SEDIMENTOLOGY OF THE FLUVIAL SYSTEMS OF THE CLEAR FORK FORMATION IN NORTH-CENTRAL TEXAS: IMPLICATIONS FOR EARLY PERMIAN PALEOCLIMATE AND PLANT FOSSIL TAPHONOMY

by

Sharane Simon

Submitted in partial fulfilment of the requirements

for the degree of Doctor of Philosophy

at

Dalhousie University

Halifax, Nova Scotia

October 2016

To my family, friends, and mentors

I am energized by your endless love and support

TABLE OF CONTENTS

LIST OF TABLES

LIST OF FIGURES

ABSTRACT

The Lower Permian Clear Fork Formation of north-central Texas is a ~350 m thick redbed deposit with extensive paleosols and well-preserved plant and vertebrate fossils. Deposited on the western equatorial margin of Pangea under (semi)arid conditions on the stable Eastern Shelf of the Midland Basin, the formation experienced shallow burial, which minimized diagenetic effects and allowed the preservation of paleoclimatic indicators. This study investigates the spatial and stratigraphic variations of the alluvial systems and provides a parallel assessment of Early Permian paleoclimatic trends established from previous studies.

Four fluvial styles were identified, representing fine-grained meandering and coarser ephemeral sandbed channels. The meandering channels exposed in cliff sections and as exhumed point bars represent a continuum between sustained lateral accretion of bedload composed of quartzose sediments and reworked pedogenic mud aggregates, and oblique accretion of suspended sediments. Swept ripples were formed as water levels declined rapidly to near-dryness and as overbank floodwaters re-entered the channels downstream. Mud aggregates are unusually well-preserved in some channel bodies due to rigid surrounding grains and cements, rapid burial within the migrating point bar, and shallow long-term burial. Abandoned channel fills contain variegated laminated mudstone with well-preserved plant leaves derived from the vegetated riparian zone. The ephemeral channels are represented by tabular sandstones that cut across the landscape and show evidence for strong but fluctuating flow.

In the formation, cements and nodules change upward from mainly calcite and ankerite in the lower unit to dolomite and gypsum with minor celestine in the middle and upper units, implying increasingly saline groundwater and supporting progressive regional aridification, which is also evident in other Late Paleozoic studies. In the meandering channel bodies, upper flow regime bedforms are confined to the lower unit, and the occurrence of plant and animal fossils decreases upsection. However, tabular sandstones and avulsive meandering bodies in the middle unit imply more humid periods with higher discharge. Many features of the Clear Fork Formation are similar to the Channel Country of central Australia, making it an appropriate modern analogue.

LIST OF ABBREVIATIONS USED

Sites/Locations					
BIO	Bedford Institute of Oceanography	BC	Mouth of Brushy Creek	CCP	Colwell Creek Pond
CR	Craddock Ranch	KWTP	Know Where To Park	MB	Mixing Bowl
MR1	Montgomery Ranch 1	MR2	Montgomery Ranch 2	MR3	Montgomery Ranch 3
NSCQ	North Soap-Creek Quadrangle	RT	Red Tank	TN	The Narrows
Facies/ Sedimentary features					
VF	very fine sand	F	fine sand	M	medium sand
C	coarse sand	VC	very coarse sand	Gm	massive pebble conglomerate
Gt	trough cross-bedded pebble conglomerate	St	trough cross-bedded sandstone	Sp	planar cross-bedded sandstone
Sh	planar stratified sandstone	Sr	ripple cross-laminated sandstone	Sm	massive or weakly laminated sandstone
Fl	finely laminated mudstone	Fm	massive ripple cross-laminated mudstone	lc	load cast
sc	scour	Mf	microfault	lcl	low angle cross-lamination
ob	overturned bed	Lp	loop bedding	con	concretion
er	eroded surface	Dr	sediment drape	P	plant fragments
A	abundant	C	common	R	rare
Fluvial Elements					
CB	channel body	CD	channel-base deposits	LA-1	quartz-rich inclined strata

LA-2	mud-rich inclined strata	LA-3	mud- and quartz-rich inclined strata	TS	tabular sandstone
LM	laminated mudstone	DM	disrupted mudstone	MM	massive mudstone
			Minerals		
A	mud aggregate	Ab	albite	Ap	apatite
Ba	barite	Ca	calcite	Ce	celestine
Ch	chlorite	Cl	clay minerals	D	dolomite
F	feldspar	Fe	ferruginous grains	G	goethite
Gy	gypsum	H	hematite	I	illite
ILM	ilmenite	Ka	kaolinite	Kf	K-feldspar
Ol	oligoclase	Pl	plagioclase	Pb	Lead fragments
Q	quartz	Sm	smectite	Ti	titania minerals
U	undifferentiated clays	Z	zircon	ZnO	zincite
			Mineralogical Techniques		
EDS	electron dispersive spectroscopy	SEM	scanning electron microscopy	XRD	X-ray diffraction
			Other		
d	grain size	D_a	long axis of grain	D_b	intermediate axis of grain
D_c	short axis of grain	G	gravity	HCL	hydrochloric acid
OOIP	original oil in place	ρ_s	density of sediment	ρ_w	density of water
Penn	Pennsylvanian	pCO_2	partial pressure of CO_2	R_o	vitrinite reflectance
T_{ci}	dimensionless shield criteria/parameter	T_{cr}	critical shear stress	u_{cr}	critical shear stress

ACKNOWLEDGMENTS

I thank God for renewing my strength daily and providing me with the knowledge, wisdom, and energy to finish this thesis. I am very thankful for the support I received from my church Jesus House Halifax, my partner Christian Kperegbeyi, friends, and family members: Allister, Anna, Melissa and Shaniah.

I am extremely thankful to my supervisor Martin Gibling who is very supportive, understanding, and encouraging. I am also grateful to my committee members Anne-Marie Ryan, John Calder, and Mike Melchin, for their constant support, guidance, and advice. It was truly a pleasure to work alongside Bill DiMichele, Dan Chaney, Neil Tabor, Lu Zhu, and Rebecca Koll. I am grateful to Gordon Brown and Dan MacDonald of Dalhousie University, Georgia Pe-Piper, Xiang Yang, and Randolph Corney of Saint Mary's University, and David Piper, Owen Brown, Lori Campbell, and Jenna Higgins of Bedford Institute of Oceanography for their willingness to always help. I thank the staff members in the Earth Science department, especially Norma Keeping, Darlene Van de Rijt, and Ann Bannon for their due diligence in all affairs. I thank Cindy Looy, Peter Holterhoft, Gresley Wakelin-King, and Dioni Cendón for informative discussions. I also thank Brent Wilson for believing in my potential and encouraging me to pursue this degree.

I thank A. B. Wharton and G. Willingham of the W. T. Waggoner Estate, James Edwards of Montgomery Ranch, and Bill Whitley of Craddock Ranch, for property access to the outcrops. Also, I acknowledge the financial support I received via a Discovery Grant assigned to Martin Gibling from the Natural Sciences and Engineering Research Council of Canada, and research grants from the Society for Sedimentary Geology and the Geological Society of America.

CHAPTER 1 INTRODUCTION

1.1 STATEMENT OF PROBLEM AND SIGNIFICANCE

The Lower Permian Clear Fork Formation was deposited on the Eastern Shelf of the Midland Basin in north-central Texas, between 0° and 5° north of the equator in the western coastal zone of Pangea. The formation comprises fine-grained, terrestrial red-beds with a diverse range of vertebrate and exquisitely preserved plant fossils, which have attracted the attention of paleontologists and paleobotanists for over a century. These fossils have contributed significantly to our understanding of prehistoric life and ancient habitats during the Late Paleozoic. In recent years, studies have used upward changes in paleosol types and plant biomes worldwide, including north-central Texas, as proxies for understanding the paleoclimatic conditions that existed during the Permo-Pennsylvanian (DiMichele et al. 2006). These proxies were strongly linked to perturbations in atmospheric pCO_2 and surface temperatures in southern Gondwana (Montañez et al. 2007).

Despite the wealth of fossil information and the contribution of these findings, the lack of geological data has precluded a broader understanding of the paleoenvironmental conditions that existed in this region. For paleobotanists, understanding the depositional setting is crucial because plant biomes tend to change with proximity to water sources. Floras such as seed plants can occupy a large ecological space and as such, constraining their habitat by studying the physical environment is one way of determining the plants' tolerance levels (W. DiMichele, personal communication). Additionally, the quality and selective preservation of plant fossils are closely linked to burial conditions, which reinforce the need to understand Early Permian surface and shallow sub-surface conditions.

In a recent study, Gibling and Davies (2012) suggested that the coevolution of fluvial systems and vascular plants occurred during the Paleozoic. During the Carboniferous, the authors noted that the diversification of gymnosperms (e.g. conifers), the expansion of vegetation across the dry alluvial plains, and the appearance of large log jams occurred in tandem with the prominent occurrence of two, distinct fluvial styles: fixed sand-filled narrow channels encased in floodplain mudstones, interpreted as anastomosing or anabranching rivers, and braided-river deposits with logs filling deep channels, similar to modern island-braided systems. Currently, the authors are extending their research into the Permian and this dissertation contributes to that study by summarizing the major plant groups present in the formation and providing detailed accounts of the depositional environments in which the plants lived and were eventually preserved.

At the end of the Permian, numerous studies have shown that significant environmental and biotic changes occurred where more than 50% of terrestrial vertebrates and plants became extinct (familial extinction rates; McElwain and Punyasena 2007). However, there are few localities where a complete section across the Permian-Triassic boundary is well-preserved. When researchers focus on that narrow interval, a more meaningful discussion of the conditions prior to the mass extinction event is prevented. Studies such as this project describe the conditions leading up to the event, providing clues about the magnitude of the disaster.

As previously mentioned, researchers have used plant biomes and paleosol types to estimate the Late Paleozoic climatic conditions in the equatorial regions of Pangea. However, there are a number of caveats associated with these proxies. For example, paleosols represent a balance between autogenic factors (e.g. sediment accumulation rate, parent material, dust flux and drainage conditions) and basin- to regional-scale allogenic processes (e.g. climate and eustasy; Tabor and Montañez 2004). In studies with few profiles, it is often difficult to differentiate

between changes related to local drainage conditions and climate (Wright et al. 1991; Kraus 1999). Additionally, paleosols may undergo burial-diagenetic alteration, which may be unrelated to paleoclimate, but mimics pedogenic features (Pimentel et al. 1996; Kraus 1999). Although plants are also regarded as "crystallized visible climate" (Claussen 1998), the fossil record is strongly biased, as it mostly comprises floras from lowland basins that grew in close proximity to water sources (DiMichele et al. 2006). As a result, the climatic signature interpreted solely from plant fossils tends to be significantly wetter than other proxies (DiMichele et al. 2006).

Another important point for consideration is that in north-central Texas, the proxies are used to interpret long-term changes that occurred during the Permo-Pennsylvanian. Identifying intraformational changes (e.g. within the Clear Fork Formation) is potentially beyond the resolution of these proxies. Therefore, qualitative sedimentary features and quantitative data such as the mineralogy of the rocks and discharge estimates can be used as indirect paleoclimatic indicators at a much finer scale. In so doing, the stratigraphic evolution of the Early Permian landscape can be linked to trends established from the plant fossils and paleosols, provided that tectonic activity is minimal, presenting a higher-order examination of paleoclimate during the deposition of the Clear Fork Formation.

Since the Clear Fork Formation is composed of red-beds, this dissertation advances our knowledge of ancient, fine-grained dryland systems, which remain poorly understood (Sambrook Smith et al. 2015). The lack of fine-grained studies in the literature is related, in part, to the difficulty of studying these systems and the low economic value of these deposits in comparison to coarse-grained channel bodies. The findings from the papers in this thesis not only document these ancient red-beds, but, we hope, may establish a benchmark for subsequent studies through some of the novel approaches used.

The Clear Fork Formation exposed at surface in north-central Texas can be traced westward into the greater Permian Basin where it is a major reservoir with nearly 1 billion barrels of original oil-in-place (OOIP; Montgomery et al. 1998). Although these reservoirs are composed of shallow-water platform carbonates, the upslope clastic beds are of interest to oil and gas companies, as they attempt to understand the regional geology of the basin. This project evaluates the time-equivalent non-marine beds and describes the fluvial styles, size, and composition of the channel bodies, as well as discusses the sediment sources that aid regional correlations.

1.2 TECTONOSTRATIGRAPHIC EVOLUTION OF THE EASTERN SHELF

The Lower Permian Clear Fork Formation was deposited on the Eastern Shelf of the Midland Basin, at the southern margin of Laurentia (Fig. 1-1), which experienced an early to middle Paleozoic passive margin phase followed by a complex collisional and post-orogenic phase in the late Paleozoic. In this section, we briefly consider the Late Paleozoic events that deformed the southern margin of Laurentia and its impact on the deposition of the Lower Permian Clear Fork Formation (Fig. 1-1; 1-2).

During the Early Pennsylvanian, the Ouachita belt which is buried unconformably below Mesozoic-Cenozoic strata in Texas, developed during the closure of the Rheic Ocean and the assembly of Pangea, and is considered the southwestward extension of the Appalachian fold and thrust belt (Fig. 1-1; Walper 1977; Nicholas and Waddell 1989). The onset of collision between Gondwana and Laurentia was marked by the upthrusting of allochthonous Mississippian foredeep flysch and tephras onto middle Paleozoic passive margin chert and novaculite exposed in the Ouachita foldbelt (Morris 1989; McBride 1989; Niem 1977; Nance and Linnemann 2008). The southward-verging oblique subduction resulted in the eastward flexure of the southern margin of Laurentia and led to the development of the Fort Worth Basin (foredeep), Bend Arch (forebulge), and Concho Platform (back-bulge; Walper 1982; Fig. 1-2C). The westward onlap and eastward thickening of the Mississippian Barnett Shale recorded the initial onset of deformation (Fig. 1-2C). The Fort Worth Foredeep Basin is fault-bounded to the north by the Red River and Muenster arches, which are interpreted as part of the Amarillo-Wichita uplifts, created when basement faults associated with the Oklahoma aulacogen were reactivated during Ouachita compression (Fig. 1-2; Walper 1977; 1982).

During the Morrowan and Atokan, terrigenous sediments (Lower Pennsylvanian Series) from the Ouachita foldbelt, the Red River, and Muenster Arches prograded into the foredeep basin as turbidites and distal flysch deposits of black shales (Brown et al. 1973; Thompson 1982; Walper 1982). As subsidence slowed during the Desmoinesian, fluvial-deltaic complexes (Strawn Group) filled the Fort Worth Basin and spilled across the Bend Arch onto the Concho Platform, marking the end of the Fort Worth Basin as a significant depocenter (Fig. 1-2C; Brown et al. 1973; Cleaves 1982; Walper 1982). The activation of the Central Basin Platform coincided with gentle uplift of the Fort Worth Basin during the Desmoinesian and led to a phase of flexural subsidence with the highest rates just east of the platform and gradually decreasing towards the Bend Arch (Fig. 1-2A). This created the asymmetric Midland Basin with a ramp-like eastern margin, i.e. the Eastern Shelf (Brown et al. 1973), which received a consistent supply of detritus from the highlands. The ramp-like geometry was maintained and a well-defined shelf/slope system was formed (Adams et al. 1951; Jackson 1964).

During the Missourian, laterally-continuous carbonate banks of the Canyon Group developed in the basin, suggesting reduced sediment input from the uplifts in contrast to the underlying Strawn Group (Fig. 1-2C; Brown et al. 1973). However, the Ouachita and the exposed Wichita-Amarillo and Arbuckle highlands were rejuvenated during the late Missourian to early Virgilian, resulting in the progradation of Virgilian to Leonardian fluvial-deltaic complexes, Cisco-Albany Groups and Clear Fork Formation, over the tectonically stable Eastern Shelf (Fig. 1-2C; 1- 3). During this period, there was a steady decline of sediments from the uplifts and thicker carbonate banks developed along the shelf edge (Brown et al. 1973). The shelf/slope system continued to prograde to the west until the Midland Basin was filled and sediment bypassed into the Delaware Basin during the Middle Permian (Van Siclen 1958; Brown et al. 1990).

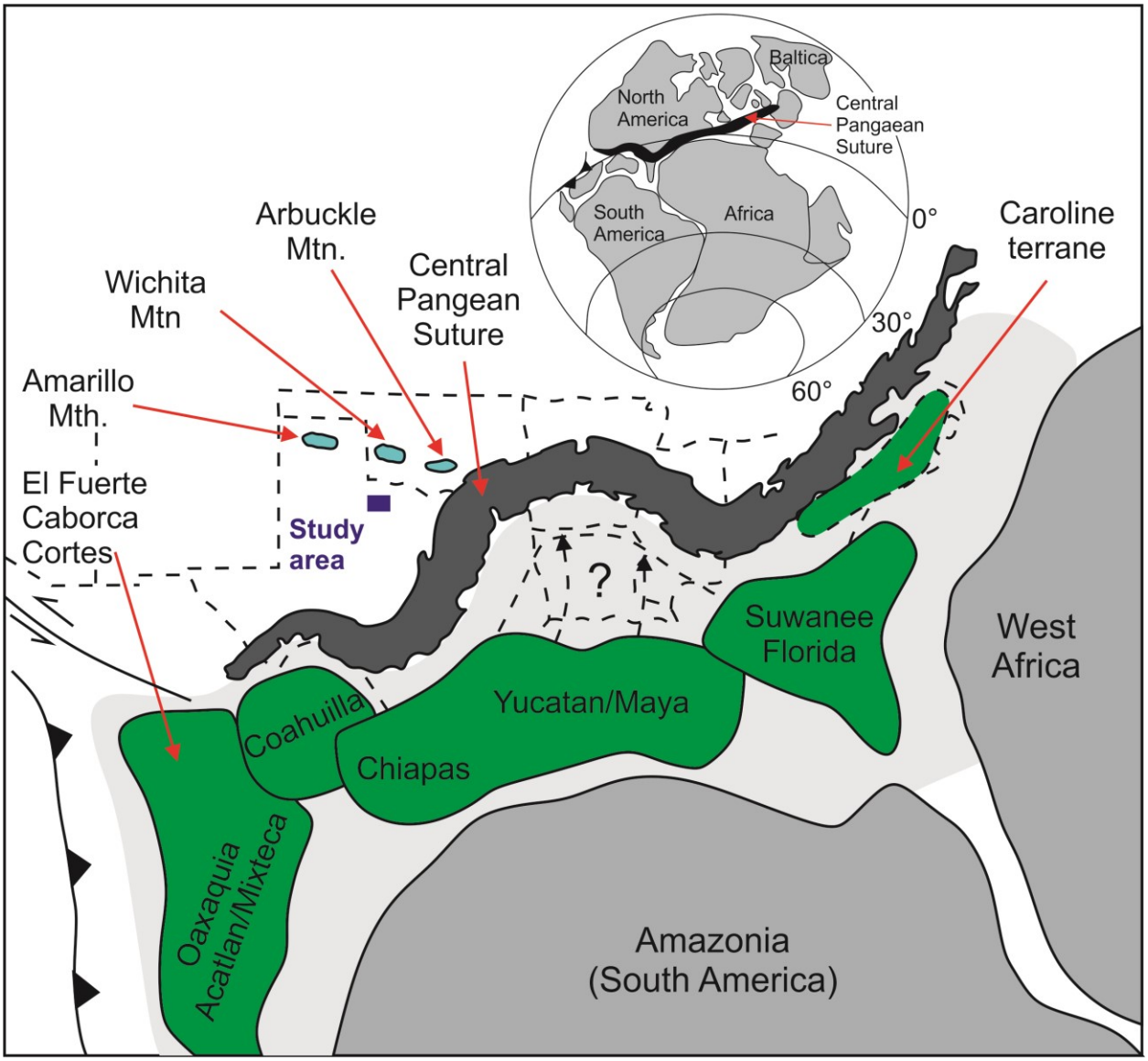

Figure 1-1 Map depicting terranes accreted and uplifted by Permian time, including Central Pangean Suture (Ouachita-Marathon orogenic belt), Arbuckle, Wichita, and Amarillo Mountains. Top inset shows larger tectonic context as the terranes assembled across the equator. Modified from Soreghan and Soreghan (2013).

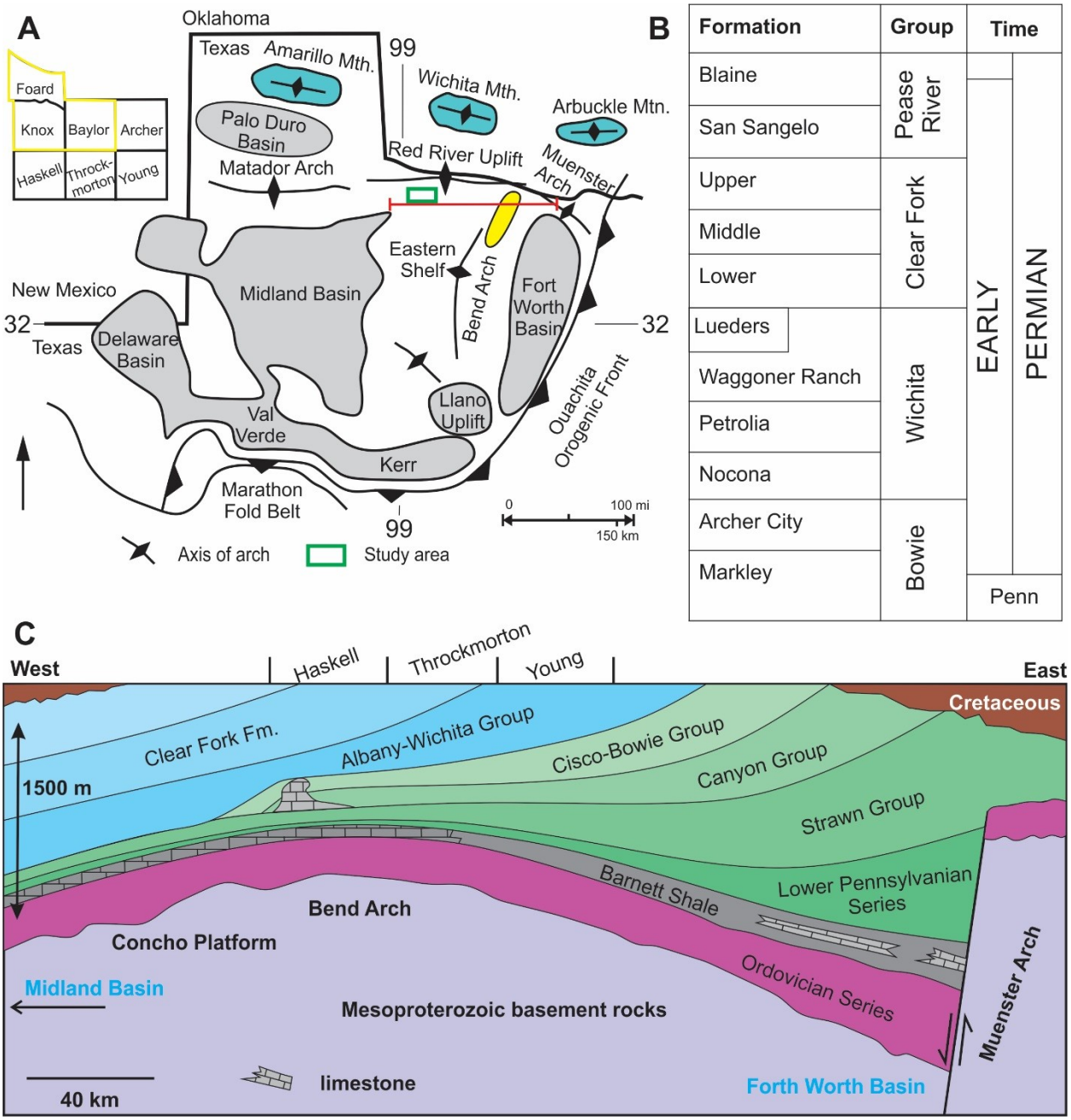

Figure 1-2(A) Permo-Pennsylvanian paleogeography of north-central Texas, showing the main uplifts and basin areas (modified from Brown et al. 1990). The study area is located in the Eastern Shelf and indicated by the green box. The red transect marks the position of Figure 1-2C. The yellow ellipse shows the study area of Hackley et al. (2009) where the authors studied the thermal maturity of the Upper Pennsylvanian Cisco Group (equivalent to Bowie Group; see Chapter 3). (B) General stratigraphic framework for the Upper Pennsylvanian and Lower Permian of the Eastern Shelf of the Midland Basin. Here, Clear Fork is defined as a group, but in this thesis, the convention set out by Nelson et al (2013) is used where the unit is described as a formation. Unit thickness on chart does not correspond to lithostratigraphic thickness or temporal duration (modified from Brown et al. 1973). (C) Schematic east–west cross-section showing stratigraphy on the Bend Arch and the main Pennsylvanian-Permian depocenters (modified from Hackley et al. 2009). Vertical and horizontal scales are approximate, with strong vertical exaggeration.

1.3 BASIN STRATIGRAPHY

During the Leonardian (Kungurian), the Clear Fork Formation was deposited on the Eastern Shelf of the Midland Basin, which lay between 0° and 5° N of the equator across the western coastal zone of Pangea, by rivers that transported sediments southward and westward along the delta plain from the degraded topographic uplifts (Fig. 1-2A; Hentz 1988). The formation comprises fluvio-continental deposits, predominantly interlayered red shale with minor sandstone, conglomerate, dolomite, and evaporites (Fig. 1-3; Olson 1958; Hentz 1988); the occurrence of dolomite and evaporite increases up-section and they are most prevalent in the upper interval. Today, the Clear Fork Formation is exposed in small vertical sections along a north-south outcrop belt in badland terrane, extending for nearly 400 km from the Oklahoma border to central Texas and dipping toward the WNW at about 1° (Fig. 1-4; Edwards et al. 1983; Nelson et al. 2013).

In the north-central region of Texas, the undifferentiated Clear Fork is recognized as a formation (Nelson et al. 2013) composed entirely of continental deposits and subdivided into three informal units: lower (55-75 m thick), middle (125-160 m thick), and upper (165-180 m thick; Fig. 1-3; 1-4). The study area lies within the north-central region and spans three counties: Baylor, Foard, and Knox (Fig. 1-4). To the south (central Texas) and west (subsurface of the Eastern Shelf), the Clear Fork is considered a group and subdivided into the Arroyo, Vale, and Choza Formations where marine interbeds occur (Olson 1958, 1989; Olson and Mead 1982), whereas in the Midland Basin, the group remains undivided (Jones 1953). Shelf- to-basin correlation is problematic because of limited paleontological data and rapid facies changes along the basin margin (Nelson et al. 2013).

In north-central Texas, the formation is underlain by terrestrial red-beds of the Bowie and Wichita Groups, upslope facies equivalents of the open marine Cisco and Albany Groups to the south (Fig 1-2B; 1-4); the lateral gradation between these facies tracts follows the general line of the Brazos River (Jones and Hentz 1988). The Markley and Archer City Formations of the Bowie Group and the Nocona Formation of the Wichita Group exhibit sedimentary features characteristic of piedmont and upper coastal plain environments (Hentz 1988). The Petrolia, Waggoner Ranch, and Lueders Formations of theWichita Group record a shift from piedmont and upper coastal plain environments to lower coastal plain settings (Hentz 1988). The Lueders Formation, which lies conformably below the Clear Fork Fomation (Fig. 1-3; 1-4), is interpreted as a tidal deposit on the basis of channels with terrestrial plants and tetrapods intercalated with carbonate rocks containing marine invertebrates such as cephalopods (DiMichele et al. 2006). Conformably overlying the Clear Fork Formation is the San Angelo Formation of the Pease River Group, which comprises an upward-fining clastic wedge derived from the Llano Uplift.

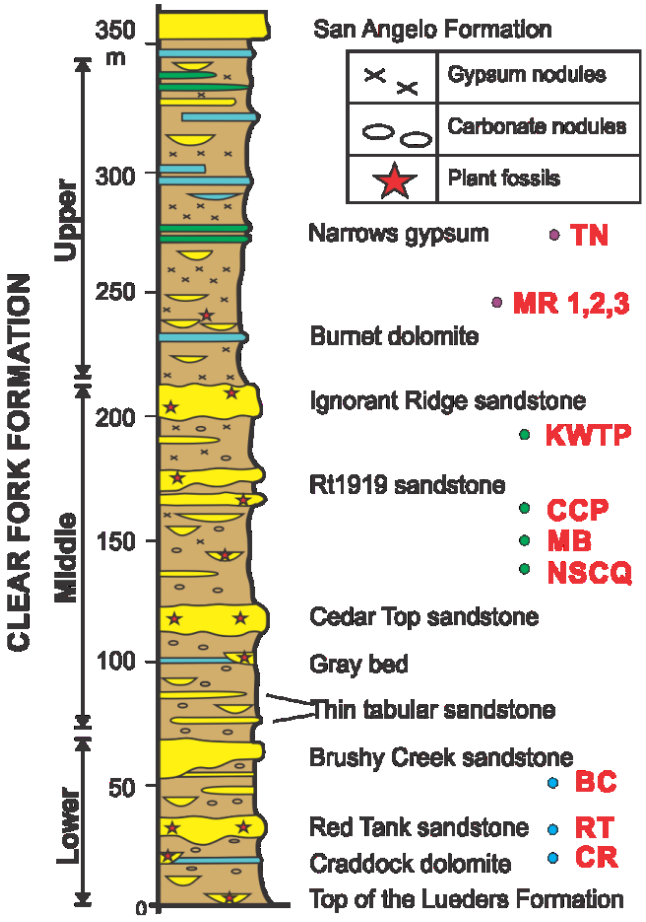

Figure 1-3 Composite log of the Clear Fork Formation along the Wichita River, showing the occurrence and relative thickness of the main channel bodies studied (modified from Nelson et al., 2013). Eleven sites were studied; TN and CR were briefly visited, but the other nine sites contain detailed outcrop descriptions. The lower Clear Fork sites (blue dots): Craddock Ranch (CR), Red Tank (RT), and Mouth of Brushy Creek (BC); the middle Clear Fork sites (green dots): North Soap-Creek Quadrangle (NSCQ), Mixing Bowl (MB), Colwell Creek Pond (CCP), and Know Where To Park (KWTP); the upper Clear Fork sites (purple dots): Montgomery Ranch 1, 2 and 3 (MR 1, 2, 3) and The Narrows (TN).

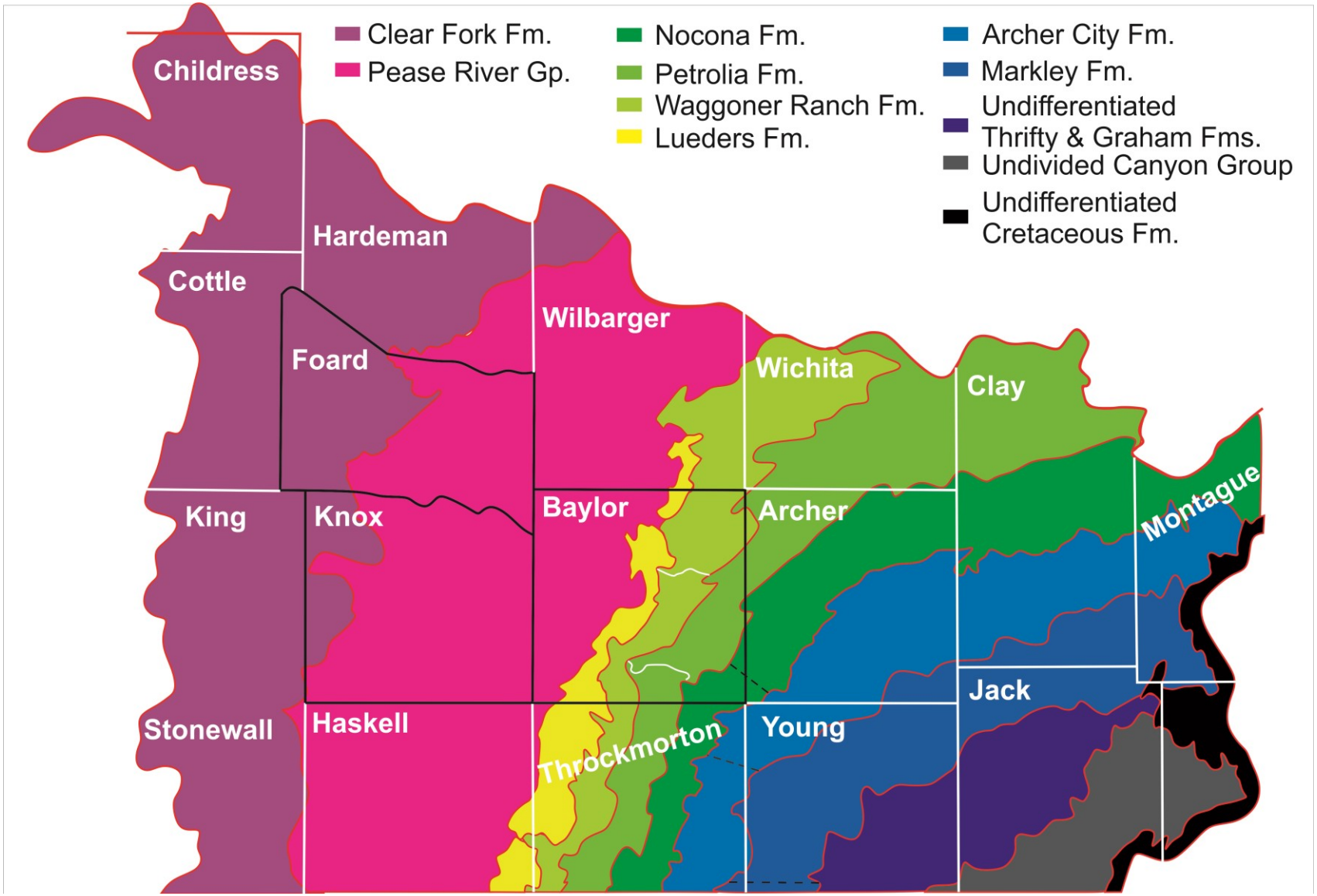

Figure 1-4 Generalized geologic map of upper Pennsylvanian and Permian marine and continental rocks in north-central Texas. The black dashed lines mark the northern extent of the marine beds of the Cisco (Bowie) and Albany (Wichita) Groups.

1.4 PERMO-PENNSYLVANIAN PALEOCLIMATIC INDICATORS

As previously highlighted, plant biomes and paleosol types are used as paleoclimatic indicators within the north-central Texas for the Permo-Pennsylvanian period (Fig. 1-5).

In north-central Texas, Tabor and Montañez (2004) noted that histosols, ultisols, inceptisols, and vertisols are common in the Upper Pennsylvanian section. These soils contain abundant redoximorphic features, widespread bituminous coals or organic-rich layers with rooting systems, and kaolinite-rich clays, which are characteristic of soils that formed in an everwet or humid tropical environment. In contrast, alfisols, vertisols, and aridisols are prominent in Lower Permian strata (Archer City, Wichita Group, and Clear Fork Formation) with features such as pedogenic carbonate, deep fossil roots, and smectite-dominated clay compositions, which most likely developed under seasonal climatic conditions. This upward increase in aridification is also inferred from stratigraphic changes in plant biomes.

Plants such as pteridosperms, marattialean ferns, lycopsids, and calamites, which have reproductive biologies and architectures that are closely linked to wet substrates, were prominent in the Late Carboniferous (DiMichele and Phillips 1994; DiMichele et al. 2006). In general, everwet plants release spores into the environment, from which a haploid (which produces both sperms and eggs) develops; a haploid is generally small and inconspicuous and lives freely and separately from the more macroscopically conspicuous diploid generation, which produces spores (W. DiMichele, personal communication). The female reproductive organs of lycopsids appear to be water dispersed and their rooting system is broadly spreading and shallow with growth tips and appendages, structurally incapable of penetrating hard substrates (Phillips 1979; Phillips and DiMichele 1992). Marattialean tree ferns are homosporous, and release spores that require moisture to complete their life cycle (DiMichele et al. 2006). Calamitean sphenopsids are

commonly found in disturbance-prone environments (e.g. streamside, bayside, and lakeside deposits), as their underground rhizomes permit them to recover from repeated rapid, shallow burial (e.g., Gastaldo 1992).

In the Early Permian, the everwet floras were replaced by seed plants such as conifers, gigantopterids, peltasperms, taeniopterids, and cordaites that bear some or all of the following morphological characteristics (depending on the extent to which they are known; Algeo and Scheckler 1998): "small or reduced foliage, sunken stomatal pores, various kinds of water-retention attributes of the leaf surface, reduced stature if broad-leaved, and deep, vertical patterns of rooting" (DiMichele et al. 2006). Unlike the pteridophytes (everwet plants), seed plants avoid the need for external water for fertilization, as the female phase of the life cycle is present in the seed, and the male phase is present in the pollen grain (W. DiMichele, personal communication). As a result, seed plants can occupy ecological space outside of poorly drained or wet terrestrial areas, making them tolerant of drier conditions. To determine the water and temperature tolerance levels of seed plants, researchers are unable to use first principle analysis (as is used for the everwet plants), but instead assess the habitat of the seed plants through links to physical and environmental indicators (W. DiMichele, personal communication). This approach is limited as linkages among physical indicators and various taxa vary in quality and reliability; additionally, such a comparison is only possible at the species level because of the great variability among species even in the same genus.

In the upper Lower Permian to lower Middle Permian, precocious taxonomic occurrences appear millions of years prior to previously well-established ranges and are referred to as "Methuselah" taxa (Looy et al. 2014). For instance, the cycad *Dioonitocarpidium* and some conifers such as *Podozamites* are present in the Pease River Group, although elsewhere they are only known from

the Mesozoic (DiMichele et al. 2001, 2004). These taxa were deposited under a seasonally dry climate as evident from the presence of gypsum and weakly developed paleosols within the section (DiMichele et al. 2006).

Within the lower and middle units of the Clear Fork Formation, floras commonly represent riparian habitats with an assemblage composed of callipterids, gigantopterids, comioids, taeniopterids, and conifers with isolated patches of everwet plants as singletons or, rarely, as the dominant element in nearly monotypic assemblages (Chaney and DiMichele 2007). The upper Clear Fork unit is generally depauperate, consisting of monotypic assemblages with one or two elements. Plant fossils die out upwards where evaporites appear, suggesting a sparsely vegetated or unvegetated landscape and/or a change in taphonomic parameters such that plant remains were not preserved (Chaney and DiMichele 2007).

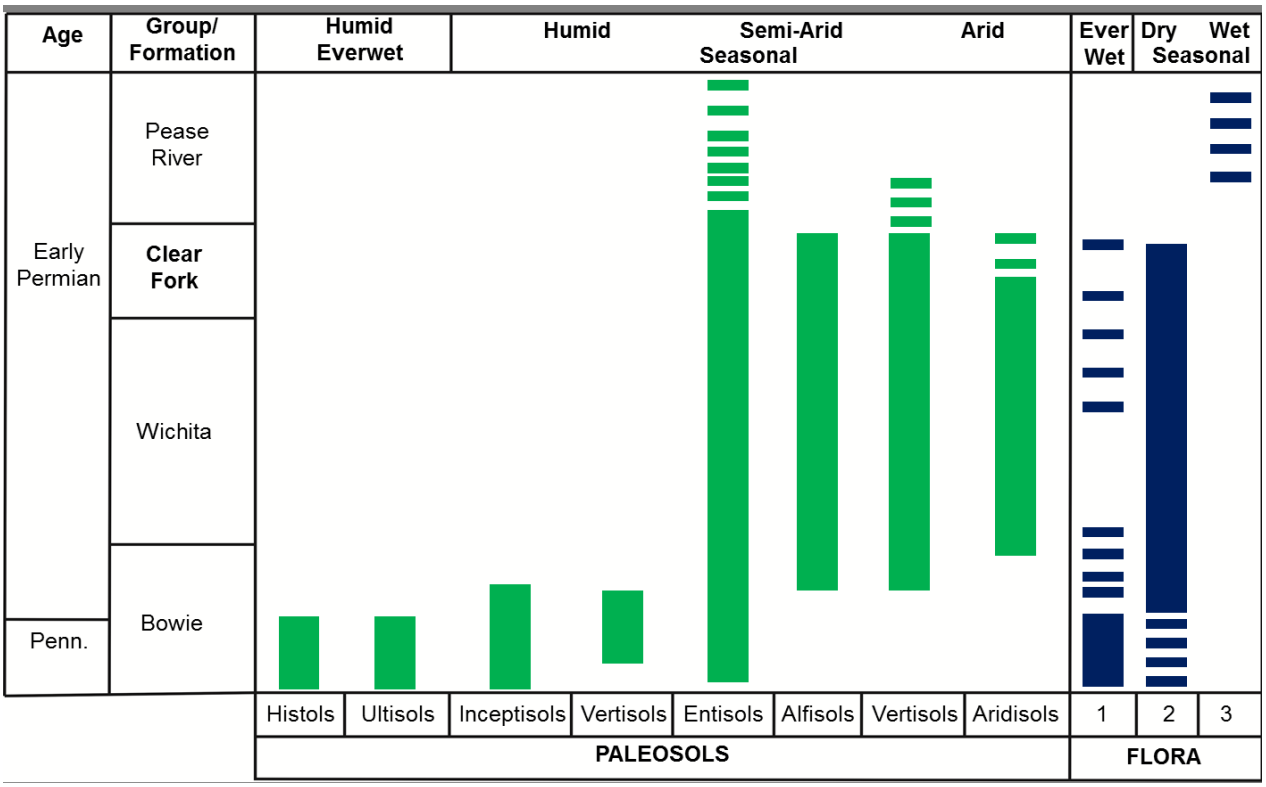

Figure 1-5 Stratigraphic distributions of pedotypes and paleofloras, showing that conditions were everwet in the Pennsylvanian and seasonal in the Permian (modified from Tabor and Montañez 2004). Formational thicknesses not drawn to scale.

1.5 OBJECTIVES AND APPROACH

Although paleobotanists showed great interest in north-central Texas since the late 1800s, it was not until the early 1990s that workers recognized the quality, quantity, and importance of the floras in the red-beds (Chaney and DiMichele 2007). In 1994, numerous plant compression fossils were discovered in the lowermost Clear Fork in north-central Texas, which highlighted the need for a strong understanding of the depositional environments and paleoecological conditions (Nelson et al. 2013). In response, Nelson et al. (2001; 2013) established a stratigraphic framework for the Clear Fork Formation in the north-central regions of Texas. This framework incorporated published and unpublished field notes, reports, maps, and cross-sections from pioneering workers such as E.C. Olson, N. Hotton and L.F. Brown Jr. in the preliminary stages and an extensive, multi-year field investigation to better understand the depositional systems. Prior to this study, Edwards et al. (1983) described an exhumed, fine-grained point bar in the middle unit of the Clear Fork Formation and discussed the occurrence of oblique ripples and the conditions responsible for their formation. In this thesis, these studies were used as a guide to stratigraphic relationships, expanding our limited understanding of the spatial and stratigraphic variations of the alluvial systems throughout the formation. In so doing, the paleoclimatic conditions under which the plants grew were also constrained.

In order to achieve this, several objectives were established (Table 1-1) and are addressed in the subsequent chapters. Over the course of three field seasons, eleven sites were visited across three counties (Baylor, Foard, and Knox), nine of which were carefully and systematically described (Fig 1-6). These sites were selected based on accessibility of the outcrop within ranchlands, availability of paleosol profiles and fossil information, and representation of the Clear Fork members. These localized outcrops, oriented variably to strike and in planform, required a

certain level of ingenuity to properly assess the beds (see Section 2.4). Since mudstones are the predominant rock type within the formation and sandstone bodies tend to be mostly fine-grained, petrographic analysis was essential for documenting detrital and diagenetic components of the rocks, a key part of understanding surface and shallow sub-surface processes. Over 100 samples were collected and analysed using various mineralogical techniques such as scanning electron microscopy (SEM) with electron dispersive spectroscopy (EDS) and X-ray diffraction (XRD; Table 1-2). Detailed accounts of the methods, as they pertain to specific objectives, are presented in subsequent chapters.

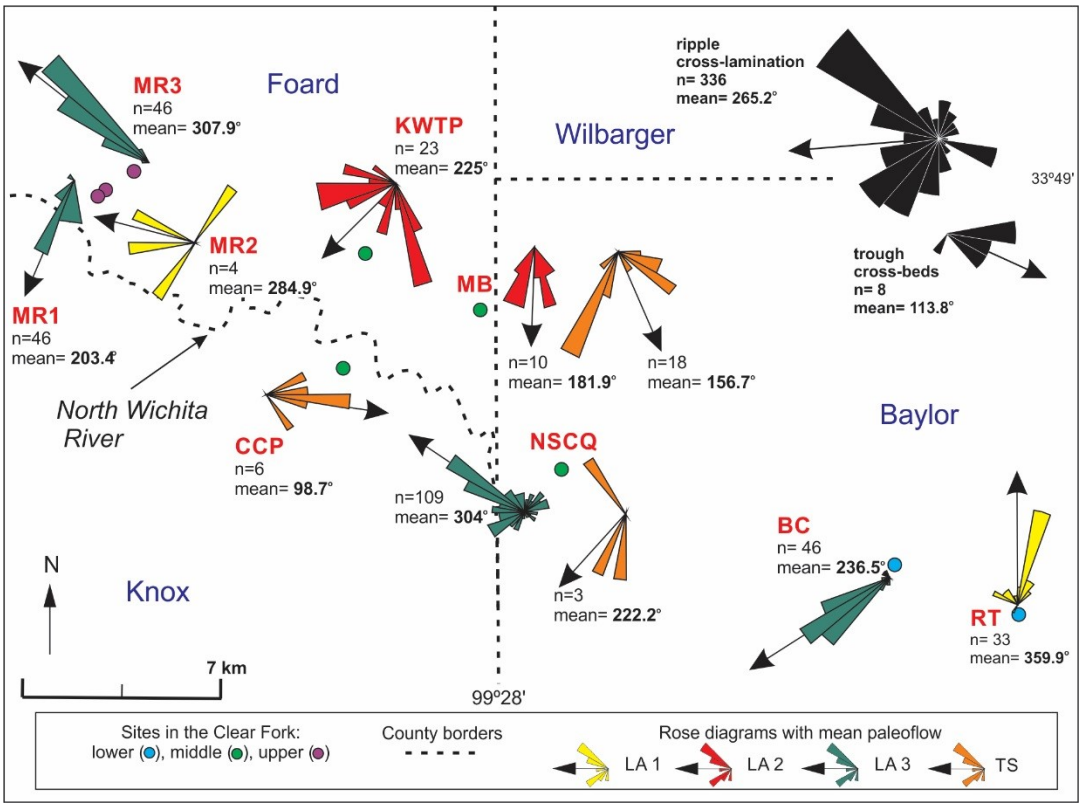

Figure 1-6 Eleven sites studied in Baylor, Foard and Knox counties. The lower Clear Fork sites (blue dots): Craddock Ranch (CR), Red Tank (RT), and Mouth of Brushy Creek (BC); the middle Clear Fork sites (green dots): North Soap-Creek Quadrangle (NSCQ), Mixing Bowl (MB), Colwell Creek Pond (CCP), and Know Where To Park (KWTP); the upper Clear Fork sites (purple dots): Montgomery Ranch 1, 2, and 3 (MR 1, 2, 3), and The Narrows (TN). The Narrows (TN) which is located west and north of the map area and contains no channel bodies, and Craddock Ranch (CR) were briefly visited, but the other nine sites contain detailed outcrop descriptions. The rose diagrams represent paleoflow data from all sites. Note that trough cross-beds were from tabular sandstone units, which exhibit somewhat different paleoflow patterns than other units (see Chapter 2).

Table 1-1 Main objectives of the thesis as discussed in the subsequent chapters.

Chapters	Primary Objectives
2	▪ To document the fluvial styles present within the Clear Fork Formation and determine the formative conditions through direct comparison with analogues. ▪ To document the mineralogical composition of the fluvial systems and predict sediment sources. ▪ To highlight the presence of oblique ripples and describe their formative conditions. ▪ To estimate discharge based on the channel dimensions. ▪ To compare paleoflow values from the channel bodies to the basin configuration. ▪ To document the facies in which plant fossils were preserved throughout the formation. ▪ To refine the Early Permian paleoclimatic trend using sedimentological and mineralogical data from the formation.
3	▪ To document the first known example of well-preserved mud aggregates as the main sediment component in a fine-grained meandering channel. ▪ To describe the form, shape, size and composition of the mud aggregates. ▪ To describe how mud aggregates are formed in smectite-poor settings and compare to analogues. ▪ To describe how mud aggregates are transported and deposited in the meandering channel. ▪ To assess the conditions responsible for preservation and compare to existing hypotheses established in the literature.
4	▪ To document the most heavily collected plant-bearing locality in the Leonardian redbed section of north-central Texas. ▪ To describe the facies and geometry of the alluvial strata, as well as the sedimentary structures, mineralogical composition and organic content of the laminated beds. ▪ To document the main plant taxa present and determine the conditions responsible for preservation.

1.6 THESIS ORGANIZATION AND CONTRIBUTIONS

This thesis comprises seven chapters: (chapter 1), three technical papers (chapters 2 to 4), additional facies information (chapter 5), discussion (chapter 6), and conclusions (chapter 7). The contributions of various authors and researchers are highlighted in Table 1-2.

Chapter two describes the fluvial styles present within the Clear Fork Formation and examines the processes responsible for the deposition of fine-grained meandering channels. The mineralogical and geochemical compositions of the channel bodies were also assessed to predict sediment sources and shallow sub-surface processes; detailed petrographic descriptions are also presented in Appendix C- Section 10.4. At the end of this chapter, the combination of physical sedimentology with petrography yielded strong evidence to refine existing paleoclimatic models for the Early Permian in this region. This chapter is derived entirely from:

> Simon, S., and Gibling, M.R., accepted 2016, Fine-grained meandering systems of the Lower Permian Clear Fork Formation of north-central Texas, USA: lateral and oblique accretion on an arid plain: Sedimentology.

Chapter three documents the first known example of well-preserved pedogenic mud aggregates as the main sediment component in a fine-grained meandering channel. I also discuss the origin of the mud aggregates and document the internal/external features of the aggregates as well as estimating the original grain size for the flattened aggregates. The depositional setting and the post-burial conditions responsible for the exquisite preservation are also assessed. This chapter is derived entirely from:

Simon, S., and Gibling, M.R., in review 2016, Pedogenic mud aggregates within a fine-grained meandering channel in the Early Permian Clear Fork Formation of north-central Texas, USA. Journal of Sedimentary Research.

Chapter four presents a multidisciplinary paper which documents the sedimentology and mineralogy of a fine-grained abandoned channel deposit that contains exquisitely preserved plant leaves with evidence of herbivory. The environments in which the plants grew and were eventually preserved are described in detail, as well as a summary of the plant groups present. This chapter is derived entirely from:

Simon, S., Gibling, M.R., DiMichele, W.A., Chaney, D.S., Looy, C.V., and Tabor, N.J., 2016, An abandoned-channel fill with exquisitely preserved plants in redbeds of the Clear Fork Formation, Texas, USA: an Early Permian water-dependent habitat on the arid plains of Pangea: Journal of Sedimentary Research, v. 86, p. 944-964

Chapter five presents a brief description and interpretation of three additional facies (debris-flow deposit, stromatolite bed, and playa-lake deposits), which were identified within the Clear Fork Formation but were not mentioned in previous chapters.

Chapter six presents a broad overview of the body of work and describes the Early Permian landscape based on the findings from the previous chapters. *Chapter seven* summarises the key findings of this thesis and appendices containing supplementary data (figures and diagrams) are attached at the end of the thesis.

Table 1-2 Contributions made by various authors and researchers for Chapters 2 to 4.

Activity	Contributions
Fieldwork	▪ Conducted by the first author with the assistance of Martin Gibling. Bill DiMichele and Dan Chaney of the Smithsonian Institute, Neil Tabor and Lu Zhu of the Southern Methodist University, and Rebecca Koll of the University of Florida provided logistical support. The data were interpreted, and collated by the first author with the assistance of Martin Gibling. ▪ 114 samples were collected during fieldwork by the authors. ▪ Three field seasons: 15th April to 7th May 2013; 22nd April to 8th May 2014; 7th to 18th March 2015.
Thin section	▪ 77 unpolished and 17 polished thin sections were prepared by Gordon Brown of Dalhousie University and Vancouver Petrographics Limited. ▪ The first author examined and described each thin section with periodic assistance from Martin Gibling and Anne-Marie Ryan.
Point counting and grain size analysis	▪ Randolph Corney of Saint Mary's University trained the first author to use the point counting and grain size analysis microscope/software. ▪ The first author point counted 12 thin sections with 300 (6 slides)-400 (6) points per slide and measured the axes of 1800 grains from 6 thin sections.
Total organic carbon and total carbon	▪ The first author prepared nine samples, which were analysed by Lori Campbell of Bedford Institute of Oceanography (BIO) using a Leco TruSpec analyser.
X-ray diffraction (XRD) analysis	▪ Owen Brown and David Piper of BIO trained the first author to prepare XRD samples and interpret the spectra. Lori Campbell conducted the analysis using the Siemens Kristaloflex diffractometer. ▪ The first author prepared 83 random powder mounts and 24 <2 μ fractions and interpreted the results.
Scanning electron microscopy (SEM)	▪ Xiang Yang and Georgia Pe-Piper of Saint Mary's University trained the first author to use the Scanning Electron Microscope and interpret the data. ▪ 17 polished thin sections and 5 rock samples were analysed by the first author using the TESCAN MIRA Scanning Electron Microscope with the EDS system.

Activity	Contributions
Drafting and editing	▪ The first author wrote the original manuscript and designed all figures and tables. Constructive criticism was provided by Martin Gibling, Anne-Marie Ryan, Bill DiMichele, and Neil Tabor. Lu Zhu studied the paleosols within the formation and her results were incorporated in this study but represents less than 5% of the paper. The three papers were submitted to two jorunals: Journal of Sedimentary Research and Sedimentology. ▪ The paper in Chapter 2 was accepted pending edits suggested by Greg Sambrook Smith, Colin North, an anonymous reviewer, and Associate Editor Christopher Fielding. ▪ The paper in Chapter 4 was accepted pending edits suggested by the Associate Editors Elizabeth Gierlowski-Kordesch (deceased) and Gary Weissmann as well as John Southard, and two other expert reviewers: Steven Driese and Anne Raymond with an August 2016 publication date. Bill DiMichele, Dan Chaney, and Cindy Looy wrote the "Plant fossils" section (5 pages) and provided two figures in support of their interpretations. Field descriptions of the paleosols as well as XRD data were obtained from Neil Tabor and Martin Gibling interpreted the results. Comments and suggestions were provided by the coauthors prior to submission and they contributed to editing the manuscript.
Contributions	▪ The author also received useful comments or information from Peter Holterhoft, Gerilyn Soreghan, Bethany Theiling, Gresley Wakelin-King, Dioni Cendón, Matt Stimson, and Alessandro Ielpi.

CHAPTER 2- Fine-grained meandering channels and sheet sandstones in the Lower Permian Clear Fork Formation of north-central Texas, USA: lateral and oblique accretion on an arid plain

2.1 ABSTRACT

Facies models that adequately represent the diverse range of fine-grained fluvial systems are currently lacking from the literature. In this paper, the spectrum of these systems on the arid plains of western equatorial Pangea is explored, as well as the source and nature of the fine-grained sediments. Eight fluvial elements in the Early Permian Clear Fork Formation of north-central Texas represent channel systems up to 7 m deep with coarse basal deposits, three types of lateral-accretion deposits, and sandstone sheets, with laminated, disrupted, and massive mudstones laid down in abandoned channels and on floodplains. The three fine-grained fluvial styles represent a continuum between two end-members: sustained lateral accretion of bedload composed of quartzose sediments and mud aggregates on point bars, and oblique accretion of suspended sediment on steep accretionary benches and banks with limited lateral migration. This spectrum is controlled in-part by grain size and the proportion of suspended to bedload sediments. The presence of rarely documented swept ripples on exhumed accretion surfaces is attributed to rapid decline in water levels and downstream re-entry of overbank floodwaters into the channel. Rill casts, roots, and disrupted mudstones low down in channel bodies indicate periods of near-dryness. Laterally extensive sheet sandstones were formed by episodic flows in broad, sandbed channels. The fluvial sediments were primarily intrabasinally sourced with extrabasinal sediments brought in during major floods from upland source areas or reworked from local storage in the basin, representing a supply-limited system. The upward change in

cement composition from mainly calcite and ankerite to dolomite and gypsum with minor celestine implies increasingly saline groundwater and progressive aridification, supporting Late Paleozoic paleoclimatic models. By integrating petrographic data with sedimentology, a plethora of information about ancient landscapes and climate is provided, allowing a fuller comparison between the Clear Fork Formation and modern dryland alluvial plains.

2.2 INTRODUCTION

Modern fine-grained fluvial systems have been documented in dryland settings far from upland source areas (Taylor and Woodyer 1978; Gibling et al. 1998; Brooks 2003a; Page et al. 2003; Fielding et al. 2009), or where fine-grained glacial detritus or loess is abundant (Fahnestock 1969; van Gelder et al. 1994; Sambrook Smith et al. 2016). Such systems are poorly represented in facies models (Brooks 2003a; Ghosh et al. 2006; Wright and Marriott 2007), in part because fluvial style and architecture is influenced by the proportions of bedload and suspended load, which may be difficult to distinguish in ancient fine-grained systems. Furthermore, fine-grained sediments derived directly from upland erosion and weathering are difficult to distinguish from those reworked from floodplains, derived from older sediments within the basin, or mobilised by aeolian processes.

In meandering systems, a key problem is distinguishing lateral from oblique accretion (Jackson 1981; Brooks 2003a, 2003b; Page et al. 2003; Makaske and Weerts 2005). Lateral accretion involves "the deposition of inclined layers by the lateral outbuilding of sediment on the surface of a river point bar" (Allaby 1999), "resulting in channel migration where point-bar advance is matched by cutbank retreat" (Eke et al. 2014). Page et al. (2003) defined oblique accretion as "the lateral accumulation of fine-grained floodplain sediment by progradation of a relatively steep convex bank in association with channel migration." Essentially, fine-grained suspended

sediment drapes the channel bank during waning flow, a process that may be decoupled from cutbank retreat. Sambrook Smith et al. (2016) suggested that lateral and oblique accretion are end-members in meandering systems, controlled by grain size and sediment load.

In the rock record, sand-rich channel fills in mud-rich formations are commonly interpreted as fixed or anastomosing channels (Smith and Putnam 1980; Rust et al. 1984; Warwick and Stanton 1988; Eberth and Miall 1991; Nadon 1994). Mud is typically a minor component that draped inclined surfaces or accreted vertically in abandoned channels. In contrast, few examples exist for active, fine-grained fluvial channel fills (Stewart 1983; Mack et al. 2003; Ghosh et al. 2006; Gruszka and Zieliński 2008), due to the lack of well-exposed sections, their susceptibility to deformation and diagenesis, difficulty in determining the sediment source, and the overwhelming attention given to economically important coarse-grained deposits. A particular problem is that pedogenic mud aggregates have rarely been identified in ancient channel fills, despite their prominence in some modern rivers (Rust and Nanson 1989; Gierlowski-Kordesch and Gibling 2002; Müller et al. 2004; Wright and Marriott 2007; Gastaldo et al. 2013). Although composed of clay flakes, these aggregates are typically sand-sized and transported as bedload.

In this study, we evaluate the intrabasinal processes responsible for the deposition of the fine-grained fluvial deposits of the Lower Permian Clear Fork Formation in north-central Texas. This formation was deposited in a relatively arid equatorial region under tectonic quiescence when source areas were distant or degraded. Shallow burial minimised diagenetic effects and aided the preservation of primary features such as mud aggregates, allowing us to (a) determine the nature and origin of the fine-grained sediments, (b) distinguish between mud transported as bedload and suspended load, and (c) identify lateral and obliquely accreted deposits through comparison with modern dryland rivers, leading to a robust link to a modern analogue. This paper also highlights

the importance of integrating petrographic analysis with field descriptions as fine-grained deposits are cryptic in outcrop and heterogeneous at various scales. The combination of physical sedimentology with petrography has also yielded important information regarding surface and shallow sub-surface processes, providing evidence in support of existing paleoclimatic models for progressive aridification in the Early Permian.

2.3 TECTONIC AND STRATIGRAPHIC SETTING

The Lower Permian Clear Fork Formation was deposited on the Eastern Shelf of the Midland Basin in north-central Texas, between 0° and 5° north of the equator in the western coastal zone of Pangea (Golonka et al. 1994; Ziegler et al. 1997; Scotese 1999; Fig. 1-2A). Uplifts to the north and east included the Wichita and Arbuckle Mountains, which are remnants of the Pennsylvanian Ancestral Rocky Mountains orogenic belt, and the Ouachita Mountains along the Late Palaeozoic suture zone of Pangea (King 1937; Oriel et al. 1967; Houseknecht 1983). During the Early Permian, tectonic quiescence prevailed with intermittent strike-slip movement along the Matador and Red River Uplifts (Regan and Murphy 1986; Budnik 1989; Brister et al. 2002). The upward decrease in grain size, thickness, and abundance of fluvial channel bodies (Fig. 1-3) suggests that uplifts were progressively denuded and onlapped during the Early Permian (Hentz 1988; Tabor and Montañez 2004; Soreghan et al. 2012).

Clear Fork strata extend for 400 km south of the Oklahoma-Texas border, and in north-central Texas the formation is subdivided into informal lower, middle, and upper units (Nelson et al. 2013). This study focused on outcrops in Baylor, Foard, and Knox counties where the formation is 350-365 m thick and dips gently (< 1°) WNW, with no faults observed (Fig. 1-3 and 1-6; Edwards et al. 1983; Hentz 1988; Nelson et al. 2013). The formation is Leonardian in age, equivalent to the earliest Kungurian (Wardlaw 2005; Lucas 2006). The formation rests

conformably on dolostone and mudstone of the Lueders Formation, and comprises mudstone (80-85%), sandstone (10-15%), carbonates and evaporites (<5%; Fig. 1-3; Olson 1958; Hentz 1988; Nelson et al. 2013). Ridge-forming sandstones up to 12 m thick, commonly with lateral accretion sets, represent meandering channel bodies with southwesterly paleoflow; they are separated by red floodplain mudstones with paleosols (Olson 1958; Edwards et al. 1983; Hentz and Brown 1987; Behrensmeyer 1988; Jones and Hentz 1988; Nelson et al. 2001; Tabor and Montañez 2004; DiMichele et al. 2006; Nelson et al. 2013). Unusually, the upper surfaces of many channel bodies are exhumed at the land surface (Edwards et al. 1983). In the upper unit, channel bodies are fewer and thinner, and gypsum is abundant as nodules, dikes, and thin beds. Open-marine intervals are present in coeval Clear Fork strata ~200 km to the south (Olson 1958; Nelson et al. 2013).

The formation has yielded freshwater sharks and palaeoniscoid fish, failed aestivation assemblages of lungfish and lysophorid amphibians, and skeletons and footprints of amphibians and reptiles (e.g. Broili 1904; Romer 1928; Olson 1958; Murry and Johnson 1987; DiMichele et al. 2006; Anderson et al. 2008; Lucas et al. 2011; Milner and Schoch 2013). Well-preserved plant fossils include roots, charcoal, and leaves of callipterids, comioids, gigantopterids, taeniopterids, and coniferous seed plants with rare occurrences of pecopterid tree ferns (DiMichele et al. 2006; Chaney and DiMichele 2007). Other fossils include invertebrate burrows, myriapod trackways, and rare bivalves (Nelson et al. 2013). Fossils generally decrease in abundance upwards and the uppermost known occurrence of plants and vertebrates lies just above the Burnet dolomite. The paleoclimate during deposition of the Clear Fork Formation was semi-arid to arid based on paleosol and plant information (DiMichele et al. 2006).

The formation is conformably overlain by the San Angelo Formation of the Pease River Group. The depth of burial under later Permian and younger strata may not have exceeded ~1100 m based on regional stratigraphic considerations and maturation studies of Eastern Shelf strata (Bein and Land 1983; Hackley et al. 2009).

2.4 METHODOLOGY

Eleven sites were studied over three field seasons (Fig. 1-6). Nine are summarised here, Colwell Creek Pond is described elsewhere (Simon et al. 2016), and a site at The Narrows had no channel bodies. Site selection was based on accessibility, availability of paleosol profiles and fossil information, and representation of Clear Fork units. Techniques depended on the type of outcrop, with cliff faces oriented parallel, perpendicular or oblique to local paleoflow. Channel components were commonly partially exposed, and were in places dug out. The data were combined to produce a synthesis of fluvial styles, while respecting individual site differences. Paleoflow measurements were made mainly on ridge-and-furrow features formed by ripple migration on bed surfaces and are accurate to ±5°.

To reconstruct exhumed surfaces, eroded ridges up to 20 m long formed by inclined sandstone bedsets were mapped using GPS readings accurate to ±3 m. Depending on ridge length, at least three readings (upstream, medial and downstream sites) were recorded, encompassing grain size and sedimentary features, strike/dip, and paleoflow. Using a range finder accurate to ±1 m or a tape, ridge length and the distance between ridge crests was measured as a field check for the GPS. At some sites, the ridges terminated against a cliff, allowing direct correlation with overlying or adjacent deposits. Directional data were imported into a Google Earth image geo-rectified into ArcGIS, allowing calculation of the overall radius of curvature ($R_c = \frac{H}{2} + \frac{W^2}{8H}$,

where W is the length of the chord defining the base of the arc and H is the height measured at the midpoint of the arc's base). For cliff sections, key stratigraphic surfaces and sedimentological observations were recorded on photomosaics. Eight fluvial elements were identified (Table 2-1) drawing on the elements and facies codes of Miall (1996); the term “mudstone” implies varied proportions of clay and silt.

The exposures allow measurement of channel-body thickness, a proxy for depth in single-storey bodies, and rarely of channel width. Channel-body thickness was estimated as the maximum vertical extent of inclined surfaces or the thickness of an abandoned-channel fill from the basal contact to the base of the overlying channel body or floodplain deposit. Channel width was measured for abandoned-channel fills, as the horizontal distance between the last lateral-accretion surface and the onlap of channel fill onto flat-lying floodplain deposits, assuming that abandonment was concurrent with the termination of cutbank retreat. For the North Soap-Creek Quadrangle site, discharge was calculated by using hypothetical flow velocities (0.5, 0.75, and 1.0 m/s) and the bankfull cross-sectional area of the channel (bankfull width * bankfull depth). Using the radius of curvature (R_c), bankfull width (W_b) and depth (D_b) were calculated using equations from Williams (1986), where $W_b = 0.71R_c^{0.89}$ and $D_b = 0.085R_c^{0.66}$. Due to the presence of suspended clays and bedload transported mud aggregates, a range of hypothetical flow velocities was used to simulate the flow strengths required for entrainment and the range of conditions that probably existed during low and high energy floods.

A total of 77 unpolished thin sections was examined under plane-polarised light and 17 polished thin sections were studied using SEM/EDS analysis. The chemical composition of the carbonate clasts and cements was determined using EDS data (see Appendix B). X-ray diffraction (XRD) analysis was conducted on 83 random powder mounts and 24 samples were selected for <2 μm

fraction analysis. Details of the sample preparation and analytical techniques are presented in the Appendix B.

Table 2-1 Elements for meandering channel, sheet sandstone, and floodplain deposits in the Clear Fork Formation. Facies codes from Miall (1985, 1996), Tucker (2003), and Long (2011). Redoximorphic spots and Fe-oxide staining are prominent in all facies, which are red, brown and grey. Plants include woody fragments and leaves; trackways refer to diplichnitid forms. Detrital grains: quartz, K-feldspar, plagioclase, titania minerals, zircon, apatite and ilmenite; clays: illite, Fe-rich chlorite, kaolinite and mixed-layer clay. VF, F, M and VC = very fine, fine, medium, and very coarse sand, respectively. Gm: massive or crudely bedded pebble conglomerate; Gt: trough-cross bedded pebble conglomerate; St: trough cross-bedded sandstone; Sp: planar cross-bedded sandstone; Sh: planar-stratified sandstone; Sr: ripple cross-laminated sandstone; Sm: massive or faintly laminated sandstone; Fl: finely laminated mudstone; Fm: massive to weakly ripple-cross laminated mudstone. A = abundant, C = common, R = rare.

Elements	Grain Size	Sedimentary features and fossils	Petrography	Interpretation
Channel-base Deposits (CD)	Pebble conglomerate, VF-F sandstone	Gm, Sh, Sr, as lenses and linear mounds. Current lineation, flute casts, trackways (C), plants (R), wood (R).	Calcitic, dolomitic, siliciclastic and ferruginous clasts in a matrix of detrital grains, hematite, and clay.	*Channel-lag deposits* laid down during and after scouring events, generally thin. Carbonate pebbles reworked from local paleosols.
Quartz-rich Inclined Strata (LA-1)	VF-F sandstone	St, Sp, Sh, Sr, Sm. Waning-flow cosets and reactivation surfaces. Inclined bedsets <4 m thick, surfaces dip <17^{o}. Paleoflow along strike and in places directly or obliquely updip of surface. Trackways (C), plants (R), root traces (C).	Calcite, ankerite, gypsum, celestine, and barite cement, with clay and hematite matrix. Clay aggregates with long axis parallel to the bed strike. Minor dolomite with hollow or calcite cores.	*Lateral accretion deposits* formed by point-bar migration. Strong component of helicoidal flow. Lower to upper flow regime. Stacked storeys suggest avulsive patterns. Well vegetated.
Mud-rich Inclined Strata (LA-2)	Mudstone (mainly siltstone) with VF sand grains	Sm, Sr, Sp. Inclined bedsets of grey and red beds <4 m thick, surfaces dip 12-15^{o}. Paleoflow along strike and rarely updip. Lateral extent of inclined bedsets <20 m, with erosional breaks. Inclined bedsets locally at low levels in channel bodies. Plants (C), root traces (R), bivalves (R), bone fragments (R).	Detrital grains, ferruginous clasts, and a few mud aggregates in a prominent clay matrix with patches of dolomite cement. Couplets contain mud-rich and detrital-rich lenses.	*Oblique accretion deposits* laid down mainly as suspension drapes on steep accretionary banks or low-level benches. Helicoidal flow not prominent. Mainly lower flow regime. Short migration distances and erosional breaks suggest periodic flood events. Locally vegetated.

Elements	Grain Size	Sedimentary features and fossils	Petrography	Interpretation
Mud- and Quartz-rich Inclined Strata (LA-3)	Alternate discrete bedsets of a) massive to weakly ripple cross-laminated mudstone (>90% of strata) and b) VF to F cemented sandstone 5 to 44 cm thick	Sr, Sh, St in sandstone beds and at channel bases. Inclined heterolithic stratification in bedsets <2.2 m thick, with mean dip of 14.5^{o}, maximum 22^{o}. Paleoflow obliquely updip but locally downdip. Exhumed topography with quartzose sandstone scarps forming curvilinear traces. Rill casts from top to base of inclined beds, scours, erosional surfaces at base of quartzose bedsets, small channels, and symmetrical ripples. Trackways (C), plants (C), root traces (R), bone fragments (R), and U-shaped burrows (R).	Mudstone: elongate, red and grey sand-sized mud aggregates, clay matrix, dolomite rhombs, detrital and ferruginous grains. Sandstone: detrital grains in a hematite and clay matrix with patches of barite, calcite and dolomite cement. Detrital grains finer upsection and finely crystalline dolomite more abundant.	*Lateral and oblique accretion deposits* formed by point-bar migration. Bedload transport of sand-sized quartzose grains and mud aggregates with some suspension deposits. Mainly lower flow regime, with erosive flood events and local ponding. No indication of scroll bars. Paleoflow patterns suggest swept ripples linked to falling flow, with local down-surface flow of flood water; only minor helicoidal flow. Locally vegetated.
Tabular Sandstone (TS)	VF-C sandstone; minor conglomerate with clasts <1 cm in diameter	St, Sh with large antidune form, Sr (ripple-drift prominent), Sm, Gm, Gt with waning-flow bedsets. Units locally >6.5 m thick and hundreds of metres in extent, with stacked erosionally based bedsets. Scours up to 1 m deep are prominent. Root traces (R), charcoal (R), bone fragments (R).	Dolomite-cemented detrital grains with hematite and clay rims. Dolomite also as finely and coarsely crystalline clasts, interlocked patches of coarsely crystalline rhombs, and inequigranular crystals that fill vugs and line ferruginous or mud clasts.	*Short-lived ephemeral flow in poorly confined and/or unconfined settings.* Sheet form of channel body. Upper and lower flow regime with waning-flow events prominent. Erosive events common. Locally vegetated.

Elements	Grain Size	Sedimentary features and fossils	Petrography	Interpretation
Laminated Mudstone (LM)	Claystone to coarse siltstone	Fl, reddish brown, yellow and grey variably graded laminae. Lenses up to 3 m thick between inclined bedsets and channel cutbanks. Loop bedding, microfaults, load casts, scours, soft-sediment deformation, overturned beds. Plants (C), bone fragments and shark coprolites (R to A).	Silt or clay layers commonly grading from silt-sized quartzose and ferruginous grains in a clay matrix to nearly pure clay with hematite. Abrupt and planar to wavy laminar contacts with some erosion evident.	*Channel abandonment fill formed in standing water*. Laminae from low-energy flows and suspension settling. Fresh or possibly with modest salinity levels. Leaves from nearby riparian vegetation.
Disrupted Mudstone (DM)	Claystone to VF sandstone	Fm, Sm, with mud aggregates. Lenses at low levels in channel bodies. Desiccation cracks filled with red mudstone, soft-sediment deformation. Plants (C), root traces (R), charcoal (R), bone fragments (C).	Mud aggregates and mud clasts with clay and hematite rims and silt-sized detrital grains in a matrix of clay and hematite. Apatite derived from bone fragments.	*Channel abandonment fill or low-stage deposits subject to desiccation*. Syn- or post-depositional modification due to exposure and water escape. Minor vegetation.
Massive Mudstone (MM)	Claystone to siltstone with some VF sand, rare discrete sandstone beds	Fm, Sr. Lenses in channel bodies and extensive sheets up to 4 m thick Slickensides, peds with clay coats, clastic dykes, angular mud chips, vertical drab mottles up to 5 mm wide and 20 cm long. Plants (R to absent), charcoal (R), bone fragments (R).	Detrital grains, rare coarse sand-sized mud clasts, and isolated or grouped euhedral dolomite rhombs. Clay and hematite matrix and vugs filled with dolomite crystals.	Thick and extensive *floodplain deposits* and part of *abandonment fills* at low and high levels in channel bodies. Incipient to moderately developed soils (see text for soil types). Deep root traces in channel settings.

2.5 FLUVIAL ELEMENTS

Eight fluvial elements were identified in the Clear Fork Formation (see Fig. 1-3; 1-6 for full site names and abbreviations and Table 2-1 for a summary of each element). Channel-base deposits (element CD) form thin layers and lenses at the base of channel bodies throughout the formation. They are overlain by tabular sandstone (TS) up to 6.5 m thick or one of the three elements with inclined strata (LA-1, 2 or 3), which are up to 4 m thick and vary in the proportion and disposition of quartz- and mud-rich material (Fig. 2-1). Laminated and disrupted mudstones (LM and DM) are present at low levels in many channel bodies, typically as abandonment fills that abut cutbanks. Massive mudstone with minor sandstone (MM) is present as floodplain sheets and in channel fills. Petrographic information is provided for each fluvial element (Table 2-1), and the formation of carbonate and other cements is briefly discussed later for the formation as a whole. The composition of the detrital grains (quartz, K-feldspar, plagioclase, titania minerals, zircon, apatite, and ilmenite) and clays (illite, Fe-rich chlorite, kaolinite, and mixed-layer clay) is relatively consistent throughout the formation.

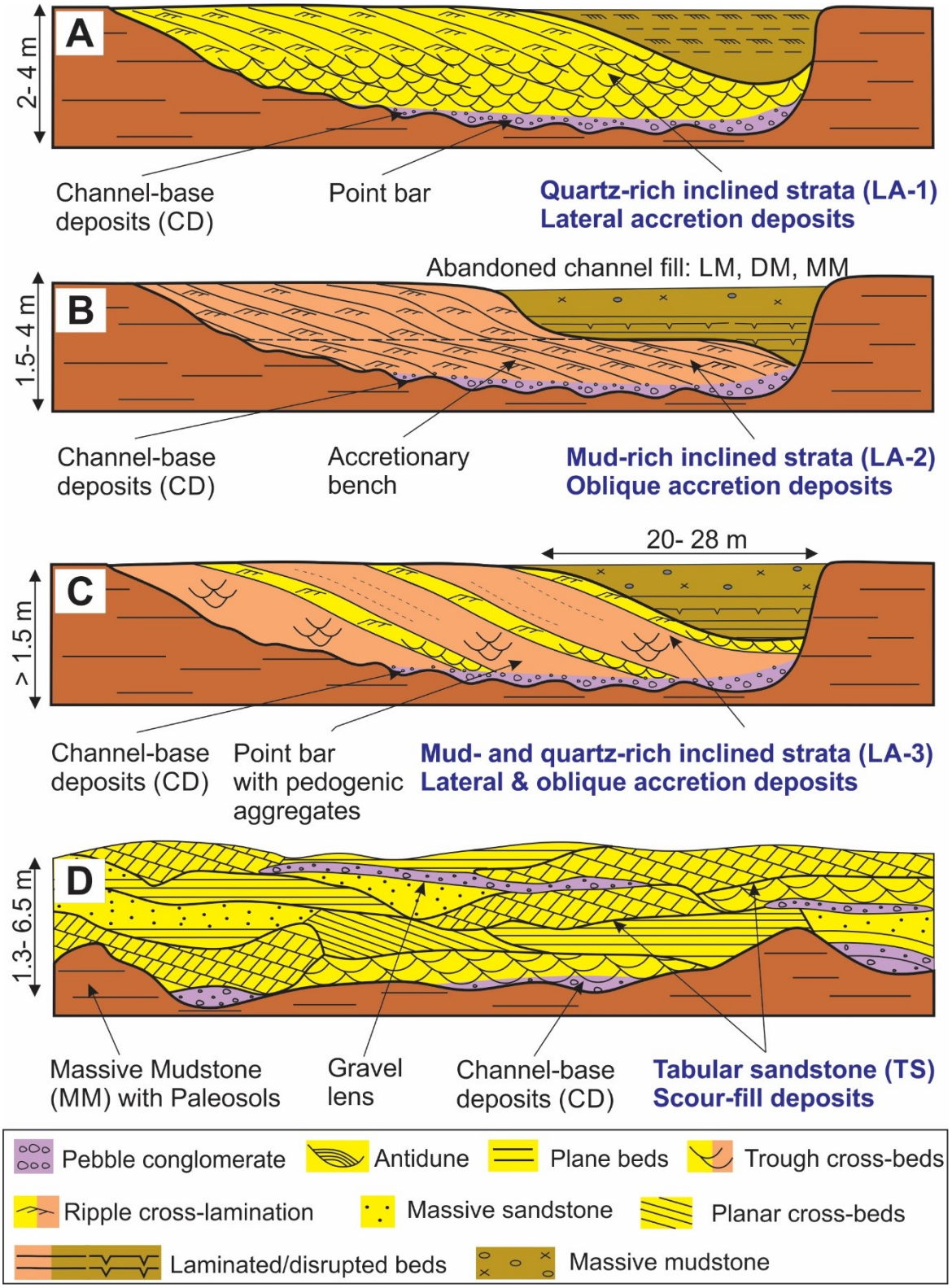

Figure 2-1 Four types of fluvial channel present in the Clear Fork Formation. The schematics illustrate the main architectural elements and sedimentary features present within the three meandering systems: quartz-rich channel with a point bar (A), mud-rich channel with an accretionary bench (B), and mud- and quartz-rich channel with a point bar (C). The fourth type is tabular sandstone (D). Outcrop images of each type are displayed in subsequent figures.

2.5.1 Channel-base Deposits (CD)

Description: Pebble conglomerate with carbonate, siliciclastic, and ferruginous clasts forms massive or thinly bedded units up to 40 cm thick (Fig. 2-2A). Carbonate is also present as crystals, commonly with rhombic form, and cements (sparry and poikilotopic), predominantly calcite and ankerite in the lower unit and dolomite in the middle and upper units, regardless of texture (Fig. 2-2B to C). Thin lenses of ripple cross-laminated and plane-laminated sandstone have flute casts and current lineation. The element rests erosionally on massive mudstone (MM) and forms sheets or lenses with form-concordant layers. One exposure shows three linear mounds draped over eroded mudstone (Fig. 2-2A), oriented near-parallel to the paleoflow and tapering downflow.

Interpretation: The clasts constitute channel-lag deposits derived from local paleosols during or shortly after erosional events of some power, as indicated by plane-laminated sandstones. The linear mounds may lie downflow from obstacles such as mud blocks or upright trees that were not preserved.

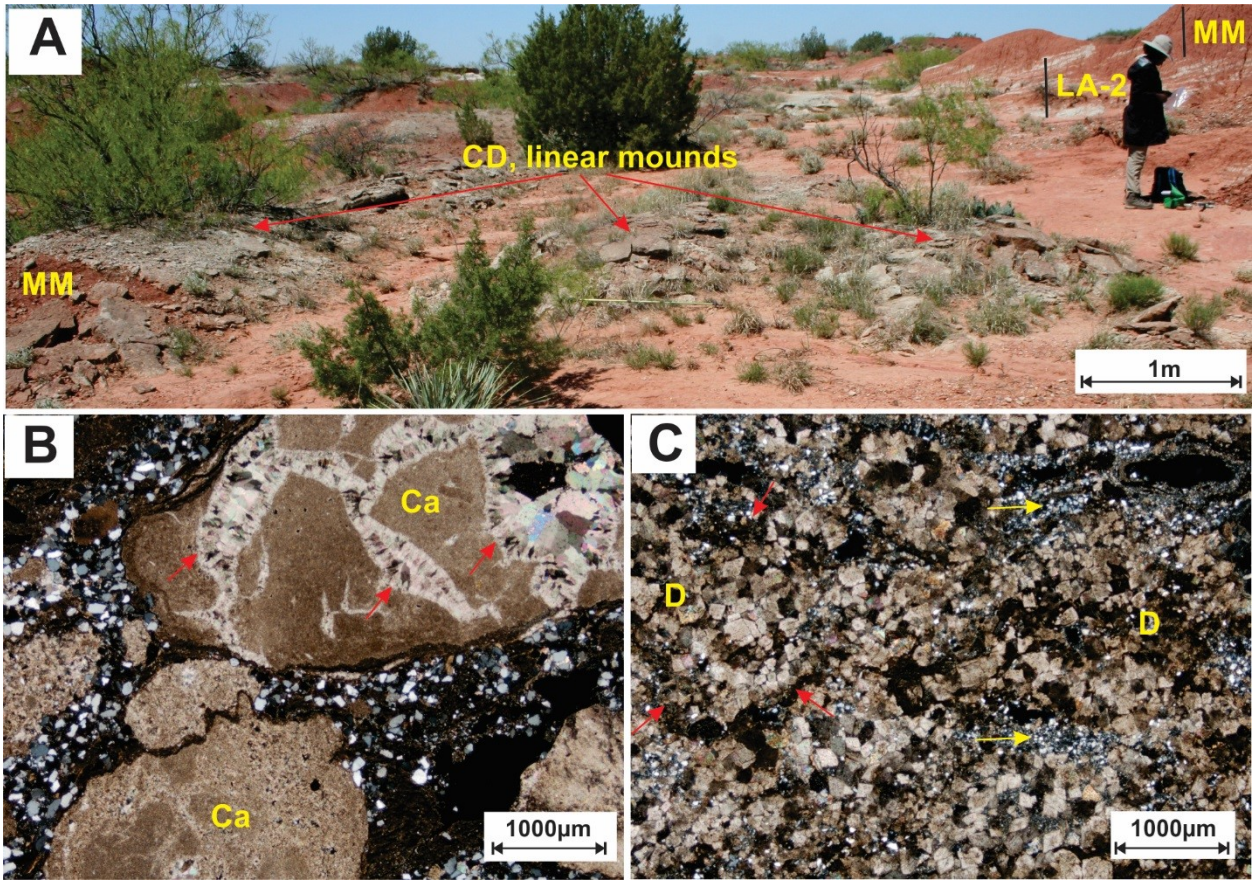

Figure 2-2 Channel-base Deposits (element CD). (A) Three linear conglomerate mounds composed of pedogenic carbonate and mudstone clasts taper downstream (away from the camera) and rest erosionally on massive red mudstone (MM; lower left). The mounds are 2 m wide, 3-9 m long, and up to 0.5 m high. Element CD is overlain by element LA-2 in cliffs to the right. Know Where To Park. (B) Calcitic clasts, finely crystalline and sub-rounded to rounded with hematite and vugs of bladed microspar (red arrows) with silt-sized quartz. Clasts are surrounded by a matrix of clay and angular to sub-rounded detrital quartz and feldspar of very fine sand to silt grade, with micritic cement. XRD indicated the presence of ankerite. Mouth of Brushy Creek. (C) Patches of interlocked euhedral to subhedral dolomite rhombs (red arrows outline patch) with very fine sand- to silt-sized grains of quartz and feldspar with minor heavy minerals and clay matrix (yellow arrows). North Soap-Creek Quadrangle. B-C under cross-polarised light. Dolomite (D), calcite (Ca).

2.5.2 Quartz-rich Inclined Strata (LA-1)

Description: The element is composed of inclined and subsidiary flat-lying layers of very fine- to fine-grained quartz-rich sandstone with <5 % of mudstone. It is present at RT in the lower unit and at MR2 in the upper unit, with RT being coarser.

At RT, four erosionally based storeys consist of flat-lying (storeys 1 and 4) and inclined sandstone beds with a mean dip of 17^{o} (storeys 2 and 3; Fig. 2-3A to C). The sandstones are composed of detrital grains and elongate, sand-sized clay aggregates cemented by barite, calcite, and ankerite (Fig. 2-3G). Storey 1 consists of trough cross-bedded and ripple cross-laminated sandstone, with a prominent scour that contains plane-stratified beds with hematite-stained root traces (Fig. 2-3B). Storey 2 comprises 4 m of inclined cosets of trough and rare planar cross-strata capped by ripple cross-laminated beds and thin plane-stratified units (Fig. 2-3B). The inclined cosets pinch out within a few tens of metres along strike. Storey 3 comprises 1.5 m of inclined beds of ripple cross-laminated sandstone (Fig. 2-3C) with drab root traces up to 0.5 cm wide and 50 cm in vertical extent (Fig. 2-3D) and trackways of Diplichnites gouldi commonly oriented along strike. Storey 4 comprises 2.5 m of ripple cross-laminated sandstone with Walchia impressions (Fig. 2-3C, 2-3E). Paleoflow is north to northwest for the four storeys (Fig. 2-3A), and ridge-and-furrow forms -in storeys 2 and 3 are oriented near-parallel to strike or obliquely up the inclined surfaces.

At MR2, inclined strata extend for tens to hundreds of metres along strike, with a minimum vertical extent of 2 m below eroded tops and a mean dip of 13^{o} (maximum 15^{o}). At the channel base, the inclined strata downlap onto ripple cross-laminated beds and mounds of massive siltstone (CD). Trough and planar cross-sets and cosets exhibit paleoflow directly or obliquely up the inclined surfaces and are overlain by ripple cross-laminated layers with similar paleoflow

(Fig. 2-3F). Cemented lenses of ripple cross-laminated sandstone mark erosion surfaces parallel to or steeper than the underlying inclined strata. Gypsum nodules up to 10 cm in diameter are present. Unlike RT, the inclined sandstones are cemented by poikilotopic gypsum and celestine, and grains typically appear to float in cements (Fig. 2-3H).

Interpretation: The inclined sandstone strata are interpreted as lateral-accretion deposits formed by bedload deposition and point-bar migration (Fig. 2-1A), with repeated superimposition of channels with varied orientation. At MR2, cross-beds formed by 2D and 3D dunes migrated up the inclined surfaces, implying a component of helicoidal flow. At RT, 2D and 3D dunes are prominent in the lateral-accretion sets, with episodes of high flow strength represented by plane beds; fining-upward cosets indicate waning-flow events. The steep dips of the inclined surfaces may in part reflect a relatively low width:depth channel (Thomas et al. 1987). The prominence of Walchia and of roots at numerous levels suggests that the point bars were well vegetated at times, and Diplichnites indicates the presence of arthropods. The mud aggregates at RT were derived from mud banks or reworked floodplain paleosols and, although flattened during burial, they retained their identity due to protection by framework grains (Rust and Nanson 1989).

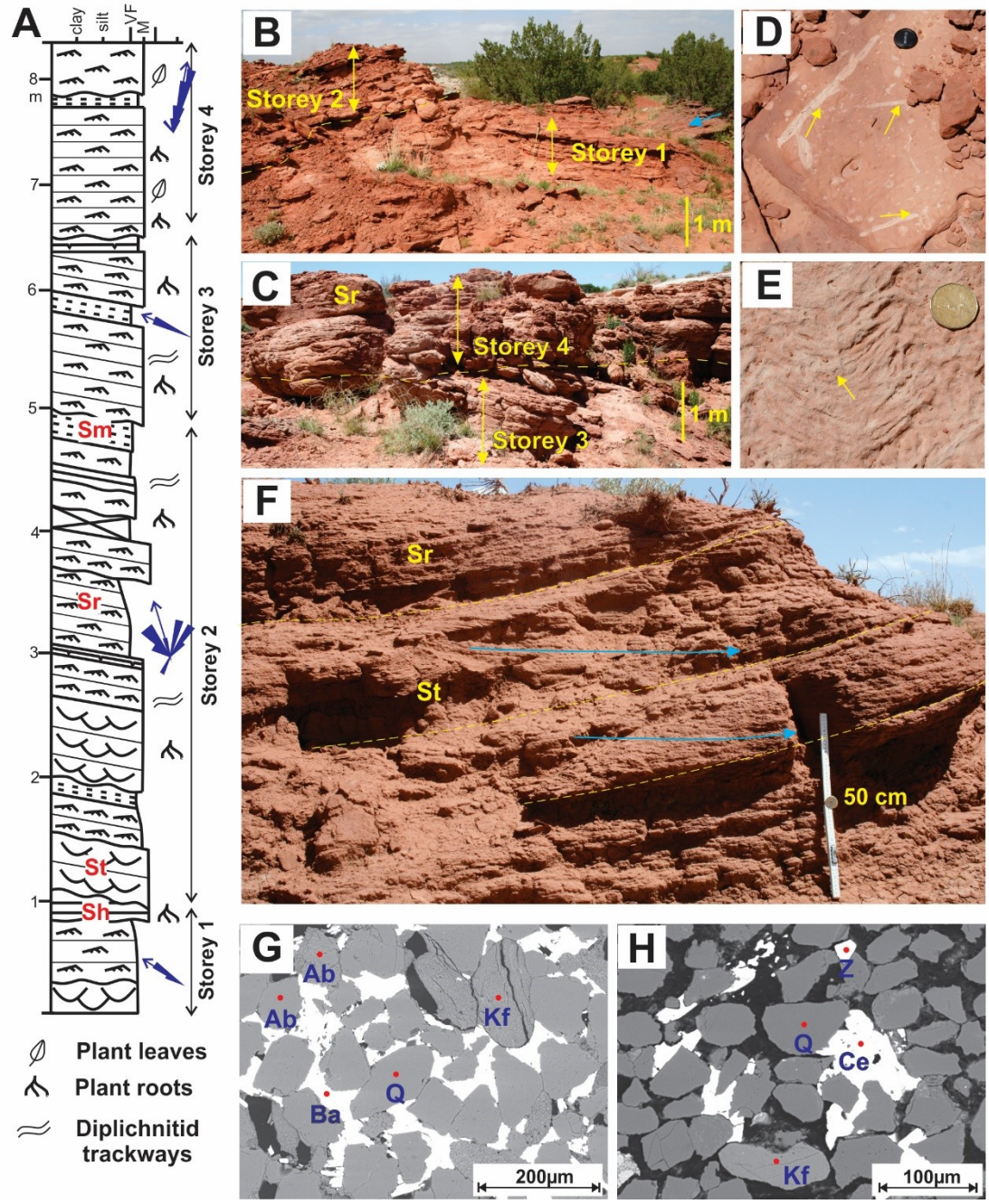

Figure 2-3 Quartz-rich inclined strata (element LA-1). A-E and G from Red Tank; F and H from Montgomery Ranch 2. (A) Composite log showing the main sedimentary features within storeys 1, 2, 3 and 4. The rose diagram presents the average paleoflow direction of each storey measured from 2D and 3D ripple crests; storey 1- 303° (3 readings), storey 2- 347° (13 readings), storey 3- 299° (1 reading) and storey 4- 012° (16 readings). (B) Flat-lying beds of storey 1 containing a broad scour (blue arrow) >1 m wide and inclined beds of storey 2 with trough cross-sets up to 45 cm thick dipping to the left. (C) Inclined beds of storey 3 capped by the flat-lying storey 4 composed of ripple cross-laminated sandstone (Sr). (D) Plane bed with redoximorphic haloes (yellow arrows) around root positions within storey 2. (E) Walchia imprint on ripple cross-laminated surface. Arrow points to leaf midrib. (F) Trough cross-sets (St) up to 40 cm thick with migration directions (blue arrows) up the dip of inclined surfaces (dashed yellow lines). The cross-sets are overlain by ripple cross-laminated sandstone (Sr). (G) Backscatter image showing grains of quartz, altered K-feldspar and albite cemented by pore-filling barite. (H) Backscatter image showung quartz, zircon and K-feldspar partially cemented by celestite, with grain boundaries partially etched. Quartz (Q), altered K-feldspar (Kf), albite (Ab), zircon (Z), barite (Ba), celestite (Ce). Lens cap and coin in E-G are 55 mm and 30 mm in diameter, respectively.

2.5.3 Mud-rich Inclined Strata (LA-2)

Description: Element LA-2 comprises mud-rich inclined beds, with 12-15° dips and paleoflow oriented near-parallel to their strike, that terminate downdip against coarse-grained strata (CD), as observed in cliffs at KWTP, MB, and CR. Inclined bedsets comprise alternate red and grey beds of massive to weakly ripple cross-laminated mudstone to very fine-grained sandstone, typically <50 cm thick (Fig. 2-4A). Most beds are siltstones composed of detrital grains, minor ferruginous clasts, and some sand-sized mud aggregates in a clay matrix with patches of dolomite cement. Excavated beds reveal no apparent difference in grain size between the red and grey layers, but hematite-rich laminae and lenses are prominent in the red layers (Fig. 2-4D) whereas couplets of mud and coarser grains are common in grey samples (Fig. 2-4E).

At KWTP, four storeys with inclined strata are superimposed (Fig. 2-4A). Storey 1 comprises inclined sets with a vertical extent of up to 4 m, traceable in the dip direction for up to 20 m (Fig. 2-4B). The storey cuts steeply into a thick sheet of massive mudstone. The grey and red inclined beds fade out up-dip into massive to weakly laminated red mudstone (MM) that shows faint inclined surfaces in the lower parts. In places, inclined grey beds terminate up-dip at a similar elevation, generating a sub-planar sheet up to 140 cm thick with a diffuse upper boundary (arrow in Fig. 2-4B). Inclined beds in the overlying three storeys have a maximum vertical extent of 3.5 m (Fig. 2-4A) and terminate downdip against thin CD layers. Isolated planar cross-sets in Storey 3 have foresets oriented up the inclined surfaces. Storey 3 shows a systematic dip of inclined sets (Fig. 2-4A), but the sets terminate in the dip direction against a series of concave-upward erosion surfaces overlain by element MM (Fig. 2-4C). Mean paleoflow was westward, with individual storeys oriented west, north and south. At Mixing Bowl, inclined grey and red strata have eroded tops and contain solitary planar cross-sets that exhibit paleoflow directly or obliquely up the

inclined surfaces. Permineralized plant leaves are well-preserved close to the toes of the inclined beds, and sub-vertical root traces are present throughout the inclined beds. Indeterminate bivalves and bone fragments are present.

Interpretation: The inclined strata are interpreted as oblique-accretion deposits (Fig. 2-1B) where mud and very fine sand draped a steep inner accretionary bank (Bluck 1971; Jackson 1981; Brooks 2003a; Page et al. 2003). With a predominance of silt and clay and no grains coarser than very fine sand, the inclined layers were deposited mainly as suspended load during waning flow and from stagnant water, with ripple cross-lamination indicating some bedload movement. Couplets of varied grain size suggest short flow episodes. The comparable grain size of red and grey beds suggests similar flow conditions; silt layers in the grey beds (Fig. 2-4E) may have enhanced water retention and reduction during shallow burial. Planar cross-sets formed by 2D dunes that migrated up inclined surfaces indicate local helicoidal flow, in contrast to ripple migration along strike in the inclined sets. The predominance of ripple cross-lamination suggests modest flow power, although dunes are typically not developed in such fine-grained sediment.

The systematic migration of inclined beds in Storey 1 at KWTP suggests that the channel migrated across a broad tract cut into floodplain deposits (MM in Fig. 2-4C). However, the overlying storeys and those at Mixing Bowl are relatively narrow with short migration distances and prominent cutbanks, suggesting that subsequent channels reworked the underlying channel deposits. These features are characteristic of avulsive settings promoted by recurring floods of high magnitude and/or rapid alluviation in the channels (Knighton and Nanson 1993; Slingerland and Smith 2004). As indicated by the basal storey cut, the channels were probably confined within a narrow valley where floods promoted avulsion. The architecture of Storey 3 suggests episodic channel migration with flood-generated reactivation surfaces. The strongly varied

paleoflow for the storeys suggests that the channels were sinuous.

The up-dip termination of inclined grey strata at a similar level low in Storey 1 suggests the presence of an accretionary bench that advanced during seasonal flows well below bankfull level (Taylor and Woodyer 1978; Woodyer et al. 1979; Gibling et al. 1998). Oblique accretion would have involved plastering of fine sediment onto the bench slipface and the accretionary bank above during flow recession. The steep dips of the inclined beds probably reflect the steep inner bank, the cohesive nature of the fine deposits, and the low channel width: depth ratio (de Mowbray 1980; Van Der Meulen 1982; Edwards et al. 1983; Visser 1986; Thomas et al. 1987). Local roots and leaves indicate that the accretion deposits were periodically vegetated, perhaps assisting bank stabilization.

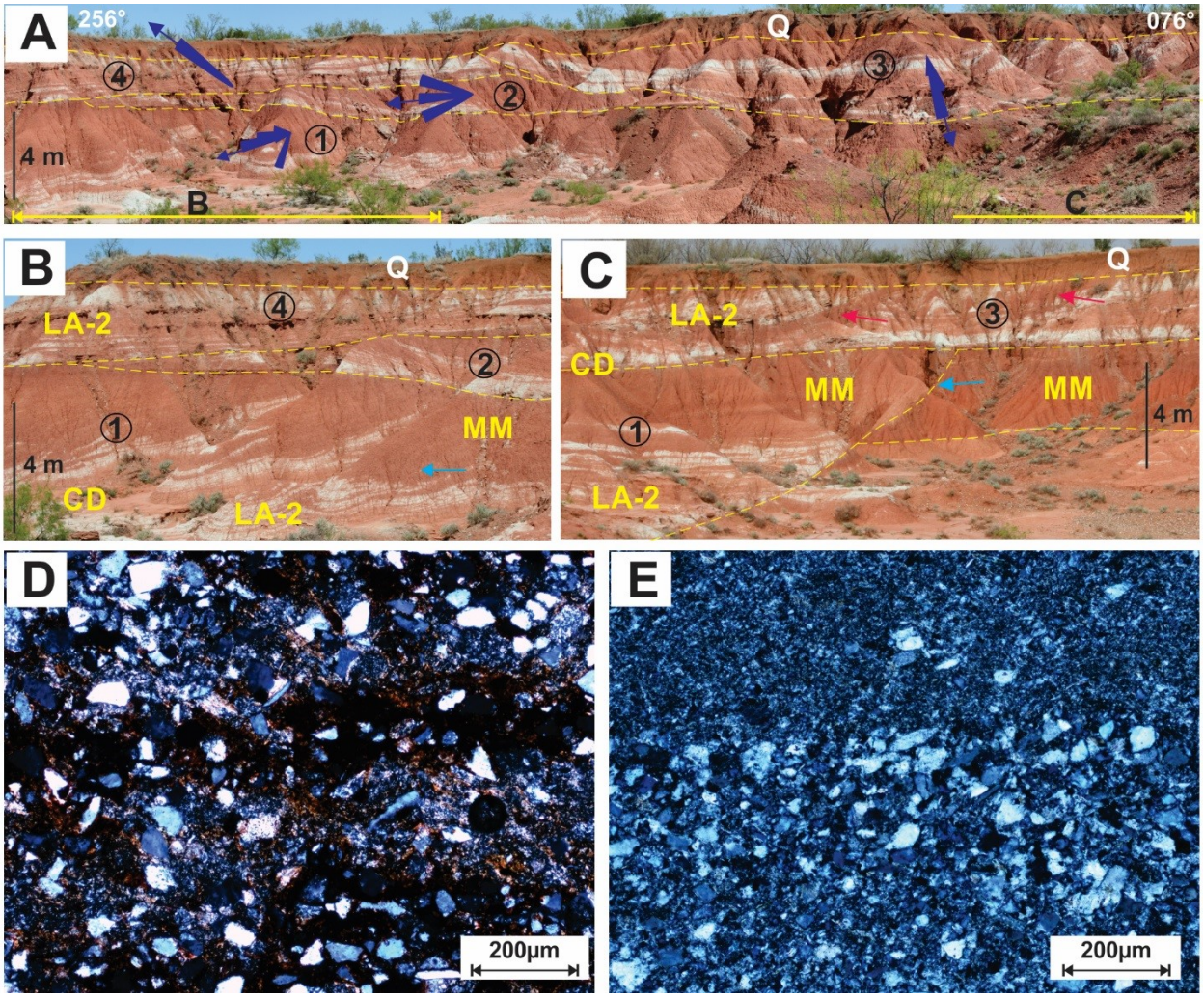

Figure 2-4 Mud-rich Inclined Strata (element LA-2), Know Where To Park. (A) Four superimposed, erosionally based storeys (numbers within circles) comprised mainly inclined strata of element LA-2 that dip in varied directions overlain by Quaternary (Q) beds. Erosional surfaces are indicated by yellow dashed lines. Rose diagrams show the mean paleoflow direction for each storey [storey 1 (252°; 10 readings), 2 (263°; 3 readings), 3 (309°; 1 reading), and 4 (164°; 7 readings)]. (B) Inclined strata of storey 1 pass upward into massive mudstone (MM) and down-lap onto channel-base deposits of element CD. The blue arrow indicates level of upward termination of dipping grey and red layers in one area, but grey layers extend to higher levels elsewhere. Inclined beds of storey 2 have a maximum thickness of 1.5 m with an 18° dip to the north. The inclined beds are truncated by storey 4, up to 4 m thick, with a dip to the west at 10°. (C) Exposure located 40 m east of (A). In storey 1, massive mudstone grades up from mud-rich inclined strata (LA-2) at left. Blue arrow indicates an erosional contact with 4 m of vertical extent, where the storey cuts into an extensive floodplain sheet of massive mudstone. In storey 3, inclined beds terminate downdip against concave-upward surfaces (red arrows) overlain by massive mudstone. (D) Red inclined bed composed of sub-angular to sub-rounded, very fine-grained sand to silt grains of quartz, feldspar and titania minerals, floating in clay and hematite matrix, with variable hematite content in layers. (E) Grey inclined bed composed of a mud-rich layer with a few, scattered silt-sized grains (top), and silt-rich layer. D-E under Cross-polarised light.

2.5.4 Mud- and Quartz-rich Inclined Strata (LA-3)

Description: Element LA-3 differs from LA-1 and LA-2 in the presence of discrete quartz-rich and mud-rich inclined beds with an average dip of 14.5° that fit the definition of inclined heterolithic stratification (Thomas et al. 1987). The inclined strata are exposed in planview across flat ground as low, discontinuous scarps that collectively show large-scale curvature (Fig. 2-5A) and can be traced into cliff exposures. Examples are found at BC, MR1, MR3, and in the superb planform exposures at NSCQ (Fig. 2-5A; Edwards et al. 1983).

The inclined bedsets comprise poorly consolidated, massive to weakly ripple cross-laminated mudstone (>90% of strata), erosionally overlain by thin layers of very fine- to fine-grained, cemented sandstone (Figs. 2-5B to E). The cemented beds partially protect the mudstone from erosion, accounting for the preservation of planforms (Fig. 2-5B). The mudstone contains poorly-developed slickensides, abundant redoximorphic spots, and root traces; where stratification is visible, dips accord with adjacent sandstone beds. At MR1, trough cross-beds in mudstone exhibit paleoflow directly or obliquely up the inclined surfaces (Fig. 2-6A). Based on petrographic analysis, the mudstone beds mainly comprise flattened sand-sized mud aggregates with scattered euhedral dolomite rhombs, detrital, and ferruginous grains (Fig. 2-6D). Subordinate layers of quartz silt have a matrix of clay and hematite with few mud aggregates, as well as clay-rich layers with few or no distinct mud aggregates.

The sandstone beds are ripple cross-laminated with 2D and rarely 3D sets visible as ridge-and-furrow structures with rare exhumed ripple forms. They are composed of detrital grains that appear in places to float in a clay and hematite matrix with patches of barite, calcite, and dolomite cement (Fig. 2-6C), with some layers of finely crystalline dolomite with few, silt-sized detrital grains. Within the upper 50 cm of the scarps, ripple cross-laminated beds thicken upward

with progressively less intervening mudstone to a well-developed sandstone bed. In a few ridges at Mouth of Brushy Creek, scoured bases are overlain by convex-upward sets of plane-laminated sandstone that grade upward into ripple-drift cross-lamination (Fig. 2-5D).

At MR1, linear sandstone mounds interpreted as dunes with small- and large-scale cross-lamination are present close to the base of an inclined bedset. These mounds have a maximum height of 20 cm, with crest-to-crest spacing of 3-5 m and steeper margins facing directly or obliquely up the inclined bed. They pass up the surfaces into straight- or sinuously-crested ridge-and-furrow structures.

At some sites, the sandstone beds flatten out updip (Fig. 2-5C), but no convex-up forms were observed. Scarp spacing ranges from <1m to 12 m depending on varying mudstone thickness between sandstones of relatively constant thickness. Between some inclined beds and parallel to the strike are a few channel forms that are up to 60 m long, 10 m wide, and have up to 50 cm of relief, as well as small elliptical scours. Bed surfaces show symmetrical ripples and rill casts that are parallel to dip, typically high but locally low on the surfaces (Fig. 2-5E). Leaves are present close to the toes of some inclined beds, as were the remains of a frog at NSCQ (Anderson et al. 2008). Abundant root traces are mainly up to 5 mm wide but locally larger (Fig. 2-6B), some low on dipping surfaces. U-shaped burrows are common, as well as Diplichnites gouldi trackways oriented parallel to oblique to strike of the beds.

From the curvature of the exhumed inclined heterolithic strata at NSCQ, channel dimensions and paleodischarge were estimated using empirical relationships. The exhumed inclined strata have an estimated radius of curvature of 140 m, which corresponds to a bankfull width and depth of 57 m and 2.2 m, respectively. Calculated as the product of bankfull cross-sectional area and

hypothetical flow velocities of 0.50, 0.75 and 1.00 ms^{-1}, bankfull discharge estimates range from 55 to 149 m^3s^{-1}. At the Mouth of Brushy Creek and Montgomery Ranch 3 sites, channels have a measured width of 28 m and 20 m (Table 2-2), corresponding to a width-to-depth ratio of 11:1 and 13:1, respectively.

Interpretation: The inclined heterolithic strata are interpreted as lateral-accretion deposits formed during migration of a point bar, with cross-strata representing 2D and 3D ripples and dunes (Fig. 2-1C). The ridges exposed across flat ground represent near-exhumed point bars and range from a few straight ridges at MR1 to numerous curved ridges that define meander patterns over hundreds of square metres at NSCQ. Based on the increase in bend radius and a change in the strike of the scarps in sector A (Fig. 2-5A), the point bars migrated mostly by expansion with some rotation (Willis 1989; Ghinassi et al. 2014; Ielpi and Ghinassi 2014). Modest changes in dip angle between successive scarps probably reflect high-discharge events and point-bar erosion, as shown by relief on sandstone bases (Fig. 2-5D). The absence of convex-up forms at scarp tops, indicative of an original ridge-and-swale topography (Gibling and Rust 1993; Ielpi and Ghinassi 2014), may reflect recent erosion (Smith 1987), but convex-up forms are absent where inclined strata are seen in cliff sections, and the point bars appear to have lacked scroll bars.

Based on the presence of sand-sized mud aggregates and the identification of a trough cross-bed within mudstone, much of the mud is inferred to have been transported as bedload after being reworked from banks and local paleosols. The apparent rarity of aggregates in some mudstones may reflect one or a combination of (a) damage during thin-section preparation, (b) destruction of aggregates during shallow burial due to lack of a supporting framework (Rust and Nanson 1989), and (c) deposition of mud from suspension, as with element LA-2, implying a component

of oblique accretion. In contrast, the sandstones were extrabasinally sourced or derived in part from extrabasinal material stored on the alluvial plain, with discrete layers laid down by near-bankfull floods based on their relatively high elevation. The flows mainly generated ripples in the lower regime, and higher energy events with a large suspended load are indicated by upper-regime plane beds that grade up into ripple-drift cross-lamination, with local scours and small channels (Kasvi et al. 2013; Lotsari et al. 2014). Symmetrical ripples indicate periodic ponding to high levels within the channel, with wind-induced oscillatory flow. The presence of low-level accretionary benches is suggested by upward flattening of some beds, and rill casts indicate that most surfaces were exposed almost to the base during waning flow. Although vegetation-induced sedimentary structures (VISS: Rygel et al. 2004) were not evident, the point bars were probably vegetated, based on root traces and leaves, and also supported arthropods and amphibians.

Table 2-2 Channel morphology and flow characteristics of the North Soap-Creek Quadrangle channel. Calculated values (Cal) with a 10% error range.

Equation		**Formula**	**Value**		
			-10%	Cal	+10%
Radius of an arc or segment, R_c (m) *W: length of the chord defining the base of the arc* *H: height measured at the midpoint of the arc's base*		$\mathbf{R_c = \frac{H}{2} + \frac{W^2}{8H}}$	126	140	154
Bankfull width, W_b (m) *R_c: radius of an arc or radius of curvature*		$\mathbf{W_b = 0.71\ R_c^{0.89}}$ *(Williams 1986)*	53	57	63
Bankfull depth, D_b (m) *R_c: radius of an arc or radius of curvature*		$\mathbf{D_b = 0.085\ R_c^{0.66}}$ *(Williams 1986)*	2.07	2.22	2.36
Bankfull cross-sectional area, A_b (m^2)		$A_b = W_b * D_b$	110	127	149
Discharge, Q (m^3/s)	*V:0.50 m/s*		55.0	63.5	74.5
V: velocity of water	*V: 0.75 m/s*	$Q = A_b * V$	82.5	95.3	111.8
discharge	*V: 1.00 m/s*		110	127	149

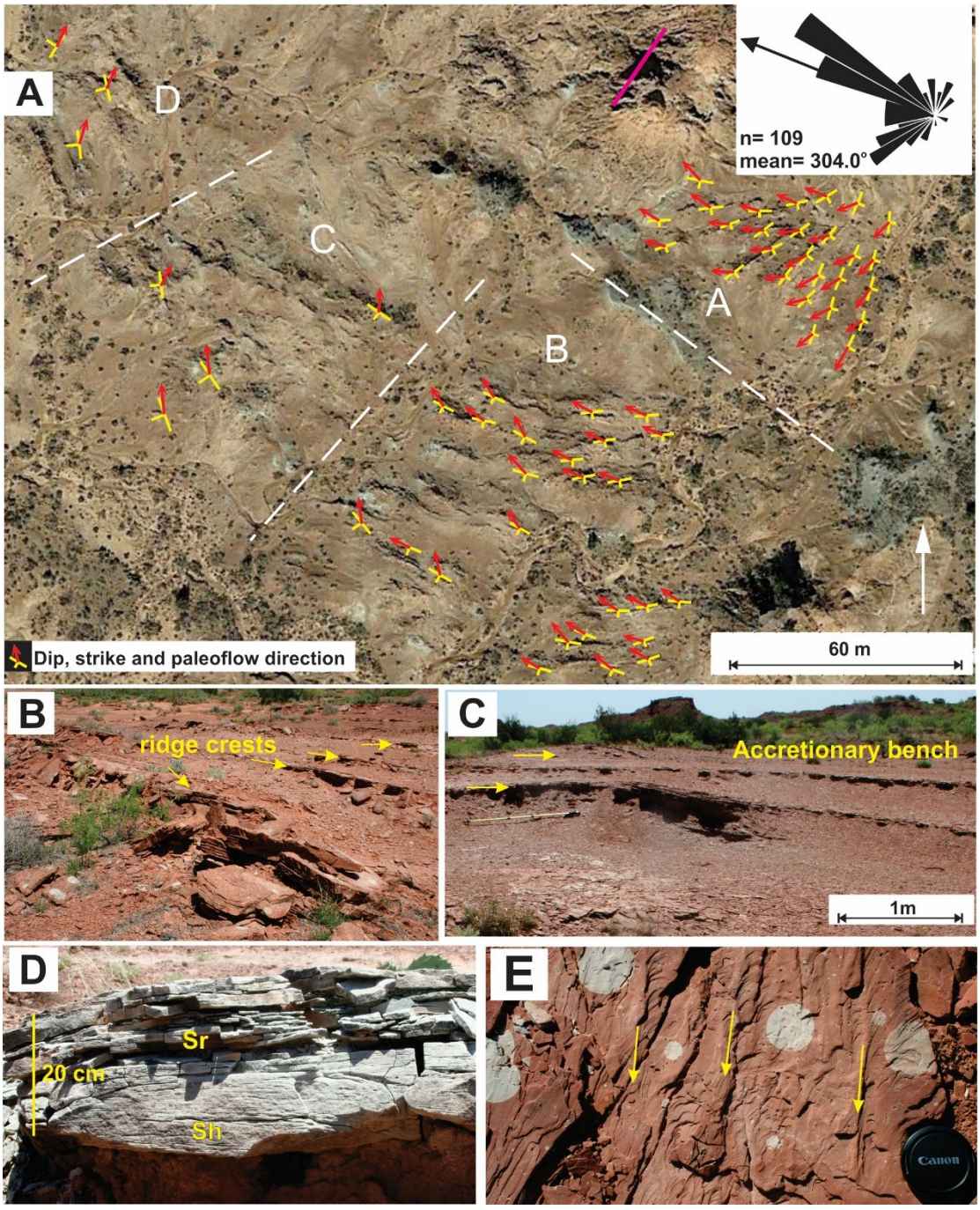

Figure 2-5 Mud- and quartz-rich inclined strata (element LA-3). A to C and E at North Soap-Creek Quadrangle. D at Mouth of Brushy Creek. (A) Planform exposure with resistant, discontinuous sandstone scarps from inclined beds, with large-scale curvature visible on Google Earth. Yellow and red lines represent scarp strike, dip and paleoflow measured from ridge-and-furrow structures on scarp surfaces. Note that, in virtually all cases, the paleoflow is oriented obliquely up the inclined surfaces. Rose diagram represents paleoflow for all inclined surfaces. Scarps defining the large-scale curvature are subdivided into quadrants A-D (see text). Pink bar notes the location of Figure 2-8A. (B) Oblique view of ridges exposed on flat ground, showing erosion of tops but near-exhumed condition. Yellow arrows highlight resistant ripple cross-laminated sandstone beds, which are separated by poorly exposed mudstone. (C) Scarps gently inclined to right, with cemented sandstone beds flattening out upwards to form a bench-like structure. (D) Sandstone scarp dipping away from the observer. The sandstone rests erosionally on red massive to weakly stratified mudstone with 10 cm of basal relief. Plane beds with convex-up form (Sh) pass upward into ripple-drift cross-lamination (Sr) with sets up to 4 cm thick. (E) Rill casts 2-3 cm wide on an inclined bed of ripple cross-laminated sandstone. Arrow denotes direction of downward drainage on the inclined surface.

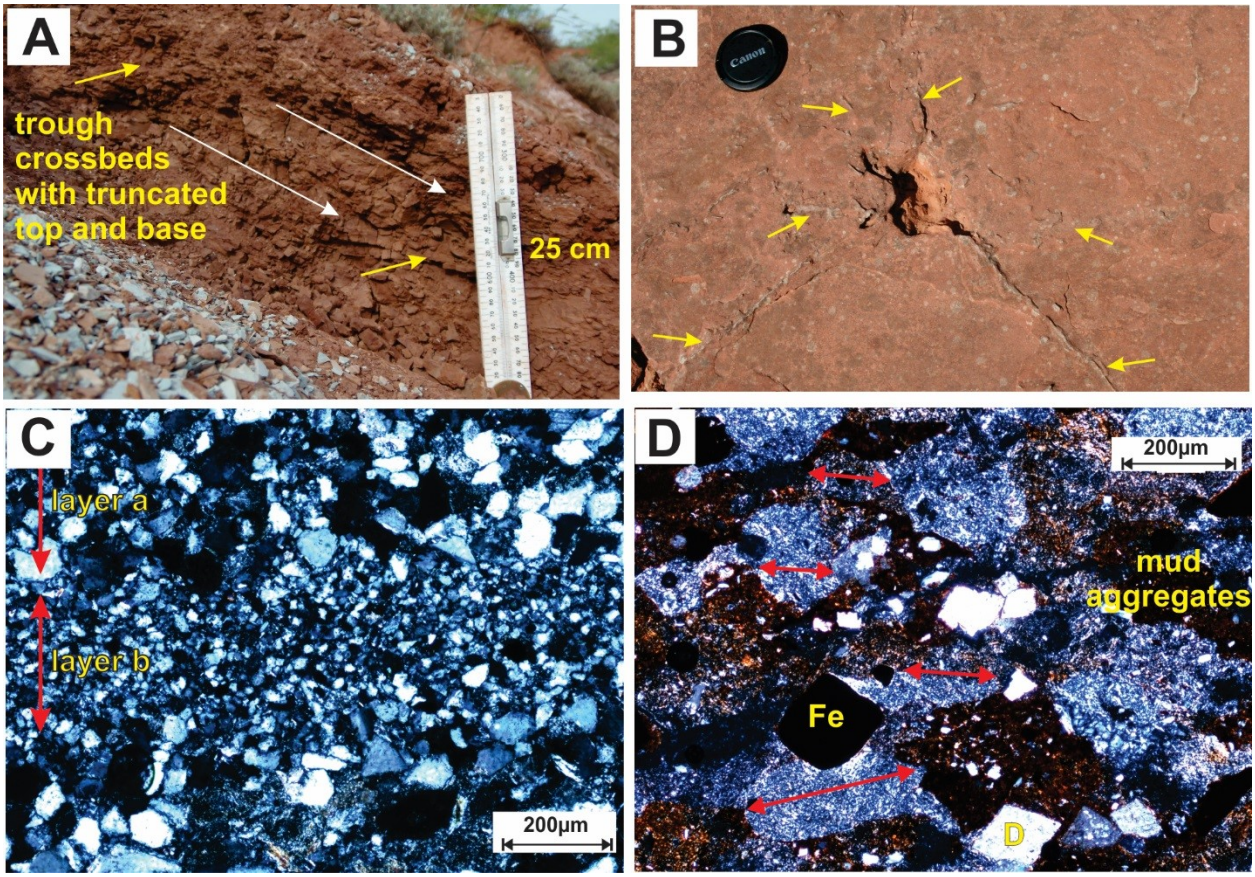

Figure 2-6 Sedimentary and mineralogical features of the mud- and quartz-rich inclined strata (element LA-3). A at Montgomery Ranch 1, B and D at North Soap-Creek Quadrangle, C from Mouth of Brushy Creek. (A) Isolated trough cross-bed 26 cm thick in mudstone. Yellow arrows indicate the base and the truncated top of the cross-set and the white arrows show foreset dips. The mudstone underlies a resistant sandstone that dips to the left of the image, and the cross-set migrated directly or obliquely up-dip. (B) Radiating plant roots up to 1 cm in diameter (arrows) with central cavity 6 cm wide that probably marks the position of a standing tree on an inclined bed. Lens cap: 55 mm in diameter. (C) Cross-laminated sandstone beds with sub-angular to sub-rounded quartz, feldspars, and some heavy minerals, with detrital grains that locally "float" in clay matrix. Laminae are up to 1 mm thick and mainly of coarser grains (layer a) with lenses < 0.2 mm thick of sub-angular silt (layer b). The b/a boundary is abrupt in this instance but is commonly gradational. (D) Sand-sized clay aggregates with euhedral dolomite crystals, ferruginous grains, and silt-sized quartz, feldspar and heavy minerals. The quartz grains are considerably smaller than the mud aggregates, which appear flattened sub-parallel to bedding (apparent long axes shown with red arrows). Dolomite (D), ferruginous clasts (Fe). C-D under cross-polarized light.

2.5.5 Tabular Sandstone (TS)

Description: Element TS consists of flat-lying sheets of fine- to coarse-grained quartz-rich sandstone with <5 % of mudstone, variably cut across LA and MM elements and extending for at least tens to hundreds of metres. The occurrences are widely separated and, although their full extent was not established, they appear to be separate channel bodies.

At NSCQ (Fig. 2-7A), the tabular sandstone is at least 1.3 m thick above a basal lens of carbonate-pebble conglomerate (CD). Scours up to 30 cm deep contain ripple-drift cross-laminated sandstone and are cut by pebble-conglomerate lenses with plane-laminated and ripple cross-laminated sandstone. At MB (Fig. 2-7B), the sandstone is at least 3.4 m thick with basal units of trough cross-bedded gravel up to 30 cm thick. Scours up to 1 m deep contain planar and trough cross-bedded sandstone and plane beds with convex-upward forms. Within the upper metre, scours are shallower and contain stacked units of plane beds, planar and trough cross-beds, and ripple-drift cross-lamination. At CCP, the 6.5 m thick tabular sandstone comprises five units that fine upward from pebble conglomerate to very fine-grained sandstone, with an antidunal bedform or trough cross-beds passing up into plane-beds, climbing and non-climbing ripple cross-lamination (Simon et al. 2016). The tabular sandstone is composed of dolomite-cemented detrital grains and few mud aggregates with hematite and clay matrix (Fig. 2-7C). Dolomite is abundant in the conglomerates as clasts, patches, vug-fills, and cements (Fig. 2-7D).

Interpretation: The sheet-like geometry and nature of the sandstone units is consistent with a broad ephemeral channel that transected floodplain and channel deposits (Fig. 2-1D). The fining upward cycles and scour-and-fill units represent repeated high-energy, short-lived floods that laid down sand and gravel dunes, plane beds and antidunes, followed by waning-flow deposits of non-climbing and climbing ripples. The mud aggregates, dolomite and mud clasts were reworked

from channel banks or paleosols, whereas isolated dolomite crystals and cements were probably formed during shallow burial.

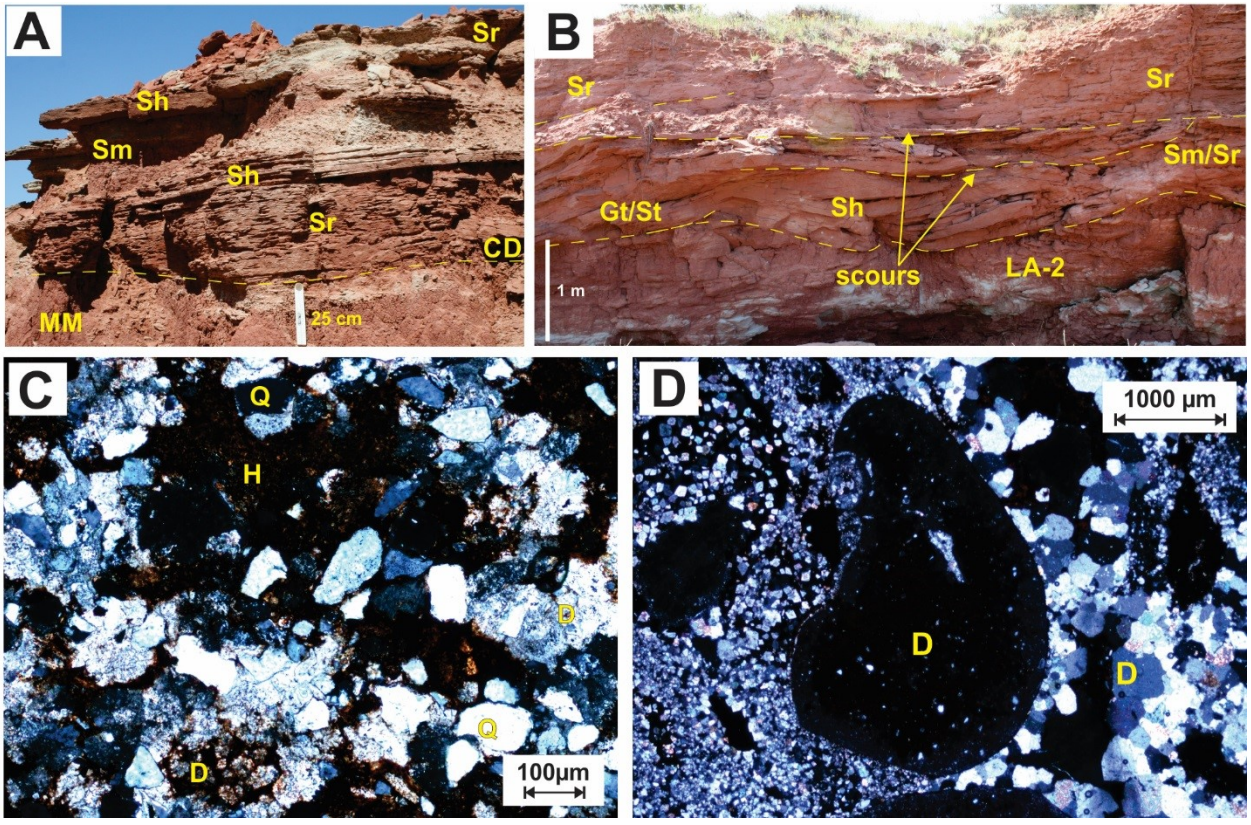

Figure 2-7 Tabular sandstone (element TS). A and C from North Soap-Creek Quadrangle; B and D from Mixing Bowl. (A) Tabular sandstone composed of fine- to medium-grained ripple cross-laminated sandstone (Sr), plane beds (Sh), and massive to weakly cross-laminated sandstone (Sm). The base of the plane beds is commonly lined with patchy lenses of pebble conglomerate. Element CD is present locally at the lowermost contact. (B) Scours in the lowermost strata, filled with plane beds (Sh) and trough cross-bedded conglomerate and sandstone (Gt/St). Scours at higher levels are smaller and filled with climbing- and straight-crested ripples (Sr). (C) Angular to sub-rounded monocrystalline quartz, very fine- to fine sand-sized, with finely crystalline dolomite cement, clay and hematite matrix. (D) Conglomerate lenses with rounded dolomite clasts that contain embedded silt-sized quartz grains, interlocked patches of euhedral to subhedral rhombs, and isolated, inequigranular dolomite rhombs in hematite matrix. Quartz (Q), Dolomite (D), Hematite (H). C-D under cross-polarized light.

2.5.6 Laminated Mudstone (LM)

Description: Element LM consists of laminae and very thin beds of claystone and silty claystone 0.3 to 2 cm thick. At BC, a 2 m unit overlies CD and forms a lens within a channel form, lapping onto the downdip side of inclined strata on one side and onto a steeply dipping channel margin cut into ripple cross-laminated sandstone on the other side. At NSCQ, four laminated intervals up to 3 m thick rest on inclined strata or rest on or are interbedded with massive mudstone (MM, Fig. 2-8A). At MB and CR, laminated units up to 40 cm thick lap onto inclined strata and are interbedded with disrupted and massive mudstone. At CCP, 2 m of laminated beds rests abruptly on CD above a channel base (Simon et al. 2016).

The laminae include ungraded, normally and inversely graded layers of silt or clay, with hematite prominent in red laminae and goethite in yellow laminae. Microfaults, loop bedding, soft-sediment deformation, scours, and overturned beds associated with load casts are also present in the mudstone (Fig. 2-8B to C). At BC, the beds contain desiccation cracks with abundant vertebrate material and coprolites up to 20 cm long, probably from aquatic vertebrates (Fig. 2-8D). Permineralized leaves are commonly exquisitely preserved as three-dimensional goethite petrifactions (Looy 2013; Fig. 2-8E) or as carbon films, with local evidence for herbivory (Schachat et al. 2014).

Interpretation: The laminated intervals are interpreted as low-flow and suspension deposits in standing water low in the channel thalweg, and their common position between laterally accreted beds and a steep channel margin indicates that deposition followed channel abandonment. The absence of roots and desiccation cracks at most sites and the presence of large coprolites at BC indicates that the water was relatively deep and perennial, but interbedded laminated, massive and disrupted mudstone suggests periodic drying up (see interpretations for other elements).

Normal grading is attributed to sediment-charged density underflows and inverse grading to velocity reversals. The absence of evaporative and carbonate minerals suggests that water influx exceeded evapotranspiration, although some degree of enhanced salinity cannot be ruled out. Microfaults and loop-bedding reflect near-surface compaction of laminae with subtle competency differences (Simon et al. 2016).

The preservation of lamination implies a scarcity of bioturbation, with Early Permian freshwater ecosystems mostly underpopulated by infauna at this early stage in colonization (Miller and Labandeira 2002). Elevated salinity, fluctuations in bottom- or pore-water oxygenation and high sedimentation rates may have restricted bioturbation, if infauna were present. Early biomineralization linked to iron-rich waters and rapid burial may explain the exceptional preservation of plants as goethite petrifactions (Looy 2013; Simon et al. 2016).

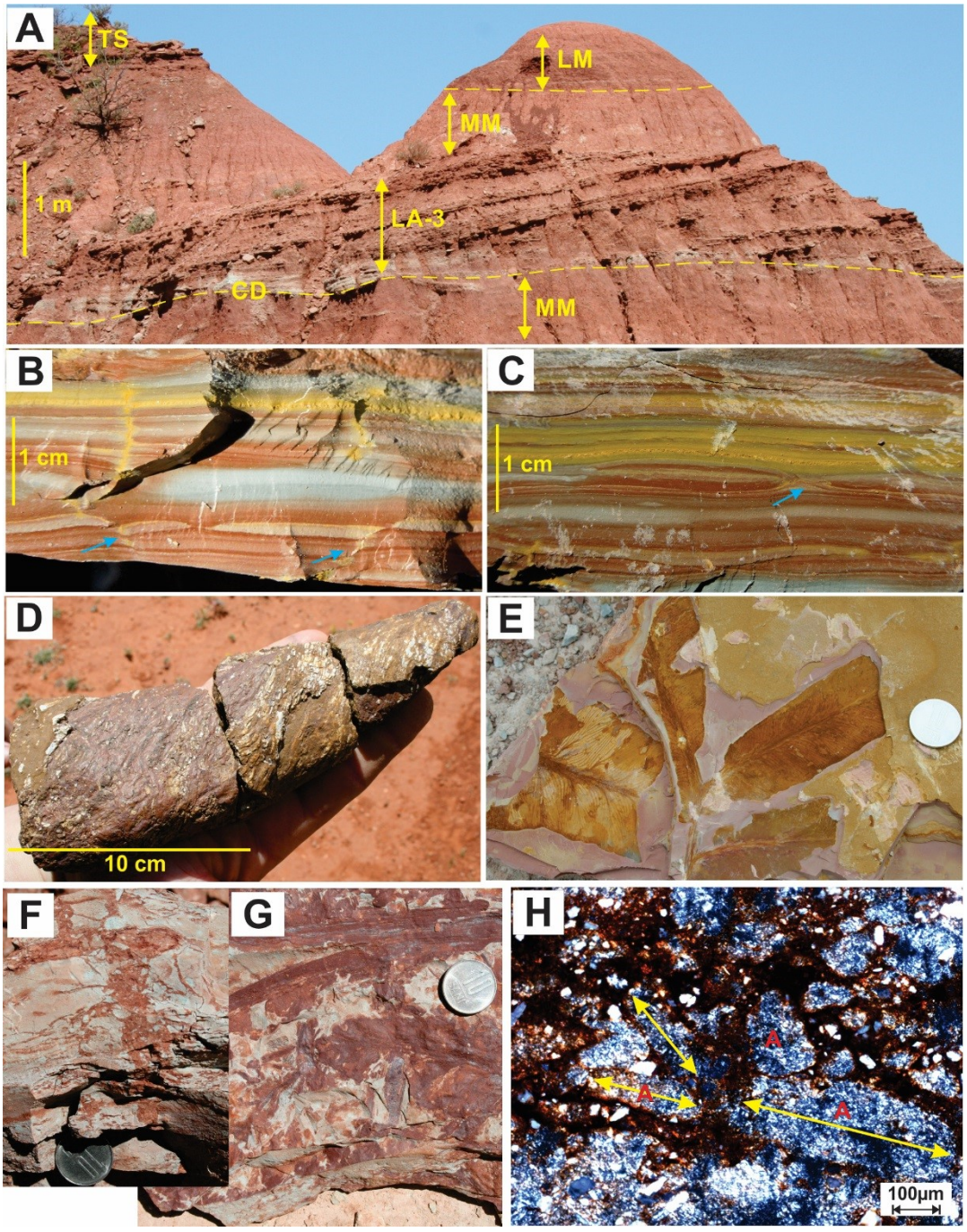

Figure 2-8 Laminated (element LM) and disrupted (element DM) mudstone. A from North Soap-Creek Quadrangle; B, C, and E from Colwell Creek Pond; D from Mouth of Brushy Creek; F to H from Know Where to Park. (A) Laminated beds deposited above massive mudstone (MM), which rests conformably on a channel body with basal coarse deposits (CD) and inclined strata (LA-3). TS denotes overlying tabular sandstone. Location of picture noted in Figure 2-5A. (B) Laminated beds with variably colored laminae. The blue arrows indicate normal microfaults that are lined with goethite (yellow). (C) Loop bedding (blue arrow), with red arrow showing a microfault associated with a loop. (D) Coprolite 20 cm long, weathered from laminated mudstone. (E) Leaves in laminated mudstone. (F) Disrupted bed of grey weakly stratified mudstone with desiccation cracks up to 1 cm wide filled with red sediment slightly coarser than the grey beds. (G) Hematite staining of plant fragments. (H) Disrupted beds composed of grey, sand-sized mud aggregates (yellow arrows show long axis) coated with hematite and detrital grains. The aggregates have average apparent long-axis length of 0.4 mm, maximum 1 mm. Desiccation cracks are filled with sub-angular mudstone clasts containing clay aggregates and detrital grains in a clay and hematite matrix. Coin 22 mm in diameter. H under cross-polarized light. Mud aggregates (A).

2.5.7 Disrupted Mudstone (DM)

Description: Element DM comprises units up to 30 cm thick of disrupted grey to red claystone to very fine-grained sandstone, with silt and clay predominant and finer layers especially disrupted (Fig. 2-8F to G). The element is present at all sites except RT. The units form thin, discontinuous lenses near the base of channel forms, in places between inclined strata and a channel margin, and are locally interbedded with laminated and massive mudstone. Beds are weakly stratified with discontinuous, planar or wavy bedding. The grey layers are <3 cm thick and pinch out rapidly. Element DM is composed of sand-sized mud aggregates (Fig. 2-8H), mud clasts, detrital and apatite grains that appear to float in a clay and hematite matrix. A prominent feature is cracks <2 cm wide and 7 cm deep, filled with red siltstone and very fine-grained sandstone (Fig. 2-8F). Hematite-stained plants are present (Fig. 2-8G), but root traces are rarely observed, although readily obscured by the cracks. At KWTP, charcoal fragments are present.

Interpretation: The element formed in the lower parts of abandoned channels. Like the laminated mudstone, the disrupted mudstone comprises layers of varied grain size with microfaults, and is interpreted to have been laid down in standing water from underflows and suspension. However, the layers are largely grey and are generally coarser, thicker and more discontinuous, suggesting higher energy conditions. Desiccation cracks indicate that the water body dried up, disrupting the sediment. Roots and leaves indicate that the deposits were vegetated, probably in shallow water or during desiccation, contributing to the disruption. Bone material may have been derived from organisms in the channel or reworked from floodplains or paleosols. The mud aggregates and clasts have more uniform colour and composition than those in other elements, as well as clay-hematite rims (Müller et al. 2004), and many probably formed during desiccation. Where interbedded with laminated mudstone, the element may indicate discharge of coarser sediment

followed by rapid drainage, or the presence of water too shallow to prevent vegetation from destroying the lamination. The disrupted fabrics resemble those of some playa-lake deposits (Tunbridge 1984; Smoot and Olsen 1988; Smoot 1991).

2.5.8 Massive Mudstone (MM)

Description: Element MM is composed of reddish brown, massive to weakly stratified silt-clay mixtures. This element comprises the bulk of the formation and is present at all sites but was not examined in detail in this study. Detailed accounts are presented in Tabor and Montañez (2004), DiMichele et al. (2006), Zhu (2015), and Simon et al. (in press).

At most sites, thin units with slickensides, desiccation cracks, and root traces are present low in channel fills, locally resting on inclined strata, and interbedded with laminated and disrupted mudstone. Plants coated with hematite are locally abundant, and charcoal fragments are present at MR3. Thicker units grade up from inclined beds or from laminated mudstone higher in channel fills (Figs. 2-4, 2-8A). These beds are well-consolidated with conchoidal to hackly fracture, mottles, angular mud chips, and discontinuous clay skins. Ripple cross-laminated sandstone lenses are present in the upper parts of some mudstone units below a channel-base erosional surface. Samples from channel fills have similar textures and comprise very fine-grained sand to silt in clay and hematite matrix.

Extensive mud-rich sheets up to 4 m thick are interbedded with and incised by laterally accreted channel assemblages (Fig. 2-4C), and extend for hundreds of metres to kilometres. Four profiles of the massive mudstone were examined in this study (NSCQ, MB, CCP, and KWTP), and contain peds with thin clay coatings, spherical mottles, mud pellets within clastic dikes, vertical tubules, wedge-shaped slicken planes, and scattered carbonate nodules. In a more extensive,

detailed study, Zhu (2015) identified similar features within nine profiles of massive mudstone. Gypsum also occurs as rosettes, veins, and dikes in the middle unit, and as nodules up to 25 cm in diameter and sheets interbedded with silty dolomite in the upper unit (MR and TN; Nelson et al. 2013).

Interpretation: Massive units low in channel fills formed through suspension deposition from stagnant water, with slickensides and desiccation cracks formed during episodes of wetting and drying. The drab vertical mottles are interpreted as root traces, suggesting that vegetation assisted in breaking down stratification. The common interbedding of elements LM, DM and MM or an upward transition to MM suggests that water levels varied and commonly shallowed in abandoned channels, with varied degrees of paleosol development.

The thick, extensive mudstones represent floodplain deposits, and profiles examined in this study suggest the presence of paleo-Entisols and paleo-Vertisols. Zhu (2015) identified six paleosol types based on the classification of Mack et al. (1993). In the lower unit at BC, vertic argillisols, calcisols, calcic vertisols and vertic calcisols are present. In the middle and upper units, calcic vertisols are present at KWTP, and gleyed calcisols, vertisols, and calcisols at MR. The carbonate-bearing paleosols represent Stage II accumulations of Machette (1985). The scarcity of gleyed paleosols suggests that water-logged or reducing environments were uncommon, in contrast to their prominence in mudstones within channel fills. The abundance of vertic features suggests seasonal conditions.

Ripple cross-laminated sandstone lenses in some mudstones are interpreted as crevasse-splay deposits (Edwards et al. 1983). Their occurrence in places below channel bodies suggests that splays advanced across the floodplain shortly before a channel arrived at the site.

2.6 OBLIQUELY ORIENTED RIPPLE CRESTS ON ACCRETION SURFACES

In sinuous channels, helicoidal flow generates a pattern of 'net outward and inward flows in the upstream and downstream segments' of point bars (Bridge 2003; Fig. 2-9A). This pattern occurs in response to the changing position of the high velocity core along the point bar and the generation of helical, curvature-driven secondary flow in the downstream segment that commonly moves sediment obliquely up the point-bar surface (Fig. 2-9A; Leopold and Wolman 1960; Bluck 1971; Bathurst et al. 1977; Dietrich et al. 1979; Bridge and Jarvis 1982; Dietrich and Smith 1983). In the Clear Fork Formation, trough and planar cross-sets advanced obliquely up the inclined surfaces of LA elements at several localities, indicating helicoidal flow cells strong enough to move dunes up the point-bar surfaces. At numerous sites, ripple crests on laterally accreted surfaces similarly show an oblique updip orientation, apparently supporting helicoidal flow for these smaller bedforms. However, Allen (1968) described swept ripples which develop due to the faster migration of crests in deeper water, providing an alternative explanation for the obliquely directed ripples (see also Dietrich et al. 1979; Edwards et al. 1983).

In this section, we document the presence of these unusual sedimentary structures at four study sites (Table 2-3), including a downflow traverse around an exhumed meander bend, and discuss their formative conditions. Obliquity (O) is defined as the angle between the paleoflow direction (P) measured in this case from ridge-and-furrow structures and the strike (S) of the accretion surface, which is presumed parallel to the local channel orientation. Zero, negative, and positive obliquity values represent ripple crests directed along the surfaces, downdip, and updip, respectively (Fig. 2-9B). An average obliquity angle was calculated from numerous beds at each site (Table 2-3).

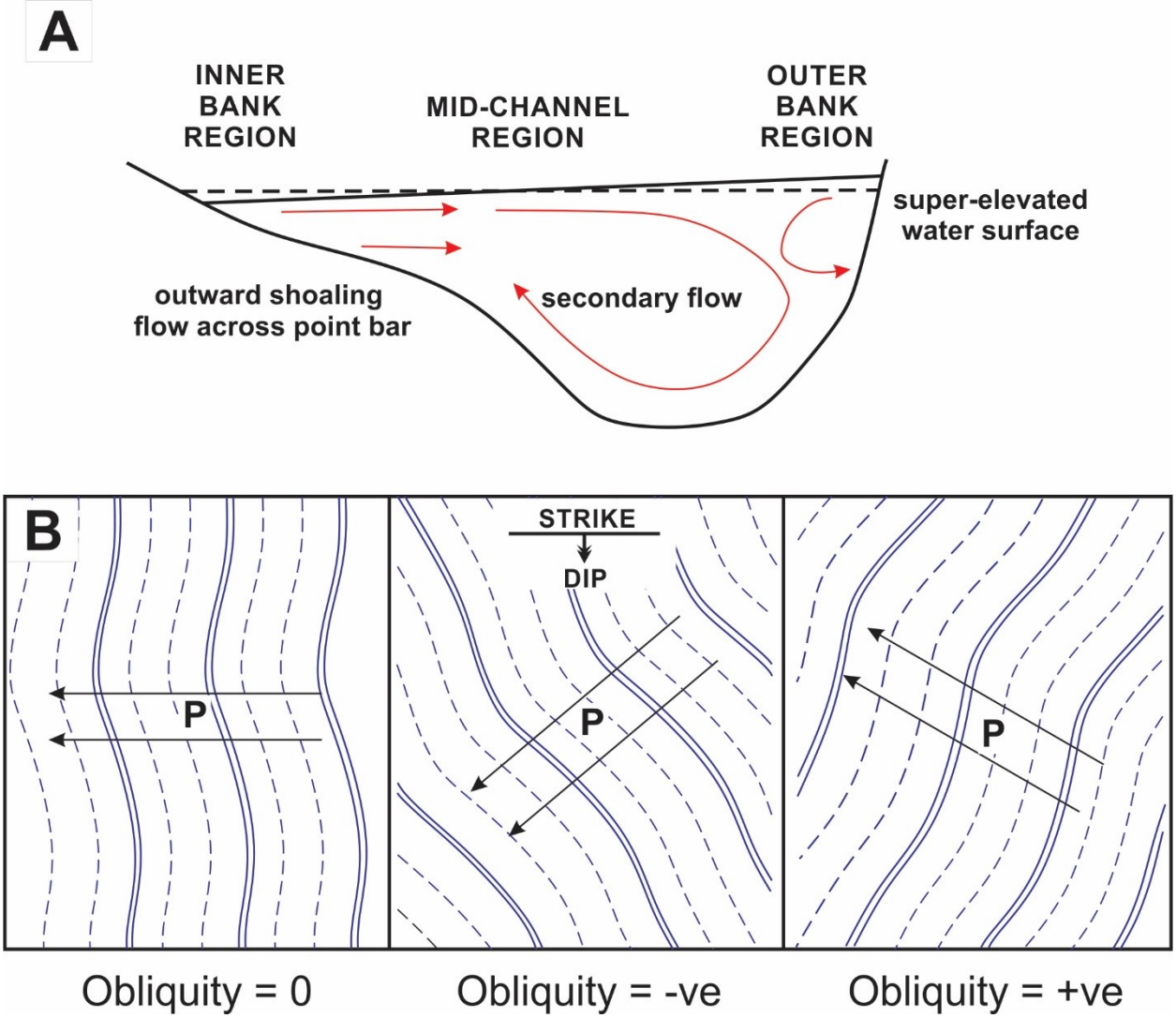

Figure 2-9 Illustration of the flow pattern in a meander: outward shoaling flow directed over the entire point bar and an inward secondary flow at the bend apex with an outer bank cell. Modified from Markham and Thorne (1992). (B) Sketch showing the relationship between the strike and dip directions of the accretion surfaces and the paleoflow direction measured from ridge-and-furrow structures. Here, the local strike of the bed is oriented parallel to the channel axis. Obliquity refers to the angle between the apparent paleoflow direction and the strike of the bed; positive and negative obliquity values represent the skewing of the ripple trains up or down the inclined surfaces whereas a value of zero refers to cases where the ripples migrate along the strike of the bed.

At NSCQ, the obliquity averages +30.6o, with ripple crests mainly oriented updip across the area. Obliquity consistently decreases downstream along the curved exhumed ridge traces from +33.9^{o}, +31.1^{o}, +20.4^{o} to +14.4^{o} in segments A to D (Fig. 2-5A), with more ripple crests oriented along and down the downstream surfaces. At MR3, obliquity is also positive (+21.7^{o}). In contrast, MR1 shows negative obliquity (-34.1^{o}), with ripple crests oriented predominantly

downdip and 2D dunes low in the channel fills directed updip. For more gently dipping beds at BC, eight were oriented downdip, six updip, and two along strike, giving a downdip average.

Edwards et al. (1983) observed positive ripple obliquity at NSCQ and suggested two possible explanations: 1) 'the large transverse gradient in local downstream sediment transport rate', implying swept ripples, and 2) 'the transverse component of the near-bed velocity which is related to helicoidal flow.' With no apparent relationship between obliquity and observed meander radius, they concluded that swept ripples were predominant, with a lesser contribution from helicoidal flow. Based on our data, a pattern of 'net outward and inward flows in the upstream and downstream segments' (Bridge 2003) was not detected at NSCQ, where a semi-complete meander bend has updip paleoflow in all segments. Although this implies swept ripples rather than helicoidal flow, such a systematic pattern across a wide area is puzzling. With good evidence for helicoidal flow at other sites, we present a composite explanation for flow patterns on the inclined surfaces that takes into account falling and overbank flow.

At bankfull stage under moderate flow conditions, ripples would migrate across all parts of accretion surfaces but would advance more rapidly in deeper water with higher shear stress, generating swept crests (Allen 1968). During falling stage, ripples high on the surfaces would be stranded but would continue to advance downstream where submerged. Rill casts are common on the surfaces down to low levels, as also noted by Edwards et al. (1983), indicating that surfaces were exposed and drained during waning flow. We agree with Edwards et al. (1983) that swept ripples were present but suggest that falling water level was a key factor for many occurrences. At MR1, dunes are directed updip (positive obliquity) low in the channel, implying helicoidal peak flow, but ripple crests are directed downward (negative obliquity) on the upper parts of the accretion surfaces. We suggest that bankfull conditions were commonly exceeded at

MR1, where thin crevasse splays are present in associated floodplain deposits, and that re-entry of overbank water into the channel caused negative obliquity of ripple crests high on the accretion surfaces. At NSCQ, more variable flow in the downstream parts of bends may indicate preferential flow routing from floodplains (cf. Gay et al. 1998; Ghinassi et al. 2013). For the ephemeral meandering river Usri in India, Purkait (2010) noted that flow was consistently directed down the point bar at one bend and was variable at three other bends.

Table 2-3 Obliquity of ripple-crest orientation measured on inclined, cemented fluvial beds in element LA-3 (mud- and quartz-rich inclined strata). See text and Figure 2-9 for an explanation of obliquity measurement.

Sites	Number of readings	Average angle of obliquity	Standard Deviation	Dominant paleoflow direction
Mouth of Brushy Creek	16	-10.4	14.3	Variable
North Soap-Creek Quadrangle	84	+30.6	16.7	Up
Montgomery Ranch 1	26	-34.1	18.1	Down
Montgomery Ranch 3	30	+21.7	19.5	Up

2.7 INTERPRETATION OF CLEAR FORK FORMATION FLUVIAL SYSTEMS

2.7.1 Fine-grained Systems

Quartz-rich systems (element LA-1) are relatively coarse-grained with steep inclined surfaces and evidence for helicoidal flow and episodic discharge (Table 2-1; Fig. 2-1). Stacked storeys and abandoned channel fills indicate an avulsive style. The fluvial deposits are attributed to sandy meandering rivers with dune trains and laterally accreted point-bars. With outcrop limitations, it is unclear whether ridge-and-swale topography formed by scroll bars (Gibling and Rust 1993) was originally present. The strata broadly resemble the deposits of modern sandy meandering rivers (Jackson 1976; Nanson 1980) and well exposed ancient analogues (Puigdefabregas 1973; Smith 1987; Ielpi and Ghinassi 2014).

Mud-rich systems (element LA-2) are fine-grained with steeply inclined surfaces. Bedforms were mainly ripples with some dunes, and sustained migration distances were short with reactivation of bar surfaces. Channels periodically dried up, as indicated by disrupted mudstone and small roots at low levels in the channel bodies. Mud aggregates are a minor component. The deposits are attributed to oblique accretion with draping of suspended sediments on accretionary banks. The deposits have many similarities with seasonal channels in low-gradient areas of central Australia (Taylor and Woodyer 1978; Woodyer et al. 1979; Page and Nanson 1996; Gibling et al. 1998; Page et al. 2003) and elsewhere (Schumann 1989; Brooks 2003a, 2003b; Marren et al. 2006). Many of these systems are anastomosing, and show limited distances of bank accretion with modest cutbank retreat (Smith and Smith 1980). Ancient analogues have been described (Rust and Legun 1983; Ghosh et al. 2006; Rygel and Gibling 2006).

Mud- and quartz-rich systems (element LA-3) comprise discrete mudstone and quartzose detrital layers with steep dips. The exceptional exposures at NSCQ display curvilinear exhumed surfaces of point bars that experienced sustained lateral migration (Edwards et al. 1983) and periods of near-dryness, with a prominent component of mud aggregates. Flow was occasionally strong but mainly of low strength and locally helicoidal, and swept ripples and rill casts formed in part during waning flow, with periodic flow back into the channel from overbank areas. No scroll bars were observed in these excellent exposures, probably due to the paucity of coarser sediment and the tendency of modest floods to deposit most sediment within the channel. Fine-grained meandering rivers with sustained point-bar migration are known (Jackson 1981; Brizga and Finlayson 1990; Page and Nanson 1996; Marren et al. 2006; Marren and Woods 2011), and the loess-sourced Bermejo River of Argentina has point bars with lateral-accretion surfaces that dip at up to 8^{o} (Sambrook Smith et al. 2016). In a classification of anabranching systems, Knighton

and Nanson (1996) identified Type 3 systems as mixed-load and laterally active. Several ancient examples are known (Stewart 1981, 1983; Mack et al. 2003; Gruszka and Zieliński 2008).

Sambrook Smith et al. (2016) suggested that fine-grained fluvial systems show a spectrum from lateral- to oblique-accretion, linked to the concentration of suspended sediment. They noted that rivers with fine sand and silt but little clay and a large suspended load tend to have point bars with lateral accretion, whereas rivers with finer grade, more clay, and less suspended sediment tend to have obliquely accreted banks. Other studies have noted a spectrum from sustained lateral accretion through short-distance oblique accretion to vertical accretion within fixed channels, with oblique and lateral accretion in adjacent reaches (Marren et al. 2006) and periods of aggradation and migration (Page and Nanson 1996). A gradation from fixed channels to channels with modest lateral accretion was noted in a Pennsylvanian example (Rygel and Gibling 2006). Fluvial style may also be influenced by bank strength imparted by vegetation, cohesive mud and paleosols.

For the Clear Fork Formation, we infer a continuum from coarse-grained meander belts with quartzose sediment (LA-1), to fine-grained meander belts with sustained point-bar migration and a bedload of sand-sized mud aggregates with some suspended clay (LA-3), to fine-grained, obliquely accreted systems with deposition of suspended load on accretionary banks and benches with limited migration (LA-2). All three LA styles are present at various levels in the formation, but exposures were not sufficiently continuous to document gradations between them. We view elements LA-2 and LA-3 as local variants on an overall fluvial style. Some systems may have been anabranching in view of their multiple storeys, avulsive nature, and common occurrence of abandoned channels with elements LM, DM, and MM. Rippled quartzose deposits include both climbing and non-climbing cross-lamination, but the deposits of climbing ripples are not

noticeably abundant, suggesting that the suspended load of detrital grains was generally modest (cf. Mack et al. 2003; Sambrook Smith et al. 2016).

The river systems of central Australia, with an arid to semi-arid climate and a prolonged dry season, provide a partial analogue for the Clear Fork fluvial systems. The Channel Country is traversed by fine-grained rivers that run some 1000 km to Lake Eyre (Nanson et al. 1992; Gibling et al. 1998), and the Murray-Darling system has both sand- and mud-rich tributaries (Taylor and Woodyer 1978; Woodyer et al. 1979; Page and Nanson 1996; Schumm et al. 1996; Page et al. 2003; Marren and Woods 2011). Channels are commonly a few metres deep and a few tens of metres wide, commonly anabranching and avulsive, with quartzose sand, mud aggregates, and a large suspension load. Points of similarity with the Eastern Shelf include a tectonically stable setting, a large distance (perhaps several hundred kilometres: Fig. 1-2A) from upland sources, and an extensive low-gradient plain. Page et al. (2003) noted that oblique accretion was favoured in central Australia by subdued relief, low gradient, fine-grained source rocks, and a tendency for decreased discharge downstream due to lower rainfall and transmission losses (Knighton and Nanson 1994a). Although the Clear Fork channels were relatively small, Channel Country channels with similar dimensions form part of continental-scale river systems.

A further point of similarity between the Australian systems and the Clear Fork Formation is the importance of mud aggregates. Across the Channel Country, pedogenic mud aggregates form in vertic soils during seasonal shrinking and swelling of clays. They are washed into the channels during rainstorms and floods where they are entrained as bedload and generate lower flow regime bedforms (Nanson et al. 1986; Rust and Nanson 1989; Maroulis and Nanson 1996). Aggregates are also released from eroding upland soils (Loch 1991; Wakelin-King and Webb 2007).

Smectite is widely considered vital for aggregate production in vertic soils (Southard et al. 2011) but is a minor constituent in some Channel Country soils, which are variably rich in kaolinite, illite, and randomly interstratified clays (Hallsworth and Beckmann 1969; Rust and Nanson 1989; Maroulis and Nanson 1996). Floodplain clays and aggregate-bearing channel sediments in the Clear Fork Formation comprise an assemblage of illite, Fe-rich chlorite, kaolinite, and mixed-layer clay. Our glycolation results suggest that these components had some swelling ability that would have promoted aggregate formation, and the lack of discrete smectite has counterparts in modern river systems where aggregates are common.

The intercalation of mud-aggregate and quartzose layers in LA-3 suggests an alternation between basinal and upland sediment sources. We suggest that the predominant mud-aggregate beds were derived from local floodplains during low-magnitude floods, whereas the quartzose beds were derived from the distant uplands or through reworking of locally stored sediment during major floods. Although some quartz may be aeolian, no unequivocal aeolian deposits were identified during this study. In central Australian channels, quartzose and aggregate layers are common, and channel incision into underlying sand sheets returns quartzose sediment to the channels at sites far out on the plains (Knighton and Nanson 1994b; Gibling et al. 1998). Considering the abundance of uplands that supplied coarse clastic sediment through geological time, fine-grained fluvial systems appear to represent unusual conditions globally. These include periods with denuded source areas, a local dearth of coarse sediment, and an unusual supply of fine sediment. We identify three broad settings for these systems with respect to the supply of fine-grained sediment: *supply-dominated, supply-limited, and supply-enhanced* (Fig. 2-10). The conditions may be basinwide or apply to certain river reaches or parts of basins.

Supply-dominated systems include the Yellow River of China (van Gelder et al. 1994; Stevens et al. 2013), the Bermejo River of Argentina (Sambrook Smith et al. 2016), and the Slims River of Alaska (Fahnestock 1969), which derive large volumes of silt and fine sand from eolian or glacial sources in their headwaters. These rivers have very large suspended loads and rapid vertical and lateral accretion in braided and meandering systems, spanning a range of climate.

In comparison, the Clear Fork Formation and many fluvial systems of central Australia are *supply-limited systems*. The quartzose sediment from distant, low-relief source areas was modest in volume and rarely exceeded fine-grained sand, and transport and accumulation rates were low. Under these conditions, reworking of clay-rich paleosols on the distal plains yielded much of the channel sediment. The supply of intrabasinal sediment reflects in part the prevalence of vertic soils with erodible aggregates, a modest vegetation cover, and seasonal flow and dryness in a semi-arid to arid basinal setting. A similar setting characterises some, as outlined above.

Supply-enhanced systems may have upland sources of coarse and fine sediment but benefit from fine-grained sediment laid down directly on the alluvial plains. The material includes loess and other eolian materials (Kessler et al. 2001; Soreghan et al. 2002) and volcanic ash (Galloway et al. 2011). The sediment is commonly reworked by and, in the case of eolian deposits, locally derived from rivers as source-bordering accumulations (Gibling et al. 2008; Nanson et al. 2008).

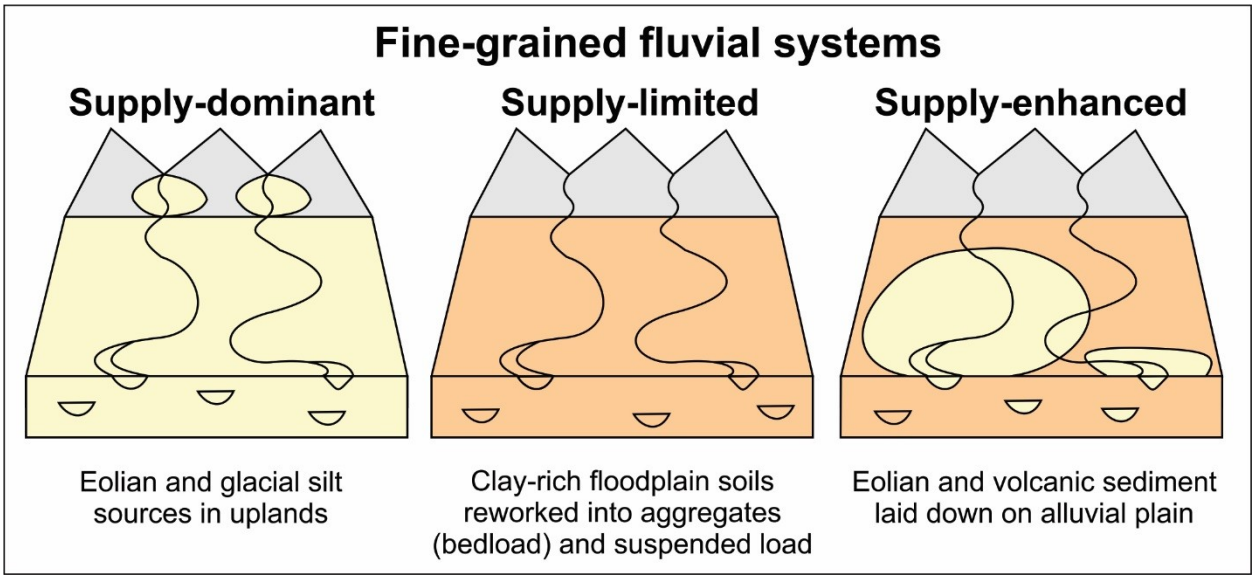

Figure 2-10 Model for fine-grained fluvial systems. The Clear Fork Formation is an example of a supply-limited system, with a limited upland source of detritus (yellow) and a considerable supply of fine material (brown), including mud aggregates, from reworking of floodplain deposits.

2.7.2 Coarse-grained Systems

Tabular Sandstone (element TS) comprises laterally extensive sandstone sheets with scours filled by high- and low-flow strength bedforms. They match in some respects the deposits of ephemeral and sheetflow-dominated rivers in relatively arid regions, including sandy braided rivers west of Lake Eyre (Williams 1971; Magee et al. 1995; Croke et al. 1996). In the ephemeral River Gash of Sudan, channel-fill sequences with prominent scour fills comprise dunes, transverse bars and waning-flow deposits, whereas sheet-flood sequences comprise plane beds and waning-flow deposits, suggesting high flow strength and rapidly varying discharge (Abdullatif 1989). McKee et al. (1967), Williams (1971) and Stear (1985) documented similar deposits laid down in catastrophic floods after heavy rain. Possible ancient analogues were described by Olsen (1989), Eberth and Miall (1991), and North and Taylor (1996).

In a tectonically stable basin such as the Eastern Shelf during the Permian, climatic fluctuation is

a possible explanation for contrasted fluvial styles (tabular sandstones and meandering systems) in rivers sensitive to modest fluctuations in water and sediment discharge (Bogaart et al., 2003). In central Australia, large meandering systems laid down thick sands during wetter parts of glacial-interglacial cycles, with muddy, low-energy anastomosing systems during more arid periods (Nanson et al. 1988; Nanson et al. 1992; Magee et al. 1995; Magee et al. 2004; Nanson et al. 2008). Nádor et al. (2003) correlated fluvial style with Milankovitch-scale cyclicity in the Pannonian Basin of Hungary, and Himalayan rivers experienced periods of aggradation and degradation in response to monsoonal fluctuations over the last glacial cycle (Gibling et al. 2005; Tandon et al. 2006).

2.7.3 Regional paleoflow

Over the 612 km^2 study area, 344 paleoflow readings were measured at nine sites using mainly ridge-and-furrow structures with a few trough cross beds on inclined beds in elements LA-1, 2, 3, and TS (Fig. 1-6; Table 2-4). One third of the readings were from the meanderbelt at NSCQ. Because ripple crests may be swept rather than transverse to the flow, the strike of the accretion surfaces was also recorded and represents a higher order paleoflow estimate (Miall 1974); using the downflow strike direction, the two datasets are closely comparable, and ridge-and-furrow was used in Figure 1C in view of the much larger dataset.

Based on 317 readings, the average paleoflow direction for the inclined fluvial beds (elements LA-1 to 3) is 269.9^o based on ridge-and-furrow and 260.5^o based on the strike of accretion surfaces. Paleoflow ranged from southwest to northwest, which is consistent with uplifts bordering the Eastern Shelf to the east and northeast (Fig. 1-2A; Edwards et al. 1983; Hentz 1988). Some paleoflow variation reflects channel sinuosity, as indicated by curved meander traces at NSCQ and inferred from varied storey paleoflow at KWTP. However, considerable

local variation is apparent: RT shows northward flow; BC, MB, KWTP, and MR1 show southward to south-westward flow, and NSCQ, MR2, and MR3 show northwestward flow. Based on 27 readings, the average paleoflow direction for the three tabular sandstones is 167.7° for ridge-and-furrow and 117.8° for trough cross-beds. At MB, paleoflow is within 20° of the paleoflow in the underlying laterally accreted channel bodies (Table 2-4 and Fig. 1-6). At CCP, the tabular sandstone shows an eastward flow, whereas the underlying abandoned channel shows westward flow (Simon et al. 2016). At NSCQ, too few (3) readings were measured from the tabular sandstone for a fair comparison. With this range of variability, the relationship between tabular and laterally accreted fluvial bodies was not fully established in the present study.

Table 2-4 Paleoflow data and channel dimensions for sites in the Clear Fork Formation. For the meandering channels, the paleoflow analysis compares azimuth of ridge-and-furrow structures (2D & 3D ripple crests) with the strike of the accretion surfaces (downflow component of strike is given). Two paleoflow values are quoted sites with tabular sandstone deposits; values with asterisks indicate paleoflow measured from trough cross-beds whereas the others were measure from ripple crests. Channel depth represents single storeys or vertical extent of inclined bedsets, and gives minimum values. Channel width represents fully exposed width of abandoned channels. n.d. = not determined; n.a. = not applicable.

Sites	Element	Paleoflow		Strike of bed		Dimensions (m)	
		Total	Mean	Total	Mean	Width	Depth
Red Tank	LA-1	33	359.9°	n.a.	n.a.	n.d.	4.0
Mouth of Brushy Creek	LA-3	46	236.5°	16	236.8 °	28	2.5
North Soap-Creek	LA-3	109	304.0°	84	257.6 °	n.d.	2.0
Quadrangle	TS	3	222.2°	n.a.	n.a.	n.d.	1.3
Know Where To Park	LA-2	23	225.0°	n.a.	n.a.	n.d.	4.0
Mixing Bowl	LA-2	10	181.9°	n.a.	n.a.	n.d.	1.5
	TS	13	165.8°	n.a.	n.a.	n.d.	3.4
		*5	*133.3°				
Colwell Creek Pond	TS	3	106.7°	n.a.	n.a.	n.d	6.5
		*3	*092.0°				
Montgomery Ranch 1	LA-3	46	203.4°	26	228.5 °	n.d.	2.2
Montgomery Ranch 2	LA-1	4	284.9°	n.a.	n.a.	n.d.	2.0
Montgomery Ranch 3	LA-3	46	307.9°	30	288.2 °	20	1.5

2.8 GEOCHEMICAL ANALYSIS AND IMPLICATIONS

Calcite and ankerite are common in cements and clasts in the lower unit of the Clear Fork Formation, whereas dolomite greatly predominates in the middle and upper units. Associated with this upward change in carbonate type, gypsum is abundant in lateral-accretion deposits and in massive mudstone in the middle and upper units. Barite is present throughout the formation and celestine is present in one laterally accreted bedset in the upper unit. Textural evidence indicates that much of the carbonate and sulphate formed under near-surface conditions or during shallow burial, as indicated by reworked clasts and poikilotopic cements with apparently floating detrital grains, suggesting precipitation from phreatic waters prior to much compaction. Cementation may have been promoted locally where water ponded due to the permeability difference between the coarse-grained deposits and underlying muds (Nash and Smith 2003), especially in element CD.

The upward transition from predominantly calcite and ankerite to dolomite cements is inferred to reflect a progressive evolution of shallow phreatic groundwater in an evaporation-dominated environment where an increased Mg/Ca ratio followed calcite precipitation. Based on the configuration of the Midland Basin and the lack of marine strata in the study area, Mg was probably derived from weathering of Mg-rich rocks in source areas and aeolian dust from tidal flats or playa lakes, such as the dolomitic lake sediments recorded by Minter et al. (2007). It is unlikely that dolomite formed by mixture of marine brines with freshwater, although brines may have been derived from saline lakes locally.

Under evaporative conditions, carbonate removal leads to sulphate enrichment and gypsum precipitation (Arakel 1986; Colson and Cojan 1996; McQueen et al. 1999; Worden and Burley 2003; Schmid et al. 2006). In the middle and upper units, gypsum nodules are prominent in

floodplain deposits with paleosols. In modern settings, pedogenic gypsum occurs in areas with <25-30 cm/yr precipitation (Birkeland 1999), suggesting arid conditions for the upper unit. Gypsum interbedded with dolomite at The Narrows was probably precipitated in playa lakes charged by saline ground- and surface-water (cf. Giles et al. 2013). The occurrence of celestine in the upper unit is consistent with a precipitation sequence in which Ca^{2+} is removed and brines enriched in Sr^{2+} relative to Ba^{2+} react with gypsum (Hanor 2000; Neubauer et al. 2010). Barite is present throughout the formation, and may have formed during shallow burial where vugs retained supersaturated solutions (Khalaf 2007).

The evidence for early, evaporative cement formation in the Clear Fork Formation accords with geochemical data from arid areas of the Australian Channel Country (Cendón et al. 2010; Tweed et al. 2011). Below the floodplains, a regional saline groundwater body with a water table at ~10 m depth has total dissolved solids (TDS) of more than 50,000 mg/L locally. The brines are of Na-Cl type, commonly at gypsum saturation (Cendón et al. 2010). Freshwater lenses underlie waterholes where floods scour sealing clays to recharge shallow aquifers, and these lenses support vegetation near the channels. Starting from a marine aerosol rainwater signature, the increase in TDS is due principally to evaporation rather than evapotranspiration, which is important in the less arid Murray Basin (Chivas et al. 1991; Cartwright et al. 2008; Cendón et al. 2010).

The petrographic analysis, along with the fluvial style of the Clear Fork Formation, supports earlier evidence from paleosols and plants for semi-arid to arid conditions for the Clear Fork Formation, as well as progressive aridification from the Pennsylvanian through the Early Permian (DiMichele et al. 2006; Tabor and Poulsen 2008; Tabor 2013). Analysis of fluid inclusions in ephemeral-lake halite from Kansas suggests that, by the uppermost Leonardian /

Kungurian, temperatures in western Pangea were more extreme than anywhere on Earth today (Zambito and Benison 2013).

2.9 CONCLUSIONS

The Lower Permian Clear Fork Formation is a continental redbed deposit in north-central Texas, which has yielded exquisitely preserved plant and vertebrate fossils. The formation was deposited under unusual conditions – the relatively arid, western equatorial margin of Pangea on a stable shelf far from upland source areas. Because shallow burial minimized diagenetic effects, primary features were exceptionally well preserved, providing clues about depositional conditions.

Three types of meandering channel were identified in the formation, which contains a spectrum of fluvial styles with two end-members that represent fundamental channel processes: lateral accretion of sandy and muddy point bars, and oblique accretion of banks and benches of fine sediment. Of particular interest are exhumed point bars composed of alternate inclined beds of quartzose sand and sand-sized mud aggregates, the latter transported as bedload with additions of suspended mud; these deposits exhibit sustained point-bar migration with components of oblique accretion, and are the first aggregate-dominated channel fills identified to date in the ancient record. A similar channel spectrum is present on the relatively arid distal plains of central Australia, where major river systems comprise suites of fine-grained channels. The ripple crests on many exhumed accretion surfaces are oriented obliquely up and down dip, an unusual circumstance linked here to a rapid decline of flood levels in seasonal channels and the stranding of bedforms, as well as re-entry of overbank water into the channel, especially in the downstream parts of bends. Abandoned channels accumulated finely laminated beds with well-preserved leaves, indicating the presence of perennial waterholes surrounded by riparian vegetation, with

disrupted beds where channels dried out completely. Coarse-grained tabular sandstones with high-energy bedforms are not part of the fine-grained spectrum, and represent ephemeral and poorly confined systems with rapid discharge variations, reflecting periodic climatic fluctuations or perhaps particular source areas.

Understanding the architectural complexity of fine-grained channel systems is a particular challenge, requiring sedimentological study of strata that are often unrevealing, coupled with petrographic analysis of grain types, their relative sizes, and the proportion of suspended to bedload sediments. Like the carbonate clasts, the locally predominant sand-sized mud aggregates were derived from paleosols on cutbanks and floodplains within the basin. In contrast, the suspended clays may reflect long-distance transport from a denuded Early Permian source, with local additions from soils and from aggregates degraded during transport and compaction. Although suspended clay and bedload aggregates may be genetically linked, their transport and deposition reflect widely different flow conditions, not apparent from an initial inspection, and channel-fill mudstone may easily be misinterpreted in the absence of petrographic data, since mud aggregates are typically only visible in thin sections. Additionally, the scarcity of certain bedforms, especially dunes, may be a function of the small grain size.

The Clear Fork Formation with its abundance of mud aggregates and suspended clay in channel deposits represents a supply-limited system with a considerable volume of sediment coming from floodplain reworking. Other fine-grained rivers are supply-dominated systems with abundant sources of eolian and glacial fines in the source areas. A third category of supply-enhanced systems receives fine-grained eolian and volcanic additions on the plains. More research is required to document these relatively understudied modern and ancient river systems.

The upward change from calcite and ankerite in the lower unit to dolomite in the middle and upper units, with increased gypsum and the occurrence of celestine, suggests increasingly saline shallow groundwater. This inference accords with a general upward fining and decrease in the proportion of channel bodies, plant and animal fossils. Sedimentological and petrographic information collectively indicate relatively arid conditions, supporting previous interpretations of progressive aridification in equatorial Pangea during the Early Permian.

CHAPTER 3- Pedogenic mud aggregates preserved in a fine-grained meandering channel in the Lower Permian Clear Fork Formation, north-central Texas, USA

3.1 ABSTRACT

The Lower Permian Clear Fork Formation of north-central Texas is the first known example from the rock record where mud aggregates are well-preserved as the main sediment component of a fine-grained meandering system. This rare occurrence provides an excellent opportunity to evaluate the origin, depositional setting, and conditions responsible for their preservation. At the study site, lateral-accretion deposits define an exhumed point bar composed of thick mudstone layers rich in aggregates, interbedded with thin layers of ripple cross-laminated sandstone. Petrographic analysis indicates that red-brown and gray aggregates comprise >68% of the mudstones, with minor amounts of quartz, feldspar, ferruginous grains and dolomite rhombs. When size estimates are corrected for 2D sections and for ~17% flattening during compaction, the aggregates are of fine-sand size and more than twice the size of associated quartz grains, which were probably size-limited on the distal plain. Despite the difference in grain size and densities, both aggregates and quartz populations were entrained at very low velocities ranging from 1.2-1.5 cms^{-1}.

Based on a relatively uniform size, variation in iron-oxide content, and association with small ferruginous concretions, the aggregates formed by reworking of associated vertic paleosols. The aggregates comprise illite, Fe-rich chlorite, kaolinite and mixed-layer clay and, in the absence of discrete smectite, their formation is attributed to swelling of illite and Fe-rich chlorite, as

indicated by glycolation results. Deficiency in smectite is probably a result of parent-rock composition, rather than burial illitization in this shallowly buried formation.

Aggregates typically lose their pelleted texture during shallow burial and compaction. Their excellent preservation is attributed primarily to rapid incorporation within a migrating point bar, set within a "compartment" of indurated paleosols that limited compactional effects. Some early cementation by dolomite, gypsum and barite of the aggregate-bearing and associated beds would have enhanced rigidity.

3.2 INTRODUCTION

Mud aggregates are transported as bedload in channels and across floodplains in modern dryland settings, in places forming the bulk of the sediment (Rust and Nanson 1989; Maroulis and Nanson 1996; Gibling et al. 1998; Wakelin-King and Webb 2007a). The aggregates form mainly in Vertisols and related soils that contain swelling clays, principally smectite, under warm seasonal climates during cycles of wetting and drying (Rust and Nanson 1989). The abundance of aggregates in channels in central Australia and elsewhere suggests that some mud-filled channels in the ancient record represent bedload transport rather than suspension settling under quiescent conditions. However, the fragile aggregates typically become unrecognizable at shallow depth due to compaction (Rust and Nanson 1989; Maroulis and Nanson 1996; Gibling et al. 1998; Brooks 2003a), which may account for their sporadic identification in ancient channel deposits.

Pedogenic mud aggregates have been identified in a small number of ancient channel and floodplain deposits (Rust and Nanson 1989; Ékes 1993; Gierlowski-Kordesch and Rust 1994; Talbot et al. 1994; Marriott and Wright 1996; Gierlowski-Kordesch 1998; Gierlowski-Kordesch

and Gibling 2002; Marriott and Wright 2004; Müller et al. 2004; Wolela and Gierlowski-Kordesch 2007; Gastaldo et al. 2013). To date, the fullest description is that of Müller et al. (2004) for the Triassic Lunde Formation of offshore Norway, in which thick accumulations of aggregates were preserved *in situ* within paleosols and were reworked within the floodplain. The authors used thin sections, scanning electron microscopy (SEM) with electron dispersive spectroscopy (EDS), cathodoluminescence and X-ray diffraction (XRD) to study the aggregates. For the Triassic Katberg Formation of South Africa, Gastaldo et al. (2013) used SEM and image-processing software to study aggregate-quartz mixtures in anabranching channel deposits, where the aggregates are present in channel lags, trough fills and the upper parts of channel fills.

Hypotheses for aggregate preservation in the rock record are based on their intrinsic properties and burial conditions (Table 3-1). Those suggested to date include selective preservation of especially durable aggregates, protection of aggregates from compaction by rigid framework grains or early-formed cement, rapid sedimentation, and overpressured burial regimes.

Simon and Gibling (in review) documented quartz-aggregate mixtures with a small proportion of aggregates in fine-grained, meandering-channel deposits throughout the Lower Permian Clear Fork Formation of north-central Texas. The formation is near-horizontal and minimally deformed, and regional evidence suggests that the strata experienced only shallow burial, which may have aided preservation of subtle depositional features. At one site in the middle unit 150 m above the formation base (North Soap-Creek Quadrangle, NSCQ, in Baylor County; Fig. 1-2A and 1-3), an exhumed point bar consists of lateral-accretion deposits composed mainly of well-preserved, sand-sized mud aggregates with few mineral grains.

In this paper, we document the depositional setting of the aggregates, extending an earlier study by Edwards et al. (1983), and use SEM/EDS, XRD and grain-size analyses to document their texture and composition and the properties of associated conglomerates and cemented quartzose sandstones. The clay mineralogy of the aggregates is compared to a recent mineralogical assessment of paleosols in the formation (Zhu 2015), which noted minor amounts of smectite in mixed-layer clay in the lower unit of the Clear Fork Formation but none in the middle and upper members (Zhu 2015). A widespread view is that pedogenic aggregates require smectite for their formation (Gierlowski-Kordesch and Gibling 2002), and some researchers consider that at least 20% smectite in the clay fraction is necessary for the development of vertic properties in shrink-swell soils (Shirsath et al. 2000). In view of this apparent discrepancy, we discuss the clay composition of aggregates and paleosols in relation to source areas and burial history for the Clear Fork Formation.

The present study has several novel points. To our knowledge, this is the first identification in the rock record of thick aggregate accumulations in channel bodies, with only minor bedrock-derived quartzose grains. This contrasts with previous studies that have documented thick aggregate accumulations in floodplain deposits but only a modest aggregate content in quartz-dominated channel sandstones. Additionally, the availability of beds dominated by aggregates allowed the integrated use of SEM/EDS and XRD to explore texture and composition (see also Müller et al. 2004). Because the aggregates were flattened, we used a statistical approach based on petrographic measurements to estimate the original size of the compacted aggregates and by extension, the amount of original strain, which is needed for a hydrodynamic assessment of the entrainment threshold and transport conditions. The study demonstrates the importance of aggregates and bedload transport in these fine-grained, laterally accreted fluvial systems, and the

exceptional aggregate preservation provides an unusual opportunity to test hypotheses for their preservation.

Table 3-1 Hypotheses proposed to explain the preservation of mud aggregates in ancient alluvial deposits.

Means of Preservation	Rationale	References
Composition of aggregates: resistance imparted by clay content, amount of swelling clays, and Fe-oxides	Enhanced preservation of unusually durable aggregates, some linked to particular soil profiles or horizons	Müller et al. 2004; this study
Buffering by a framework of rigid mineral grains in sandstone and siltstone	Mineral grains protect the aggregates and prevent their loss by compaction	Ekes 1993; Gierlowski-Kordesch 1998; Rust and Nanson 1998; Gierlowski-Kordesch and Gibling 2002; Müller et al. 2004
Cementation by carbonate, barite or iron oxides, especially during shallow burial	Increases rigidity of the sediment and enhances resistance to burial pressure	Gierlowski-Kordesch and Gibling 2002; Müller et al. 2004; this study
Rapid burial in paleosols due to cumulative sediment addition	Impedes pedogenic modification and other near-surface overprinting	Müller et al. 2004
Rapid burial in sediment bars within channel cuts	Stores aggregates in low topographic position, away from pedogenic processes, stabilized by capping sediment layers	This study
Shallow burial with less opportunity for deep-basin diagenesis	Buried strata may avoid the full range of diagenetic effects	This study
Burial in over-pressured zones	Reduces effective stress acting on grains at depth	Müller et al. 2004

3.3 GEOLOGIC SETTING

Located in north-central Texas, the Lower Permian (Kungurian) Clear Fork Formation is a 350-365 m thick interval of near-horizontal red mudstone with lesser sandstone, carbonate, and evaporite (Fig. 1-2A and 1-3; Olson 1958; Wardlaw 2005; Nelson et al. 2013). The formation was deposited between 0° and 5° N of the equator on the Eastern Shelf, a stable platform along the eastern flank of the Midland Basin, which was bounded to the north by the Wichita and

Arbuckle Mountains and to the east by the Ouachita Mountains (Fig. 1-2A; Galloway and Brown 1973; Edwards et al. 1983; Hentz 1988). The Wichita Mountains contain a Cambrian to Proterozoic bimodal suite of gabbros and basalts with rhyolites and granites, as well as Cambrian to Ordovician carbonates (Gilbert 1982). The Arbuckle Mountains comprise Cambrian to Devonian carbonates and Devonian to Mississippian clastic deposits on a Precambrian granite and gneiss basement (Ham 1973). The Ouachita Mountains consist of Paleozoic strata that were thrust onto the southern margin of North America during the late Paleozoic (Viele and Thomas 1989; Gleason et al. 1995; Ingersoll et al. 1995). The study site lies about 250 km west of the present Ouachita Orogenic Front and ~150-250 km from the Wichita and Arbuckle Mountains (Fig. 1-2A).

After the Fort Worth foreland basin was filled in the Late Pennsylvanian, sediment accumulated on the Eastern Shelf from the westward progradation of detritus shed from the uplifts, including recycled Pennsylvanian sediments (Fig. 1-2A and 1-2C; Brown 1973; Galloway and Brown 1973; Hentz 1988; Ziegler et al. 1997; Tabor and Montañez 2004). At the end of the Pennsylvanian, tectonic quiescence prevailed with intermittent strike-slip movement along the Matador-Red River uplifts (Regan and Murphy 1986; Budnik 1989; Brister et al. 2002) and the partial burial of the Wichita and Arbuckle Mountains by Lower Permian strata (Soreghan et al. 2012). The paleoclimate during deposition of the Clear Fork Formation was semi-arid to arid based on paleosol and plant information (DiMichele et al. 2006).

In a study of Pennsylvanian and Lower Permian paleosols of the Eastern Shelf, Tabor and Montañez (2004) estimated a maximum burial depth for the Virgilian Markley Formation (Bowie Group: Fig. 1-2C) of less than 1600 m; the formation lies up to 500 m below the Clear Fork Formation, suggesting ~1100 m of burial at the base of Clear Fork Formation. This estimate

is supported by regional data, which suggest that the Clear Fork Formation was overlain by ~1150 m of Middle to Upper Permian, Mesozoic, and Cenozoic strata (thus ~1500 m to the base of the formation; Roth et al. 1941; Smith 1974; Barnes et al. 1987; Johns and Granata 1987; Kocurek and Kirkland 1998; DiMichele et al. 2004; Nelson et al. 2013). This estimate contains many uncertainties due to original thickness variations and unconformities at the base of the Triassic, Cretaceous and Quaternary sections.

The region contains ~1300 m of Permian strata (including beds below and above the Clear Fork Formation) deposited in ~50 million years (301 ± 2 Ma to 251 ± 4 Ma: Fracasso and Kolker 1985; Rasbury et al. 1998; Lucas and Anderson 1993). This corresponds to a low long-term accumulation rate of 0.03 mm/yr, comparable to other mid-plate cratonic basins (<0.06 mm/yr: Schwab 1976).

Assuming a burial depth of 1500 m, a geothermal gradient of 20-30^{o}C/km appropriate for cratonic settings (Robbins and Rhodehamel 1976; Ruppel et al. 1995), and surface temperatures similar to modern equatorial settings, the maximum temperature experienced at the base of the Clear Fork Formation may have been as low as 60^{o} to 75^{o}C.

Establishing the formation's thermal history more directly is challenging due to the paucity of organic-rich beds and maturation data, requiring proxy data from nearby areas. Hackley et al. (2009) documented the vitrinite reflectance (R_o) of coal and carbonaceous shale in the Upper Pennsylvanian Cisco Group which lies stratigraphically ~500 m below the Clear Fork Formation southeast of the study area (Fig. 1-2A and 1-2C). Mean R_o ranges from 0.4-0.8%, equivalent to subbituminous C to high volatile bituminous A coal rank and near the onset of thermogenic gas generation (e.g., Rice 1993; Hunt 1996; Tang et al. 1996); peak gas generation typically occurs

at 1.0-1.2% (Tissot and Welte 1984; Michael et al. 1993; Tang et al. 1996). Using maturation data and bottom-hole temperatures from wells in the Middle to Late Permian San Andreas Formation of the Palo Duro Basin (Fig. 1-2A), Bein and Land (1983) concluded that the strata are immature (R_o = 0.4) and burial temperatures did not exceed 40-45 °C. This estimate may be geologically unreasonable because the authors suggested similar original brine temperatures, which implies little change in temperature during burial. Collectively, however, these datasets suggest that the Clear Fork Formation attained a low level of thermal maturity, at or below the threshold for gas generation.

In summary, the Clear Fork Formation was deposited on a slowly subsiding cratonic margin and experienced minimal deformation. The strata were shallowly buried with periods of exhumation and are thermally immature with low burial temperatures.

3.4 METHODS

Field Description. – The NSCQ field area was mapped in detail (Fig. 3-1). A 12.5 m stratigraphic log was measured through the exposure, and lithofacies identified within the exhumed point bar (Channel Body 1), two other Channel Bodies (2 and 3) and intervening floodplain deposits are described in Table 3-2. Twelve samples were collected from the three channel bodies and intervening mudstone unit, with a list of petrographic analyses conducted outlined in Table 3-3.

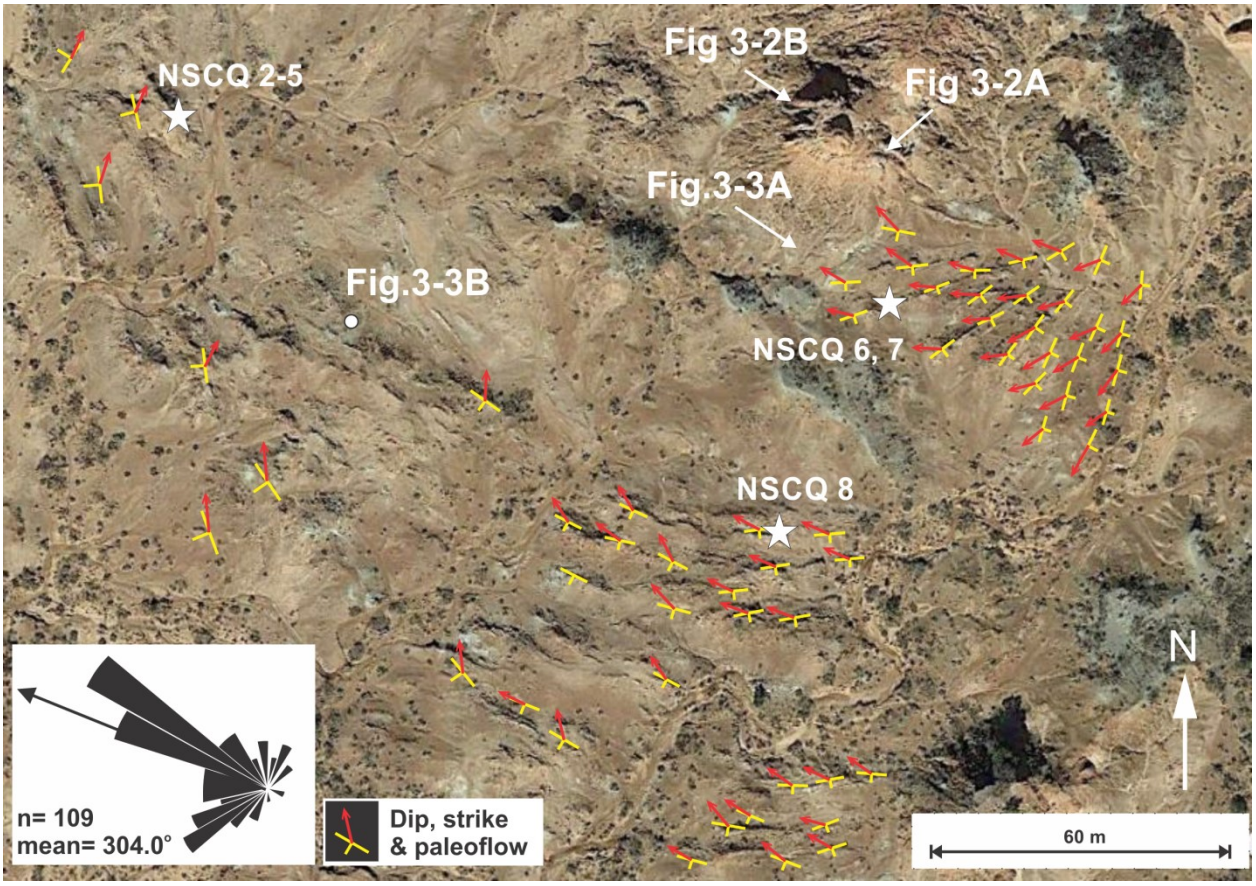

Figure 3-1 Planform exposure of exhumed point bar at North Soap-Creek Quadrangle (Google Earth image) showing resistant, discontinuous scarps formed by inclined sandstone beds, with large-scale curvature. Paleoflow was measured from ridge-and-furrow structures on scarp surfaces and the rose diagram represents paleoflow for all inclined surfaces. In virtually all cases, paleoflow is oriented obliquely up the inclined surfaces, confirming the presence of swept ripples (see text). The viewing direction for Fig. 3-2A-B and 3-3A is indicated by the white arrows and the position of Fig. 3-3B is shown by the white circle. The white stars indicate the position of the Channel Body 1 samples in Table 3-3. A stratigraphic log was measured at NSCQ 2-5 and is displayed in Fig. 3-3D.

Petrographic Description. – Twelve unpolished thin sections were examined using a Nikon Eclipse E400 Pol petrographic microscope with a Pixe-Link digital camera. Four out of five thin sections of mudstone in Channel Body 1 contain well preserved aggregates (NSCQ 2, 3 5, 6). Six thin sections were systematically counted with 400 points per slide of the key components (aggregates plus matrix, quartzose, dolomite, and ferruginous grains; Table 3-4). Aggregates and clay matrix could not always be distinguished, and the two components were counted together; however, inspection of the thin sections indicates that aggregates form the bulk of the finer material in the four key samples.

Using TESCAN MIRA 3 LMU Variable Pressure Schottky Field Emission SEM with INCA X-max 80 mm 2 Energy Dispersive X-ray Spectroscopy (EDS) system, two samples of cemented quartzose sandstone and basal coarse deposits and five aggregate samples were imaged using polished thin sections, and in the latter case on broken rock surfaces where aggregates were projecting from the matrix. During the preparation of polished thin sections, aggregate surfaces were commonly plucked, leaving pits that aided the imaging of internal features. Elemental analysis using the EDS system was problematic (clays < 10 μm spot size) and the resulting spectra typically represent mixtures. Consequently, the EDS data with an average error margin of 10% were used to determine the presence of quartz, feldspar and carbonate minerals and to qualitatively identify clay and mica minerals.

Five samples were selected for <2 μm XRD fraction analysis (Table 3-3). Approximately 20 g of crushed sample was suspended in a burette containing a weak solution of sodium hexametaphosphate. After 16 hours, the <2 μm fraction was isolated, flocculated with 4 ml of $MgCl_2$ solution, and centrifuged. The mixture was decanted and the clay fraction was re-suspended in a 500 ml cylinder. A 20 ml aliquot was withdrawn, dried and weighed to determine the appropriate weight (5 %) for the internal standard, zincite. The zincite was added to the re-suspended sample and dissolved using a laboratory shaker, after which the sample was centrifuged and smeared on a normal glass slide and a second heat-resistant glass. Using the Siemens Kristaloflex diffractometer with Co Kα radiation and scan properties of 2-77^o 2θ with a 0.02^o step increment and 2 s step time, XRD analysis was carried out on the <2 μm fractions that were smeared on normal glass. The slides were then placed in a desiccator containing vapors of ethylene glycol for ~4 hours to investigate peak shifts, after which they were analyzed immediately to prevent the glycol from evaporating, using a 2^o-30^o 2θ range with a 0.2^o step

interval and 2 s step time. The heat-resistant slides were placed in a preheated furnace at 150°C for at least 30 minutes, and were analyzed using a 2°-30° 2θ range with a 0.2° step interval and 2 sec step time. This process was repeated for 300°C, 500°C, and 650°C, which allowed clay minerals to be identified by revealing changes in crystal structure spacing. At temperatures >500°C, most clay smears started to flake or bubble, and XRD analysis was not conducted on these samples. Minerals were identified using the d-spacings from tables in Moore and Reynolds (1997) and the Joint Committee on Powder Diffraction Standards PDF system. The composition of mixed-layer clays was not determined. For the four key aggregate samples, the XRD results largely represent the composition of the predominant mud aggregates.

Grain Size Analysis. – Because the aggregates could not be separated for sieving, thin-section techniques were used to estimate grain size for six samples (Table 3-3). In the following text, major and minor axes denote measurements of grains in 2D thin sections, and long, intermediate and short axes denote true grain dimensions in 3D.

A total of 300 mud aggregates and 300 quartz and feldspar grains were selected from each of the four samples that contained well preserved aggregates (1200 particles for each type). The major axes of 600 quartz and feldspar grains were measured from two thin sections (300 points per thin section) of cemented sandstones in the inclined beds. The lengths of major and minor axes were measured for each aggregate, with the major axis measured first, and the major axis of each quartz grain was measured, providing a set of raw data (Table 3-5). The aggregates were selected individually after inspection because some were difficult to distinguish from matrix (see also Müller et al. 2004); thus, they were not randomly selected by point counting, as recommended by Johnson (1994) to obtain true volume estimates. For non-aggregates, using quartz plus feldspar is

a satisfactory approach (Johnson 1994) and, with <5% of feldspar in the samples, the silicate grains are referred to below as "quartz".

Because most random cuts through grains show axial dimensions less than true values, only apparent lengths of grain axes can be measured in thin sections, underestimating grain size. To correct for this, we used the method of Johnson (1994, p. 996), which derived mathematical relationships for grain size in 2D sections using a suite of random cuts through ellipsoidal particles with a range of axial ratios. Johnson also provided estimates of standard deviation for ϕ values based on measured major axes. Based on these relationships, two measures of corrected grain size were calculated (Table 3-6):

1) *Corrected Length of Major Axis*. This was calculated by multiplying the mean length of major axes by 1.3 for millimeter values, or by adding -0.4 to the equivalent ϕ values, with results estimated to lie within 6% of the true value (Johnson 1994). This approach was used for samples from aggregate layers (1200 mud aggregates and 1200 quartz grains from 4 thin sections) and quartzose layers (600 grains from 2 thin sections).

2) *Corrected Nominal Diameter*. Yielding the closest approximation to grain volume, nominal diameter is defined as the diameter of a sphere with the same volume as the grain, calculated as $\sqrt[3]{(D_a D_b D_c)}$, where D_a, D_b and D_c are the long, intermediate and short axes of the grain, respectively (Wadell 1932; Koster et al. 1980; Cui and Komar 1984). For the thin sections, a corrected nominal diameter was calculated by multiplying the mean length of the major axes by 0.95, or by adding 0.05 to the equivalent ϕ values, with results estimated to lie within 5% of the true value (Johnson 1994). Cui and Komar (1984) noted that the long axis alone is a reasonable

predictor of nominal diameter, although using all three axial measurements improves the predictive capability.

Inspection of the aggregates shows that many have been flattened in the plane of the bedding during compaction, in contrast to aggregates preserved with minimal compaction within a framework of detrital grains (Gastaldo et al. 2013). This would have decreased the length of the short (vertical) axis and increased the length of the long and intermediate (horizontal) axes, and thus estimates of size based on major-axis length in thin sections will be overestimates. To correct for this, we assumed that a newly released aggregate was spherical but was flattened evenly during burial such that the volume remained constant. Linking these assumptions with the nominal diameter equation, D_a and D_b will lie approximately in the bedding plane and D_c will be normal to bedding. Because D_a and D_b cannot be distinguished for flattened grains in 2D images, we assumed that $D_a = D_b$ for evenly flattened aggregates. Thus, the major axis is representative of $D_a = D_b$ and the minor axis is representative of D_c. For each of the 1200 aggregates, these values were used to calculate a value of the nominal diameter for each aggregate and a mean value for the population (*Nominal Diameter for Flattened Aggregates*: Table 3-6). No correction was made for the 2D thin-section effect at this point.

This approach assumes that volume reduction through loss of water and gas was negligible. Aggregates in modern soils are partially compacted due to shrink-swell pressures and are durable during reworking (Maroulis and Nanson 1996); thus, they should compact relatively evenly with limited further volume loss. No material additions to aggregates in vugs or along fractures and micro-faults were observed.

An additional approach was used to estimate the original major-axis length of the aggregates. Because D_c becomes shorter and D_a and D_b become proportionally longer during flattening, the minor: major axis ratio provides a measure of the extension. For example, a hypothetical aggregate with $D_a = D_b = 1$ mm and $D_c = 0.5$ mm yields a short:long axis ratio of 0.5 and has a nominal diameter of 0.794 mm. Thus, an originally spherical grain 0.794 mm in diameter has extended its long axis to 1 mm during flattening, an increase of 20.6%. The corrected major-axis length for the aggregate population was reduced by this percentage to correct for long-axis extension during flattening (*Corrected Length of Major Axis for Flattened Aggregates*: Table 3-6).

Although the grain-size estimates for aggregates and quartz provide a reasonable assessment, they are liable to a considerable error margin with 2D uncertainties compounded by aggregate compaction. However, a key purpose was to compare the relative size of quartz grains from the cemented quartzose sample to those from the mudstone layers, as well as to compare aggregates and quartz grains in the same bed, in order to assess their hydrodynamic response; the same methods were used for both groups of grains.

Flow Hydraulics. – To estimate the critical flow velocities required for entrainment of the aggregates and quartz grains (Paphitis 2001; Vermont Agency of Natural Resources 2003; Table 3-7), the critical shear stress (τ_{cr}) was first calculated using the grain densities and corrected grain sizes (quartz grains: d is the *Corrected Length of the Major Axis*; mud aggregates: d is the *Corrected Length of Major Axis for Flattened Aggregates*; Table 3-6) using Shields (1936) equation:

$$\tau_{cr} = \tau_{ci} \times g(\rho_s - \rho_w)d$$

where τ_{ci} is the dimensionless Shields parameter, g is acceleration due to gravity (981 cms^{-2}), ρ_s is the density of the sediment, ρ_w is the density of water (1 gcm^{-3} at 20°C), and d is the grain size (cm). Values of τ_{ci} were obtained from Table 7.1 in Julien (1995) where coarse silt, very fine and fine sand have dimensionless values of 0.165, 0.109 and 0.072, respectively. Aggregates in central Australia had densities of 2.27-2.31 gcm^{-3} (Maroulis and Nanson 1996), considerably lower than quartz at 2.65 gcm^{-3} (Paphitis 2001). Grain-size measurements from thin sections were corrected as set out above.

Using the critical shear stress values calculated for the aggregates and quartz grains, the critical flow velocities (u_{cr}) required for entrainment were calculated using:

$$u_{cr} = \sqrt{\tau_{cr} \times \rho_w}$$

Table 3-2 Lithofacies in the Clear Fork Formation at North Soap-Creek Quadrangle, using terminology from Miall (1985, 1996), Tucker (2003) and Long (2011). VF, F, M and VC = very fine, fine, medium, and very coarse grains, respectively.

Facies code	Lithofacies description	Sedimentary structures	Unit contacts	Fossils	Interpretation
Gm	Pebble conglomerate	Massive units of carbonate clasts, 1-3 cm in diameter	Abrupt, planar or irregular, erosive	Not observed	Channel lag associated with erosive events, probably linked to channel cutting, with clasts probably derived from paleosols
Sh	Planar-stratified sandstone	VF-M; plane lamination	Undulating to planar contacts	Not observed	Plane beds formed under upper flow regime conditions
Sr	Ripple cross-laminated sandstone to siltstone	VF-F; non-climbing and climbing asymmetrical ripples, with paleoflow obliquely updip of inclined bed surfaces; symmetrical ripples; rill casts; elliptical scours; gypsum dikes	Sharp, planar basal contacts	Root traces; *Taenidium barretti* / *Planolites montanus*, *Diplichnites gouldi* and putative tetrapod trackways	Migration of current ripples under lower flow regime conditions; on inclined beds, updip paleoflow attributed primarily to swept ripples formed during waning flow; lenses in mudstone represent crevasse splays
Fl	Laminated mudstone	Finely laminated, largely clay grade with minor silt; normally graded beds, varicolored (red-brown, gray, yellow)	Abrupt base and top; laminar contacts parallel- to nonparallel-planar and wavy	Permineralized leaves	Low-flow and suspension deposition in standing water during channel abandonment; leaves derived from riparian vegetation
Fm	Massive mudstone	Massive to locally weakly stratified, red-brown; slickensides, faint irregular mottles, wedge-shaped peds, redoximorphic spots, carbonate nodules	Abrupt, locally irregular	Rare root traces	In channel bodies, lateral accretion deposits composed largely of sand-sized mud aggregates; in sheets, suspension deposition from standing water, with pedogenic overprinting to form vertic paleosols

Table 3-3 List of samples from the NSCQ field area with their relative stratigraphic position and the various analyses conducted.

Sample numbers	Lithofacies description	Context	Analyses				
			Thin section	Point counting	Grain size	SEM/EDS	XRD
NSCQ 1	Pebble conglomerate	Basal deposits in downstream segment of exhumed point bar, Channel Body 1	✓	--	--	✓	
NSCQ 2	Massive mudstone	Inclined beds in 1.7 m section in downstream segment of exhumed point bar, Channel Body 1	✓	✓	✓	✓	✓
NSCQ 3			✓	✓	✓	✓	✓
NSCQ 4			✓			✓	
NSCQ 5			✓	✓	✓	✓	✓
NSCQ 6	Massive mudstone	Inclined beds in upstream segment of exhumed point bar, Channel Body 1	✓	✓	✓	✓	✓
NSCQ 7	Ripple cross-laminated sandstone	Inclined cemented beds in upstream segment	✓	✓	✓	--	--
NSCQ 8		Inclined cemented beds in midstream segment	✓	✓	✓	--	--
NSCQ 9	Massive mudstone	Thick sheet blanketing Channel Body 1	✓	--	--	--	✓
NSCQ 10	Pebble conglomerate	Basal deposits, Channel Body 2	✓	--	--	--	--
NSCQ 11	Ripple cross-laminated sandstone	Flat-lying cemented beds, Channel Body 3	✓	--	--	✓	--
NSCQ 12	Pebble conglomerate		✓	--	--	--	--

3.5 FIELD ANALYSIS

Description. -- At NSCQ, inclined bedsets of Channel Body 1 extend for ~300 m across a flat-lying area of four hectares (Fig. 3-1). The outcrop comprises scarps that represent the slightly eroded crests of dipping, cemented sandstone and poorly consolidated mudstone beds, with 1-12 m spacing between the more resistant sandstones (Figs. 3-2A, 3-3A). The scarps are curvilinear in overall planform with a radius of curvature of 140 m.

In the measured section (Fig. 3-2D), Channel Body 1 commences with a 24 cm sheet of pebble conglomerate composed of dolomite clasts with an average size of 0.5-3 cm (Gm: Table 3-2), overlain by a 6 cm lens of very fine- to fine-grained, ripple cross-laminated sandstone (Sr). The deposits mantle an erosion surface cut into red massive mudstone (Fm) with redoximorphic spots, slickensides, faint irregular mottles, and wedge-shaped peds. The mudstone and basal channel deposits are visible only in small outcrops scattered across the plain, precluding a fuller description.

Inclined heterolithic sets of mudstone and cemented sandstone (Thomas et al. 1987) downlap onto the coarse deposits and have a vertical extent of 2.2 m and an average dip of 14.5^{o}. They consist mainly of red-brown mudstone (Fm, >90% of strata), massive to weakly ripple cross-laminated, with thin lenses of very fine sandstone to siltstone (Fig. 3-3B-D), local root traces, poorly-developed slickensides, and abundant redoximorphic spots. Where the mudstone contains poorly-developed stratification, dips accord with those of the associated sandstone beds. Based on the average dip value and an estimated maximum ridge spacing of 12 m, the mudstone beds are up to 3 m thick measured orthogonal to bedding.

The inclined bedsets of cemented sandstone are erosionally based, very fine- to fine-grained, and up to 0.5 m thick. They extend to the surface of the plain with little change in thickness, forming scarps that partially protect the underlying mudstone and in places flatten out updip (Fig. 3-3B). They are ripple cross-laminated (Sr) and bed surfaces show straight-to-sinuous ridge-and-furrow forms attributed to climbing and non-climbing ripples, with paleoflow mainly directed obliquely up the inclined surfaces (compare red paleoflow arrows and strike of beds in Fig. 3-1). Other features include symmetrical ripples high on the surfaces, rill casts oriented down-dip, and elliptical scours oriented near-parallel to strike. Root traces low in the beds, vertical and horizontal burrows of *Taenidium barretti* / *Planolites montanus* (Baucon et al. 2014) and putative tetrapod tracks are present locally, as well as trackways of *Diplichnites gouldi* oriented parallel or oblique to the strike of the sandstones. Gypsum dikes up to 3 m long and 8 cm wide cut through the beds.

The inclined bedsets grade upward into a 4.4 m thick sheet of red-brown massive mudstone (Fm), consolidated at the base but more friable above, with carbonate nodules, redoximorphic spots, slickensides, and discontinuous 5 cm lenses of ripple cross-laminated siltstone (Fig. 3-2B and D). The mudstone is overlain erosionally by Channel Body 2, which commences with a 12 cm gray pebble conglomerate composed of 1-2 cm dolomite clasts (Gm). Above, a 1.5 m unit comprises steeply dipping (up to 18^{o}) heterolithic bedsets of very fine-grained sandstone, siltstone and mudstone (Sr and Fm: Fig. 3-2B). The sandstone is ripple cross-laminated with paleoflow along strike and dies out to the west into a 2 m unit of massive mudstone with poorly developed inclined beds. This is overlain abruptly by 1 m of laminated claystone (Fl) with red-brown, gray and yellow laminae, normally graded beds, and permineralized plant leaves.

Capping the outcrop is a 1.3 m erosionally based sheet sandstone (Channel Body 3). The sheet comprises scours filled with lenses of pebble conglomerate with 0.5-1 cm dolomite clasts and fine- to medium-grained, plane-laminated and ripple cross-laminated sandstone (Gm, Sh and Sr: Fig. 3-2C).

Interpretation. – For Channel Body 1, the curvilinear bedsets of inclined mudstone and sandstone strata, exposed across flat-ground, are interpreted as lateral-accretion deposits formed during the migration of a point bar, which is currently exhumed at surface. Based on paleoflow readings, the point bar was deposited by a northwesterly flowing meandering channel with a minimum estimate of bankfull depth, width and discharge of 2.2 m, 57 m and 64-127 m^3s^{-1}, respectively (Simon and Gibling in review). The basal coarse-grained deposits represent a channel lag formed during or shortly after erosional events. The underlying mudstones are interpreted as floodplain deposits modified to vertic paleosols, as indicated by slickensides and wedge-shaped peds; elsewhere at this site, similar pedogenic units were interpreted as paleo-Vertisols (DiMichele et al. 2006; Zhu 2015). The dolomite clasts were probably derived from the paleosols, although concretions were not observed in the outcrops.

For the inclined mudstone and cemented sandstone beds, the apparent absence of bedforms larger than ripples reflects a grain size at the lower limit of the stability field for dunes (Southard and Boguchwal 1990), precluding a full analysis of flow strength. Additionally, the massive appearance of the laterally accreted mudstone precludes identification of bedforms other than a few poorly preserved ripples; dunes were rarely identified in mudstone channel fills elsewhere in the formation (Simon and Gibling in review). For the cemented sandstones, the abundance of ripples may reflect low-flow conditions at the point of deposition during waning flow. The up-surface orientation of the ridge-and-furrow structures (Fig. 3-1) is attributed primarily to swept

ripples, which formed during waning flow as bedforms were stranded at high levels on the point-bar surface but continued to advance under water lower in the channel; helicoidal flow may also have contributed to this effect in the sinuous channel (Edwards et al. 1983; Simon and Gibling in review). Other sedimentological evidence indicates seasonal discharge variation. Following high discharge and ponding of flow, as indicated by symmetrical ripples high on the surfaces, rill casts and some small root traces low on inclined surfaces indicate waning flow, drainage of sediment, and probably periodic drying up of the channel.

As with the underlying mudstone beds, the thick sheet of mudstone blanketing Channel Body 1 is interpreted as floodplain deposits with paleo-Vertisols. Channel Body 2 is interpreted as a meandering-fluvial body with lag deposits and steeply dipping lateral-accretion deposits of mudstone and rippled sandstone. The overlying laminated mudstone is interpreted as an abandoned-channel fill laid down as fine, graded laminae during flow events, with additional deposition from suspension and leaves derived from the adjacent riparian vegetation (see detailed description of a similar unit at Colwell Creek Pond: Simon et al. 2016).

Channel Body 3 is interpreted as a sheet-like ephemeral channel that blanketed underlying floodplain and channel deposits. The coarser grain size, presence of scour-and-fill units, plane beds, and reworked dolomite clasts at several levels suggest that floods were high-energy and short-lived, capable of reworking dolomite from paleosols or channel banks (Simon and Gibling in review).

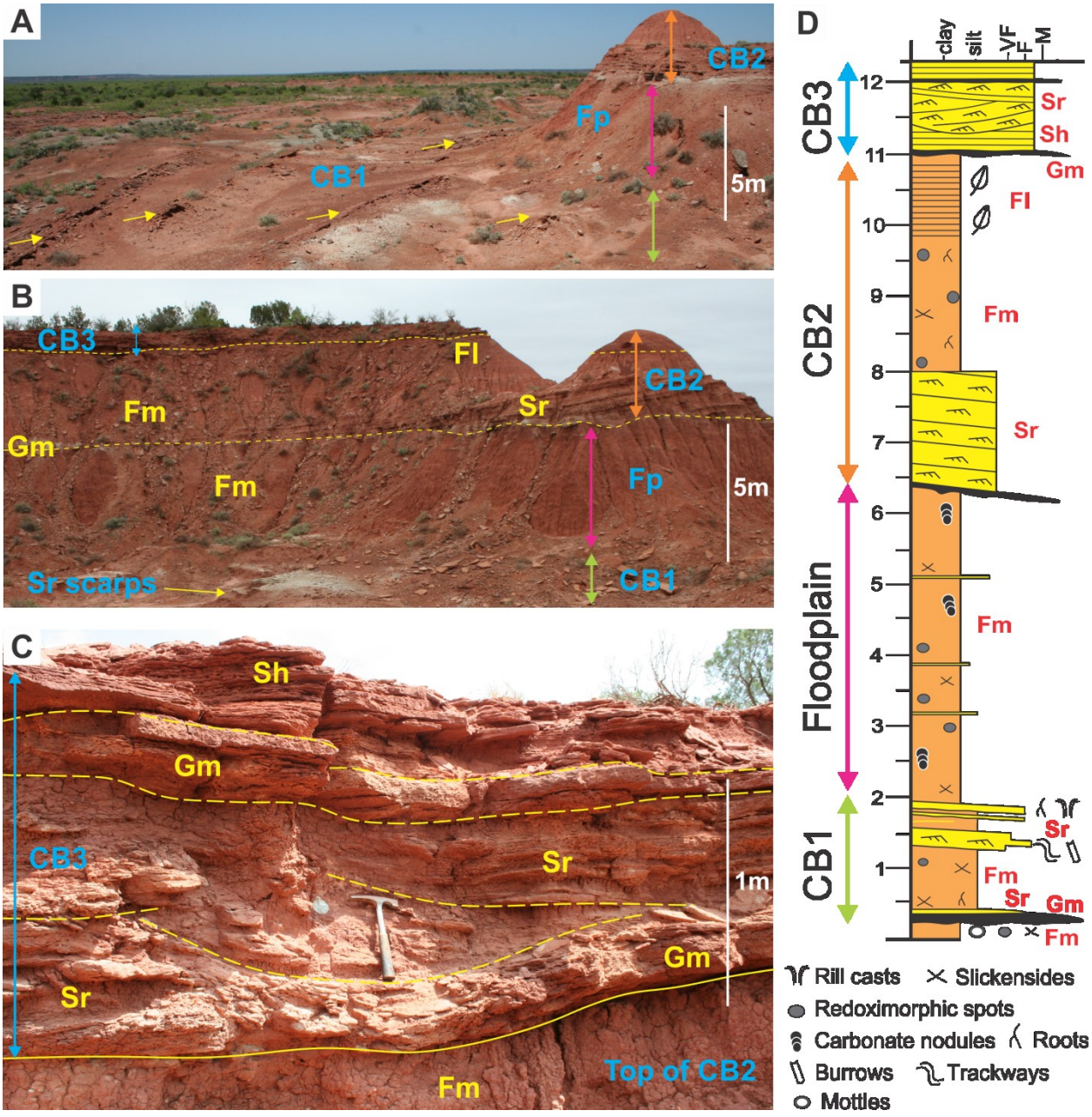

Figure 3-2 Field context of the exhumed point-bar deposits. The positions of the pictures are indicated in Fig. 3-1. (A) Oblique view of sandstone scarps (yellow arrows) in the exhumed point bar of Channel Body 1 relative to the cliff section at the upstream end. The inclined strata terminate upward into a thick sheet of massive mudstone interpreted as floodplain deposits (Fp), overlain by Channel Bodies 2 and 3. (B) Downview of cliff face section in A. Mudstone sheet (Fp) is cut by Channel Body 2 with steeply-dipping lateral accretion deposits of ripple cross-laminated siltstone and sandstone (Sr). The accretion deposits pass upward into massive mudstone (Fm), capped abruptly in the small dome -at right by laminated mudstone (Fl). Channel Body 3, tabular sandstone, forms the cliff top. (C) Close-up of Channel Body 3 with pebble conglomerate lenses (Gm) and plane-laminated (Sh) and ripple cross-laminated (Sr) sandstone filling shallow scours. (D) Composite log of the cliff section shows three channel bodies (CB 1, 2, 3) and intervening massive mudstone (Fp).

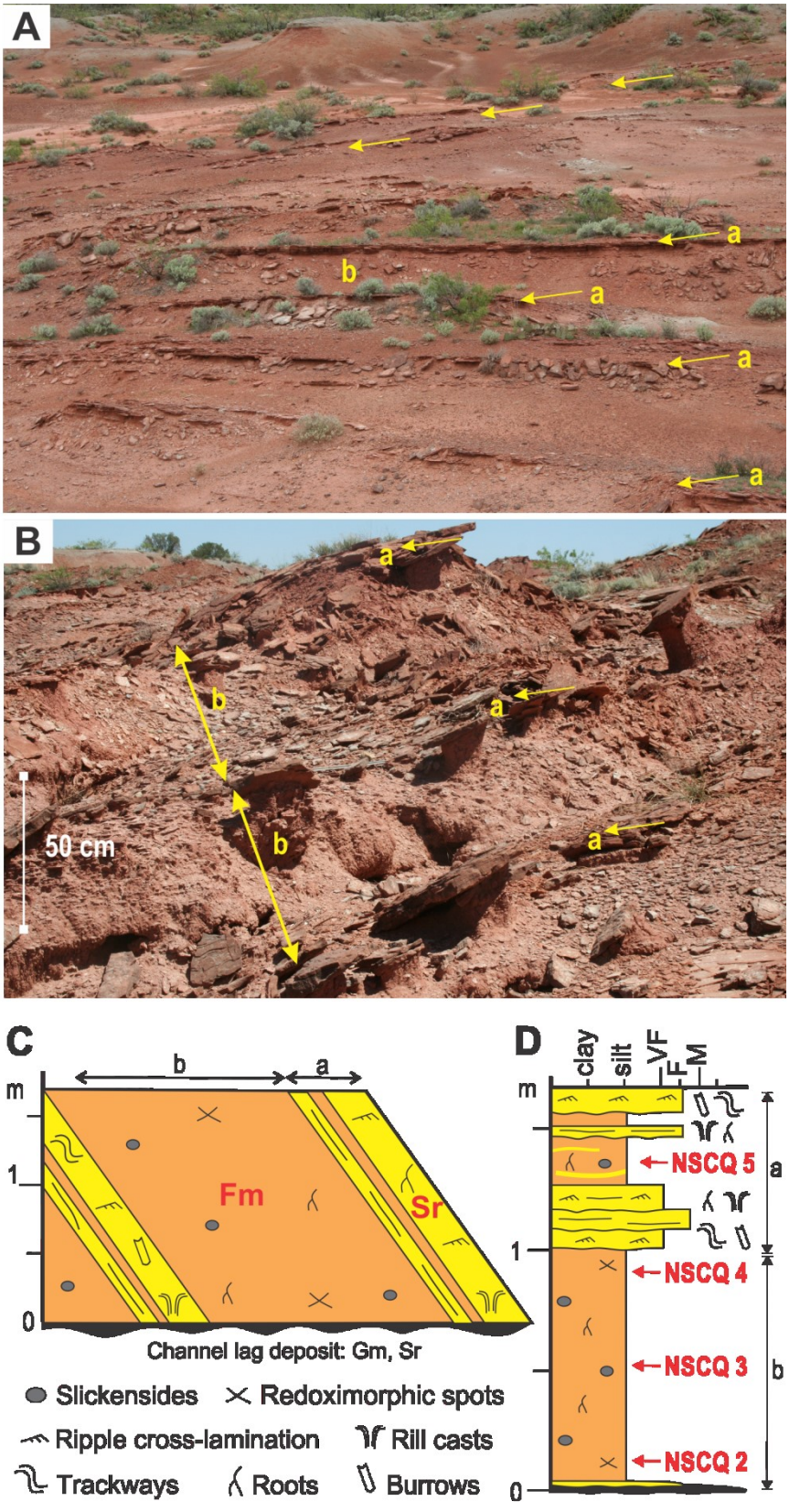

Figure 3-3 Sedimentology of the exhumed point bar at North Soap-Creek Quadrangle. (A) Oblique view of resistant, discontinuous sandstone scarps (a) separated by massive mudstones (b) that represent point-bar lateral-accretion deposits in near-horizontal strata, exposed on flat ground. The scarps in the foreground show a different orientation to those in the background, representing changes in point-bar accretion direction. (B) Inclined lateral-accretion deposits with resistant ripple cross-laminated sandstone units (a) separated by thicker intervals of poorly exposed mudstone (b). (C) Schematic diagram to show the relative thickness of the sandstone (a) and mudstone units (b). The basal contacts of the sandstone units are gradational or abrupt, and the sandstone beds contain rill casts, root traces, vertical burrows, and diplichnitid trackways. (D) Log of sandstone and mudstone units as measured in a strike exposure of inclined beds (Fig. 3-1), showing sample positions.

3.6 PETROGRAPHIC ANALYSIS

3.6.1 Thin sections of aggregate-rich mudstone. --- The mudstone units contain layers 0.7-1.5 mm thick composed of aggregates with minor amounts of matrix (68-76%), quartz (2-15%; a few grains with overgrowths), ferruginous grains (12-18%) and dolomite crystals (3-9%; Table 3-4; Fig. 3-4). Some aggregates contain small silicate and ferruginous grains. The quartz grains also form layers and lenses up to 0.2 mm thick that rest with abrupt or gradational contacts on aggregate-rich layers. Redoximorphic spots up to 3 mm in diameter extend across quartz and aggregate layers. Some layers of matrix-supported aggregates and mineral grains are present.

Table 3-4 Points and percentages for 400 points counted in thin sections of mudstone and cemented sandstone in channel deposits at North Soap-Creek Quadrangle.

Samples	Quartz	Dolomite	Ferruginous grains	Mud aggregates + clay matrix
Mudstone				
NSCQ 2	43 (11%)	13 (3%)	72 (18%)	272 (68%)
NSCQ 3	33 (8%)	34 (9%)	62 (16%)	271 (68%)
NSCQ 5	7 (2%)	22 (6%)	67 (17%)	304 (76%)
NSCQ 6	58 (15%)	12 (3%)	49 (12%)	281 (70%)
Sandstone				
NSCQ 7	174 (44%)	158 (40%)	12 (3%)	56 (14%)
NSCQ 8	243 (61%)	120 (30%)	20 (5%)	17 (4%)

The aggregates are variably gray or red-brown in plane-polarized light (Fig. 3-4A and D) and their boundaries are best seen in cross-polarized light (Fig. 3-4B, C and E). Some gray aggregates contain irregular patches of hematite. The aggregates are ellipsoidal to circular in cross-section, and they are sutured with concavo-convex, tangential and long contacts, with long

axes near-parallel or oblique to bedding (Fig. 3-4B). A small amount of hematite-rich clay matrix is present, with rims around some grains (Fig. 3-4C). The colour contrast between gray aggregates and red-brown rims and matrix is pronounced, whereas the red-brown aggregates commonly appear to merge with the matrix (Fig. 3-4C and E).

Medium crystalline, euhedral dolomite rhombs or patches are dispersed between the mud aggregates and are less than half the size of the aggregates (Fig. 3-4A and D). Ferruginous grains of similar size or slightly larger than the aggregates are common (Fig. 3-4B and D). They are typically more equant than the aggregates but range from ellipsoidal to sub-circular, with a few prismatic grains with sub-planar or curved boundaries (lower right in Fig. 3-4D). Long axes range from sub-parallel to oblique and locally perpendicular to bedding. Some contain embedded silt-sized quartz, and a few are slightly displaced along microfaults parallel to bedding. The varied degree of opacity (Fig. 3-4E) suggests that they contain varied amounts of hematite. Those with especially sharp outlines are probably small ferruginous concretions (see Discussion), but others may be iron-rich aggregates. Discrete, hematite-rich lenses up to 3 mm long and 0.5 mm thick are also common.

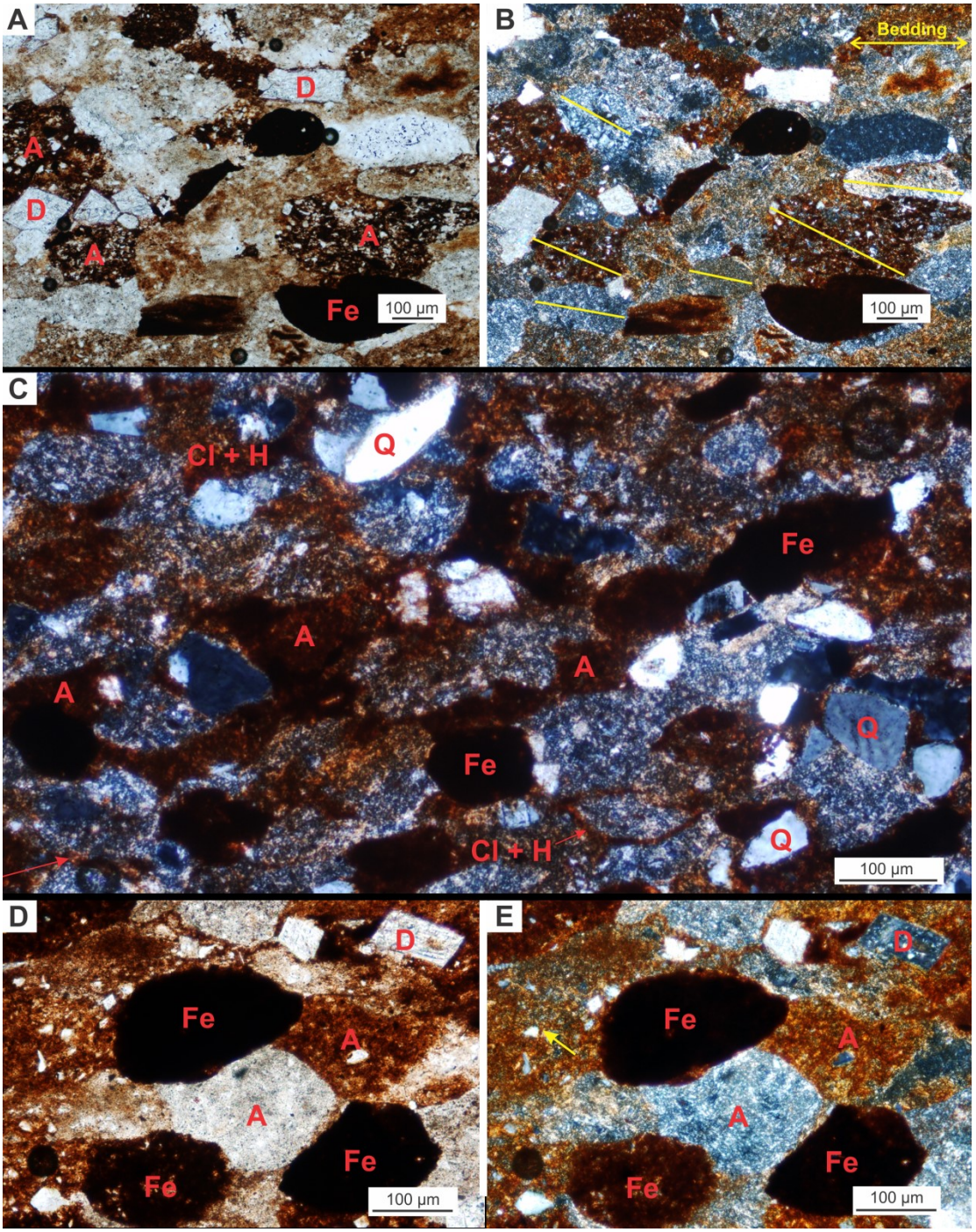

Figure 3-4 Petrographic features of massive mudstone beds in channel bodies at North Soap-Creek Quadrangle. Plane-polarized (A and D) and cross-polarized light (B, C, and E). (A, B) Sutured sand-sized mud aggregates with minor amounts of euhedral dolomite rhombs, ferruginous grains, and silt-sized quartz grains, some of which are embedded within the aggregates. The aggregates vary in proportions of clay, silt grains, and hematite and in color from red-brown to grey, as seen in plane-polarized light (A). Yellow lines in B denote the apparent long axes of some aggregates, which are oriented sub-parallel to oblique to bedding. (C) Subangular to angular sand-sized quartz grains between aggregates. Grey aggregates are prominent and locally have a thin rim of clay and hematite (red arrow). Red-brown aggregates vary from well preserved to strongly deformed. (D, E) Close-up of discrete, lensoidal aggregates with rounded ferruginous grains of similar size and dolomite crystals. Other areas (yellow arrow) represent sutured, less distinct aggregates of similar color. Samples are NSCQ 3 (A, B); NSCQ 6 (C); NSCQ 2 (D, E). A = aggregate; Cl = clay minerals; H = hematite; D = dolomite; Fe = ferruginous grain; Q = quartz.

3.6.2 SEM and XRD analysis of aggregate-rich mudstone. --- Preparation of polished sections for these soft materials resulted in partial plucking of aggregates between areas of more resistant detrital grains with interstitial clay (Fig. 3-5). Both plucked surfaces and imaging of broken rock surfaces (Fig. 3-6) yielded valuable information on aggregate texture and composition using SEM/EDS analysis.

The aggregates are mainly sutured together, and some show rims (arrowed in Fig. 3-5A) of clay and mica with a high iron content (FeO <35 %), probably hematite. Fractures are prominent between some aggregates; they may define boundaries between aggregates with indurated outer zones, but most lie within regions rich in detrital grains (Fig. 3-5A-C) and are probably artefacts of thin-section preparation. Within the aggregates, clay flakes a few microns in length are oriented sub-parallel to the major axis and packed around embedded detrital silt grains.

Detrital patches consist mainly of silt- to very fine-sand sized, angular to sub-rounded grains of quartz, K-feldspar and albite (Fig. 3-5B and D). Minor titania minerals, apatite, lithic fragments, and ferruginous and chlorite-rich grains were identified. Some ferruginous grains contain silt-sized quartz (Fig. 3-5C), and a few quartz grains have overgrowths. The detrital patches have an interstitial matrix of clay and hematite and are locally matrix-supported.

On broken mudstone surfaces, the aggregates emerge as rounded, sub-circular to bladed forms that are typically 75 to 250 μm long (Fig. 3-6A to C). EDS analysis shows that they contain discrete quartz grains and flakes of kaolinite, chlorite and illite (Fig. 3-6D), and they are surrounded by detrital grains, hematite and clay. Dolomite crystals are common as isolated, euhedral to subhedral rhombs with slightly pitted surfaces (Fig. 3-6E). Dolomite crystals with rims of hematite form a loosely interlocked cement in vugs up to 2 mm wide, and poikilotopic

dolomite cement encases detrital grains locally. The matrix contains rare patches of barite cement (Fig. 3-6F).

Based on XRD analysis, the <2μ fractions of the mudstone samples comprise illite, Fe-rich chlorite, kaolinite, and mixed-layer clays (Fig. 3-7). The mixed-layer clays were identified where profile and peak intensities changed during glycolation (red arrows in Fig. 3-7). The response to glycolation indicates that discrete smectite is not present and that illite and Fe-rich chlorite have some swelling potential.

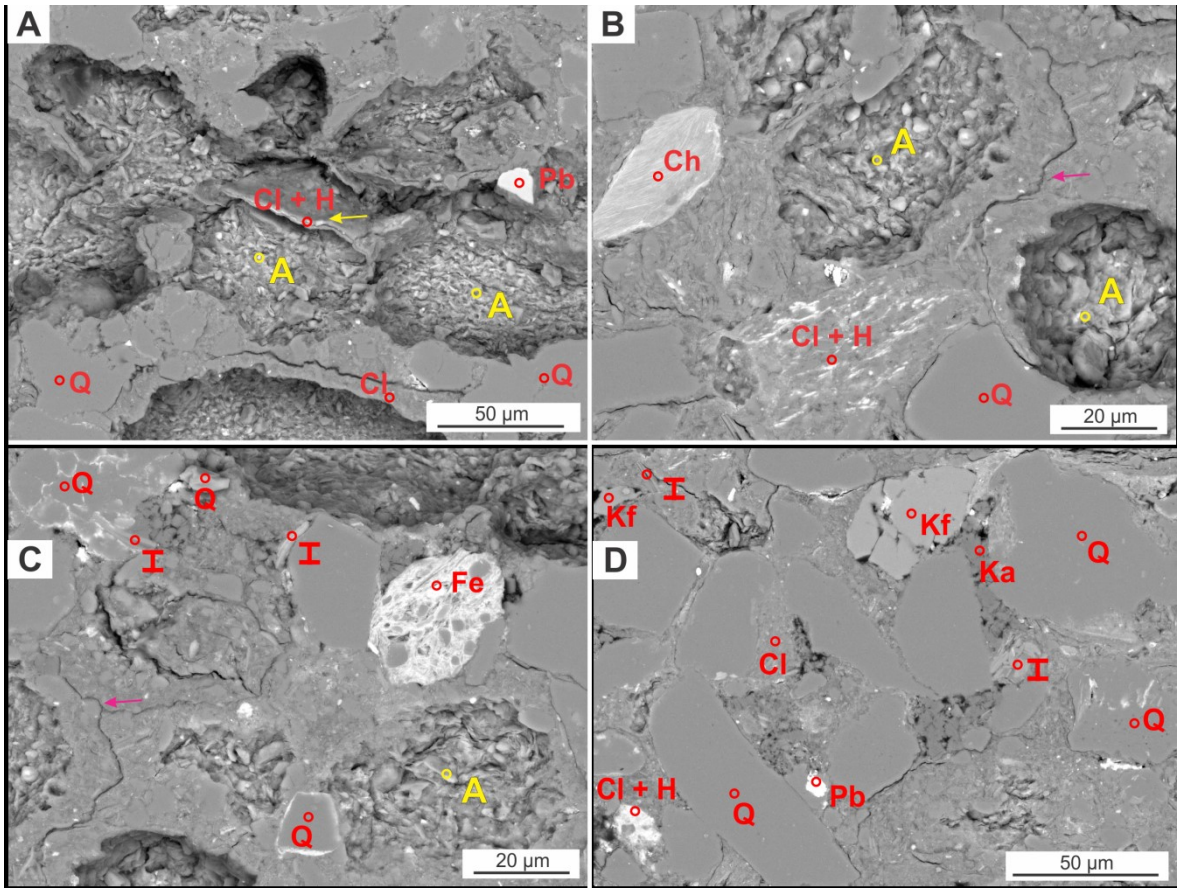

Figure 3-5 Backscatter images from a polished thin section of sample NSCQ 4. (A-C) Aggregates seen as elongate to sub-circular pits generated during thin-section preparation and polishing. Pits expose the fine internal features of the aggregates, which are composed of stacked clay flakes and silt-sized detrital grains. Surrounding elevated, more resistant areas comprise quartz, K-feldspar, illite, ferruginous grains, and altered chlorite in a matrix of clay and hematite. Aggregates are sutured with thin resistant clay rims (yellow arrow in A) or partially bordered by detrital grains. Fractures (pink arrows) may define aggregate boundaries or represent artefacts of the preparation process. (D) Subrounded, silt- to sand-sized quartz and K-feldspar grains in a matrix of clay and hematite. Kaolinite and illite are present in the pores between the grains. A = aggregate; Ch = chlorite; Cl = clay minerals; H = hematite; Fe = ferruginous grain; I = illite; Ka = kaolinite; Kf = K-feldspar; Q = quartz; Pb = lead fragments from section preparation.

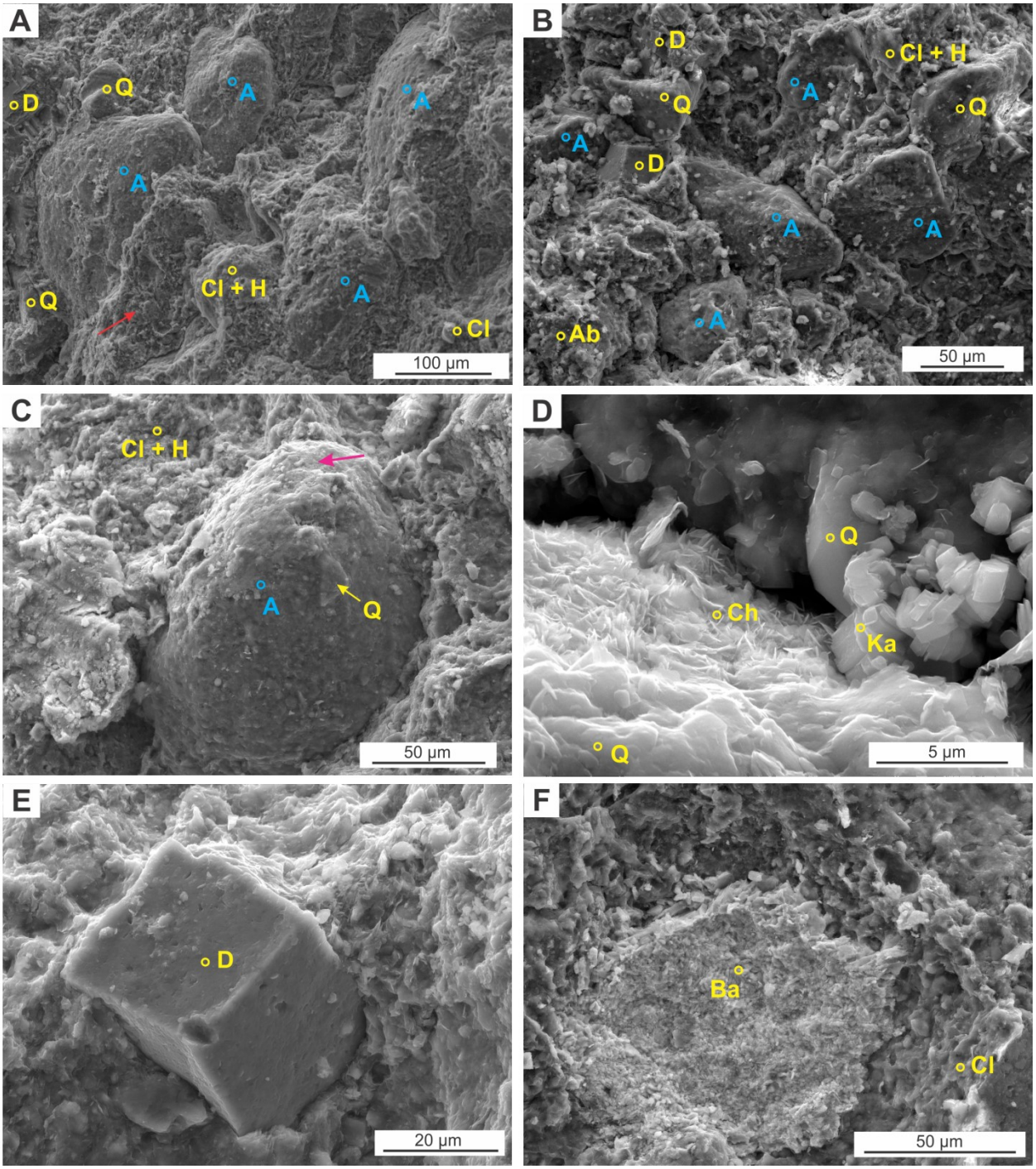

Figure 3-6 Backscatter images from broken mudstone surfaces. (A, B) Sand-sized mud aggregates with minor quartz and albite grains and euhedral dolomite crystals, in a matrix of clay and hematite. The aggregates are rounded with sub-circular, bladed and irregular forms, and EDS analysis indicates clay and quartz compositions. (C) Close-up of an aggregate nestled in a matrix of clay and hematite. The aggregate is composed of silt- and clay-sized grains of quartz, clay and hematite. (D) Close-up of top of aggregate in C (pink arrow), with chlorite, kaolinite and quartz; illite is also abundant but was not identified in this image. (E) Euhedral dolomite crystal with pitted, irregular surface. (F) Barite cement patch in clay matrix. Samples are NSCQ 2 (A, C, E); NSCQ 3 (B); NSCQ 5 (D, F). A = aggregate; Ab = albite; Ba = barite; Ch = chlorite; Cl + H = clay with hematite; D = dolomite; Ka = kaolinite; Q = quartz.

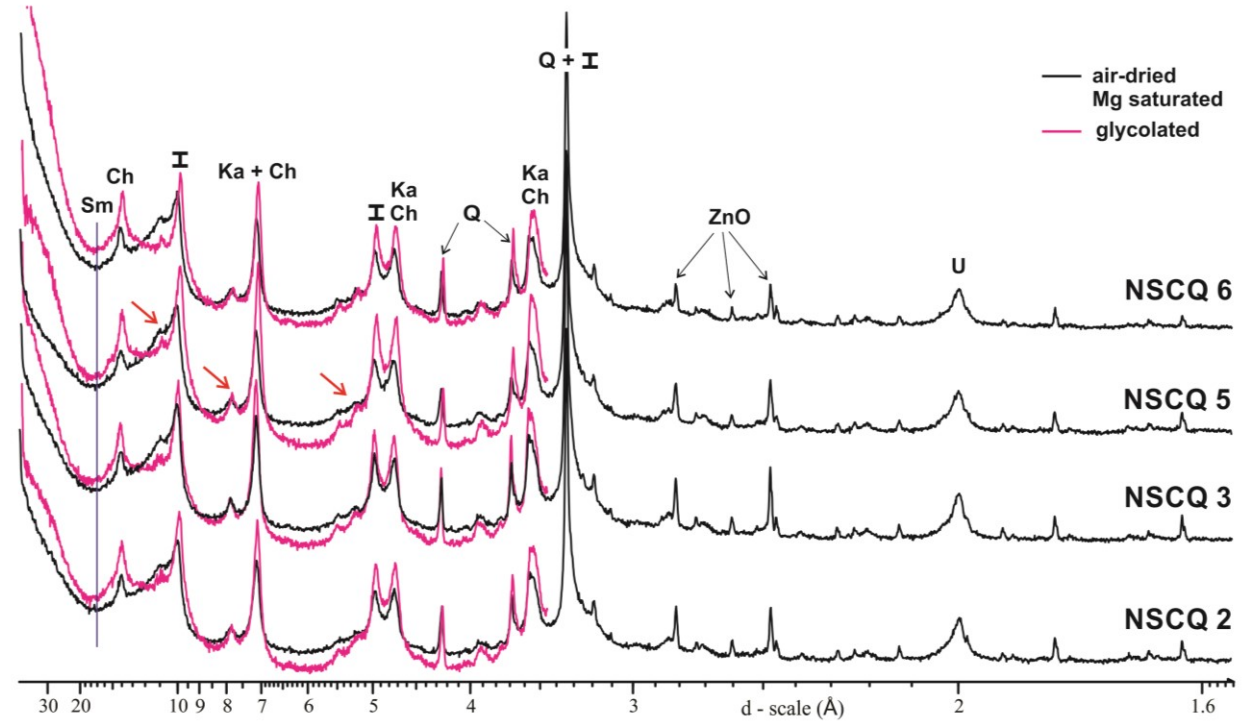

Figure 3-7 Diffractograms of <2µm clay fractions from four samples, in air-dried and glycolation modes. Illite, Fe-rich chlorite, kaolinite, and mixed-layer clays (red arrows) were identified. During glycolation, the peak intensity of illite and Fe-rich chlorite increased, suggesting some swelling potential. Glycol-treated samples with smectite should typically produce a strong 001 reflection at 16.9 Å (vertical blue line), but this was not observed in any samples. Sm = smectite; Ch = chlorite; I = illite, Ka = kaolinite; Q = quartz; ZnO = zincite standard; U = undifferentiated clay minerals.

3.6.3 Petrography of basal deposits, cemented sandstones, and mudstone sheets. – The coarse basal deposits in Channel Bodies 1 and 2 comprise patches of interlocked coarsely crystalline euhedral (planar-e) to subhedral (planar-s) dolomite rhombs and finely crystalline dolomite clasts (Fig. 3-8A-C). They are associated with minor amounts of quartzose grains, clay minerals and patchy gypsum, barite and dolomite cements (Fig. 3-8B and C)

The cemented sandstones comprise quartz, feldspar and ferruginous grains cemented by poikilotopic dolomite with a matrix of illite, Fe-rich chlorite, kaolinite, mixed-layer clay and hematite (Fig. 3-8D). Point counts indicate 44-61% quartz, 30-40% dolomite cement, 4-14% mud aggregates, and 3-5% ferruginous grains (Table 3-4).

The mudstone sheet that caps Channel Body 1 is composed of silt-sized quartz, hematite, illite, Fe-rich chlorite, kaolinite and mixed-layer clay, with isolated or grouped euhedral dolomite rhombs in the matrix or filling vugs. Based on XRD analysis, clay compositions are similar to those of the aggregates in Channel Body 1.

The tabular cemented sandstones in the Channel Body 3 consists of quartzose grains floating in dolomite cement with a hematite-rich clay matrix (Fig. 3-8E). The conglomerate lenses are composed of inequigranular dolomite rhombs that form patches or fill vugs in a hematite-rich clay matrix with minor amounts of quartzose grains (Fig. 3-8F).

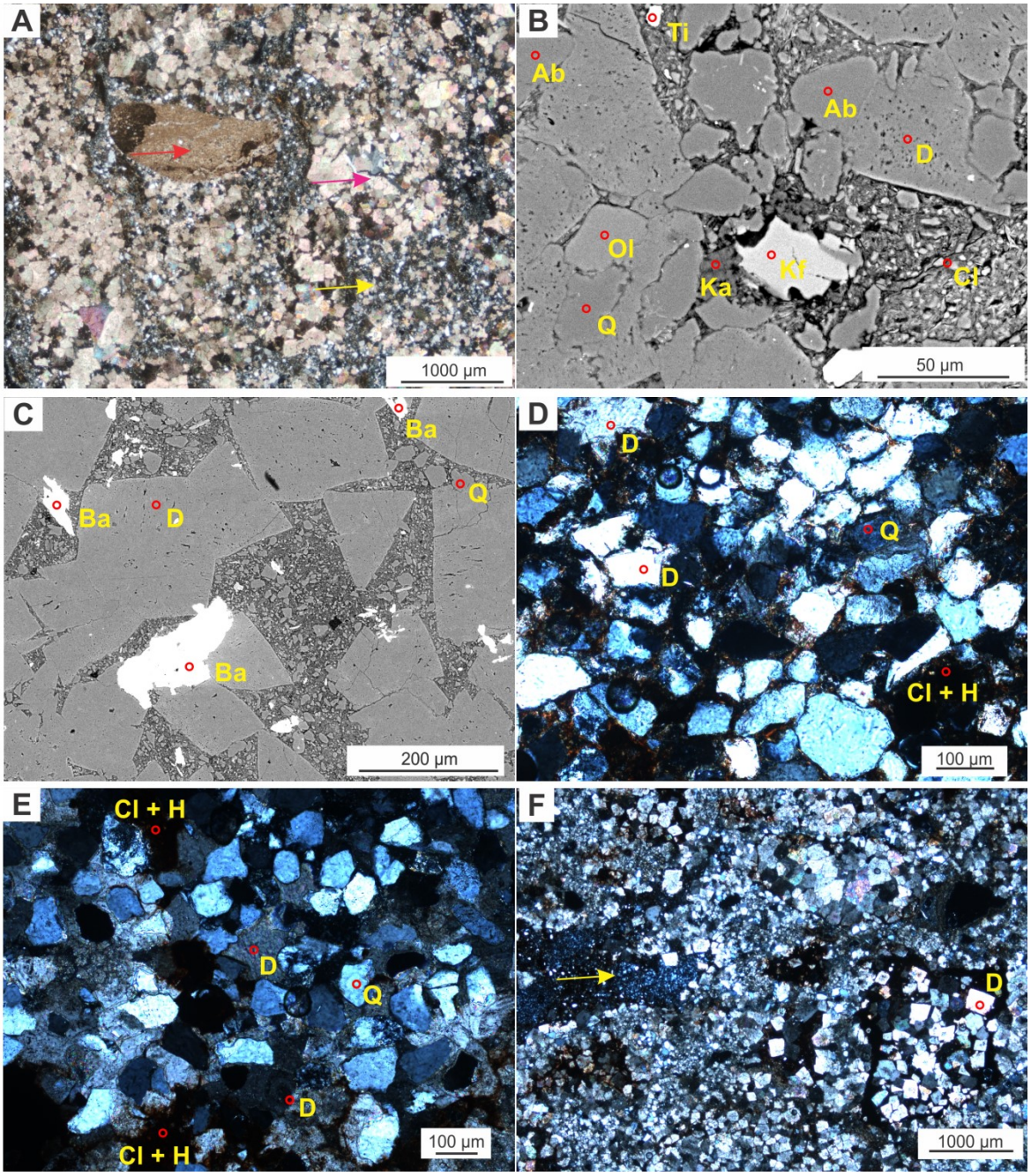

Figure 3-8 Petrography of coarse-grained basal deposits (A-C), inclined cemented sandstones (D) in Channel Body 1, flat-lying, cemented sandstone (E) and conglomerate lenses (F) in Channel Body 3. (A) Pebble conglomerate composed of finely crystalline dolomitic clasts (red arrow) and interlocked patches of euhedral to subhedral dolomite rhombs (pink arrow) with very fine-grained sand and silt grains of quartz and feldspar, minor heavy minerals and clay matrix (yellow arrow). (B) Backscatter image showing grains of quartz, albite, oligoclase, K-feldspar and titania minerals cemented by dolomite, with clay minerals and booklets of kaolinite. (C) Backscatter image showing medium to coarsely crystalline, euhedral dolomite with irregular patches of barite and a matrix of clay and silt-sized quartz grains. (D) Very fine-grained to silt-sized quartzose grains with patches of dolomite cement and a matrix of hematite and clay. (E) Very fine-grained sand to silt-sized quartzose grains floating in dolomite cement with a matrix of hematite and clay. (F) Inequigranular dolomite rhombs in hematite matrix, forming patches or filling vugs with minor amounts of quartzose grains and clay minerals (yellow arrow). Samples are NSCQ 1 (A-C), NSCQ 7 (D), NSCQ 11 (E) and NSCQ 12 (F). Q = quartz; Ab = albite; Cl = clay minerals; Cl + H = clay with hematite; Ol = oligoclase; Ti = titania minerals; D = dolomite; H = hematite; Ka = kaolinite; Kf = K-Feldspar; Ba = barite. Cross-polarized light (A, D, E and F).

3.6.4 Grain size of aggregates and quartz. --- For the aggregate-rich samples, analysis is based on uncorrected thin-section measurements. The mean major axis length of aggregates is 0.163 mm and of associated quartz grains is 0.067 mm (Table 3-5). Samples NSCQ 2 and 5 contain larger mud aggregates and smaller grains of quartz than samples NSCQ 3 and NSCQ 6, suggesting that the samples are a mixture of the two components derived from separate sources. For the cemented sandstones with a high proportion of quartz grains (Table 3-4), the mean length of 600 quartz grains is 0.113 mm, i.e., 1.6 times larger than the quartz grains associated with the aggregates.

Table 3-5 Raw major-axis measurements for 300 quartz grains and 300 aggregates in four thin sections (NSCQ 2, 3, 5, 6) and 300 quartz grains only in two thin sections (NSCQ 7, 8) from North Soap-Creek Quadrangle.

Sample	**Major Axis of Quartz (mm)**			**Major Axis of Aggregates (mm)**		
	Mean	St. Dev.	Range	Mean	St. Dev.	Range
	Aggregate-rich Mudstone					
NSCQ 2	0.066	0.021	0.023- 0.194	0.153	0.038	0.068- 0.319
NSCQ 3	0.070	0.017	0.027-0.130	0.147	0.033	0.071- 0.252
NSCQ 5	0.053	0.034	0.016- 0.316	0.214	0.072	0.076- 0.708
NSCQ 6	0.079	0.018	0.040- 0.147	0.139	0.028	0.074- 0.236
Mean	**0.067**	0.025	0.023- 0.316	**0.163**	0.055	0.064- 0.708
	Cemented Sandstone					
NSCQ 7	0.132	0.024	0.076- 0.217	--	--	--
NSCQ 8	0.095	0.012	0.068- 0.138	--	--	--
Mean	**0.113**	0.027	0.068- 0.217			

Using the correction method of Johnson (1994) for the aggregate-rich samples, the compacted aggregates have a mean corrected major-axis length of 0.212 ± 0.071 mm (2.281 ± 0.422 φ), which corresponds to fine sand (Table 3-6; Fig. 3-9A) with a sorting estimate of very well sorted. In contrast, the associated quartz grains are much smaller, with a mean major-axis length of 0.087 ± 0.033 mm (3.601 ± 0.571 φ), which corresponds to very-fine sand (Table 3-6; Fig. 3-9B). Quartz grains in the cemented sandstones have a mean corrected major-axis length of 0.147 ± 0.035 mm (2.780 ± 0.325 φ; Table 3-6; Fig. 3-9C). Both suites of quartz grains have a sorting

estimate of moderately sorted. The quartz population associated with aggregates is positively skewed with a tail of fine silt particles (mostly coarse silt), whereas the quartz population in the cemented sandstones is negatively skewed.

The corrected mean nominal diameter of the mud-aggregate population is 0.155 ± 0.052 mm (2.731 ± 0.422 φ; Table 3-6). The values for populations of quartz grains from the mudstone beds and cemented sandstone are 0.064 ± 0.024 mm (4.051 ± 0.571 φ) and 0.108 ± 0.025 mm (3.254 ± 0.325 φ), respectively.

Correcting for flattening, the nominal diameter of the aggregate population is 0.133 ± 0.044 mm (2.937 ± 0.400 φ; Table 3-6). Using an approach based on the ratio of the minor to the major axes measured in thin sections, the minor axes of the aggregates are on average 0.57 times the length of the major axes (major: minor axis ratio 1.75), with a wide range of values (Fig. 3-9D). If on average Da = Db = 1.0 mm and Dc = 0.57 mm, an average aggregate now has a nominal diameter of 0.829 mm and an initially spherical grain 0.829 mm in diameter would have extended its long axis by 17.1% during flattening. Based on Johnson's (1994) approach, the aggregates have a corrected mean long-axis length of 0.212 mm (Table 3-6) which, reduced by 17.1%, yields a mean long-axis length of 0.176 mm prior to compaction, in the fine sand range.

A plot of aggregate size in phi (corrected using Johnson's method) against minor:major axis ratio shows no apparent relationship between aggregate size and shape (Fig. 3-9E). This suggests that grains were variably compressed, irrespective of their size.

In view of the complex problems associated with thin-section analysis and flattening, no unique solution was possible to assess the original size of the aggregates. However, the results using several approaches suggest that the aggregates were originally of fine-sand grade, two to three

times the size of the associated quartz grains in the same samples, and about 1.2 to 1.4 times larger than quartz grains in cemented sandstones. Quartz grains in the cemented sandstones are about 1.7 times larger than those associated with the aggregates.

Table 3-6 Estimated grain-size parameters for 1200 quartz grains and 1200 aggregates in four samples (NSCQ 2, 3, 5, 6) and 600 quartz grains in two samples (NSCQ 7, 8; Quartz_ cemented) of channel deposits from North Soap-Creek Quadrangle. See text for description of approaches used.

Grain size Estimates		**Aggregate-rich Mudstone**				**Cemented Sandstone**	
		Aggregates		**Quartz**		**Quartz**	
		mm	**phi**	**mm**	**phi**	**mm**	**phi**
Corrected Length of Major Axis[1]	Mean	**0.212**	2.281	**0.087**	3.601	**0.147**	2.780
	St. Dev.	0.071	0.422	0.033	0.571	0.035	0.325
	Range	0.088-0.92	0.098-3.48	0.021-0.411	1.262-5.568	0.088-0.282	1.807-3.485
Corrected Nominal Diameter[1]	Mean	**0.155**	2.731	**0.064**	4.051	**0.108**	3.254
	St. Dev.	0.052	0.422	0.024	0.571	0.025	0.325
	Range	0.06-0.673	0.055-3.928	0.02-0.30	1.71-6.018	0.064-0.206	2.281-3.959
Nominal Diameter for Flattened Aggregates[2]	Mean	**0.133**	2.937	--	--	--	--
	St. Dev.	0.044	0.400	--	--	--	--
	Range	0.059-0.666	0.574-3.994	--	--	--	--
Corrected Length of Major Axis for Flattened Aggregates[3]	Mean	**0.176**	2.51	--	--	--	--

[1] Correction made to mean length of major axes measured in thin sections (Johnson 1994).
[2] Long and intermediate axis lengths are assumed to be equal for flattened grains.
[3] A theoretical measure based on mean ratio of the length of the minor and major axes measured in thin sections.

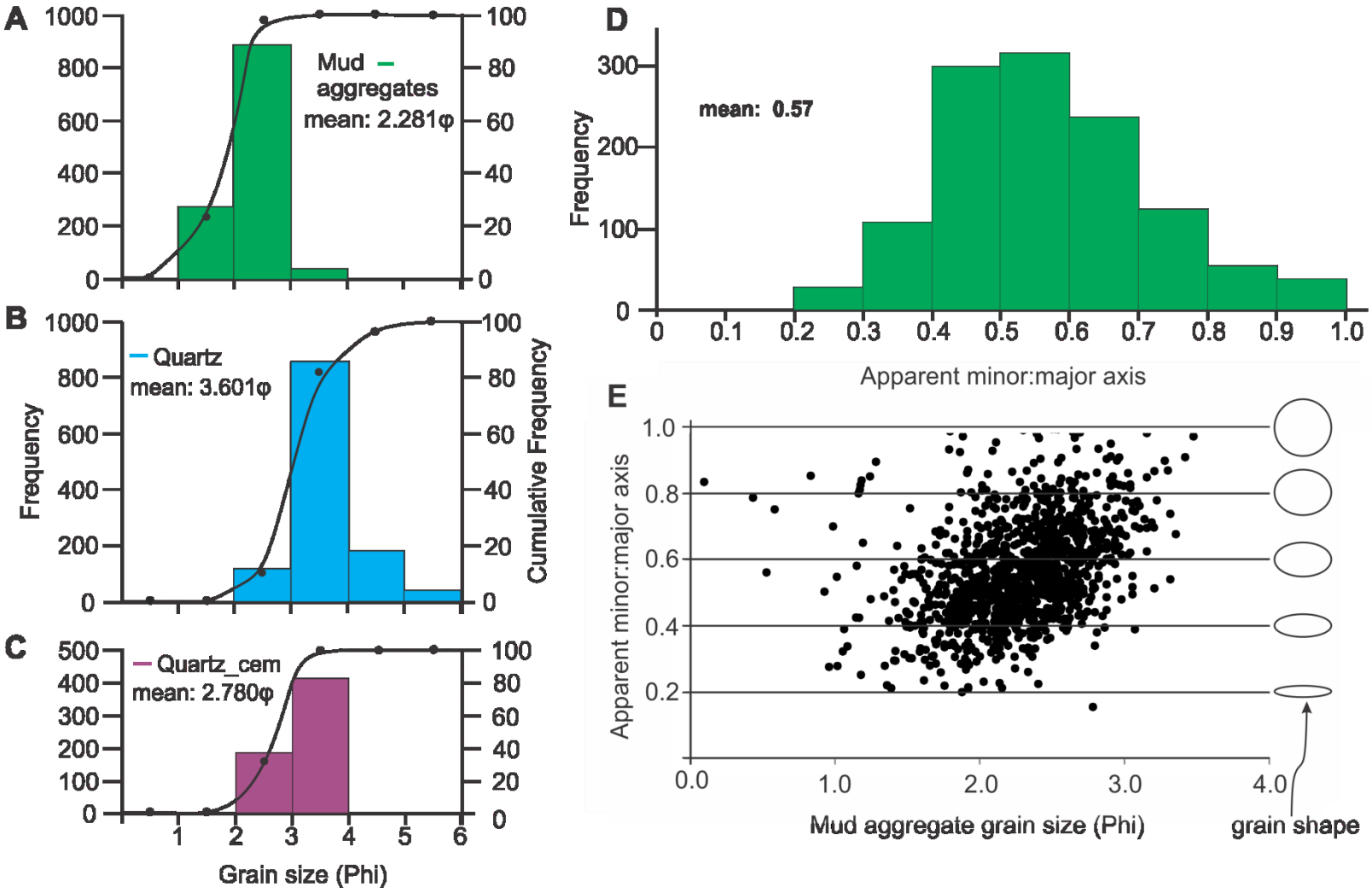

Figure 3-9 Grain-size distribution and cumulative frequency curves of 1200 mud aggregates (A), 1200 quartz grains from the same beds as the mud aggregates (B), and 600 quartz grains from a cemented sandstone layer (C) in phi units. The corrected lengths of the major axes are used as the sizes of the individual mud aggregate and quartz grains, and the mean values are from Table 3-6, corrected based on the method of Johnson (1994) as set out in the text. (D) Histogram of the ratio of the apparent minimum to maximum axis of the 1200 mud aggregates. The mean ratio is 0.57, and the data are positively skewed with an excess of grains with a ratio up to 1. (E) Plot of mud aggregate grain size versus the ratio of the apparent minimum to maximum axis for 1200 grains; little correlation between shape and size is apparent for the bulk of grains between 2 and 4 phi.

3.7 DISCUSSION

3.7.1 Origin of Mud Aggregates

In central Australia, mud aggregates are widely recognised in modern channel and floodplain deposits (Nanson et al. 1986; Rust and Nanson 1989; Maroulis and Nanson 1996; Tooth and Nanson 2000) and in upland areas (Wakelin-King and Webb 2007a,b). Climatic conditions are semi-arid to arid and strongly seasonal, with annual rainfall ranging from 120 to 500 mm in the Channel Country of Queensland (Gibling et al. 1998) and 200 mm with an average annual potential evaporation of ~2800 mm at Fowler Creek, New South Wales (Wakelin-King and Webb 2007a,b). Although aggregates may form during bank collapse (e.g., Müller et al. 2004), most are attributed to pedogenic processes, formed when soils with swelling clays repeatedly expand and contract during seasonal wetting and drying (Rust and Nanson 1989; Loch 1991). They may also originate as fecal grains or eolian pellets (Bowler 1973). However, Rust and Nanson (1989) suggested that (a) the abundance, variable size, and angular nature of freshly released aggregates argue against a biogenic origin, especially in dry climatic conditions, and (b) eolian sediments are uncommon in Australian rivers and tend to occur with hematite-coated quartz grains.

The NSCQ aggregates are attributed largely to pedogenic processes operative under relatively arid, seasonal conditions. They are relatively similar in form and size, and consist of densely packed clay with flakes wrapped around embedded quartz grains, features common to many paleosols. They are accompanied by ferruginous clasts, some of which probably formed as soil concretions. Channel Body 1 cuts into red paleosols with slickensides and wedge-shaped peds indicative of shrink-swell processes, from which some aggregates may have been derived. No search was made for aggregates within *in situ* paleosols, but paleo-Vertisols, Argillisols and

Calcisols are present in the Clear Fork Formation and, along with plant taxa, suggest seasonal, relatively arid conditions (Tabor and Montañez 2004; DiMichele et al. 2006; Chaney and DiMichele 2007). Although invertebrate trace fossils are present, they are not abundant, and a biogenic origin for most of the aggregates is unlikely (see also Müller et al. 2004). Previous Clear Fork studies have hypothesized that microbial activity played a key role in the preservation of plant leaves (Looy 2013), but the contribution of micro-organisms to aggregate formation is not known. Eolian deposits were not unequivocally identified at NSCQ or elsewhere in the formation, and hematite-coated quartz grains (commonly associated with eolian clay pellets: Rust and Nanson 1989) were not observed in the NSCQ deposits. The modest amount of bedrock-derived grains and the presence of relatively unaltered feldspars and other detrital grains preclude aggregate formation through the alteration of unstable grains during burial of the channel fills.

In other parts of the formation, larger and more irregular mud clasts in basal channel deposits were probably eroded from cutbanks. Disrupted mudstones with desiccation cracks and mud fragments are present in basal channel deposits elsewhere (Simon and Gibling in press).

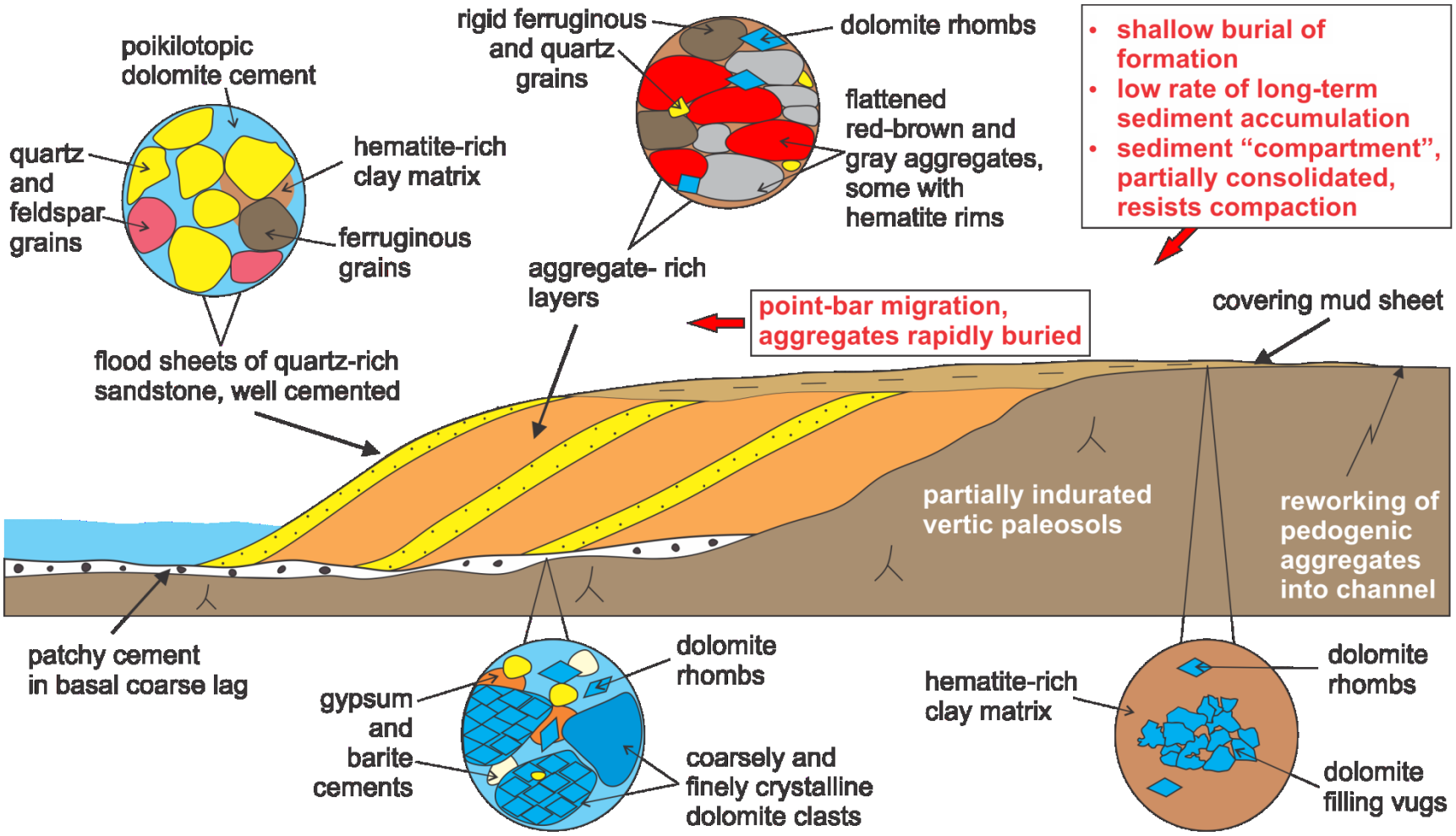

Figure 3-10 Model for preservation of aggregates through point bar migration and rapid sediment burial within a "compartment" of relatively indurated alluvial sediments. Circles show petrographic sketches for stratal components, with modest to pervasive early cementation of sediments that would have aided resistance of the aggregates to compaction. Not drawn to scale.

3.7.2 Contribution of Smectite to Aggregate Formation

The formation of pedogenic aggregates is widely understood to require clay-rich soils with at least a minor amount of swelling clay (Rust and Nanson 1989). Expandable, montmorillonite-rich (smectite) clays with minor kaolinite were identified at several Australian sites with aggregates (Maroulis and Nanson 1996; Wakelin-King and Webb 2007a, b), but kaolinite predominates elsewhere (Hallsworth and Beckmann 1969; Nanson et al. 1988; Rust and Nanson 1989, 1991). Illite is a major component of Vertisols in southern Australia (Norrish and Pickering 1983) and is co-abundant with kaolinite in parts of northern Australia (Hubble 1984). Based on these examples and the variable clay composition of Vertisols generally (Coulombe et al. 1996; Southard et al. 2011), smectite, especially in large quantities, may not be *required* to generate mud aggregates.

At NSCQ and throughout the Clear Fork Formation, clays are dominated by illite, Fe-rich chlorite, and kaolinite with some mixed-layer clays. Discrete smectite was not identified in the aggregates at NSCQ, nor in channel deposits elsewhere in the formation, and previous paleosol studies indicate that smectite is rare as a discrete mineral or is present in modest amounts in mixed-layer clays (Zhu 2015). For the NSCQ samples, the shift in peak positions of illite and Fe-rich chlorite during glycolation (Fig. 3-7) suggests that these clays would have experienced volume changes during wetting and drying, and their presence may have facilitated aggregate formation; additionally, the mixed layer clays probably had some swelling potential. For the Triassic Lunde Formation, Müller et al. (2004) noted a high illite and relatively low smectite and interlayered illite/smectite content in some aggregate-bearing samples.

The absence of discrete smectite in the aggregates and elsewhere in the Clear Fork Formation may reflect parent material, climatic conditions, and/or burial diagenesis. The eroding parent

material commonly controls the clay mineralogy of modern surficial sediment. In the Mississippi River Basin, smectite-rich clays are abundant in western regions with Tertiary and Cretaceous rocks, whereas an illite-chlorite-kaolinite assemblage is prominent in eastern regions with Paleozoic rocks (Potter et al. 1975). Piper and Slatt (1977) documented a marine illite-chlorite assemblage adjacent to metamorphic terrains in eastern Canada, with kaolinite adjacent to younger sedimentary rocks. Climatic changes can also modify clays. Srivastava et al. (1998) noted that, during arid conditions, biotite may weather to vermiculite and smectite in soils, whereas warmer and more humid conditions result in smectite-kaolinite mixed clays and ultimate alteration of smectite to kaolinite. Under mildly alkaline conditions (pH: 9-10), smectite can be altered to authigenic minerals (e.g. Fe-illite, analcime, and K-feldspar) over timescales <100 ka in very rare cases (Hay et al. 1991; Savage et al. 2010). Laboratory experiments have shown that illitization of smectite can occur during wetting and drying cycles in the presence of a potassium source (Mamy and Gaultier 1975; Eberl et al. 1986, 1993; Mora et al. 1998). During deep burial, illitization of smectite may take place (Dunoyer de Segonzac 1970; Rust and Nanson 1989).

For the Clear Fork Formation, the scarcity of smectite may be related to Precambrian and Paleozoic bedrock sources in the Wichita, Arbuckle and Ouachita uplands, which probably yielded predominantly illite, chlorite and kaolinite. Burial was relatively shallow and did not achieve a maturation level associated with the smectite-to-illite transition (Heroux et al. 1979); additionally, well-preserved feldspar and biotite in the strata and minimal evidence for pervasive alteration and cementation argues against deep-burial diagenesis and illitization. Despite a paucity of smectite in some intervals, Müller et al. (2004) found little indication that smectite had converted to illite during burial diagenesis of the aggregate-bearing Lunde Formation.

3.7.3 Entrainment of Aggregates and Quartz

The nature of the lateral-accretion deposits indicates that flow conditions and sediment sources varied periodically. During lengthy periods, aggregates appear to have been supplied in abundance from nearby paleosols and were reworked into thick layers on the point bars, probably by low-magnitude floods that were largely confined to the channel. In contrast, thin, erosionally based sandstone bedsets with near-constant thickness extend to high levels in the lateral-accretion sets and indicate shorter periods of flow that reached or exceeded bankfull levels. These high-discharge periods brought quartz-rich sediment directly from the uplands or remobilised sediment stored within the channels or elsewhere in the landscape (Simon and Gibling in review).

Due to their lower density, aggregates in modern settings are transported as bedload along with denser quartz, feldspars, and ferruginous clasts of smaller size (Nanson et al. 1986). Maroulis and Nanson (1996) conducted flume experiments that used aggregates collected in central Australia. The aggregates had a density of 2270-2310 kgm^{-3}, 15% less than quartz with a density of 2660 kgm^{-3}, and the samples had a mean d50 value from sieving of 0.13 mm, in the fine-sand range and similar to the size of aggregates in the present study. They found that, although bedform transitions accorded closely with those for quartz-rich sediment in bedform-existence diagrams (see Southard and Boguchwal 1990), the aggregates were entrained at flow velocities of <0.1 ms^{-1} at shallow water depths, indicating a much lower entrainment threshold than previously documented for quartz-rich sediment (Maroulis and Nanson 1996). Suspended sediment progressively generated by aggregate attrition settled on the bed, increasing the entrainment threshold.

The grain-size analysis of the NSCQ aggregates and quartz allows some assessment of entrainment thresholds for the sediment types (Table 3-7). Based on the Shields equation, the critical shear stress for aggregates with a mean corrected long-axis dimension of ~0.176 mm ranges from 1.58-1.63 $gcm^{-1}s^{-2}$, depending on the density of the grains [2.27-2.31 gcm^{-3} (Maroulis and Nanson 1996)], which corresponds to a critical flow velocity for entrainment of 1.26-1.28 cms^{-1}. For the population of quartz grains with a corrected mean long-axis dimension of ~0.087 mm, the critical shear stress and flow velocity range from 1.53-2.32 $gcm^{-1}s^{-2}$ and 1.24-1.52 cms^{-1}, respectively, depending on the value of the dimensionless Shields parameter which varies when the quartz population is considered as a mixture of very fine sand and silt. In comparison, quartz grains within the cemented sandstones with a corrected mean long-axis dimension of ~0.147 mm would have needed a critical shear stress and flow velocity of 1.71 $gcm^{-1}s^{-2}$ and 1.31 cms^{-1} for entrainment, respectively.

Table 3-7 Estimation of critical shear stress and flow velocities required for entrainment of aggregates and quartz populations. The dimensionless Shields parameters were obtained from Julien (1995) where coarse silt, very fine and fine sand have values of 0.165, 0.109 and 0.072, respectively. The grain density for the aggregates and quartz grains were obtained from Maroulis and Nanson (1996) and Paphitis (2001), respectively.

Sample population	**Unitless Shields parameter**	**Grain density gcm^{-3}**	**Grain size cm**	**Critical shear stress $gcm^{-1}s^{-2}$**	**Critical flow velocity cms^{-1}**
Aggregates	0.072	2.27	0.0176	1.58	1.26
	0.072	2.31	0.0176	1.63	1.28
Quartz with aggregates	0.109	2.65	0.0087	1.53	1.24
	0.165	2.65	0.0087	2.32	1.52
Quartz in cemented sandstone	0.072	2.65	0.0147	1.71	1.31

Although these values are not tightly constrained, they suggest that both quartz grains and aggregates could have been entrained at very low flow velocities, in the order of 1.2-1.5 cms^{-1}. Despite the differing grain density and size of associated aggregates and quartz grains in the mudstones, these varied grain populations were probably close to hydraulic equilibrium at the

time of entrainment. This result reflects in part the increase in critical shear stress τ_{ci} for smaller grains in imperfectly sorted grain populations. Larger grains project into the turbulent flow and experience a greater hydrodynamic force for a given shear stress, whereas smaller grains are shielded by the larger grains and require a higher critical shear stress for entrainment (Julien 1995).

The calculations yield estimates only for entrainment and not for the maximum shear stress and flow velocity experienced by the grains. For quartz grains with a diameter of ~0.15 mm and a water depth of 1 m, ripples would be the stable bedform at a velocity of up to ~1 ms^{-1} (Southard and Boguchwal 1990), considerably higher for the NSCQ channel with an estimated depth of 2.2 m. In view of the distance from upland source areas (Fig. 1-2A), it is probable that the maximum size of available bedrock-derived grains was small, well below the size that the flows were capable of transporting (McKee et al. 1967). Nevertheless, in contrast to the sheet sandstone of Channel Body 3, Channel Body 1 contains little indication upper flow regime conditions, such as plane beds or prominent erosion surfaces within the channel fill, suggesting that flow strength was modest. In this respect, the channel dynamics match the modest levels of flow typical of the Channel Country rivers of Australia (Gibling et al. 1998).

The matrix of the aggregate beds represents a washload, perhaps supplemented by suspended sediment formed by mechanical wear (Maroulis and Nanson 1996). The matrix probably infiltrated the pore spaces when the aggregates were deposited on the accretionary surfaces during waning flow (Rust and Nanson 1989; Gierlowski-Kordesch 1998; Gierlowski-Kordesch and Gibling 2002; Müller et al. 2004).

3.7.4 Aggregate Preservation

Based on the evidence for grain flattening and sutured contacts, the aggregates were compacted during burial but, unusually, retained their pelleted texture. In contrast, aggregates on modern floodplains typically lose their texture at burial depths of a few meters (Rust and Nanson 1989; Maroulis and Nanson 1996; Brooks 2003a). We evaluate several possible explanations for the exceptional degree of aggregate preservation in the Clear Fork Formation (Table 3-1; Fig. 3-10).

Aggregate type. -- An alluvial basin may yield a range of pedogenic aggregates, and the clay type, cement, percentage of non-clay minerals, and organic material (Probert et al. 1987; McGarry 1996; Kay and Angers 2000) may govern their strength (Gierlowski-Kordesch and Gibling 2002; Müller et al. 2004). If aggregates are eroded from a single paleosol profile, their composition and texture will depend on the source horizon, linked to such factors as drainage conditions, sediment accretion, and chemical accumulation (Müller et al. 2004; Gastaldo et al. 2013). Aggregates in a single channel may also be derived from different soil types.

At NSCQ, the variably gray and red-brown aggregates, with variable amounts of silt-sized quartz, probably were eroded from different soil horizons or profiles, among the range of paleosol types documented in the Clear Fork Formation (Tabor and Montañez 2004). The ferruginous grains are probably reworked, durable paleosol concretions that formed under conditions of poor drainage and redox fluctuations, or from weathered Fe-rich sources (Stiles et al. 2001; Wilson et al. 2012; Löhr et al. 2013). Apart from the evidently rigid ferruginous grains, there is no clear evidence that aggregates with varied composition had markedly different strength.

Protection by framework grains and cements. -- Aggregates deposited with mineral grains (Rust and Nanson 1989; Ékes 1993; Gastaldo et al. 2013) or encased by carbonate and hematite cements during early burial (Müller et al. 2004) may have higher preservation potential. Aggregates shielded by the predominant quartz grains are present in channel bodies at numerous sites in the Clear Fork Formation (Simon and Gibling in review). However, at NSCQ, aggregates are the main component of the channel mudstones (68-76%), and other mineral grains (2-15%) were too few and small to serve a protective function, although the non-compactible ferruginous grains (12-18%), similar in size to the aggregates, may have provided some protection. The small proportion of dolomite rhombs and poikilotopic dolomite cement (3-9%) and patches of barite cement may have imparted some rigidity to the sediment. Although the timing of cement formation is not well-constrained, cementation most likely took place during early burial. This is suggested by the euhedral form of rhombs between the mud aggregates, implying displacive growth in weakly consolidated sediment. No soil-formed carbonate crystallaria networks (Müller et al. 2004) were observed. Hematite-bearing rims around a few aggregates and an encasing matrix of clay and hematite may also have provided some protection.

Rapid near-surface burial. -- For *in situ* and reworked aggregates in Triassic soil profiles and floodplain deposits, Müller et al. (2004) suggested that cumulative addition of sediment to soil profiles resulted in high short-term sedimentation rates, rapidly burying aggregate-bearing materials and reducing pedogenic modification and overprinting. In contrast, floodplain mud accumulates at a very low rate at Cooper Creek in Australia where muds in the shallow subsurface are commonly indurated, contributing to aggregate destruction (Rust and Nanson 1989; Gibling et al. 1998).

For the NSCQ site, we suggest that rapid accumulation and burial of bedload aggregates in the channel was a key factor in their preservation (Figs. 3-2C and 3-10). The aggregates were deposited at the base of a meandering channel, in a low topographic position on the landscape where preservation potential was enhanced. The channel was cut into paleosols that were probably partially indurated. Basal channel sediments contain dolomite clasts and, although carbonate concretions were not observed in the underlying paleosol, reworked fragments suggest induration of nearby soils. Thus, the aggregates accumulated in an eroded "compartment" with relatively rigid boundaries (Fig. 3-10) that would have resisted compaction during burial. The channel deposits yielded no evidence for soft-sediment deformation that might indicate a saturated condition and early water loss and compaction.

The inclined aggregate-bearing layers are up to 3 m thick and were incorporated into the body of the point bar as it migrated laterally. The channel deposits contain evidence for waning flow and periods of near dryness, including swept ripples, rill casts and roots at low levels, implying rapid drainage of the newly deposited layers and perhaps incipient induration. Periodic deposition of quartzose sandstone bedsets on the point bar would have shielded the aggregate layers from surface modification, and field and petrographic analysis yielded little sign that the aggregate beds were overprinted by pedogenesis, other than a few root traces and slickensides. Aggregate-bearing point bars on the Red River plains of Manitoba migrated at long-term rates of 0.04 to 0.35 m/yr over the past ~8000 years (Brooks, 2003b); if similar rates apply to the NSCQ point bar, an aggregate layer could have been covered by younger bedload sediment within decades to centuries. Subsequently, a thick sheet of floodplain mud covered the point bar, further isolating the aggregates from near-surface processes.

Early diagenesis of the channel and overlying floodplain sediments may have promoted resistance to compaction (Fig. 3-10). The aggregate accumulations themselves are only modestly cemented, but associated strata yield evidence for partial cementation. The coarse basal beds of Channel Bodies 1 and 2 contains patchy dolomite, gypsum and barite cement, and inclined sandstone beds of Channel Body 1 and the tabular sandstone of Channel Body 3 are well-cemented with poikilotopic dolomite. Dolomite rhombs are also present in the mudstone sheet above Channel Body 1. Poikilotopic dolomite cement indicates precipitation under phreatic conditions, probably during shallow burial, and is consistent with observations from other Clear Fork sites (Simon and Gibling in review). There are numerous examples of phreatic dolomite formation in arid settings, commonly during early diagenetic stages when groundwater becomes enriched in magnesium (Spötl and Wright 1992; Armenteros et al. 1995; Henares et al. 2016) and/or when fresh groundwater mixes with saline brines (El-Sayed et al. 1991; Colson and Cojan 1996).

In summary, the sedimentological context would have promoted aggregate preservation. An important consideration is that dryland channel and floodplain sediments commonly undergo some degree of early lithification (Nanson et al. 2005) and are less prone to compaction than subaqueous deposits. Müller et al. (2004) noted that desiccation cracks in the Triassic aggregate-bearing paleosols showed only limited ptygmatic folding, implying <15% compaction, and some paleo-Vertisols experienced as little as 10% compaction (Caudill et al. 1996).

Burial depth. – In principle, shallow long-term burial should promote the preservation of aggregates, which would experience a more limited range of diagenesis. The Clear Fork Formation is near-horizontal and was deposited on a cratonic platform with low rates of long-term sediment accumulation and shallow burial (~1100 m). However, the Linde Formation

aggregates documented by Müller et al. (2004) survived burial to 2500-3500 m depth during a thermal subsidence phase that followed rifting, suggesting that burial depth *per se* is not the sole factor. Neither the Linde nor Clear Fork Formations appear to have experienced overpressuring that might have inhibited compactional dewatering.

3.8 CONCLUSIONS

This paper documents the only known example in the rock record to date of channel deposits dominated by mud aggregates. At the North Soap-Creek Quadrangle location in the Early Permian Clear Fork Formation of Texas, lateral-accretion deposits of an exhumed point bar are composed of well-preserved, flattened and sutured aggregates with a small proportion of quartz and other detrital grains. The varied hematite and detrital content of the aggregates and their association with reworked ferruginous concretions support a derivation by reworking of paleo-Vertisols and related soil types, which are prominent in the formation. The aggregates were probably reworked from the paleosols during modest seasonal floods, and corrections for compactional flattening as seen in 2D thin sections suggest that they were originally of fine-sand size. They are two to three times larger than associated quartz grains of silt to very fine-sand size, which may have been supply-limited on the distal alluvial plain. Entrainment considerations suggest a low threshold for aggregate mobilization. Beds of fine-grained quartz sand were probably emplaced on the point bars during stronger floods that periodically brought detrital sediment into the basin from distant source areas or mobilized sediment stored in the landscape.

The aggregates contain illite, Fe-rich chlorite, kaolinite and mixed-layer clays, and are similar in clay composition to paleosols in the formation. Smectite is widely considered important for aggregate formation on account of its shrink-swell properties, but glycolation results suggest that the illite and Fe-rich chlorite had some swelling potential. The apparent absence of discrete

smectite is attributed to parent rocks of Precambrian and Paleozoic age, which are unlikely to have yielded much smectite. Because the formation was only shallowly buried on the stable Eastern Shelf and experienced a low degree of thermal maturity, it is unlikely that smectite was lost due to illitization.

The preservation of mud aggregates, which are usually destroyed by compaction during shallow burial, is attributed to a combination of factors. Although the aggregates are the main sediment component, a small proportion of rigid detrital and ferruginous grains may have partially buffered the aggregates, along with early-formed dolomite rhombs and cements of dolomite, gypsum and barite, as well as hematite rims and encasing clay matrix. However, the key factor was probably the rapid incorporation of aggregate-rich beds within a migrating point bar set in a rigid "compartment" cut into tough and relatively non-compactible paleosols. Inclined flood sheets of sandstone with early-formed poikilotopic dolomite cement would have isolated them further from pedogenic and other surface processes, as would overlying floodplain and channel deposits. Early cement formation in these strata would have enhanced the rigidity of the sediment package.

The Clear Fork Formation study site indicates that aggregates may dominate channel sediments on distal alluvial plains. In view of the problems of identifying them by petrographic means, aggregate-rich channel fills may be much more widespread in the geological record than is currently recognized.

CHAPTER 4- An abandoned-channel fill with exquisitely preserved plants in redbeds of the Clear Fork Formation, Texas, USA: an Early Permian water-dependent habitat on the arid plains of Pangea

4.1 ABSTRACT

A well preserved plant assemblage at the Colwell Creek Pond locality of Leonardian (Kungurian) age provides an opportunity to evaluate taphonomic conditions in a dryland alluvial setting. A narrow channel body incised to 5 m depth through red paleo-Vertisols contains 2 m of varicolored laminated mudstone with graded layers and plant material. X-ray diffraction analysis of individual laminae indicates the presence of chlorite, illite, kaolinite, and mixed-layer clay, with hematite in red and gray layers and goethite in yellow-brown laminae. No carbonate was identified, and the total organic carbon content is minimal. The fine sediment accumulated in a shallow abandoned channel from suspension and gentle underflows, probably linked to seasonal inflow, and analysis of lamina thickness suggests that standing water may have persisted for up to a few millennia. The preservation of lamination is attributed to a lack of bioturbation, possibly linked to a paucity of subsurface oxygen, low productivity, elevated salinity, rapid deposition, or a combination of these factors; minimal bioturbation may also reflect the limited use of freshwater ecospace during the Early Permian. Clay-rich paleo-Vertisols complete the fill, with drab root traces that indicate growth of vegetation in a strongly seasonal setting.

Abundant plant material in the laminated beds includes branches of walchian conifers, the possible cycadophyte *Taeniopteris* spp., and the comioid, possible peltasperm, *Auritifolia waggoneri*. They were derived from an adjacent riparian zone and preserved as 3D goethite petrifactions. Much of the foliage shows evidence of arthropod herbivory. Although a humid

climatic episode cannot be ruled out, the exceptional abundance and preservation of the plants probably reflects the persistence of an oxbow lake on a relatively arid alluvial plain, where riparian plants experienced periodic moisture stress but had access to groundwater nearly year round. Rapid burial in standing water, the lack of bioturbation in the laminated sediments, and early biomineralization probably explain the exceptional preservation of the plant remains.

4.2 INTRODUCTION

As the supercontinent Pangea assembled through the Late Pennsylvanian and Permian, alluvial plains across Euramerica experienced progressive aridification, with thick loess accumulations and arid paleosols (Kessler et al. 2001; Tabor and Poulsen 2008; Tabor 2013). Based on the analysis of fluid inclusions in halite, estimated surface temperatures were at times as extreme as in any place on Earth today (Zambito and Benison 2013). Floral assemblages across western Euramerica changed in step with this climatic evolution (DiMichele and Aronson 1992; Rees et al. 2002; DiMichele et al. 2006; Montañez et al. 2007).

Surprisingly in view of this aridity, well-exposed Pennsylvanian and Permian alluvial formations across north-central Texas have yielded rich assemblages of exquisitely preserved plant fossils and a diverse range of vertebrates (Olson 1958; Olson and Bolles 1975; Olson and Mead 1982; Murry and Johnson 1987; Olson 1989; DiMichele et al. 2006; Chaney and DiMichele 2007; Chaney et al. 2009; Mamay et al. 2009; Tabor et al. 2013). Rare occurrences of plant fossils have been recorded in upper Permian and Triassic redbeds elsewhere, where plant remains were commonly preserved in gray lenses and within laminated sediments in lakes and abandoned channels (Demko 1995; Clausing and Boy 2000; Galtier and Broutin 2008; Bercovici et al. 2009). Hypotheses to explain these occurrences include 1) periodically humid and well vegetated conditions that reflect climatic change, 2) local groundwater-dependent habitats in an otherwise

dry landscape, 3) plant preservation under unusual taphonomic conditions, or 4) a combination of these factors (DiMichele et al. 2006; Montañez et al. 2007; Looy 2013).

In the Clear Fork Formation of Texas, a prominent floral site is Colwell Creek Pond, interpreted as an oxbow lake (Chaney et al. 2009; Looy 2013; Schachat et al. 2014). Excavated periodically over 20 years, the site is the most heavily collected plant-bearing locality from a single depositional environment in the Leonardian redbed section of north-central Texas. The flora was briefly discussed by Schachat et al. (2014) in the course of their characterization of insect damage on the plants.

The plant fossils are preserved in thinly laminated beds with subtle layer-by-layer color variation, for which no sedimentological or technical analysis was previously available. Although abandoned-channel fills worldwide commonly contain laminated intervals, such thinly laminated beds constitute a rarely documented facies that is prominent at numerous localities in the Clear Fork Formation. Plant fossils are present at many of these sites, and understanding the nature and origin of the laminated beds at Colwell Creek Pond is central to an assessment of plant preservation in this unusual facies. The present study documents 1) the facies and geometry of the alluvial strata, 2) the sedimentary structures, mineralogical composition, and organic content of the laminated beds, 3) the main plant taxa, and 4) the characteristics of the associated paleosols. We conclude that the locality represents a local well-watered habitat in a relatively arid landscape, where water influx to the channel offsets a high rate of evapotranspiration. A well vegetated channel margin supplied leaves and branches to standing water where favorable taphonomic conditions included early biomineralization.

4.3 GEOLOGIC SETTING

The Clear Fork Formation was deposited on the Eastern Shelf of the Midland Basin, which lay between 0° and 5° N of the equator across the western coastal zone of Pangea during the Late Paleozoic (Fig. 1-2A; Ziegler et al. 1997). The Wichita, Arbuckle, and Ouachita Mountains to the east rose during the Pennsylvanian, but early Permian tectonic activity was limited to intermittent strike-slip movements along the Matador—Red River uplifts (Regan and Murphy 1986a; Budnik 1989; Brister et al. 2002). During the Permian, clastic sediments were sourced mainly from recycled Pennsylvanian fan deltas and fluvial facies, reflecting substantial denudation of the uplifts (Brown 1973; Hentz 1988; Tabor and Montañez 2004). The formation is near horizontal with a gentle WNW dip (< 1°) but with little other evidence of deformation (Edwards et al. 1983; Hentz 1988).

The Clear Fork Formation rests conformably on dolostone and mudstone beds of the Lueders Formation, which is interpreted as a tidal deposit based collectively on an assemblage of brackish-water invertebrates, plants, and tetrapods with channel deposits that intercalate or correlate with carbonate rocks containing marine invertebrates (DiMichele et al. 2006). In north-central Texas, the Clear Fork Formation comprises 350—365 m of terrestrial deposits, mainly red mudstone with minor sandstone, carbonates, and evaporites (Fig. 1-3; Olson 1958; Nelson et al. 2013). In this area, Nelson et al. (2013) subdivided the formation into informal lower, middle, and upper units, with the Colwell Creek Pond site in the middle unit. The paleoenvironment northwest of Seymour has been interpreted as continental on the basis of sedimentology and biota, with possible marine influence in the basal strata (Olson 1958; Murry and Johnson 1987; DiMichele et al. 2006) and playa-lake deposits at a locality to the southwest (Minter et al. 2007). Fine-grained meandering-channel and floodplain deposits are prominent, with plants, vertebrates,

and tetrapod and myriapod trackways and paleoflow to the southwest (Olson 1958; Edwards et al. 1983; Lucas et al., 2011; Nelson et al. 2013). Pedogenic carbonate and gypsum nodules are present, the latter increasing in prominence upwards (DiMichele et al. 2006). Approximately 200 km to the south, the Clear Fork contains open-marine limestone and dolomite (Olson 1958, 1989; Olson and Mead 1982; Nelson et al. 2013). Although marine influence cannot be discounted for the low-gradient plain of the study area, no evidence currently supports such an interpretation at the level of the Colwell Creek Pond site. Conformably overlying the Clear Fork is the San Angelo Formation of the Pease River Group, laid down in multi-channel systems and suspended-load meandering rivers (DiMichele et al. 2006).

The burial history of the Eastern Shelf is not well documented, but the maximum burial depth of the Virgilian strata, less than 500 m below the Clear Fork Formation, may not have exceeded 1600 m (Tabor and Montañez 2004). Virgilian coals and carbonaceous shales have low R_o values of 0.4—0.8% (Hackley et al. 2009), and burial temperatures of less than 40—45^{o}C were estimated from Early Permian strata along the flanks of the Midland Basin (Bein and Land 1983; Tabor and Montañez 2004). These data collectively suggest that the Clear Fork Formation experienced shallow burial and a low degree of thermal maturation, implying only modest diagenetic change in clays and other minerals during burial.

4.4 METHODS

The outcrops at Colwell Creek Pond, which derives its name from a nearby creek draining into the North Fork of the Wichita River, are exposed along cliffs (10 m high), partially covered by a weathered layer and sparse vegetation (Fig. 4-1). Located in Knox County, the exposures extend for 60 m across 0.85 hectares and are oriented northeast to southwest. Lithology, grain size, and sedimentary features were recorded, leading to the identification of seven lithofacies (Table 4-1).

Two profiles were measured and combined to create a composite section divided into channel bodies 1 and 2, in upward succession (Fig. 4-2A). A profile was measured in a floodplain section under the margin of Channel Body 1 (Fig. 4-2B).

To reconstruct the orientation and geometry of Channel Body 1, the strike and dip of the beds were recorded with GPS locations accurate to ± 3 m. Paleoflow readings were measured from rib and furrow structures on ripple cross-laminated beds to an accuracy of ± 5°. Location coordinates were used to map the basal surface of the channel body in ArcGIS (Fig. 4-3). Using photomontages of the cliffs, the distance above the channel base was determined with a precision of ± 0.1 m. For points measured away from the cliffs where photomontages were unavailable, the height of each point above the channel base was obtained from a Google Earth elevation profile with a precision of ± 0.3 m. A cross section was generated by projecting data points of known elevations onto a line perpendicular to the mapped channel margin (line A—A′; Fig. 4-3). A best-fit curve was generated, broadly defining the base of the channel body.

The laminated beds containing the plant fossils were studied for lamina thickness and geometry and for sedimentary structures (Figs. 4-4, 4-5), and three unpolished thin sections were studied under plane-polarized light (Figs. 4-6A and B). Thickness measurements were acquired from thin sections rather than block samples because the layers contain sub-laminae that could not be distinguished in hand specimens. Furthermore, the layers pinch out laterally within a few centimeters in block samples and are commonly contorted, whereas thin sections provide a narrow, high-resolution cut through the layers, aiding precise thickness measurement. Due to the delicate nature of the rocks, large mudstone slabs were not collected in the field, which precluded analysis of trends in lamina characteristics. A polished thin section studied using a LEO 1450 VP Scanning Electron Microscope with an INCA X-max 80 mm 2 EDS system

provided semiquantitative elemental information. Because mineral grains are smaller than the analyzed spot size of 10 μm, the results yield only a general guide to the minerals present. The thin section was polished with a lead block, and embedded lead fragments were recorded as artefacts. The backscatter images were used to determine grain size and composition and to highlight textural variations (Figs. 4-6C to F).

X-ray diffraction (XRD) analysis was conducted at Bedford Institute of Oceanography on nine randomly oriented powder mounts of individual laminae with varied color (Fig. 4-7A). The surfaces of laminae were exposed using a hammer and a metallic file, and material was removed using a thin blade, with the first scraping avoided to reduce contamination. The samples were crushed using a mortar and pestle, and powder colors were estimated using a Munsell Geological Rock Color Chart. XRD was carried out with a Siemens Kristaloflex diffractometer using Co-Kα radiation. Bulk slides were scanned from 2^{o} to 77^{o} 2θ, with a 0.2^{o} step interval and 2 s step time.

Two samples were selected for a < 2 μm fraction analysis. Approximately 20 g of crushed sample was suspended in a burette containing a weak solution of sodium hexametaphosphate. After 16 hours, the < 2 μm fraction was isolated, flocculated with 4 ml of $MgCl_2$ solution, and centrifuged. The mixture was decanted and the clay fraction was resuspended in a 500 ml cylinder. A 20 ml aliquot was withdrawn, dried, and weighed to determine the appropriate weight (5%) for the internal standard, zincite. The zincite was added to the resuspended sample and dissolved using a laboratory shaker, after which the sample was centrifuged and smeared on a normal glass slide and a second heat-resistant glass. Using the scan properties described above, XRD analysis for the < 2 μm fraction was carried out using the normal glass slides. The slides were then placed in a desiccator containing vapors of ethylene glycol for ~ 4 hours to investigate peak shifts, after which they were analyzed immediately to prevent the glycol from evaporating,

using a 2°—17° 2θ range with a 0.2° step interval and 2 s step time. The heat-resistant slides were placed in a preheated furnace at 150°C for at least 30 minutes, and were analyzed using a 2°—30° 2θ range with a 0.2° step interval. This process was repeated for 300°C, 500°C, and 650°C, which allowed clay minerals to be identified by revealing changes in crystal structure spacing (Fig. 4-7B). At temperatures > 500°C, most clay smears started to flake or bubble, and XRD analysis was not conducted on these samples.

For three samples from the floodplain interval, oriented aggregates were treated to produce potassium- and magnesium-saturated mounts, with and without glycerol solvation, and analyzed at Southern Methodist University using a Rigaku Ultima III X-ray diffractometer with Cu-Kα radiation from 2° to 30° 2θ with a 0.05° step interval per s. The potassium-saturated samples were heated in a furnace at 500°C for at least two hours. Mineral identification of the laminated beds and floodplain deposits followed Moore and Reynolds (1997) and the JCPDS (Joint Committee on Powder Diffraction Standards) Powder Diffraction File system. Components of mixed-clay layers were not identified, and no attempt was made to quantify clay-mineral proportions, although general comparisons were possible using peak intensities.

A split from each of the nine samples was ground and freeze-dried, and ~ 100 mg was analyzed for total carbon using a Leco TruSpec CHN (detection limit 0.01 wt. %). Another split was leached overnight with 10% HCl to remove inorganic carbon. A total of 100 mg of the leached sample was analyzed for organic carbon, and the inorganic-carbon content was calculated by difference (Table 4-2).

Figure 4-1 Outcrops at Colwell Creek Pond. Yellow arrows denote the positions of detailed lithological logs. A) Main cliff section 7 m high, subdivided into Channel Bodies 1 and 2. The lower stratigraphic interval is subdivided into lithofacies shown in Table 4-1 (Fm, massive mudstone; Fl, laminated mudstone; Sr, ripple cross-laminated sandstone; Sh, planar-stratified sandstone; and Gm, massive pebbly conglomerate). B) Adjacent cliff section highlighting the contact of the two channel bodies and that of the lower channel body with underlying floodplain deposits (Fm). The cliff lies parallel to and 20 m northwest of the main cliff section.

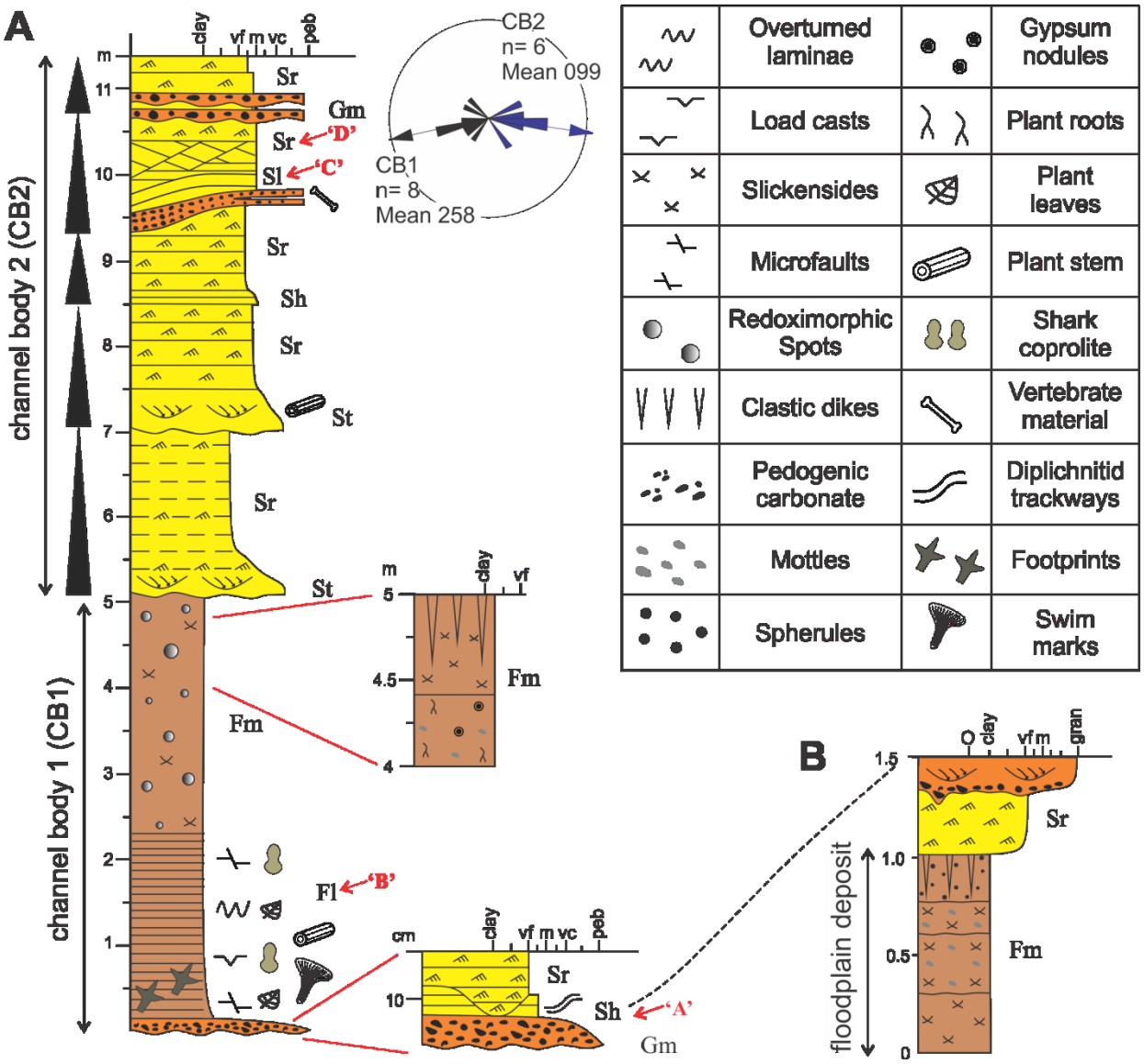

Figure 4-2 Lithological logs at Colwell Creek Pond. A) Log illustrating the sedimentological features of Channel Bodies 1 and 2. A detailed section of the basal 20 cm and upper 1 m of Channel Body 1 are also shown. Five fining-upward cycles are noted in Channel Body 2 by black-filled triangles. The rose diagram represents ripple cross-lamination; with mean westward and eastward paleoflow for Channel Bodies 1 and 2, respectively. Sand grain size: vf = very fine, m = medium, vc = very coarse; gravel grain size: gran = granule, peb = pebble. B) Log of floodplain deposits below Channel Body 1 with position shown in Figure 4-1B.

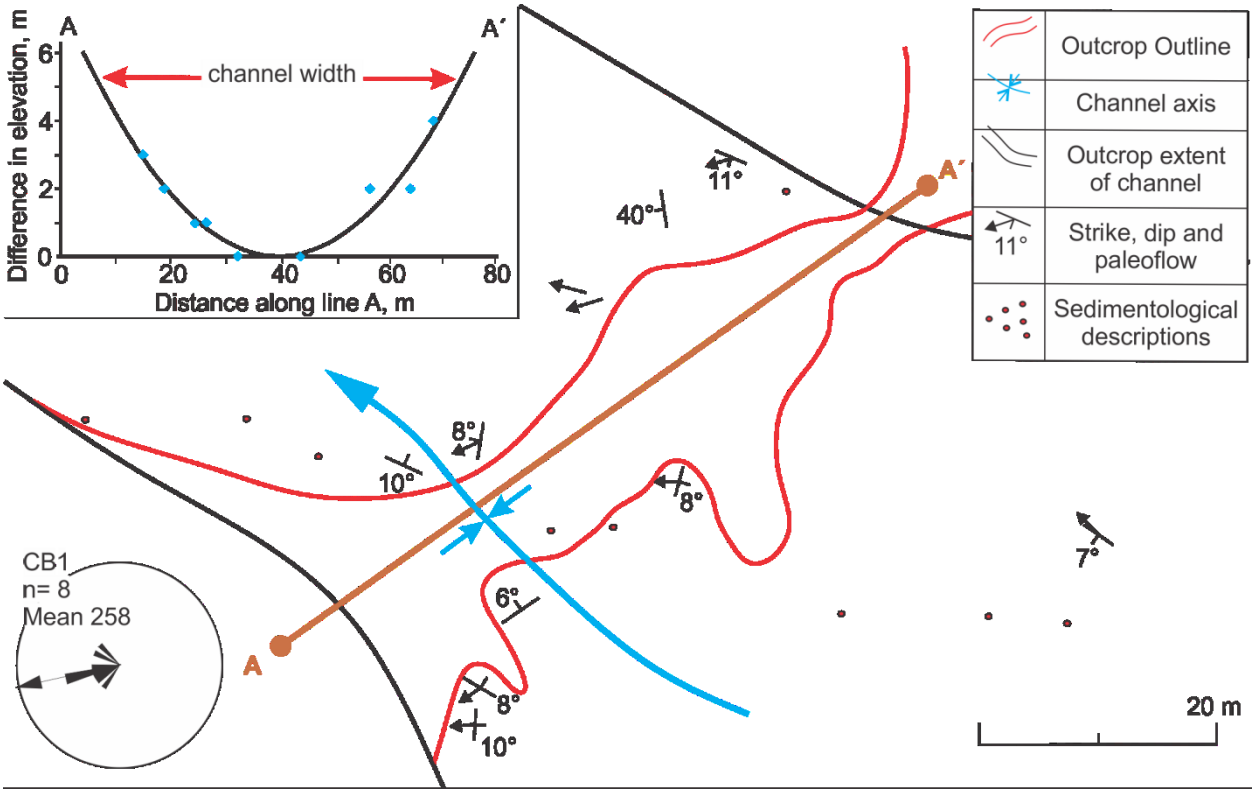

Figure 4-3 Map of Channel Body 1 at Colwell Creek Pond, showing the outcrop outline and the traceable extent of the channel margin. Circles represent sites with sedimentological descriptions and GPS locations, with strike/dip and paleoflow data from other sites. Line AA′ is perpendicular to the channel axis, with the original inferred SW edge of the channel defined as Point A. The rose diagram for Channel Body 1 is also shown. B) Cross section AA′ of Channel Body 1. Using a parabolic model, a thickness of 5 m produces a channel width of 65 m. If 1 m of section in Channel Body 1 was eroded below the overlying channel body, the minimum channel width would have been 72 m

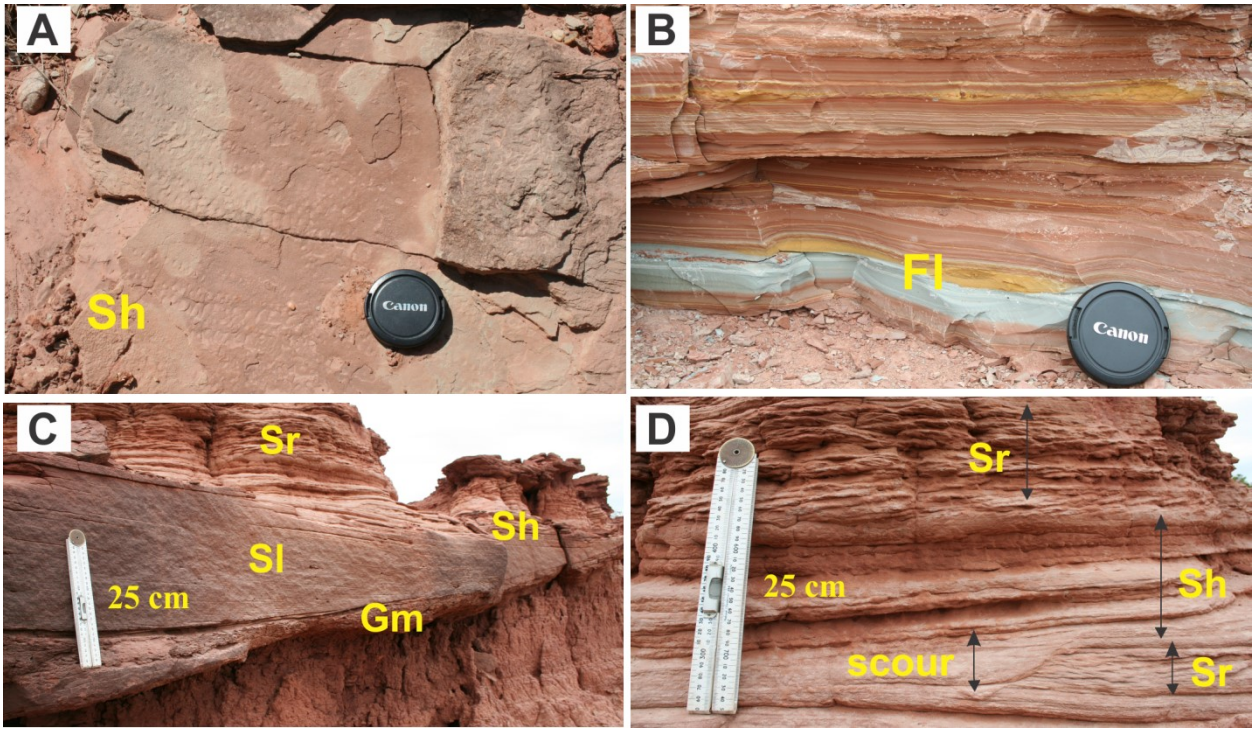

Figure 4-4 Field photos. Diameter of lens cap is 6 cm. A) Plane beds with trackways of *Diplichnites gouldi* in basal deposits of Channel Body 1. B) Variegated, laminated mudstone (Fl), close to the base of Channel Body 1. C) Antidune bedform (Sl) in the fourth cycle of Channel Body 2, resting on a thin lens of pebble conglomerate (Gm) and passing laterally into plane beds (Sh) and upwards into ripple cross-laminated beds (Sr). D) Closeup of the upper part of the fourth cycle. Smaller rhythms comprise alternate layers of plane beds (Sh) and ripple cross-lamination (climbing and nonclimbing, Sr), with scour fills. The positions of photos are noted on the logs in Figure 4-2.

Table 4-1 Lithofacies in the Colwell Creek Pond outcrops, using terminology from Miall (1985, 1996), Tucker (2003), and Long (2011). VF, F, M, and VC = very fine, fine, medium, and very coarse grains, respectively.

Facies Code	Lithofacies Description	Sedimentary Structures	Unit Contacts	Fossils	Interpretation
Fl	Variegated, laminated mudstone	Lamination; cross lamination; graded bedding; loop bedding and microfaults; soft-sediment deformation; load casts; overturned beds; scours	Parallel-planar at base, to parallel to nonparallel wavy at top	Plant leaves and stems abundant	Suspension deposition from density underflows with minor compactional deformation
Fm	Brown, massive mudstone	Massive; locally weakly stratified; redoximorphic spots; slickensides	Poorly developed or irregular	Plant roots rare	Suspension deposition from standing water, with pedogenic overprinting. Paleosol development on the floodplains
Gm	Gray, massive pebbly conglomerate	Massive units of carbonate and mudstone clasts; locally weakly stratified and trough cross-stratified	Abrupt, planar or irregular, locally erosional	Vertebrate material rare	Channel lag associated with scouring events
Sl	Red, M sandstone, low-angle cross-stratified	Convex-up mound with form-concordant plane lamination	Sharp basal contact, gradational top	Not observed	Antidune formed under upper-flow-regime conditions
Sh	Red, VF to M sandstone, planar-stratified	Planar lamination	Undulating to planar contacts	Diplichnitid trackways abundant	Plane beds formed under upper-flow-regime conditions
St	Red, VC sandstone with minor granules, trough cross-bedded	Trough cross-beds; minor ripple cross-lamination	Sharp or erosional contacts	Plant stems rare	Accretion and migration of lower-flow-regime 3D dunes
Sr	Gray/red, VF to M, ripple cross-laminated sandstone	Ripple cross-laminated (non-climbing and slightly climbing); scours	Sharp, planar contacts	Not observed	Accretion and migration of current ripples under lower-flow-regime conditions

4.5 LITHOFACIES

4.5.1 Laminated Mudstone (Fl)

Description. --- Laminated mudstone forms a single unit 203 cm thick that rests abruptly on coarser beds of facies Gm, Sr, and Sh in Channel Body 1. The laminae are predominantly red-brown with light brown, yellow, and gray layers (Table 4-2; Figs. 4-4B, 4-5). Grains of fine to coarse silt predominate as discrete layers and the coarser parts of graded beds.

Based on thin-section analysis of 34 laminae from three thin sections, the layers range from 0.2 mm to 2.1 mm thick, with an average of 0.7 ± 0.4 mm (1-sigma range). The gray and red-brown layers have a combined average thickness of 0.8 ± 0.5 mm, and the yellow laminae have an average thickness of 0.4 ± 0.1 mm. The lowermost laminae are thicker and slightly coarser grained (coarse silt). The gray and red-brown layers are difficult to discern in thin section, and no attempt was made to distinguish them (Fig. 4-6A). The collected blocks of laminated mudstone show little indication of systematic change in thickness.

The laminae are commonly ungraded, but some are normally graded and a few are inversely graded (Figs. 4-6A and B). Backscatter images show abrupt contacts between layers of similar silt grade but with different degrees of compaction and proportion of clay (Figs. 4-6C to F). Low-angle cross-lamination is rarely present in the yellow laminae (Fig. 4-5A), and no evidence of desiccation features or bioturbation was noted. Laminar contacts are planar- or wavy-parallel (Fig. 4-5B), and minor scours up to 0.5 cm deep are filled with different-colored laminae (Figs. 4-5A and B). Load casts and overturned beds are present where gray laminae overlie interbedded yellow and red- brown layers (Figs. 4-5A).

Normal microfaults with a vertical extent of 1 cm contort the layers and commonly terminate within gray laminae (Figs. 4-5A, 4-6B). Loop bedding is present where laminae up to 0.5 cm thick wedge out along low-angle discontinuities, ranging from simple structures with laminae bending symmetrically on both sides of a boudin neck to complex loops with faulted boudin necks (Fig. 4-5B; Calvo et al. 1998). Roll-over geometries are preserved with slight draping over some microfaults (Fig. 4-6B). Microfaults and loop bedding are more prominent in the uppermost 70 cm, yielding an upward change from parallel to wavy lamination.

Complete and fragmentary permineralized plant leaves, branches and stems (up to 15 cm long and 4 cm wide) are preserved in the laminated mudstone. It is unclear whether the plant remains lie preferentially on the tops or the bases of the laminae, but they are common in red-brown layers, and yellow layers viewed in thin section contain greenish black patches at lamina tops or in the layers, attributed to plant fragments (Fig. 4-6B). One blattoid insect wing was identified, and a few indeterminate three-toed footprints and discontinuous surface marks in the lowermost part of the unit are attributed to fish or amphibians, probably swimming traces.

Coprolites up to 5 cm long are uncommon, and are provisionally attributed to xenacanth sharks, which are known from numerous sites in the formation (Murry and Johnson 1987; Johnson 2012).

Based on XRD, the laminae comprise quartz, undifferentiated feldspar, hematite, goethite, titania minerals, illite, kaolinite, Fe-rich chlorite, and mixed-layer clay (Figs. 4-7A, B). As used here, illite includes muscovite and hydromuscovite. The gray (CC 4a and 4c) and brown (CC 3r, 4d and 4e) laminae have similar spectra and contain a higher proportion of quartz, feldspar and illite than the yellow laminae (CC 1a, 1b, 1c and 3j). Goethite was only identified in yellow laminae,

and a fossilized plant preserved on a yellow lamina surface (CC 1b) yielded the strongest peak intensities for goethite. The leaves were rarely preserved as a carbonaceous film surrounded by a bluish gray zone of reduced iron. All samples had less than 0.27% carbon, with an average of 0.17% (Table 4-2). The carbon content showed no apparent correlation with color, and total organic carbon was virtually identical to the total carbon, indicating that inorganic carbon (e.g. carbonate) was minimal or absent.

Table 4-2 Summary of technical information for nine individual laminae in laminated mudstone (facies Fl).

Sample	Munsell Color	Description	Total carbon (TC %)	Total organic carbon (TOC %)
CC 3j	7.5YR 6/6	Reddish yellow	0.27	0.27
CC 1a	10YR 6/6	Brownish yellow	0.15	0.14
CC 1b	10YR 6/4	Light yellowish brown	0.20	0.20
CC 1c	10YR 5/8	Yellowish brown	0.18	0.18
CC 3r	10YR 7/4	Very pale brown	0.17	0.17
CC 4d	7.5YR 6/3	Light brown	0.09	0.09
CC 4e	5YR 6/4	Light reddish brown	0.13	0.13
CC 4a	Gley1 7-8/N	Light gray	0.23	0.23
CC 4c	Gley1 7-8/N	Light gray	0.11	0.08
		Average	0.17	0.017

Interpretation. --- Based on the fine grain size and grading, the silt-to-clay laminae are attributed to flows that entered standing water within the water column or along the bed, with deposition under waning flow. Generally flat and non-erosional contacts imply weak currents, but currents were periodically strong enough to transport bedload (ripple cross-laminated lenses) and erode scours, and inverse grading suggests velocity reversals. The coarser-grained and thicker laminae low in the unit suggest stronger initial flows.

Loop bedding (see Calvo et al. 1998) has been attributed to desiccation (Bradley 1931), synaeresis, or diagenetic cracking (Donovan and Foster 1972; Cole and Picard 1975), extensional

stress (Dean and Fouch 1983), seismicity (Hesselbo and Trewin 1984), shear stress produced by turbidity currents (Trewin 1986), and gas-bubble leakage (Fregenal-Martinez and Melendez 1994). Calvo et al. (1998) inferred an interplay between ductile deformation during lithification and extensional stress (micro-seismic shocks from tectonic activity), acting on competency differences between layers. Based on the minimal degree of deformation of the Clear Fork Formation and a quiescent Permian tectonic setting (Nelson et al. 2013), seismic effects and extensional stress are improbable causes of loop formation. No evidence was found for desiccation or bubble effects, and flows appear to have been gentle. Consequently, loop bedding and microfaults are attributed to near-surface compaction, and their association with load casts and overturned laminae indicate partial consolidation; textural heterogeneity (Fig. 4-6) may have provided competency contrasts. The up-section increase in deformational features may reflect in part progressive drying and stress as the channel filled.

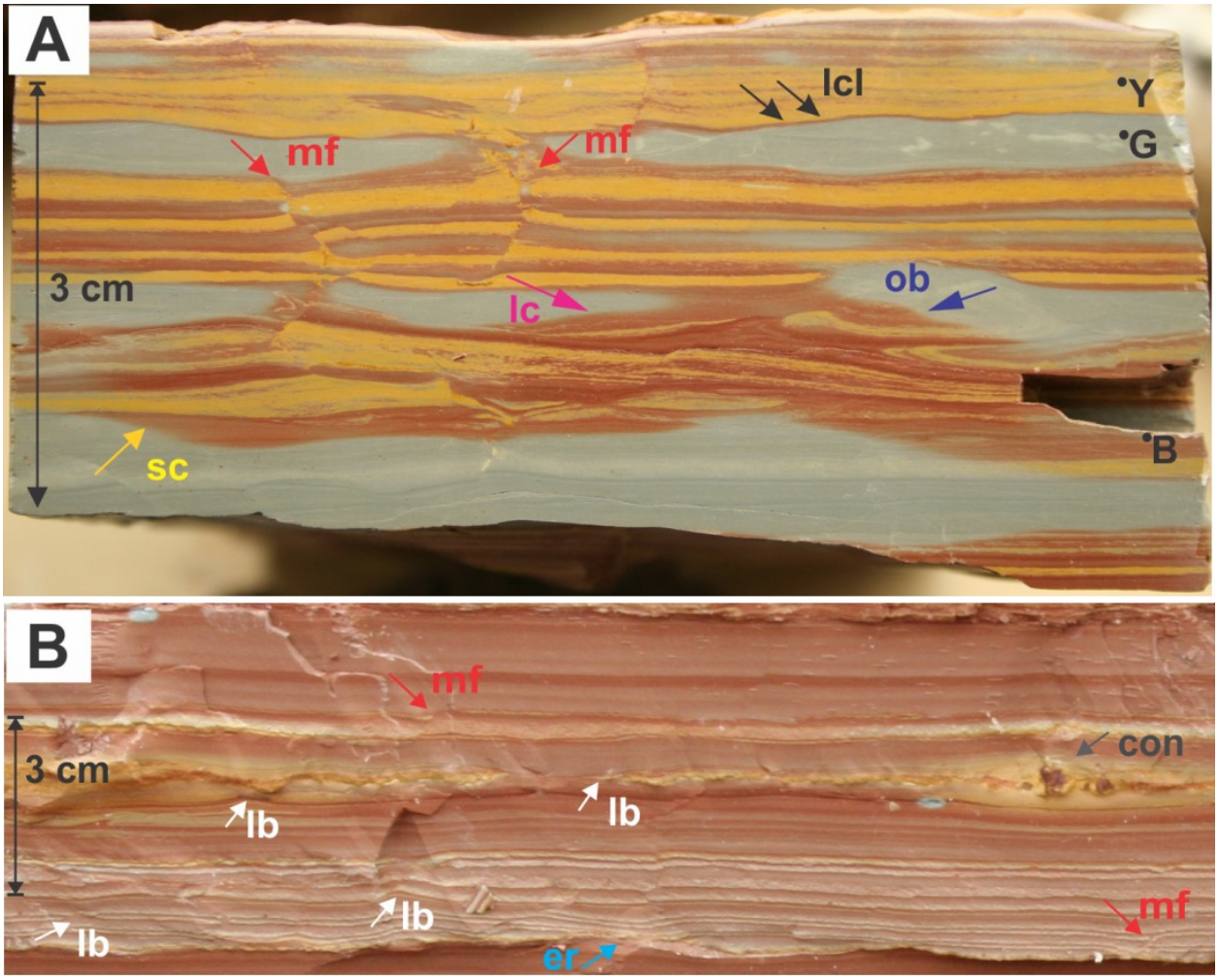

Figure 4-5 Syn- and post-deformational features in the laminated mudstone of Channel Body 1. A) Interbedded red-brown "B" and yellow "Y" layers are truncated by normal microfaults (mf), which terminate in the overlying or underlying gray "G" laminae. Load casts (lc) are visible in the gray layers, and the underlying interbedded red-brown and yellow layers are commonly overturned (ob). The bases of the laminae are locally scoured (sc), and low-angle cross-lamination (lcl) is observed in yellow laminae. B) Laminated beds with loop bedding (lb) and microfaults (mf). Laminae bases are mainly non-erosional planar- or wavy-parallel; in rare cases, the bedding contacts are irregular and erosional (er). Concretions (con) around permineralized plant leaves are common in the yellow laminae

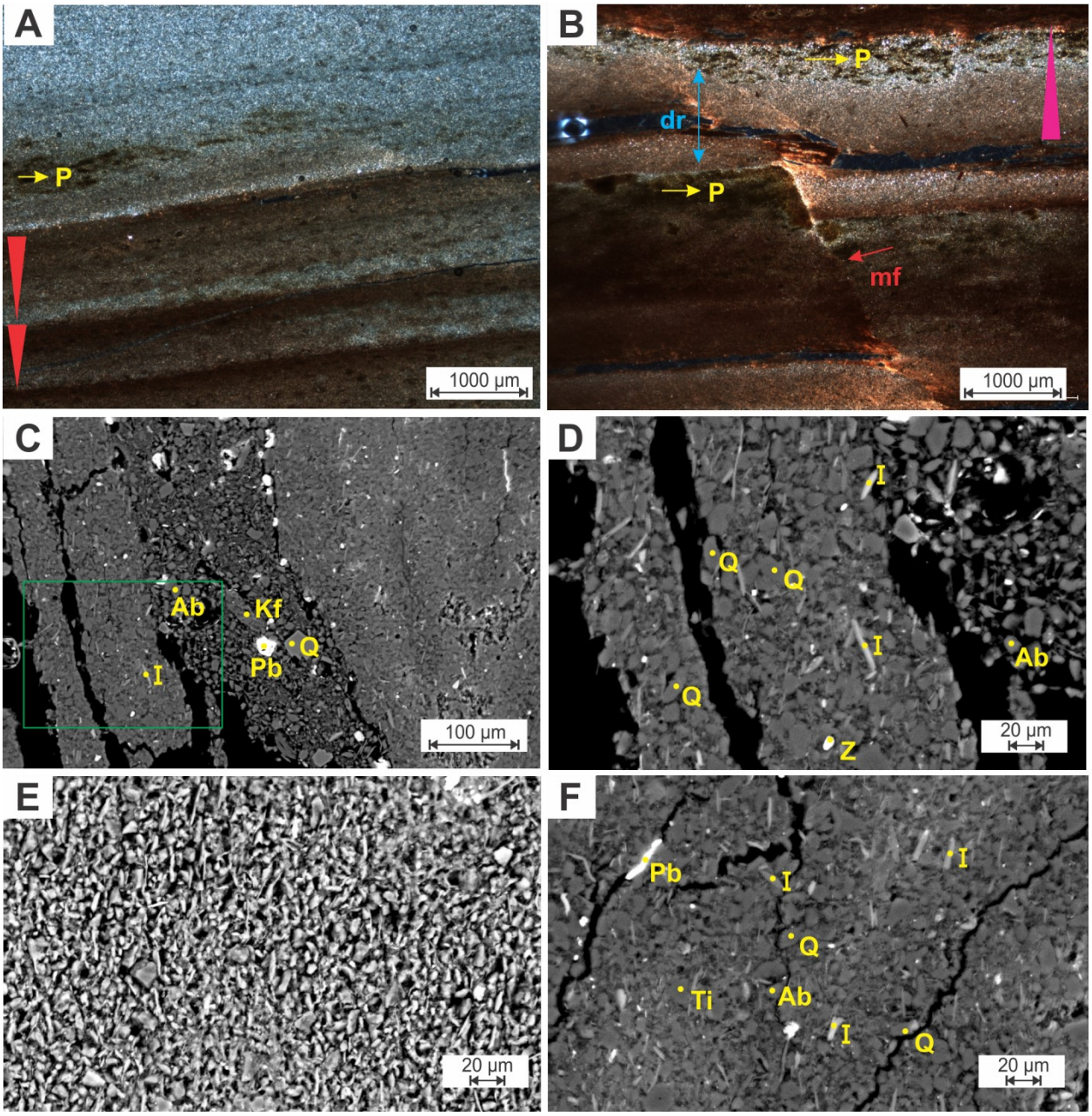

Figure 4-6 Photomicrographs of laminated mudstone (facies Fl) in plane-polarised light (A, B) and as SEM backscatter images of polished thin sections (C—F). A) Planar-laminated mudstone with graded bedding (red arrows) and quasi-horizontal to concave-downward bedding surfaces. Dark particles (P) present discontinuously along the laminae are interpreted as plant fragments. B) Microfaults (mf) cutting laminae, with draping (dr) of overlying sediments across the fault trace. The overlying laminae are variously nngraded or inversely graded (pink arrow). C) Layers with distinct textures and sharp boundaries, with coarse silt-size grains in a loosely compacted lamina at center. In the more compacted layer at right, irregular pits are a product of the thin-section preparation process. White fragments (Pb), commonly along fractures, are contaminants from lead block used in the thin-section preparation. D) Close-up of area in the green box in part C, showing silt-size grains of varied composition. E, F) Abundant silt-size (medium to fine) grains and clay matrix. Q = quartz; Ab = albite; Kf = K-feldspar; I = illite with bladed habit; Z = zircon; Ti = titania minerals.

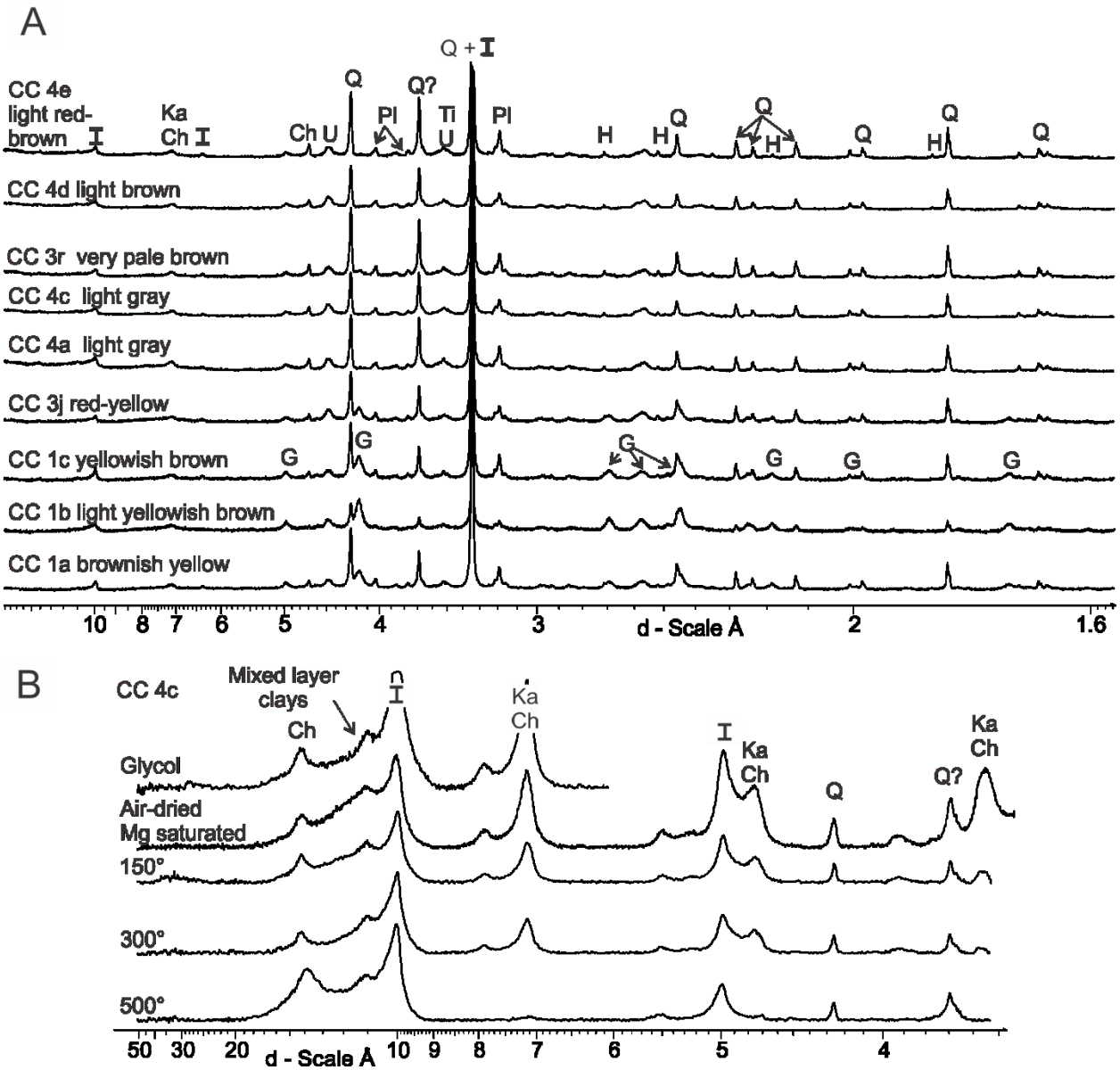

Figure 4-7 X-ray diffraction spectra for < 2 µm nonoriented samples of laminated mudstone. A) Nine spectra for individual laminae, arranged by color (see Table 4-2). Criteria used for mineral identification are shown in Table 4-3. Samples CC 4a, 4c, 3r, 4d, and 4e are composed of illite, kaolinite, chlorite, undifferentiated clays, quartz, feldspar, hematite, and titania minerals. Samples CC 1a, 1b, 1c, and 3j also contain goethite; sample CC 1b has the strongest peak intensities for goethite. B) Diffractograms of the < 2 µm clay fraction in CC 4c, showing the effects of heat treatment and glycolation, with identification of chlorite, kaolinite, illite, and mixed-layer clays. Q = quartz; Pl = plagioclase; I = illite; Ch = chlorite; Ka = kaolinite; U = undifferentiated clays; Ti = titania minerals, H = hematite; G = goethite.

Table 4-2 Criteria used for identification of minerals during X-ray diffraction analysis (Moore and Reynolds 1997).

Mineral	Identification
Low Quartz	Characteristic 100 and 101 reflections at 4.26 Å and 3.34 Å. An anomalous peak at 3.7 Å is provisionally attributed to quartz based on the examination of 75 spectra from the Clear Fork Formation in which the intensity of this peak is similar to that of the quartz 100 reflection and it only occurs when quartz is present within the sample.
Feldspar	Characteristic peaks at 3.20 Å, 3.7- 3.83 Å, 4.0- 4.1 Å and 6.3- 6.6 Å.
Dolomite	Characteristic 104 reflection at 2.89 Å.
Hematite	Weak and broad 104 and 110 reflections at 2.69 Å and 2.52 Å, reflecting the low degree of crystallinity.
Goethite	Strong 110 reflection at 4.18 Å with broad 130 and 021 peaks at 2.69 Å and 2.58 Å.
Ti-oxide	Weak 101 reflection occurs at 3.51- 3.52 Å.
Illite	Characteristic 001, 002 and 003 reflections at 10.1 Å, 4.99 Å and 3.38 Å; the latter peak overlaps with the low quartz 101 reflection. Upon glycolation, the 10.1 Å peak becomes sharper with increased intensity suggesting the presence of expandable clays. The ratio of the d-spacing (001) and (002) reflectors was greater than 2.00 which indicates that the illite shows some degree of interstratification with other clay minerals.
Chlorite	Characteristic 001, 002, 003 and 004 reflections at 14.4 Å, 7.15 Å, 4.77 Å and 3.55 Å, respectively. The chlorite peak positions slightly sharpened by glycolation (presence of expandable clays), but the 001 reflection dramatically increased in intensity, while the other peaks were weakened during heating to temperatures > 300ºC. Since the odd order peaks (001, 003 and 005) have lower intensities than the even order peaks (002 and 004) and the intensity of chlorite 001 peak is less than the 003 peak, the chlorite minerals are enriched in iron within the hydroxide layer.
Kaolinite	Characteristic 001 and 002 peaks at 7.18 and 3.58 Å overlaps with the chlorite 002 and 004 peaks.
Mixed layer clays	Mixed layer clays not identified within this study but are present between 11-13 Å and a broad, weak peak appears between 30- 40 Å when the sample is heated to 150^{o}C.
Standard Zincite	Characteristic 100, 002, 102 and 110 reflections at 2.81 Å, 2.60 Å, 2.47 Å and 1.62 Å, respectively.

4.5.2 Massive Mudstone (Fm)

Description. --- At the top of Channel Body 1 (Figs. 4-1A, 4-2), 2.9 m of red-brown, noncalcareous massive to weakly stratified mudstone rests sharply but non-erosionally on laminated mudstone. It is relatively consolidated but more friable below Channel Body 2. In the topmost meter, the lowermost 40 cm has a coarse, angular blocky structure with discontinuous clay skins coating the surfaces and gypsum nodules in the basal part. A prominent feature is the abundance of vertical drab mottles that branch downward, up to 2 cm wide and 20 cm long. The uppermost 60 cm grades up to a finer blocky structure, with slickenplanes and clay skins that are independent of each other. Sandstone dikes taper down from the base of Channel Body 2. Reduction spherules are prominent throughout.

Below the margin of Channel Body 1 (Fig. 4-1B), 1 m of mudstone is yellowish red below to more intensely red above, noncalcareous, and divided into sub-units at wavy boundaries. Slickenplanes have well-oriented clay skins along their surfaces, with drab mottles and reduction spherules. The topmost part has an angular blocky structure with clastic dikes below ripple cross-laminated sandstone. Four randomly oriented bulk samples have a similar composition to that of the laminated mudstone, each with quartz, feldspar, titania minerals, and trace amounts of hematite. In the < 2 μm fraction, illite, kaolinite, and Fe-rich chlorite predominate, with traces of mixed-layer clay and goethite. Minor dolomite was identified in one sample.

Interpretation. --- Based on remnant stratification, the facies is inferred to have formed from suspension in standing water in a channel or on a broader floodplain. Following improved drainage and aeration, pedogenic processes obliterated structures as paleosols developed. The vertical drab mottles, especially prominent in Channel Body 1, are interpreted as haloes around former roots that aided the destruction of stratification. The clastic dikes are inferred to have

filled desiccation cracks. For both paleosol profiles, slickenplanes, clay skins, gleyed mottles, and desiccation cracks suggest a seasonal climate with wetting and drying that, in sediment with mixed-layer clays, resulted in shrink—swell features.

Facies Fm resembles Pedotype G of the Clear Fork Formation, attributed by DiMichele et al. (2006) to Vertisols formed in floodplain muds. This pedotype consists of red-to-brown claystone with wedge-shaped aggregates, slickensides, and clastic dikes, indicating episodic shrink—swell processes. The clay-mineral (< 2 μm) fraction in Pedotype G is dominated by smectite, trace kaolinite, and weathered micas (DiMichele et al. 2006). The presence of gypsum in the upper part of Channel Body 1 suggests comparison with gypsum-bearing soils of the Mississippi Valley, U.S.A., which formed in a humid but strongly seasonal climate (Aslan and Autin 1998). The origin of the minor dolomite in one sample is not clear, but dolomite-cemented sandstones and paleosols are prominent at other Clear Fork localities (S. Simon, unpublished data) and in Early Permian paleosols elsewhere in the region (Kessler et al. 2001). As discussed more fully under Paleoclimate, below, dolomitic paleosols are widely inferred to represent evaporative groundwater conditions.

Especially in Channel Body 1, facies Fm differs from Pedotype G in the abundance of drab vertical mottles. In this respect the facies more closely resembles Pedotype D (DiMichele et al. 2006), interpreted as paleo-Vertisols in the underlying Markley and Archer City formations, for which redox effects were attributed to a shallow water table and a relatively humid paleoclimate; this is discussed further below.

4.5.3 Other Facies

Five standard fluvial facies comprise Channel Body 2 and form a minor component at the base of Channel Body 1 (Table 4-1). *Pebble conglomerate* (Gm) forms units up to 25 cm thick of angular 2—3 cm fragments of gray dolomitic carbonate, and local mudstone chips, with Fe-oxide staining and rare indeterminate bone fragments. The units can be traced laterally for up to 5 m and are largely massive with a few 15 cm trough cross-beds. The facies rests erosionally on red siltstone of facies Fm at the base of Channel Body 1 and on sandstones in Channel Body 2, and is interpreted as a channel lag of intrabasinal material eroded from paleosols adjacent to the channels or upstream. The presence of dolomite in the floodplain paleosols of facies Fm supports a paleosol origin for the dolomitic clasts, although alteration from carbonate precursors during shallow burial cannot be ruled out. Bone material may have been derived from organisms in the channel or reworked from floodplains or paleosols.

Planar-stratified sandstone (Sh) comprises gray planar laminasets with current lineation, up to 10 cm thick. Trackways of *Diplichnites gouldi* (Gevers et al. 1971) up to 3 cm wide and 30 cm long are prominent at the base of Channel Body 1 and are oriented near parallel or oblique to the lineation (Fig. 4-4A). Units are discontinuous and sharply overlie facies Gm and underlie or grade laterally into facies Sr. *Low-angle cross-stratified sandstone* (Sl) forms a red convex-upward mound 50 cm thick in Channel Body 2, with form-concordant, low-angle stratification and an extent of 3 m within a scour. The bed rests abruptly on facies Gm and wedges out against and passes up into facies Sh (Fig. 4-4C). Both facies are attributed to upper-regime flow conditions, with the Sl mound formed as an antidune bedform when Froude numbers for transcritical and supercritical flows were exceeded (Langford and Bracken 1987), probably in shallow water (Allen et al. 2013). Rapid discharge decline may have prevented reworking of the

antidune into lower-regime bedforms (Alexander and Fielding 1997; Fielding 2006). The diplichnitid trackways in Sh were made by arthropods (Minter et al. 2007) that moved along the current direction, probably as flow waned.

Trough cross-bedded sandstone (St) forms 40 cm units in Channel Body 2, with 20 cm trough sets, mudstone clasts, and one indeterminate plant stem 10 cm long and 1 cm wide. *Ripple cross-laminated sandstone* (Sr) consists of gray or red cross-laminated sets up to 3 cm thick that are locally climbing and show FeMn oxide staining and redoximorphic spots. At the base of Channel Body 1, lenses 10 cm thick rest erosionally on other coarse facies, thickening to 40 cm in scours and overlain abruptly by facies Fl. In Channel Body 2, Sr forms units up to 1.5 m thick that rest abruptly or gradationally on facies St or Sh and locally pass upward from climbing to nonclimbing sets (Fig. 4-4D). Both facies St and Sr formed in the lower flow regime, as sinuously-crested dunes and ripples, respectively. For Sr, an upward transition from climbing to nonclimbing ripples represents progressively reduced aggradation of suspended sediment as flow strength declined, with thick beds indicating an abundant suspended load.

4.6 FACIES ARCHITECTURE AND PALEOFLOW

Channel Body 1 is 5 m thick above an erosional surface overlain by a thin, discontinuous layer of coarse deposits (Gm, Sh, Sr) formed during incision and initial flow. The remaining 4.5 m of the channel fill comprises mudstone (Fl overlain by Fm). A map of the basal contact outlines a linear channel with an axial position estimated from dip variations in the basal beds (Fig. 4-2). Elevation measurements indicate a concave-upward basal surface and a channel width of 65 m at the top of the preserved fill, based on a parabolic model. This suggests a width: thickness ratio for the channel body of 13:1, a "broad ribbon" geometry (Fig. 4-2; Gibling 2006). Erosion below Channel Body 2 probably removed the topmost fill of facies Fm, which may have overlapped the

margin to merge with floodplain deposits. A westward paleoflow for the basal beds appears oblique to the channel margin, suggesting deflection off the eastern bank.

Channel Body 2 is 6.5 m thick, with its topmost strata eroded, and comprises five erosionally based cycles, each 1-2 m thick, that fine upward from granule and/or pebble conglomerate to very fine-grained sandstone. In the sandstone, trough cross-beds (St) grade upward into plane beds (Sh) and climbing and nonclimbing ripple cross-lamination (Sr), indicating waning flow strength. In the fourth cycle, a basal erosional surface draped by lenses of pedogenic carbonate and mudstone clasts (Gm) with bone fragments is overlain by an antidune (Sl), overlain in turn by plane beds (Sh) and climbing and nonclimbing ripples (Sr; Figs. 4-2A, 4-4D). The basal surface is planar across the exposure, which is oriented normal to the eastward paleoflow, and the channel body is probably sheet-like.

4.7 PLANT FOSSILS

Description. --- Three common taxa (walchian conifers, cycadophyte foliage (?) *Taeniopteris*, and peltasperm foliage (?) *Auritifolia*) account for > 85% of the macrofloral foliage (Figs. 4-8A—G; Schachat et al. 2014). They were produced by seed plants, and their photosynthetic organs (branches or leaves) show varying degrees of robust construction. The most common floral elements are penultimate branch systems of so-called walchian conifers, an extinct paraphyletic group of small trees with a plagiotropic branching pattern. These branch systems were abscised as single units with ultimate branchlets, and their leaves still attached (Fig. 4-8A; Looy 2013). The leaves on the ultimate branchlets are bifacially flattened, ovate to awl-shaped, and distally incurved. Based on the distribution of variability of gross morphological features among these leaves, Looy and Duijnstee (2013) recognized four walchian “morphotypes” in the deposit, possibly unique species.

Taeniopteris sensu lato is nearly as common as the conifers (Fig 4-8E). This is a polyphyletic taxon (derived from more than one source, that is, not of a single line of evolution; Hale et al. 2005) that, in this deposit, consists mainly of foliage likely attributable to cycadophytic seed plants. The form most typical of *Taeniopteris sensu stricto* (Remy and Remy 1975) has elongated leaves with lateral veins that run nearly at right angles from the midvein to the leaf margin. A second form has large leaves (long and relatively wide) with venation that is much more angular in its insertion than is typical of the genus. It resembles *Lesleya*, although the veins are less flexuose than is typical of that genus (see discussion of the differences between *Taeniopteris* and *Lesleya* in Bashforth et al. in press). The third form of *Taeniopteris* is rare in the deposit and undescribed in the literature. The leaves are small with straight, right-angle, lateral veins that are widely spaced and forked near the midrib. They are of uncertain affinity and may be attributable to ferns or could represent specialized leaves associated with (unrecognized) reproductive organs (or possibly caducous pinnules, i.e. pinnules being shed at an early stage in development; Hale et al. 2005). All forms of *Taeniopteris sensu lato* at the study site appear to have been leathery in construction, indicative of long-lived leaves.

Third in abundance, but also common, is the comioid *Auritifolia waggoneri* (Fig. 4-8D; Chaney et al. 2009), a seed plant of possibly peltaspermous affinity. *Auritifolia waggoneri* has a pinnate leaf with distinctive fasciculate venation, similar to that of the genus *Comia* (Mamay et al. 2009), but within which are vein reticulations. Leaves were of robust construction with thick, woody petioles, suggesting that they stayed on the parent for several growing seasons.

Less common seed plants include *Nanshanopteris, Evolsonia, Supaia, Rhachiphyllum, Cordaites*, and cf. *Mixoneura*. The suspect peltaspermous affinity of many of these plants, based on their leaf architectures and venation patterns, is noteworthy. The peltasperms appear to have

undergone a broad evolutionary radiation during the early Permian in seasonally dry, tropical settings (DiMichele et al. 2005).

Nanshanopteris is a likely peltaspermous seed plant (Wan and Wang 2015), similar to *Brongniartites* of DiMichele et al. (2005), although Naugolnykh (1999) considered *Brongniartites* to be an illegitimate name. It is similar in form and may be closely related to *Glenopteris*, as described by Krings et al. (2005). *Nanshanopteris* has robust, unforked, once pinnate leaves, similar in shape to *Auritifolia waggoneri*, and the foliage likely had a long leaf lifespan. The habitat of the gigantopterid *Evolsonia texana* (Fig. 4-8C; Mamay 1989), a possibly peltaspermous seed plant, is unknown; some Cathaysian gigantopterids may have had liana habit (Li and Taylor 1998, 1999). Gigantopterids are common in Chinese and North American Permian strata. Whereas most older gigantopterids have distinctly forked leaves, *Evolsonia* leaves are unforked, broad, thick, and likely leathery with reticulate venation. *Supaia* sp., another likely peltasperm, is represented in the flora by a few specimens, one of which is distinctly forked at the base. White (1929) described many species of *Supaia* some of which, similar to the form described here, may belong to a single, morphologically variable species. Because of the small number of specimens in hand, we leave this material undetermined at the species level. The final probable peltasperm is *Rhachiphyllum* (Kerp 1988). Leaves are known to be forked, although that characteristic was not observed in the fragmentary Colwell Creek specimens. On each fork, leaves are twice pinnate; pinnules are flat, with steeply ascending veins and a weakly developed midrib that crosses the pinnule at an angle, macroscopically, from base to tip. Some veins originate from the rachis (rachial veins) rather than the pinnule midrib. In addition, an important character for identification is the presence of rachial pinnules, borne on the higher-order rachis between the ultimate pinnae.

Cordaites is the foliage of a group of woody seed plants closely related to the conifers (Florin 1954; Rothwell 1982). Leaves are elongate, often strap-like, with parallel veins. As a group, the cordaitaleans had an enormous ecological spectrum, from swamps in shoreline areas (Raymond et al. 2010) to upland regions under conditions of seasonal drought (Falcon-Lang and Bashforth 2005; Bashforth et al. 2014). Their leaves are easily confused in compression preservation with taphonomically flattened rachial axes of marattialean fern and medullosan seed plants, particularly if fragmentary, and are often overlooked.

Seed plants with medullosan affinities are poorly represented in the assemblage. Fragments of pinnules with fine, arcing venation and thin but well developed midveins are most similar to the medullosan seed plant *Mixoneura* (*Odontopteris*). For a recent discussion of this genus, its morphology and taxonomy, see Laveine and Dufour (2013).

Only a single species of an unquestionably pteridophytic plant, *Sphenophyllum* cf. *S. thonii*, was found. This plant is recognized by its distinctively wedge-shaped, multi-veined leaves. A terminal "fringe" of vein endings suggests the *S. thonii* affinity. Stems are jointed with clearly marked, swollen nodes. By analogy with other species of this genus (Batenburg 1982), *S. thonii* most likely was a scrambling, groundcover plant. As such, it is the only plant with that habit that has been identified in the flora. The paucity of groundcover elements, both taxonomically and in terms of abundance, in the fossil assemblage may be a taphonomic happenstance; this pattern is typical of many fossil assemblages and has been attributed to protection of small plants from the effects of wind as a natural sampling agent (Scheihing 1980). Alternatively, it is possible that there was little groundcover surrounding the site.

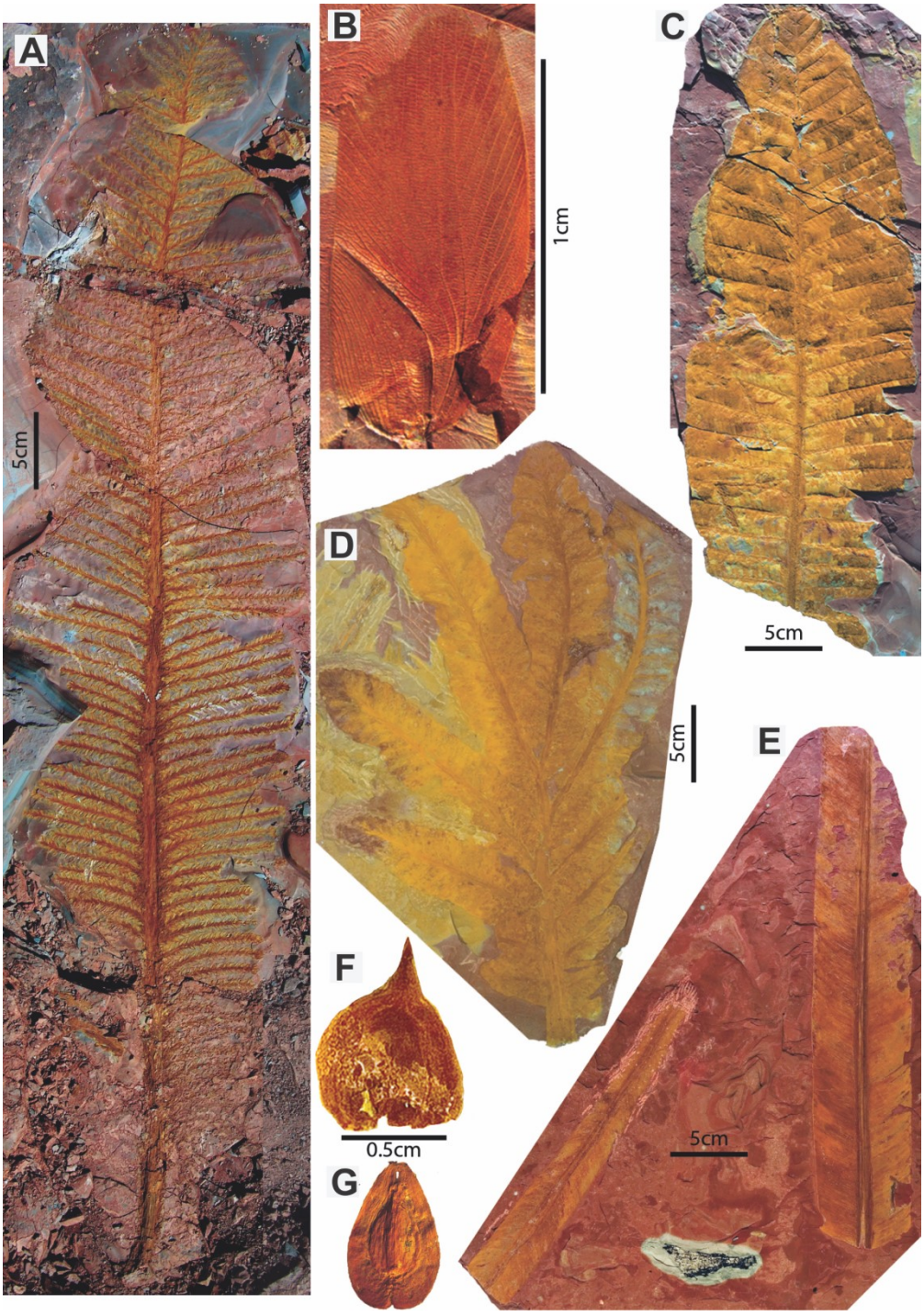

Figure 4-8 Plant and other fossils from laminated mudstone at the Colwell Creek Pond locality. A) Walchian conifer branch system (Looy and Duijnstee 2013). Morphotype IV) photographed in the field before extraction (USNM 536456). This image is a composite of a series of images. B) Blattoid wing (USNM 543850a). C) *Evolsonia texana* (USNM 528205b). D) *Auritifolia waggoneri* (USNM 508135). E) C f. *Taeniopteris*. Foliage similar to *Taeniopteris* in overall shape and in its open, dichotomous venation; however, venation angle falls outside that typical of the genus and may be indicative of a new taxon. (right: USNM 526033; left:USNM 530900). F) Type 1 seed (USNM 530907). G) Type 2 seed (USNM 539373).

Interpretation of life setting. --- The seed plants at the study site almost uniformly produced leaves that lived for more than a single season or, in the case of conifers, lateral branches with similar extended life spans. The leaves of *Evolsonia*, *Auritifolia,* and *Taeniopteris* are thick, large, and woody at the base or throughout; leaf thicknesses, measured from permineralized specimens, range from 200 to 250 μm. The branches of Colwell Creek walchian conifers appear to have formed over several seasons of growth, indicated by growth interruption points. In addition, a life span of several years is strongly suggested by woodiness and basal thickening of the branch bases (Looy, 2013). Increasingly, physiological studies of conifers with similar types of leaves show that they are mesic to tropical in their tolerances and do not prosper with water deficits (Pitterman et al. 2012). The above-mentioned groups are the four most abundant taxa in the flora (Schachat et al. 2014). These features point to a flora that, by modern standards, would be characterized as physiologically slow, within the leaf economics spectrum (Wright et al. 2004). The large size of these photosynthetic organs also suggests a large potential for transpiration and water loss, indicating that they grew in an environment with nearly year-round groundwater accessible to plants large enough to access this water source.

None of the plants represented in the flora appear to have been growing in swampy habitats. There are no tree ferns, lycopsids, or calamitalean sphenopsids, typical of equatorial regions of Pangea with high water tables but also of seasonally dry regions where sufficient moisture and occasional standing water supported their requirements (DiMichele et al. 2006). Their absence is, in fact, surprising. Wet-substrate plants, particularly tree ferns and calamitaleans, are known from numerous other deposits in the Leonardian redbeds of Texas, including sites younger than Colwell Creek Pond and much less intensely sampled. They also are known throughout western Pangea, locally in seasonally dry areas within or bordering channels (e.g., DiMichele et al.

2014), and appear to have reached even small wetland sites by virtue of their highly wind-dispersible propagules. It might be concluded, therefore, that their absence at Colwell Creek Pond is just a natural sampling happenstance. However, plant remains in abandoned channels almost invariably are drawn from the immediately surrounding area (Scheihing and Pfefferkorn 1984; Burnham 1989; Gastaldo 1989), and a largely seed-plant flora could indicate a channel with little or no area along the margins for plants requiring a nearly permanent source of water. Given the excellent preservation and evidence of minimal transport of the organic remains, these wetland plants should be represented if they were present.

We conclude that the flora is representative of the immediately surrounding vegetation, and, even in its suggestion of distinct seasonality, may indicate more mesic conditions than those of the interfluves — areas not represented or poorly represented in the assemblage. These more distant areas were likely populated by the most moisture-stress-resistant floral components, the conifers.

4.8 DISCUSSION

4.8.1 Incision and Sedimentation History

For Channel Body 1, it is surprising that the deep basal incision is draped only by thin, discontinuous coarse deposits below laminated fines (Fig. 4-9). Considerable erosive power would have been necessary to cut such a channel, implying the capability for coarse-sediment transport. Patchy basal deposits are characteristic of many Clear Fork channel bodies, and the scarcity of coarse detritus may represent a long transport distance from source areas to the east or denuded proximal (local to subregional) sources.

During incisional avulsion, flow is diverted from the parent channel onto the floodplain (Mohrig et al. 2000), commonly triggered by rapid alluviation, channel blockage, or high-magnitude floods (Miller 1991; Knighton and Nanson 1993; Slingerland and Smith 2004). If the new channel rejoins a sediment-deficient parent channel downstream, increased erosive power may increase the cross sectional area, thinning or removing entirely the pre-existing channel fill (Smith et al. 2014). In contrast, avulsion by annexation redirects the flow into other active, partially active, and abandoned channels, where part of the original channel fill is likely to be preserved (Morozova and Smith 2000; Slingerland and Smith 2004). With no indication of a pre-existing fill, incisional avulsion is the preferred model for the creation of the Colwell Creek Pond channel. Channel creation may have linked overland flow paths or erosional hollows around trees (cf. Gibling et al. 1998), rather than resulting from a single catastrophic event.

Basal gravel (Gm) overlain by plane-laminated (Sh) and ripple cross-laminated (Sr) sandstone represents waning flow after incision. As indicated by diplichnitid trackways, arthropods were active on the channel floor at this time. Although *Diplichnites* is known from marine and freshwater environments, it is common in freshwater settings (e.g., Buatois et al. 1998; Netto et al. 2009), and *Diplichnites gouldi* has been attributed to continental organisms elsewhere in the Clear Fork Formation (Minter et al. 2007).

The laminated mudstone (Fl) represents the initiation of a standing-water body, essentially a small lake, within the incision. The abrupt incoming and sustained deposition of these beds suggests complete disconnection from the parent channel (Toonen et al. 2012), and the lack of evidence for subaerial exposure, such as desiccation cracks, rainprints, or wind-blown sand, suggests permanent standing water. Sedimentary features indicate deposition from density underflows and suspension (Toonen et al. 2012), probably generated by sediment-charged

floodwater from neighboring rivers, rainwater flow along tie channels or floodplain depressions, or bank slumps (Mertes 1997; Rowland et al. 2005; Marren and Woods 2011). Groundwater discharge below a spring line can contribute water to channel systems on distal alluvial plains (Weissmann et al. 2013, 2015; Hartley et al. 2013), and this process may have assisted in maintaining standing water for prolonged periods. Retention of water would have been aided by the fine-grained, impermeable nature of underlying floodplain deposits (Marren and Woods 2011), as well as flood-derived clay that can seal channel incisions and reduce seepage into the groundwater (Knighton and Nanson 1994a, 1994b; Cendón et al. 2010). In the arid plains of Cooper Creek, where annual evaporation greatly exceeds precipitation, standing bodies of water (waterholes) above the water table can be retained in the channel over several years before flow recommences (Cendón et al. 2010) and are considered more-or-less permanent (Knighton and Nanson 1994b).

Based on the average lamina thickness, the 203-cm-thick unit contains 2900 laminae. An individual lamina may represent a multiannual or annual flow event, (Shanahan et al. 2008; Lojka et al. 2009), or several flows may have taken place during a single year. If flows were annual, the laminated unit would have taken ~ 2900 years to accumulate. Some oxbow lakes may be long-lived: in Sky Lake, in the Mississippi area, 120 cm of sediment was deposited in ~ 3600 years prior to anthropogenic effects (Wren et al. 2008), and an oxbow lake in the Czech Republic lasted for nearly 800 years before the lake filled and became a eutrophic fen (Pokorný et al. 2000). However, we suggest that multiple flooding events occurred in most years, as in many modern seasonal areas, and that the sediments accumulated in much less than 2900 years. Oxbow lakes connected to a main river via tie channels may fill in decades to centuries (Rowland et al. 2005), although the sediment is generally coarser than the laminated beds at

Colwell Creek Pond. The upward change to massive mudstone with root traces (Fm) indicates progressive shallowing, probably due to sedimentation within a fixed incision, and vegetation may have enhanced pedogenesis considerably.

In contrast to Channel Body 1, Channel Body 2 represents a major fluvial system with considerable coarse sediment (> 6.5 m) and a sheet-like form. The stacked cycles represent repeated short-lived flow events with high-flow-strength bedforms (plane beds and an antidune) followed by deposition of abundant suspended sediment (climbing ripples). The eastward paleoflow, in contrast to the westward paleoflow of Channel Body 1, remains to be explained in a basin with known topographic uplifts to the north and east (Fig. 1-2A). Sheet-like channel bodies with a change in paleoflow direction were also observed at two other outcrops in the middle Clear Fork Formation.

4.8.2 Modern and Ancient Analogues

Channel Body 1 is interpreted as an abandoned channel that was part of a meandering system, the predominant fluvial style in the formation (Edwards et al. 1983; Nelson et al. 2013). Partial analogues are found in Quaternary abandoned channels (oxbow lakes) along the Mississippi and Rhine rivers (Guccione 1993; Guccione et al. 1999; Toonen et al. 2012), although these systems have abundant coarse sediment and much larger channels than those of the Clear Fork alluvial plain. These modern oxbows locally contain up to 3 m of laminated dark silty clay to clay with disseminated organic matter and thin sandy silt beds. As the water shallowed, vegetation was established and up to 2 m of dark homogeneous silty clay to clay was laid down, with lamination destroyed by shrink—swell processes and roots. The grain size and lamina thickness of the fills reflect in-part the distance downstream from the cutoff, the water depth, and plugging of the upstream part of the oxbow, restricting access to coarser sediment. To date, we have not

identified a modern abandoned-channel fill that replicates closely the varicolored laminated mudstone of Channel Body 1.

In the Upper Triassic Chinle Formation, fossiliferous abandoned-channel deposits are composed of < 2 m of dark, laminated carbonaceous mudstone and sandstone (Demko 1995). These fining-upward deposits filled oxbow lakes and moribund channels and are thinly laminated (1—10 mm thick), locally bioturbated, and rooted at the top. In the late Permian Normandien Formation of the Karoo Basin in South Africa, an oxbow-lake fill comprises 3—4 m of olive gray shale with glossopterid leaves and other vascular plant organs (Prevec et al. 2009). Although the shale was not described in detail, the authors suggested that the water body was semiperennial based on the paucity of desiccation features, the thickness of the channel body (25 m), and the presence of discrete sediment packages. In the early Permian Wichita Group, which underlies the Clear Fork Formation in Texas, gray or yellow lenses in redbeds represent shallow abandoned channels or ponds and contain vertebrate bones and plants (Sander 1987; Hotton et al. 2002; Chaney et al. 2005; Labandeira and Allen 2007). Little information was provided about stratification, but the drab color suggests reducing bottom conditions.

In terms of its stratification, the Colwell Creek Pond mudstone resembles the deposits of some larger modern and ancient stratified lakes. These deposits are variably composed of detrital, carbonate, and organic laminae with vertebrate, invertebrate, and plant material, and the lamination is commonly attributed to annual events or flows that laid down graded beds (Wilson 1977; Ludlam 1981; Gibling et al. 1985; Demicco and Gierlowski-Kordesch 1986; Clausing and Boy 2000; Menounos et al. 2005; Shanahan et al. 2008; Lojka et al. 2009). Although some process inferences may be applicable, such large lakes are not applicable to the study site, which was little more than 5 m deep and a few tens of metres wide. A closer analogue is provided by

laminated mudstones in the Miocene Siwalik Group of Pakistan (Zaleha 1997a, 1997b), attributed to short-lived to perennial floodplain lakes less than 10 m deep; however, these deposits contain micritic calcite and sparse trace fossils.

A possible analogue for Channel Body 2 is the ephemeral sheetflow-dominated River Gash in Kassala, Sudan (Abdullatif 1989). This broad, shallow sandbed river has laid down a sheet of coarse sediment and experiences high discharge variations, evaporation, and infiltration in an arid setting. Deposits include cross-beds, plane beds, and scour-and-fill units, with successions laid down during events of high flow strength and waning flow.

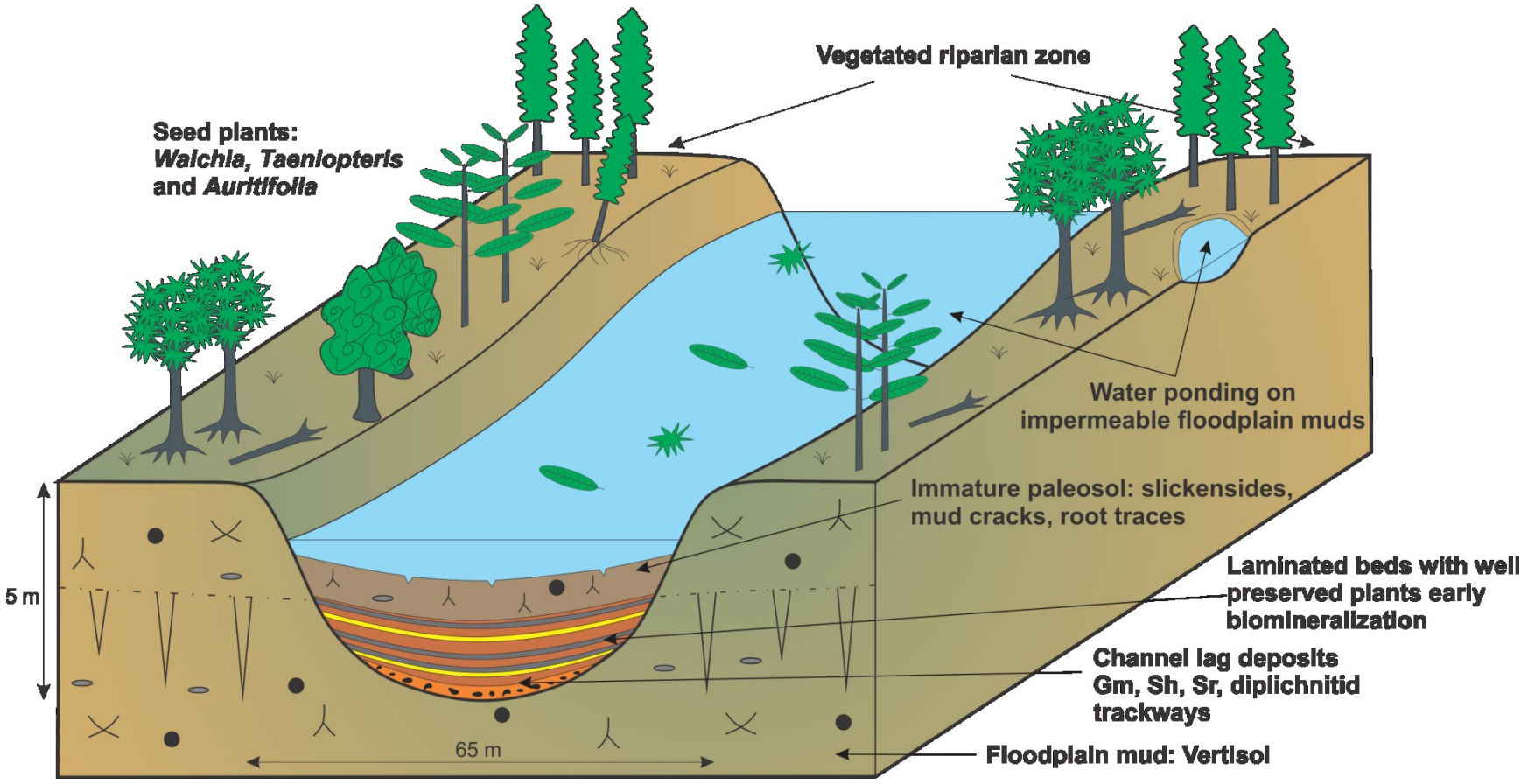

Figure 4-9 Schematic diagram showing the paleoenvironment of Channel Body 1.

4.8.3 Preservation of Lamination

The preservation of laminated mudstone in subaqueous settings is generally related to the impoverishment of benthic fauna, limiting disruption of the laminae (Cohen 1984). Paleozoic freshwater environments were dominated by epifaunal traces (Buatois and Mángano 1993), and infaunal activity is not recorded until the Permo-Triassic, since endobenthos required new ways of obtaining oxygen and completing their reproductive cycles (Miller 1984; Miller and Labandeira 2002). Sites elsewhere in the Clear Fork Formation yield diverse trace fossils characteristic of Early Permian redbeds (Lucas et al. 2011), but the presence of surface traces and the lack of open burrows suggest largely epifaunal communities (Minter et al. 2007).

Reduced benthic populations also have been related to low bottom- or pore-water oxygenation, low productivity, a high sedimentation rate, and elevated salinity (Verschuren 1999; de Gibert and Ekdale 2002). Anoxic conditions at the bottom of a permanently stratified lake is the most common explanation for the absence of bioturbation (Kelts and Hsu 1978; Anderson and Dean 1988). However, Cohen (1984) showed that, in Lake Turkana in Kenya, oxygen-saturated water was present down to the water—sediment interface due to mixing by wind action and the low depth:fetch ratio. At 4 cm below the interface, a sharp decline in oxygen was accompanied by a change from red-brown to olive-green sediment, the latter inferred to be laminated. The scarcity of benthic organisms was attributed to a subsurface oxygen deficit and to the low concentration of organic matter in the sediments, implying a limited food source. Laminae may also be preserved where rapid sediment accumulation outpaces the capacity of the macrobenthos to homogenize the sediment (Verschuren 1999), as inferred for abandoned-channel fills of the Mississippi River by Guccione (1993). Several studies have suggested a correlation between

hypersalinity and reduced diversity (Sugden 1963) and an increase in dwarfism (Kinne 1970; Price 1982).

For Miocene laminated lacustrine beds in Pakistan, Zaleha (1997a) suggested that the lake was oxygenated throughout based on wave-ripple cross-lamination and the scarcity of plant detritus. The rarity of organisms and preservation of lamination was attributed to the low availability of organic detritus as a food source, the high sedimentation rate, and chemical factors such as alkalinity, pH, total dissolved solids, and trace elements.

None of these explanations can be entirely supported or ruled out for the Colwell Creek Pond site. We hypothesize that the delayed colonization of freshwater ecospace was an important factor (Miller and Labandeira, 2002). Anoxic to dysoxic bottom or subsurface conditions may have prevailed periodically, but the presence of graded beds and other flow features, coprolites and swim marks, and cements of hematite and goethite suggest that bottom water and shallow sediment was mainly oxygenated. The low organic content of the mudstone may imply low productivity in the standing water and limited nutrient availability for benthos, although organic matter is rapidly oxidized on seasonally dry alluvial plains (Sharma et al. 2004). Evidence for active flow suggests that rapid sedimentation assisted in preserving lamination from bioturbation. Petrographic analysis failed to indicate phases associated with elevated salinity or unusual chemical conditions, such as carbonates, evaporites, or unusual clay minerals (e.g., sepiolite, palygorskite). However, calcium carbonate precipitates from sea water only when salinity is ~ 1.8 times normal values (McCaffrey et al. 1987), and elevated salinity need not be accompanied by a mineralogical signature. Although a seawater model is not applicable to the study site, elevated salinity may have excluded benthic organisms but left little other trace. In conclusion, the presence of undisturbed lamination may be attributed to delayed colonization of the

abandoned channel by benthos, supplemented by issues of water chemistry, sedimentation, and productivity.

4.8.4 Paleoclimate

Evidence relevant to a paleoclimatic interpretation was obtained at three stratigraphic levels. For floodplain deposits below Channel Body 1, the paleosols are interpreted as paleo-Vertisols formed in seasonal settings, in accord with the presence of mixed-layer clays and desiccation features. A significant observation is the presence of dolomite in the paleosols and reworked pedogenic dolomite nodules in facies Gm at the base of Channel Body 1. Detrital dolomite may have been reworked from the Wichita and Arbuckle Mountains (Ham 1973; Gilbert 1982) or derived as windblown accessions from coeval marine deposits or playa lakes (Petersen et al. 1966; Kessler et al. 2001; DiMichele et al. 2006; Minter et al. 2007). However, an upward transition from early-formed calcite and ankerite cement in the lower member to dolomite and gypsum cement in the middle and upper members (S. Simon, unpublished data) implies increasingly evaporative groundwater conditions which would have elevated Mg/Ca and promoted dolomite formation (cf. Arakel and McConchie 1982; Spötl and Wright 1992; Colson and Cojan 1996; Schmid et al. 2006). Notwithstanding a possible contribution from reworked dolomite, the stratigraphic evolution of the groundwater suggests relatively arid conditions.

For Channel Body 1, the laminated beds represent a standing-water body with no indication of desiccation over a period of centuries to a few millennia. XRD analysis indicates a terrigenous composition and the water may have been fresh, although a modest salinity increase could have gone unrecorded. Invertebrate traces are restricted to arthropod trackways, and although this suggests an inimical environment, these were early days in the colonization of benthic freshwater settings. Non-moisture-limited conditions are indicated by seed plants with large, robust thick

leaves, suggesting that the parent plants grew in riparian settings where they experienced periodic moisture stress but had access to groundwater nearly year round. A puzzling point is that the assemblage lacks plant groups characteristic elsewhere of seasonally dry settings where water sources were locally available. Paleo-Vertisols at the top of the channel fill differ from those below the channel body in the prominence of drab root traces, suggesting that shallow water tables during final filling promoted the growth of vegetation.

Collectively, these points appear to suggest a relatively humid, seasonal climate during the deposition of Channel Body 1. However, the evidence is difficult to assess because it was derived from an abandoned channel where water would have ponded against relatively impermeable paleosols (Marren and Woods 2011). Additionally, modern channels commonly exchange water with adjoining aquifers and riparian zones, receiving subsurface water by hyporheic flow during dry seasons, which influences habitat diversity and ecological processes. Cendón et al. (2010) provided evidence of such an interchange on distal river plains in Australia. At Quaternary archeological sites in Tanzania (Driese and Ashley 2015), local springs increased soil moisture, which promoted vegetation growth and enhanced pedogenic processes, resulting in an elevated estimate of mean annual precipitation in comparison with regional estimates based on other proxies. Although this spring-fed example does not accord with the context of the study site, the Tanzanian example illustrates that local water sources, such as might be derived from periodic floods or shallow aquifers, can modify soils considerably.

For Channel Body 2, thick coarse sediments with high-flow-strength bedforms, waning-flow cycles, and rapid aggradation indicate large volumes of available water and strongly seasonal flow patterns. Although this suggests a more humid climate and a change in flood patterns

(Tooth 2000), the channel body may represent a trunk channel within the drainage system, and the change in paleoflow direction suggests a different source area.

In summary, the most robust evidence for paleoclimate at the Colwell Creek Pond site comes from the floodplain soils below Channel Body 1, which suggest a relatively arid, strongly seasonal paleoclimate. In Channel Body 1, pedogenic processes were probably enhanced by local water availability, allowing riparian vegetation to take advantage of a water-dependent habitat (DiMichele et al. 2006). However, a more humid climate during this period cannot be ruled out, and Quaternary climatic and fluvial records document fluctuations over centuries to a few millennia that radically changed water and sediment budgets (Knox 1993; Gibling et al. 2005; Zhang et al. 2009; Ge et al. 2013). Additionally, the later Kungurian was marked by glaciation in Gondwana (Montañez et al. 2007; Fielding et al. 2008) and, although the level of biostratigraphic precision for the Clear Fork Formation precludes detailed correlation, the Colwell Creek Pond strata may have experienced the far-field effects of global climatic changes.

4.8.5 Taphonomy and Preservation of Plant Material

Plant material is commonly preserved as "three-dimensional goethite petrifactions" in the laminated mudstone (Looy 2013), where early mineralization preserved undistorted anatomical structures of stems and leaves (Fig. 4-10). The absence of cellular crushing or compaction prior to permineralization indicates early infiltration and hardening of iron compounds in the plant tissues (Dunn et al. 1997). In most modern leaves, the hydrophobic waxy cuticle prevents direct reaction with metals (Kok and Van Der Velde 1994; Dunn et al. 1997). However, leaves coated with bacterial biofilms bond readily with Fe^{3+} within minutes of being placed in water that contains $FeCl_3$, whereas those that lack biofilms do not (Dunn et al. 1997; see also Spicer 1977). Additionally, in environments where oxygen and uncomplexed Fe^{3+} are readily accessible, iron

bacteria such as Sphaerotilus and Leptothrix promote iron encrustation on the leaves (Caldwell and Caldwell 1980; Lütters and Hanert 1989). Bacterially induced iron deposits are present on biological and sediment surfaces in channels of the Amazon Basin (Konhauser et al. 1993). This process may be a viable mechanism for explaining the well-preserved plant remains at the Colwell Creek Pond site.

Some plant parts, especially of conifers, were coated with a layer of goethite that obscured their features. No cellular structure was associated with these coatings. We hypothesize that these layers were originally algal or bacterial films on the surfaces of plants floating in the water or on the bottom. Yellow goethite-rich laminae may indicate the presence of biofilms in the channel, although they lack microbial textures. The lack of destructive bioturbation would have assisted in preserving these remarkable plant fossils.

4.9 CONCLUSION

The Colwell Creek Pond site of the Clear Fork Formation represents a small abandoned channel or oxbow lake, with standing water and associated relatively high soil moisture in an otherwise generally dry Early Permian landscape. The 5-m-deep channel was abandoned soon after incision and was infilled with laminated and massive terrigenous mudstone, with a low organic content and no indication of carbonate or evaporite minerals. The laminae were laid down by gentle flows in a standing body of water where the impermeable nature of the underlying soils and perhaps exchange with associated aquifers helped to retain water in the abandoned channel. Abundant large plant remains include branch systems of walchian conifers, leaves of Taeniopteris and Auritifolia, and other seed plants that probably grew in the riparian zone and were blown or washed into the channel.

Due to the absence of bioturbation and roots, sediment laminae in the abandoned channel were well preserved. A combination of low productivity, high sedimentation rate, elevated salinity, and limited bottom- or pore-water oxygenation may have inhibited benthic organisms, but freshwater ecosystems were underpopulated by infauna during the Early Permian, a reflection of an evolutionary delay in colonization of such habitats.

Paleosols in underlying floodplain deposits are interpreted as paleo-Vertisols formed under relatively arid conditions, with evidence for a strongly seasonal and probably evaporative setting. In contrast, paleosols in the upper part of the channel body yield evidence for wetter conditions. Although we cannot rule out a more humid climate for the plant-bearing laminae, the most parsimonious explanation is that the abandoned channel is a site where water was available for plant growth and preservation in an otherwise relatively arid plain. The exceptional preservation of plant material is attributed to early biomineralization and rapid burial in the absence of burrowing organisms.

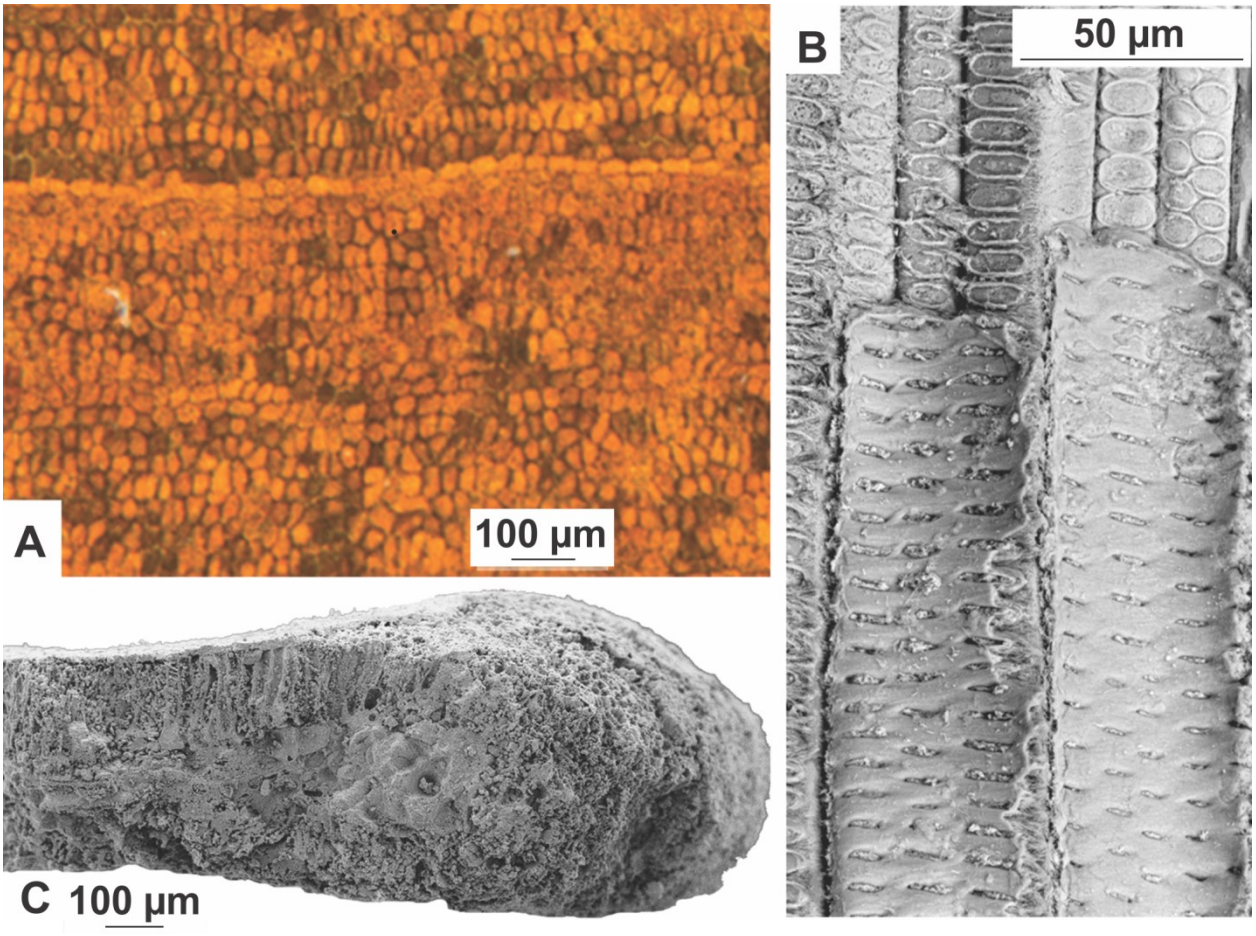

Figure 4-10 Goethite petrification of cellular structure of plant remains recovered at the Colwell Creek Pond locality. A) *Taeniopteris* (USNM 539325) true-color image of the adaxial leaf surface. The cuticle was not preserved; the adaxial ends of the palisade cells are visible and grouped into costal and inter-costal bands. B) *Taeniopteris* (USNM 539324) SEM micrograph. View of tracheid cells in the main vein of the lamina. Elongate hollow tracheid cells are broken longitudinally, exposing the internal openings to oval bordered pits. C) *Auritifolia waggoneri* (USNM 528671) SEM micrograph. View of broken edge of leaf cross section showing the palisade cells, parenchyma, and the lower adaxial epidermis. At the right, the rounded outer edge of the leaf is slightly inflated compared to the internal part of the lamina.

.

CHAPTER 5 OTHER FACIES

Three additional facies (debris-flow deposit, stromatolite bed, and playa-lake deposits) were identified within the Clear Fork Formation but were not mentioned in the previous chapters. In this section, a brief description and interpretation of these facies are presented.

5.1 DEBRIS-FLOW DEPOSIT

Description: At the Mixing Bowl site, a poorly-sorted pebble conglomerate with carbonate and rip-up mud clasts, concretions, and plant fragments forms massive or weakly stratified beds up to 70 cm thick (Fig. 5-1A). The facies rests erosionally on accretion deposits (LA-3) of mud-rich channels and is traced along a depositional low for up to 5 m but rapidly pinches out laterally into massive mudstone beds (MM). The facies is primarily composed of clasts made up of interlocked euhedral to subhedral dolomite rhombs and quartzose grains (Fig. 5-1B, D). Some clasts are finely crystalline with cracks lined with hematite and vugs filled by coarsely crystalline dolomite (Fig. 5-1C, D). Between the dolomite clasts, quartzose grains float within finely crystalline dolomite cement with clay minerals and hematite along the pores (Fig. 5-1E).

Interpretation: This facies is interpreted as a channelized debris-flow deposit laid down by the mobilisation and entrainment of sediments within a confined stream (Nettleton et al. 2005). The debris-flow could have been initiated by a landslide in the upland areas (upflow direction) or by extreme floods during periods of lengthy or intense precipitation. The flow reworked rocks and pedogenic fragments from the floodplain paleosols, flowing down a gully or depositional low, before laying down the poorly sorted deposits. The carbonate cements formed during shallow burial, linked to the permeability difference between the coarse-grained deposits and the underlying muds (Nash and Smith 2003).

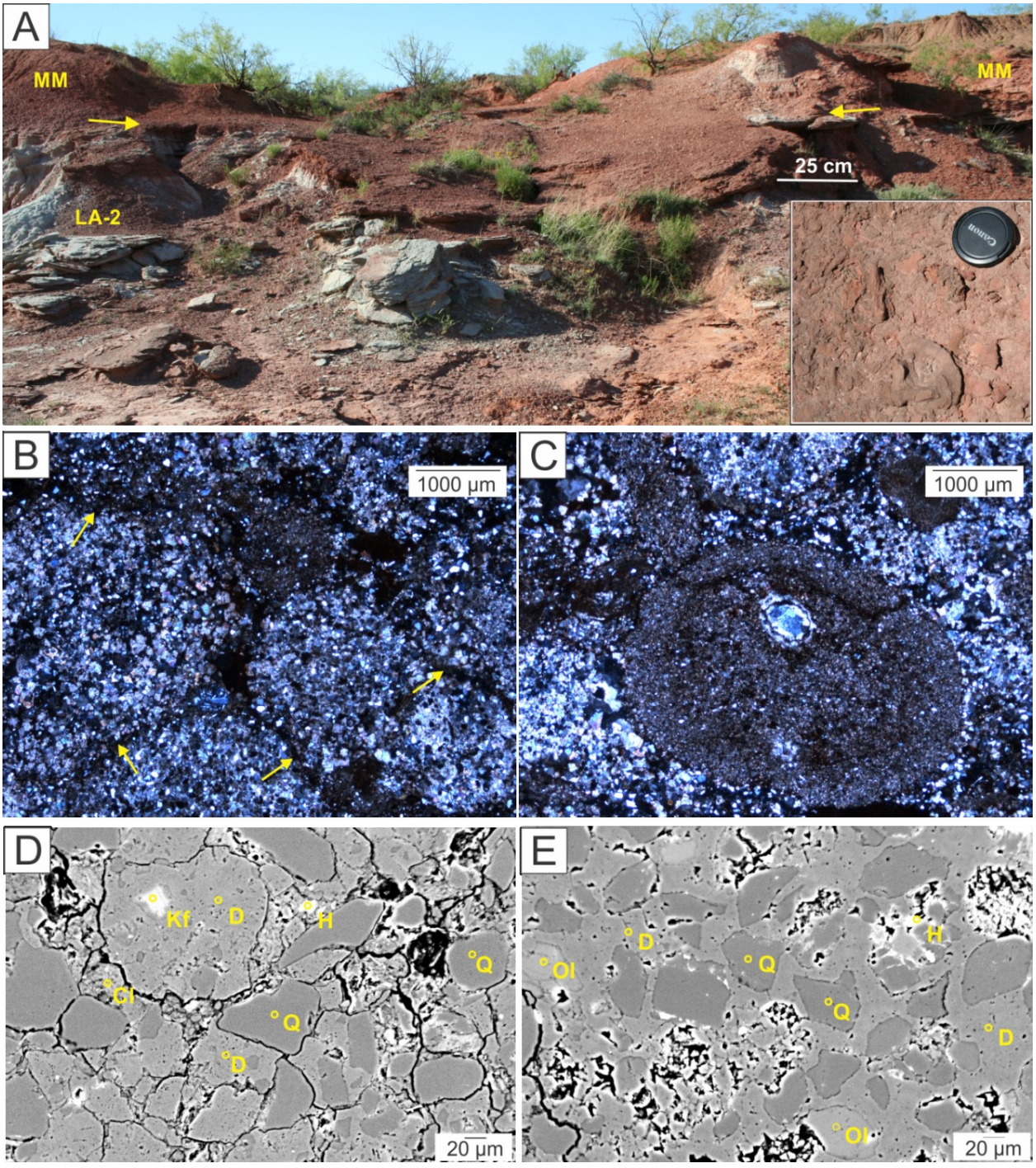

Figure 5-1 Debris-flow deposit at Mixing Bowl (MB). (A) Red, pebble conglomerate with carbonate clasts, concretions, rock fragments, rip-up mud clasts, and plant fragments forms massive to weakly stratified unit up to 70 cm thick (inset map). The conglomerate fills a 10 m wide depositional low cut into the underlying accretion deposits (LA-2) of the mud-rich channels. The deposit pinches out perpendicular to the channel axis (yellow arrows) and can be traced along the axis for up to 5 m. Flow direction is towards the observer. (B) Clasts composed of interlocked euhedral to subhedral dolomite rhombs and very fine sand- to silt-sized quartzose grains, with well-defined hematite rims. (C) Rounded, finely crystalline clast with vug filled with coarsely crystalline dolomite and cracks lined with hematite. (D) Backscatter image to show distinct dolomitic clasts and quartzose grains, lined by clay and hematite minerals, cemented by finely crystalline dolomite. (E) Backscatter image to show subangular to subrounded quartzose grains cemented by finely crystalline dolomite with pores lined with clay minerals and hematite. Quartz (Q), dolomite (D), K-Feldspar (Kf), oligoclase (Ol), and hematite (H). Lens cap in A is 55 mm.

5.2 STROMATOLITE BED

Description: Massive, blocky siltstone with dome tops is present at the base of a mud- and quartz-rich channel. (Fig. 5-2A, B) These beds are up to 20 cm thick and form an irregular patch which abruptly overlies massive mudstone (MM) deposits. In some areas, these beds are not well-developed and are significantly smaller, less than 10 cm thick, and more friable. A section through these siltstone beds reveals no internal features or prominent layering. X-ray diffraction and petrographic analysis reveal that the beds are composed primarily of very finely crystalline dolomite with few silt-sized quartzose grains (Fig. 5-2C).

Interpretation: Although columns and laminations were not apparent, the shape and composition of the massive siltstone deposits are provisionally interpreted as freshwater stromatolite beds developed within shallow playa lake settings (Freytet et al. 1999; Minter et al. 2007). The occurrence of some beds along the channel base also suggests intermittent flows with periodic development of lacustrine beds within the channels (Alley 1998). Early dolomitization masked or destroyed the original features and layering, resulting in a massive, blocky bed. Alternatively, prismatic columnar structures have been recognized in sodium-influenced (natric) argillic horizons in paleosols, which developed under semi-arid to arid environments (McCahon and Miller 1997).

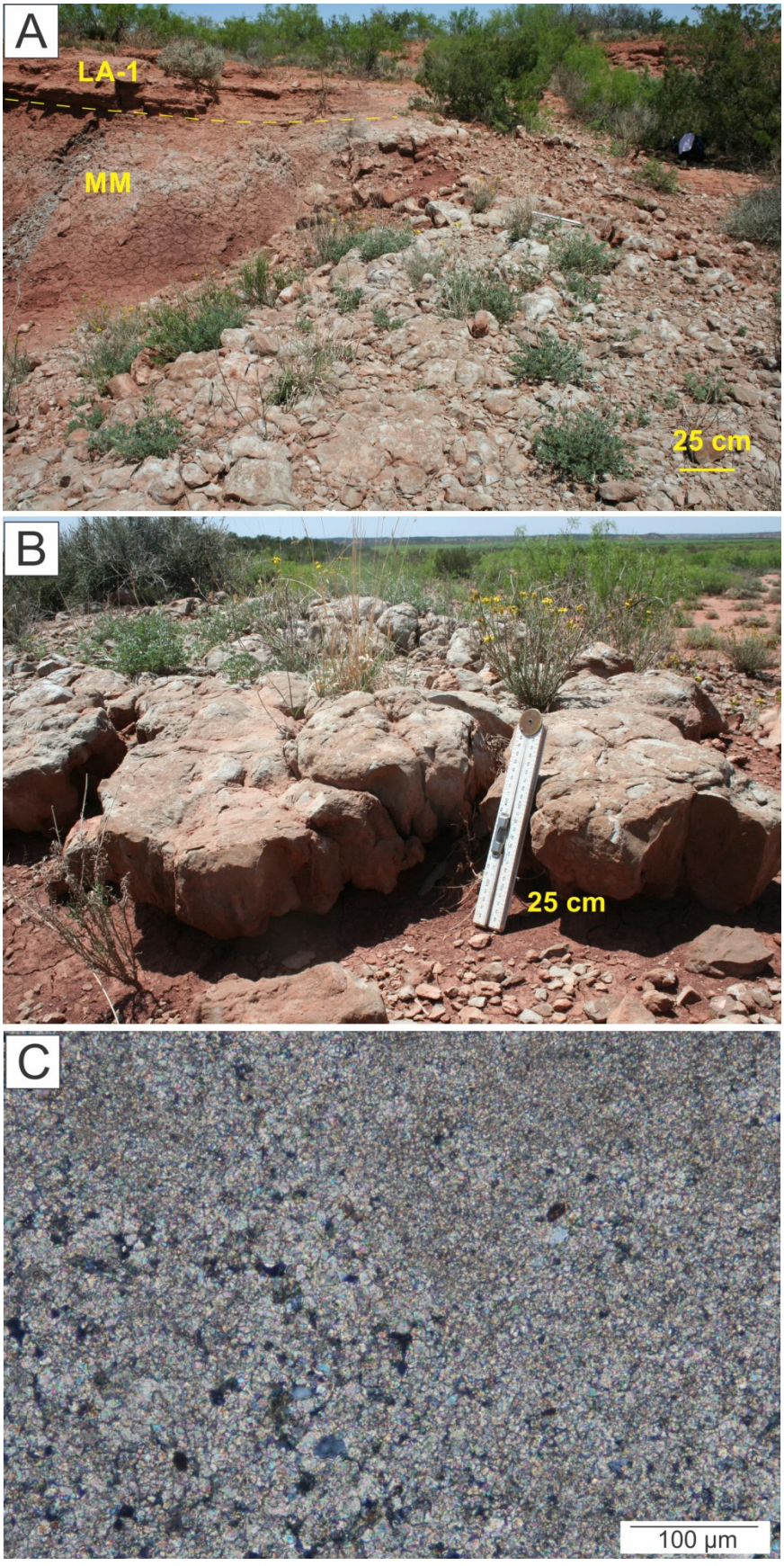

Figure 5-2 (A) Stromatolite bed at Montgomery Ranch 2 site (MR2). The stromatolite bed (nodular-weathering carbonate unit in foreground) overlies massive mudstone (MM), and is overlain by lateral accretionary deposits (LA-1) of a quartz-rich channel body in the low cliff at back left. The stromatolite bed is locally present but does not appear to extend across the base of the channel body, in the area of the dashed line. (B) Close up view of the stromatolite bed which is composed of a massive, blocky dolomite bed with domes on the top surface. A section cut through a sample of this bed in the lab revealed no internal features or prominent layering. (C) Stromatolite bed composed of finely crystalline dolomite with very few quartzose grains.

5.3 PLAYA LAKE DEPOSIT

Description: In the upper Clear Fork unit, gypsum occurs as rosettes, veins, dikes, and nodules up to 25 cm in diameter with sheets interbedded with silty dolomite. Extensive dolomite and gypsum beds overlie massive mudstones (MM) adjacent to or incised by channels, and in some areas, they occur as distinct, irregular patches, apparent in planview across flat ground (Fig. 5-3A, B). At the Narrows, couplets of gypsum and dolomite are prominent and extend for several kilometers.

Interpretation: The occurrence of extensive dolomite and gypsum beds overlying massive mudstones is interpreted as playa lake deposits (Minter et al. 2007; Giles et al. 2013). These lakes were probably sourced from saline groundwater and surficial water, allowing the primary precipitation of dolomite and gypsum. Although these beds were not studied in detail, there is no diagnostic evidence for marine influence in this area.

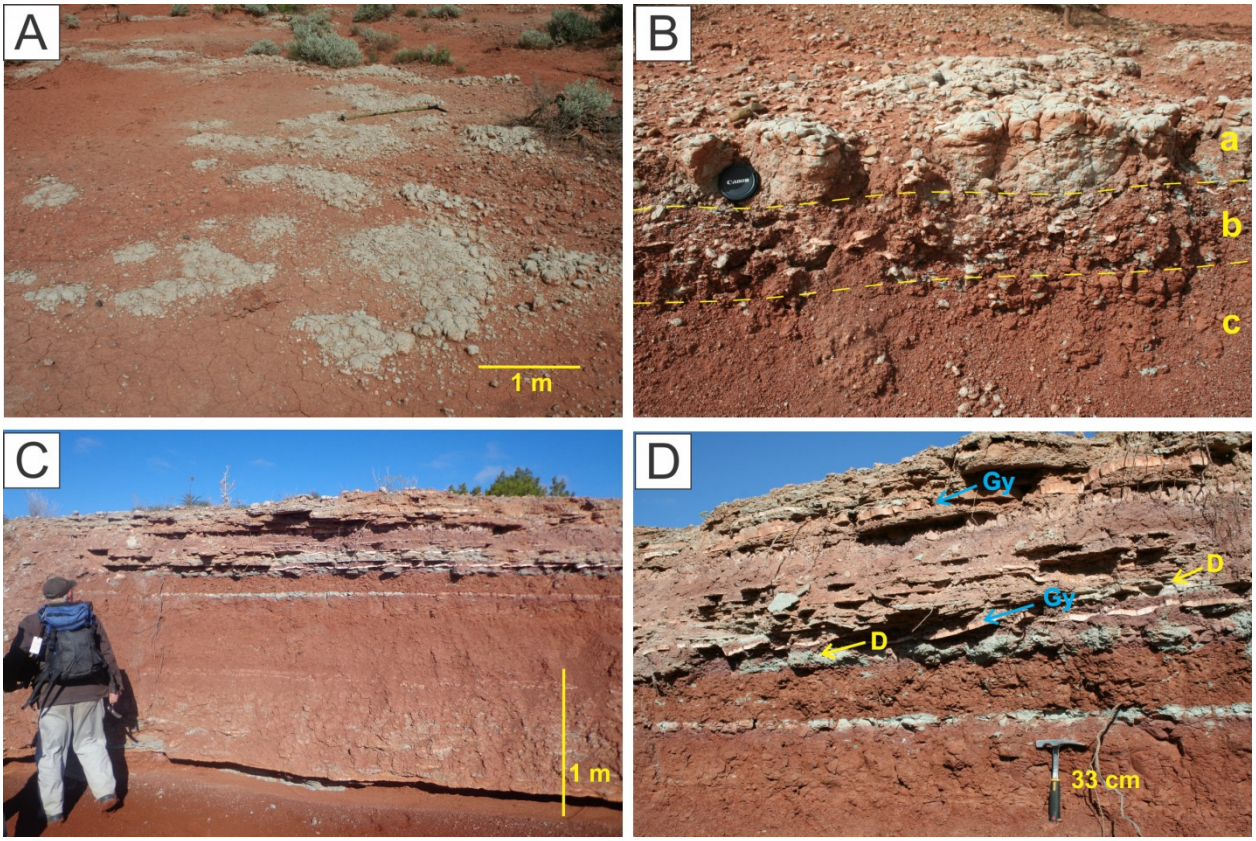

Figure 5-3 Shallow playa lake deposits in the upper Clear Fork Formation. (A) At MR 2, patchy dolomite deposits overlie massive mudstone of floodplain deposits. Individual patches are about 1-1.5 m wide and occur over a relatively large area (over 30 m square). (B) Cross-section through one of these dolomite patches. Three layers were identified and separated by gradational contacts (yellow dashed lines). The top layer 'a' is a blocky, massive dolomite with vugs filled with gypsum and calcite. This is underlain by layer 'b' which consists of stratified dolomite with gypsum nodules and red siltstone. Layer 'c' comprises blocky to weakly stratified siltstone with redoximorphic spots and mottling. (C/D) At the Narrows, couplets of gypsum (Gy) interbedded with dolomite (D) overlie red massive mudstone. The couplets are laterally extensive and can be traced for a few km.

CHAPTER 6 DISCUSSION

6.1 INTRODUCTORY STATEMENTS

In the previous chapters, we documented the objectives of the study, the methods used, and the main findings; a brief summary of the salient points is presented here.

Chapter 2 describes the sedimentary features and mineralogical composition of the fluvial channel bodies (meandering systems and tabular sandstones) within the Clear Fork Formation. The fine-grained meandering systems are the dominant fluvial style and are subdivided into three groups: quartz-rich (Q), mud- and quartz-rich (MQ), and mud-rich (M) systems, which represent a continuum between sustained lateral accretion of bedload deposits (quartzose sediment and mud aggregates) and oblique accretion of suspended sediment (clays). In the mud- and quartz-rich systems, the crests of the ripple were skewed (swept) relative to channel flow due to the rapid decline in water levels and downstream re-entry of overbank floodwaters into the channel. Thick, tabular sandstones (TS) were formed by high energy, episodic flows in broad, sandbed channels. Within the formation, progressive aridification was inferred based in part on the upward mineralogical change from mainly calcite and ankerite to dolomite and gypsum with minor celestine as cements within the channel bodies and floodplains.

Chapter 3 documents the first known example of well-preserved mud aggregates, as the main sediment component, in a fine-grained meandering channel. Under (semi)arid climates, the mud aggregates were formed in paleosols containing swelling clays of illite, Fe-rich chlorite and mixed-layer clays. During flooding events, the sand-size aggregates were washed into the channels where they were transported as bedload alongside other detrital and ferruginous grains and were eventually deposited on the point bars. The unique preservation of the mud aggregates

in the channel is attributed to (a) the encasing clay matrix and hematite rims, (b) partial buffering by detrital and ferruginous grains along with the early formation of dolomite rhombs and cements of varied composition, (c) the rapid burial of aggregates within the migrating point bar set in a rigid "compartment" cut into tough and relatively non-compactible paleosols, and (d) shallow long-term burial of the formation.

Chapter 4 presents an unusual case of exquisitely preserved leaves on laminated mudstone within an abandoned channel. The plant materials, with evidence of arthropod herbivory, were derived from seed plants growing in the riparian zone, and the excellent preservation is attributed to rapid burial in the absence of burrowing organisms and early biomineralization. The absence of benthic fauna was probably related to the evolutionary delay in freshwater colonization in the Early Permian, supplemented by low productivity, elevated salinity, and limited bottom- or pore-water oxygenation. The abandoned channel was a site of unusual water availability for plants in an otherwise (semi)arid landscape, as indicated by floodplain paleosol types, with standing water persisting for centuries to a few millennia.

Chapter 5 presents a brief description and interpretation of three additional facies (debris-flow deposit, stromatolite bed, and playa-lake deposits), which were identified within the Clear Fork Formation but were not mentioned in the previous chapters. In the following sections, we refer to these findings as we investigate the upward changes within the Clear Fork Formation. In this chapter, we also briefly summarise the key features of the formations overlying and underlying the Clear Fork Formation, in an attempt to study long-term stratigraphic changes within the Permo-Pennsylvanian section. At the end of this chapter, a future work section is included to address the limitations of this study.

6.2 LANDSCAPE RECONSTRUCTION: SOURCE TO COASTAL PLAIN

Throughout this thesis, parallels at various scales (outcrop to basin level) were drawn between the Clear Fork Formation and the Channel Country region of central Australia (Table 6.1). However, a full paleoenvironmental reconstruction cannot be adequately conducted without considering the Clear Fork Formation in the broader context of the Permo-Pennsylvanian section (Fig. 1-2B). For the underlying Bowie and Wichita Groups and the overlying Pease River Group, we summarize the key findings from Hentz (1988) and Nelson and Hook (2005), respectively (Fig. 1-4). For the Clear Fork Formation, we integrate the findings from this study with those of DiMichele et al. (2006), Chaney and DiMichele (2007), and Nelson et al. (2001, 2013).

6.2.1 Bowie and lower Wichita Groups

The Bowie (Markley and Archer City Formations) and lower Wichita (Nocona Formation) Groups exhibit features characteristic of piedmont and upper coastal plain environments (Fig. 6-1, 6-5), which include interstratified deposits of sandy braided rivers, meandering rivers, and floodplain deposits (Fig. 6-1). In the piedmont, multistory channel-fill sequences at the foothills of the topographic uplifts (Ouachita foldbelt, Muenster Arch, Arbuckle, and Wichita Mountains) comprise the deposits of gravel- and sand-bed braided rivers. These river deposits contain planar lamination and medium- to large-scale trough and tabular cross-beds with prominent chert-pebble conglomerate at the base of the channel. Mixed-load meandering channels grade westward from the braided systems in the piedmont and similarly fine upward from pebbly, very coarse sandstone with medium- to large-scale trough and tabular cross-beds to ripple cross- and planar-laminated fine sand. Interstratified with the channel bodies are floodplain deposits, which comprise predominantly red mudstone, crevasse splay sandstone, levee deposits of siltstone and mudstone, ephemeral channels, and fossiliferous floodplain ponds. By proportion, the groups are

composed of 50-90% mudstone, 10-30% sandstone, <10% conglomerate, and <1% coal (only in the Markley Formation).

In the Markley Formation of the Bowie Group and underlying Virgilian section, extensive bituminous coals and plants such as pteridosperms, marattialean ferns, lycopsids, and calamites, are present along with histosols, ultisols, inceptisols, and vertisols rich in kaolinite and illite, suggesting humid conditions (see section 1.4; Tabor and Montañez 2004; DiMichele et al. 2006). In the Archer City Formation of the Bowie Group and Nocona Formation of the Wichita Group, seed plants along with aridisols, alfisols, and vertisols rich in smectite, illite, and kaolinite are prominent, suggesting seasonal, (semi)arid climatic conditions.

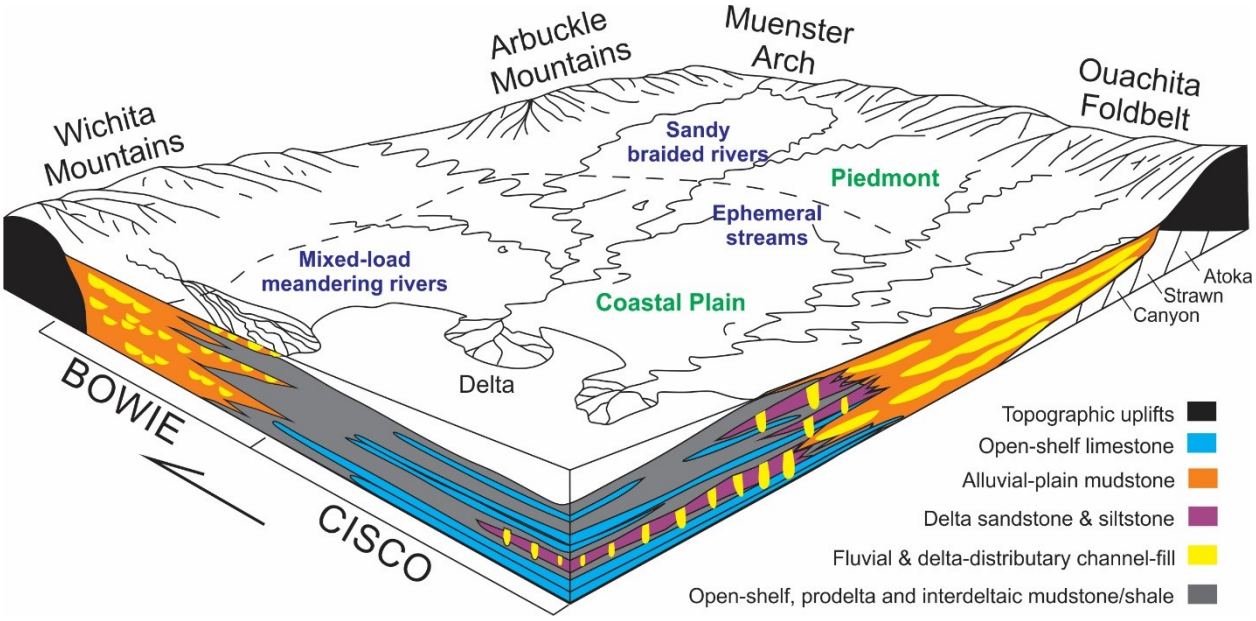

Figure 6-1 Schematic paleoenvironmental reconstruction of contemporaneous Bowie and Cisco facies (adapted from Hentz 1988). Sandy braided rivers traversed the piedmont area and were sourced from the topographic uplifts and possibly thrust-faulted Atoka, Strawn, and Canyon rocks. In the upper coastal plain, mixed load meandering rivers and ephemeral streams were prominent and associated with crevasse splays, levees, and backswamps. Regional fluvial transport directions were mostly northwest to southwest.

6.2.2 Wichita Group (middle and upper interval)

The middle and upper Wichita Group (Petrolia, Waggoner Ranch, and Lueders Formations) contains sedimentary features typical of lower coastal plain deposits (Fig. 6-2; 6-5), suggesting that the coastline advanced landward in comparison to the Bowie Group. The lower coastal plain comprises a diverse range of facies including mud-rich meanderbelts, ephemeral streams, interchannel facies (including floodbasin ponds), tidal mud-flats, coastal ponds and marshes, shallow shelf facies, and nearshore terrigenous clastic muds. By proportion, the group is composed of 80-95% mudstone, 5-20% sandstone, <1% conglomerate, and <1% limestone.

Sediments were transported to the coastal regions by highly sinuous, mud-rich meandering systems. The channel fills are composed of very fine- to fine-grained sandstone. In the lower part of the point bar, medium- to large-scale trough cross-beds and cut-and-fill scours are locally present, implying deposition of bedload by high intensity flows. In the upper 75% of the point bar, thin inclined interbeds of cross- and planar-laminated very fine sandstone and weakly stratified silty mudstone make up the lateral-accretion deposits, reflecting alternating periods of deposition from traction currents and suspension. The point bars experienced continuous lateral growth based on the regular spacing of the accretion deposits, but at some exposures, they are erosionally superimposed, suggesting episodic accretion and adjustment of channel courses during major floods. Ephemeral streams, which exhibit little evidence of lateral accretion, are also a minor component of the coastal plain and are composed of poorly sorted, massive conglomerate with clasts of calcareous nodules, mudstone, and locally, bone material. These channel bodies are generally isolated, but may be stacked with a thin layer of red mudstone separating them.

On the floodplains, floodbasin ponds contain variegated laminated claystone, with the color attributed to the abundance of organic matter, authigenic iron sulfide, mixing of green clay (illite and chlorite), malachite, and azurite. These laminated deposits are also common within oxbow lakes where they represent the final stages of infilling. Within the floodbasin ponds, carbonized floral remains (hash) are abundant, but fronds, stems, and seeds are less common (Mamay 1960, 1966; Read and Mamay 1964). Also, fossilized fish, reptiles, and amphibians are well-preserved (Sander 1987), but invertebrates such as insects are sparse.

In the shallow shelf environment, several mappable limestones, representing the nearshore termination of thicker, shallow-shelf limestones of the Albany Group, extend upslope and interfinger with the coastal plain facies. The Lueders Formation which directly underlies the Clear Fork Formation is a limestone bed used to correlate the continental deposits with the marine beds to the south. For a detailed assessment of the tidal mud-flats, coastal ponds, and marshes, see Hentz (1988).

The paleosols and plants present in the middle and upper Wichita Group are similar to those within the Archer City Formation of the Bowie Group and the lower Wichita Group (Nocona Formation). As a result, paleoclimatic conditions are also inferred to be (semi)arid with seasonal precipitation.

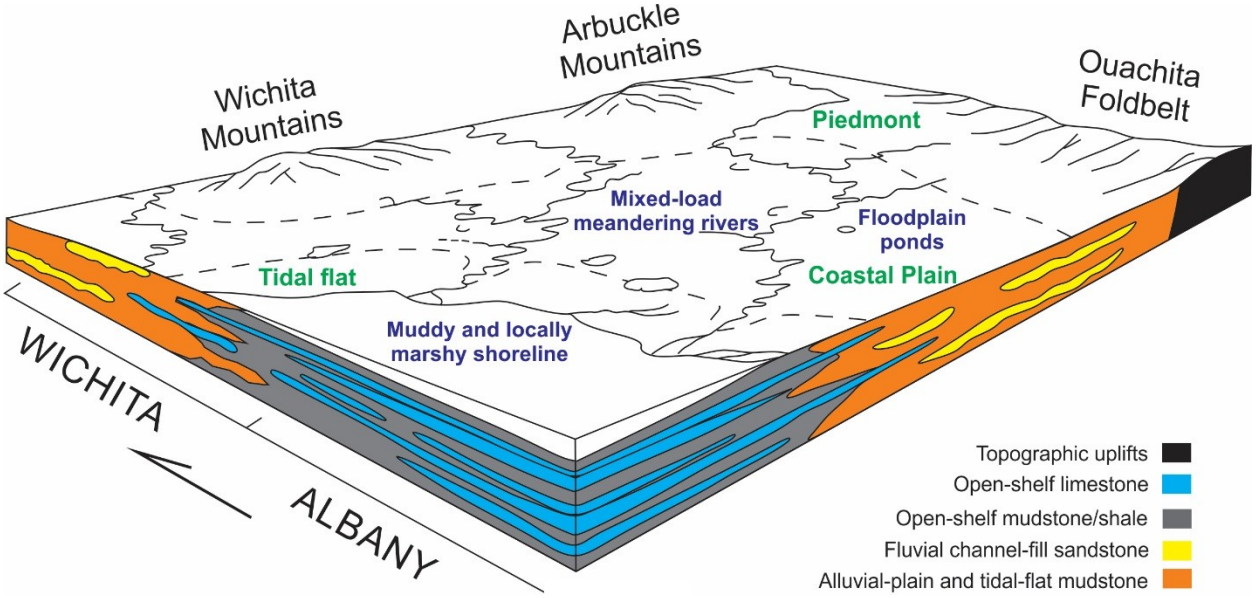

Figure 6-2 Schematic paleoenvironmental reconstruction of contemporaneous Wichita and Albany facies (taken from Hentz 1988). Sources of the fine-grained fluvial systems were primarily from the north (Wichita and Arbuckle Mountains). In comparison with the Bowie/Cisco reconstruction, source-area relief is significantly diminished and fewer and finer grained river systems existed.

6.2.3 Clear Fork Formation

The main geologic features of the Clear Fork Formation are described at length in the previous chapters, but a brief summary is provided here (Fig. 6-3) with a comparison to the Channel Country Rivers of Australia (Table 6-1). Figure 6-4 summarise the key stratigraphic changes within the Clear Fork Formation; the information presented in this figure was derived mainly from this thesis and integrates work by Hentz (1988), DiMichele et al. (2006), Chaney and DiMichele (2007), and Nelson et al. (2001, 2013). Elements of this figure are discussed in the following sections.

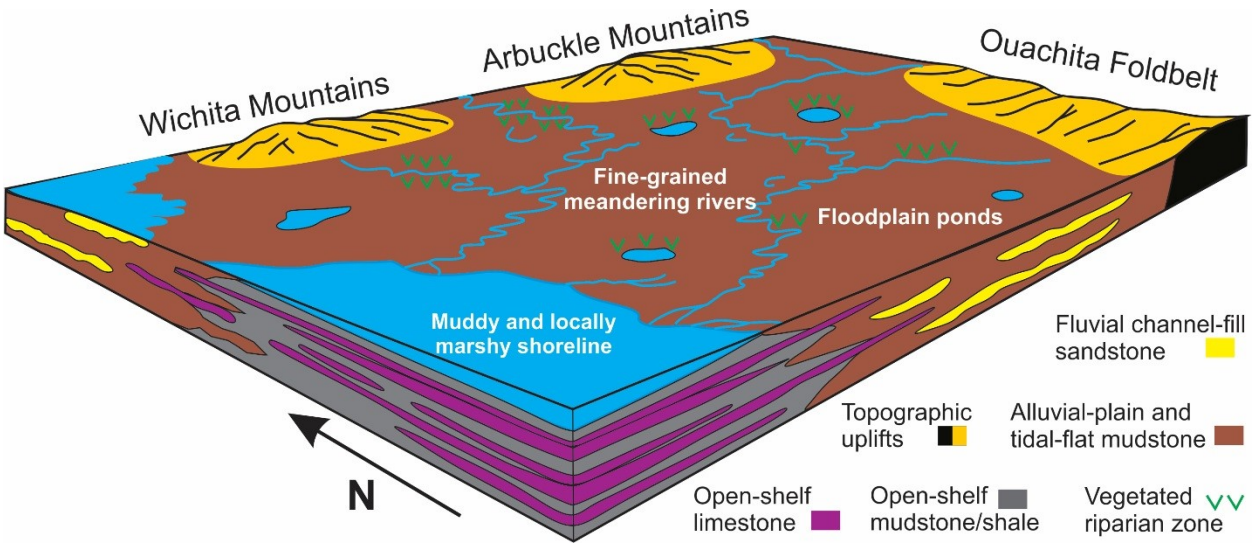

Figure 6-3 Schematic paleoenvironmental reconstruction of the Clear Fork Formation (modified from Hentz 1988). Sources of the fine-grained fluvial systems were primarily recycled from within the basin and the topographic uplifts to the north (Wichita and Arbuckle Mountains) and east (Ouachita Foldbelt).

Table 6-1 Sedimentary features of the Lower Permian Clear Fork Formation of north-central Texas and the Channel Country Rivers of Australia. Summary of the Channel Country systems are taken from Gibling et al. 1998.

Characteristics	Clear Fork Formation, north-central Texas	Channel Country Rivers, Australia
Geologic setting	Tectonically stable during the Early Permian; gently subsiding Eastern Shelf of the Midland Foreland Basin	Tectonically stable intracratonic basin
Climate	Arid to semiarid with variable precipitation; rainfall estimate < 650 mm/yr (threshold for pedogenic calcite formation)	Arid to semiarid with variable precipitation; rainfall in headwaters 400-500 mm/yr and 120 mm/yr in deserts; Diurnal temperatures range from 49 °C to -2 °C
Drainage pattern	Rivers drain uplands and flow several hundred kilometres across a broad, low-gradient plain to the coastline (south/west); exorheic basin	Rivers drain uplands and flow 1000 kilometres to Lake Eyre (a salt pan); endorheic basin
Flow pattern	Mostly low flow regime floods that do not exceed bankfull conditions; intermittent short-lived, high magnitude floods (middle unit)	Extreme flow variability; during floods, discharge of a single week can greatly exceed the river's mean annual discharge; during drought, flow ceases with stagnant water retained in waterholes
Channel type	Mostly fine-grained meandering rivers, with local tabular sandstone and debris-flow deposits	Mostly anastomosing channel systems, with meandering and braided rivers
Channel geometry	Variable width:depth ratios; single or multiple stories; thickness <8 m	Low width:thickness ratios; channel bodies up to ~10 m thick
Channel fills	Broadly fining upward point bars, accretionary benches, tabular sandstones	Single storey fills observed to date; broadly fining up; accretionary benches and channel-base sheets prominent
Sediment type	80-85% mudstone, 10-15% sandstone, <5% limestone,	Mainly sand-sized mud aggregates, with suspended

	dolomite, and gypsum; varies depending on channel type; combination of quartzose sand, mud aggregates, and suspended clay; low TOC with permineralized leaves	fines and some quartz sand; some organic material preserved in channels
Channel borders	No evidence of levees and scroll topography; thin splay deposits	Levees with modest relief, braid bars and channels; mainly mud aggregates
Deep scours (waterholes)	Deep scours up to 5 m filled with laminated and massive mudstone. Probably distal from active channel bodies. Formed by incisional avulsion through the linking of overland flow paths or erosive hollows around trees	Unusually deep waterholes along channel reaches, at constrictions between dunes and bedrock, and at confluences
Floodplains and pedogenesis	Low aggradation rate; vertic argillisol, calcisol, gleyed calcisol, vertic calcisol, vertisol, and calcic vertisol; paleosols with calcrete, dolocrete, and bedded gypsum	Vertisols with gilgai, desiccation cracks to 1 m, calcretes and gypsum at depth
Fossils	A varied assemblage of plant, vertebrates, some invertebrates, and trace fossils	Widespread vegetation; shells common; bioturbation widespread in channels, waterholes and on floodplains

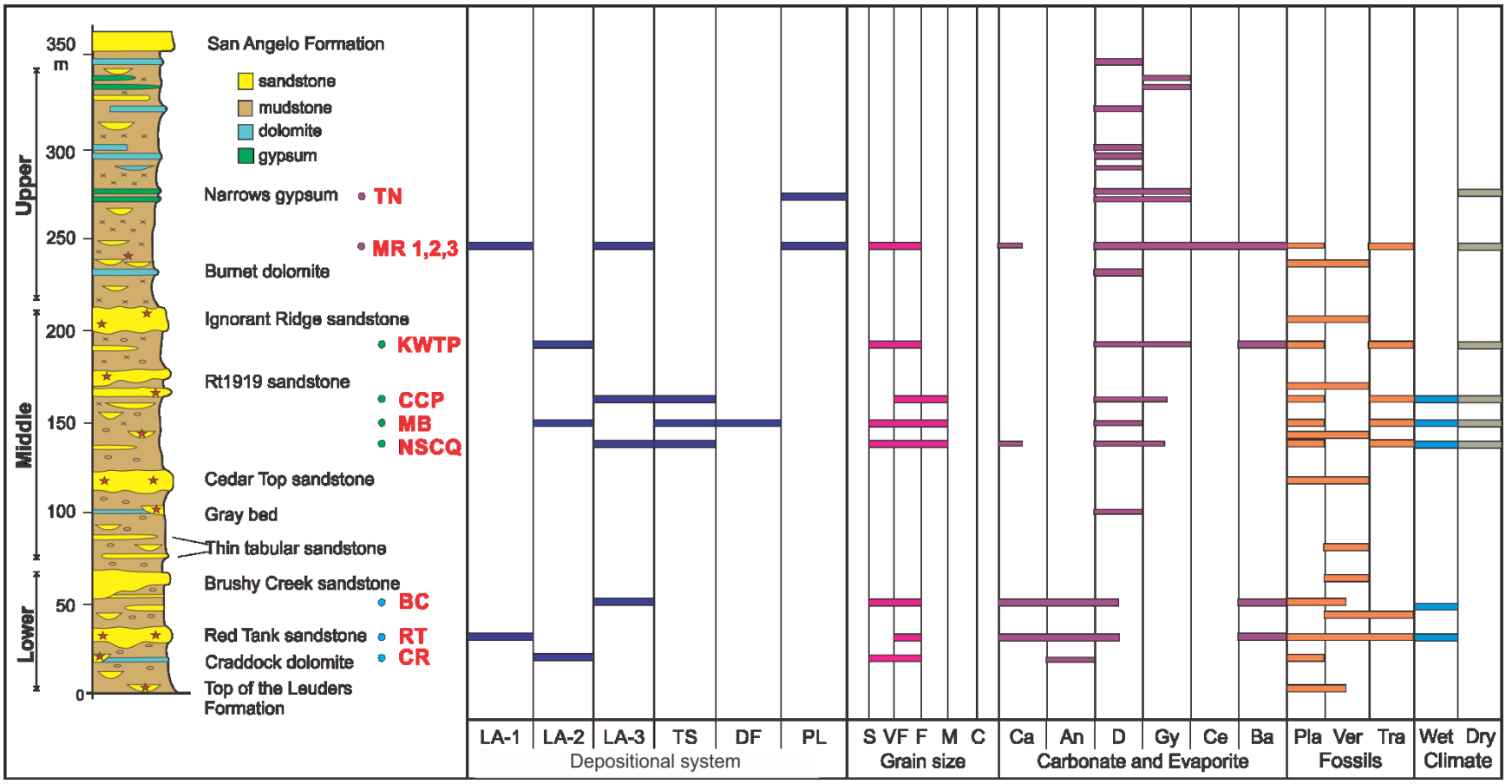

Figure 6-4 Upward changes in fluvial style, grain size, mineralogy, and fossils within the Clear Fork Formation (see text for further descriptions and semi-quantitative estimates) as well as climatic conditions. The bars mark the occurrence and relative position of sedimentary features; half bars represent rare occurrences of minerals. Fluvial styles: quartz-rich (LA-1), mud-rich (LA-2), mud- and quartz-rich (LA-3), tabular sandstone (TS), debris-flow (DF), and playa lake (PL) deposits. Grain size: silt (S), very fine sand (VF), fine sand (F), medium sand (M), and coarse sand (C). In the middle unit, the presence of medium sands is linked to the occurrence of TS. Carbonate and evaporite in the form of cement, nodules, beds, and dikes: calcite (Ca), ankerite (An), dolomite (D), gypsum (Gy), celestine (Ce), and barite (Ba). These minerals are mostly present in channel deposits but also in the less-sampled paleosols. Fossils: plant material (Pla) which include stems, leaves, and roots; vertebrate (Ver); and trace fossils (Tra) which include shark and fish coprolites, failed aestivation assemblages of lysorophoid amphibian *Brachydectes* and lungfish *Gnathorhiza,* burrows of *Taenidium barretti/Planolites montanus*, fish scales, and trackways of *Diplichnites gouldi.* For sites not visited, data were obtained from DiMichele et al. (2006), Chaney and DiMichele (2007), and Nelson et al. (2001, 2013).

6.2.3.1 Channel body type and occurrence

The Clear Fork Formation is composed of channel bodies (meandering channels and tabular sandstones) interbedded with muddy floodplain deposits. Three types of fine-grained meandering channels were identified in the formation [quartz-rich (Q), mud-rich (M), and mud- and quartz-rich (MQ) systems], but no definite stratigraphic change in their occurrences is apparent through the section (Fig. 2-15; 6-4). The three types of meandering channel bodies are present in the lower unit; in the middle interval, only M and MQ channel bodies were identified, whereas in the upper unit, Q and MQ systems were present. Overall, the M and MQ styles were more abundant, with Q channels only present at two sites. The most significant change occurs within the middle unit where tabular sandstones (TS) overlie M and MQ channel bodies at several sites. At an equivalent level, one small occurrence of debris-flow deposits (see Fig. 5-1) and highly avulsive mud-rich meandering channels were also present. Although not identified as a formal fluvial style, fossiliferous abandoned channels with prominent laminated mudstone (element LM) form part of the meandering systems (e.g. CCP; see chapter 4). Additionally, crevasse splay deposits are rare throughout the formation, implying that floods rarely exceeded bankfull conditions to carry quartzose materials onto the floodplains.

In addition to meandering channels, Nelson et al. (2013) also identified braided fluvial channels in the top of the lower unit, which (a) "are thicker and more deeply incised than the other Clear Fork channels; (b) contain a higher percentage of sand and larger grains (fine as opposed to very fine); (c) feature a predominance of grain-supported mudstone-pebble conglomerates instead of carbonate-pebble conglomerates"; and (d) exhibit planar and trough crossbed sets up to 2.5 m thick. Since Nelson et al. (2013) conducted an extensive mapping project over a decade, the identification of this additional style is not surprising. The authors also identified small

ephemeral channels within the upper 150 m of the formation based on the presence of small, single-story channel bodies with lateral accretion deposits. However, we believe that these channel bodies are analogous to the mud- and quartz-rich systems identified in this study and therefore, do not represent an additional fluvial style. In terms of channel body thickness, Nelson et al. (2013) described channel bodies 8-15 m thick, whereas in this study, the thickest channel body was less than 8 m thick, since we focused specifically on sites with fossiliferous channel bodies and paleosol data.

Another key stratigraphic change is the upward decrease in channel-body occurrence in the formation. In view of the badland nature of the outcrops and scattered exposure of near-horizontal beds, no quantitative assessment of channel-body proportions could be made, and an assessment relies on the stratigraphic column of Nelson et al. (2013), which is composed of 80-85% mudstone, 10-15% sandstone, and <5% limestone, dolomite, and gypsum (Fig 1-3). Channel bodies appear relatively evenly spaced in the lower and middle units. However, in the upper Clear Fork, few channel bodies are present and they overlie massive mudstone deposits containing tabular gypsum and dolomite beds with provisionally identified stromatolites (see section 5.2). This facies assemblage implies a progressive change from channelized and floodplain deposits in the lower and middle units to modest channel activity with floodplains and shallow playa lakes on the landscape in the upper unit (see Fig. 5-2, 5-3). To the southwest (central Texas), Minter et al. (2007) also identified small ephemeral (playa) lakes in the Clear Fork Group that developed in shallow depressions on the alluvial plain. However, the occurrence of some stromatolite beds along the channel base also suggests intermittent flows with periodic development of shallow saline lakes within the channel (Alley 1998). Nelson et al. (2013) noted that the upper unit shares similarities with other Lower Permian sequences attributed to a mud-

rich coastal to continental sabkha system in the subsurface of King, Cottle, and Childress Counties to the west (Fig. 1-4). However, the authors dismissed this interpretation based on the absence of evidence for tidal activity, suggesting that the upper unit represents up-dip continental deposits that formed on an arid, low gradient coastal plain in ephemeral streams and lakes.

6.2.3.2 Sedimentary features

The sedimentary features present within the formation are environment-specific and depend on their stratigraphic position. For example, lower and upper flow regime bedforms (2D/3D ripples, dunes, plane beds, and antidunes) are present in the quartz-rich (Q) systems and tabular sandstone (TS) deposits where they are commonly stacked based on decreasing flow strength. In contrast, lower flow regime bedforms (2D/3D ripples and a few dunes) and sedimentary features indicative of receding and low water levels (e.g. rill casts and symmetrical ripples), as well as complete drying out (e.g. disrupted mudstone and desiccation cracks) are common within the accretion and channel-fill deposits of the mud-rich (M) and mud- and quartz-rich (MQ) channels.

By evaluating the MQ channels, which are present throughout the formation, it is apparent that the flow strength varied significantly between the channels in the lower and middle/upper units. For example, at the Mouth of Brushy Creek in the lower unit, the accretion deposits are composed primarily of 3D and 2D ripples and some of the ridges contain convex-upward sets of plane-laminated sandstone; in contrast, the channels in the middle and upper units comprise primarily 2D ripples. On average, the accretion deposits are inclined at a lower angle (12.7^{o}) than the channels in the middle and upper units (14.5^{o}) and contain less rill casts. Also, elongate scours, some of which extend the full length of the exhumed point bar (up to 60 m), are associated with the inclined bedsets. This comparison shows that, although the channels were of the same style, the flows were considerably stronger and more active in the lower unit,

suggesting that more water was available on the landscape.

Since the meandering channel bodies are primarily composed of fine-grained sediments, it is not possible to conclusively interpret the original depositional conditions, because the grain size of the sediments (silt and clay) tend to preclude the formation of bedforms larger than ripples (Southard and Boguchwal 1990). Also, beds containing bedload-transported mud aggregates, which are only visible in thin section, appear massive at the outcrops as the sedimentary structures were masked during burial, precluding an assessment of the bedforms.

Similar to the quartz-rich beds in the upper unit (MRG 2), the tabular sandstones in the middle unit (MB, NSCQ, and CCP) contain upper flow regime bedforms and sedimentary features indicative of waning flows. This suggests that high energy floods were interspersed with periods when flows were consistently of low magnitude, as evident by the meandering channels.

6.2.3.3 Grain size

The grain size of the sediments varies with position on the landscape. As expected, channel bodies contain coarser sediments than the floodplains with the exception of a few splay deposits composed of thin lenses of very fine sand, which extend for a few metres. The quartzose layers in the meandering channel deposits are commonly silt to fine-grained, whereas the tabular sandstones are fine- to coarse-grained. Also, some of the mudstone beds in the channel bodies are composed of fine-grained mud aggregates. Overall, there is a slight upward decrease in the grain size of the meandering channel bodies, but this trend is punctuated by episodes where coarser quartzose material was brought into the basin and deposited as tabular channel bodies (element TS).

6.2.3.4 Mineralogy

The mineralogical composition of the Clear Fork Formation is described based on the fluvial elements and also in terms of upward changes throughout the section. The former is briefly summarised in section 2.5 of Chapter 2 but is described at length in Appendix C, whereas the latter is presented below.

Within the formation, detrital grains are composed of quartz, feldspar (K-feldspar and plagioclase), iron minerals (hematite and goethite), heavy minerals (titania minerals, zircon, apatite, and ilmenite), mud aggregates, ferruginous grains, and carbonate clasts. The preservation of unstable feldspar minerals suggest that climatic conditions were relatively arid, inhibiting chemical weathering.The relative proportion of intraclasts to mineral grains varies depending on the position in the channel; carbonate clasts are mostly present in channel lag deposits and in the small debris-flow deposit at Mixing Bowl, whereas quartzose minerals are abundant in lateral accretion deposits and tabular sandstones. In some channel bodies, mud aggregates are the main sediment component with only a minor proportion of mineral grains. Overall, the assemblage of the detrital grains appears uniform throughout the formation, with no obvious differences. However, the fine-grained nature of most quartzose samples makes it difficult to assess changes in the relative proportions of mineral types.

Clay minerals comprise Fe-rich chlorite, kaolinite, illite, and mixed-layer clays. Although the semi-quantitative proportion of clay minerals was not estimated in this study, the relative similarity of peak heights on the XRD traces suggests little variation in relative abundance between samples (see appendix D). The composition of the clays in the aggregates and matrix was similar and consistent up-section.

The most significant mineralogical change is the upward variation in the composition and abundance of carbonate and evaporite minerals. In the channels, carbonate occurs as cements in sandstones and conglomerates, crystals in mudstone, sandstones, and conglomerates, and reworked nodules in conglomerates, whereas in the under-sampled paleosols, carbonate is present as crystals, cements filling vugs and cracks, nodules, and beds. Evaporite minerals mostly occur as cements and crystals in the channels, and as nodules and beds in paleosols. Semi-quantitative analysis was not conducted because (a) each site was not sampled proportionally or extensively to capture the patchy occurrence of the minerals and (b) the carbonate and evaporite minerals are a minor constituent of the channel and floodplain composition (< 5% as indicated by Nelson et al. 2013).

Calcite and ankerite are the main carbonate minerals in the lower unit with minor amounts of dolomite, whereas dolomite is predominant in the middle and upper units with minor amounts of calcite and ankerite (Fig. 6-4). Ankerite was only identified through XRD analysis, unlike calcite and dolomite, which were easily identifiable using SEM/EDS analysis. Barite occurs sporadically throughout the formation, but gypsum abundance increases from the middle to the upper unit and celestine only occurs within the upper Clear Fork. Nodules and beds of gypsum and dolomite are present in the upper unit, whereas the minerals are present as intraclasts, rhombs, and cements in the lower and middle units.

6.2.3.5 Fossils

The Clear Fork Formation has a wide assemblage of plant, vertebrate and invertebrate fossils and trace fossils. Well-preserved plant materials are abundant at key localities throughout the formation. Leaves and stems are common in coarse basal sediment, within accretion deposits, and in laminated and disrupted mudstones in abandoned channel fills where the plant leaves are

most abundant and locally exquisitely preserved (see Chapter 2; Chaney and DiMichele 2007; Looy 2013; Schachat et al. 2014). Root traces of varied size are common in disrupted mudstone low in the channel bodies, at various levels on inclined sandstone beds, and as drab vertical traces within massive mudstones in abandoned channel deposits (Simon et al. in press). Based on the size, abundance and excellent preservation of the leaves, we infer that many channels had a riparian zone with substantial trees, from which leaves were transported a short distance to the depositional site (parautochthonous: Bateman 1991). Root traces are rarely observed in thicker mudstone sheets that represent floodplain deposits (DiMichele et al. 2006), suggesting that the floodplains were probably sparsely vegetated, although vegetation in such environments tends to have a low preservation potential (Gastaldo and Demko 2011). No upright trees, large logs, or vegetation-induced sedimentary structures (Rygel et al. 2004) were identified. Charcoal fragments at numerous sites indicate periodic wildfires on the riparian zone and distant floodplains.

In the lower and middle units, seed plants are abundant with isolated occurrences of everwet plants. The number of known plant localities and diversity diminishes significantly in the upper unit, despite intensive searching over many years, and this change is probably related to a landscape that became depauperate, and/or to a change in taphonomic parameters (Chaney and DiMichele 2007).

Paleontologists have also found a range of freshwater fish, amphibian, and reptile remains in the Clear Fork Formation over the past 130 years (e.g. Cummins 1908). In the lower unit, a large number of bonebeds and trace fossils is present, but the occurrences steadily decline up-section and the last appearance occurs just above the Burnet dolomite (Fig. 6-4). Fossils found weathering out of mud-rich channel and floodplain deposits, mostly in the lower unit, include

small palaeoniscoid fishes and fish scales, amphibamid temnospondyls, unidentifiable bone fragments, xenacanth shark teeth and "freshwater sharks (*Orthacanthus*), obligatory aquatic amphibians such as *Diplocaulus, Trimerorhachis,* and *Isodectes*, fully terrestrial amphibians such as *Dissorophus* and *Seymouria*, and higher tetrapods such as *Diadectes, Dimetrodon, Edaphosaurus, Secondontosaurus, Varanosaurus,* and *Araeoscelis*" (Broili 1904; Williston 1910, 1911; Murry and Johnson 1987; DiMichele et al. 2006; Anderson et al. 2008; Johnson 2012; Nelson et al. 2013). Invertebrate fossils such as conchostracans, myriapods (Baird 1958), indeterminate bivalves, and a blattoid insect wing at CCP are rarely found in the formation. Trace fossils are common throughout the section and include shark and fish coprolites found within muddy abandoned channels, failed aestivation assemblages of the lysorophoid amphibian *Brachydectes* (Wellstead 1991) and the lungfish *Gnathorhiza* (Olson and Bolles 1975), burrows of *Taenidium barretti/Planolites montanus* (Baucon et al. 2014) penetrating the accretion deposits, and trackways of *Diplichnites gouldi* on cemented, sandstone beds in the channels.

Although the animal fossil sites occur sporadically upsection, the presence of shark coprolites and tetrapod material in abandoned channel fills in the lower unit suggests that more water was available on the landscape, which supported larger organisms.

6.2.3.6 Paleosols

Similar to the middle and upper Wichita Group, alfisols, vertisols, and inceptisols occur within the Clear Fork Formation (DiMichele et al. 2006), but no upward trends were described by these authors. In a recent study, researchers noted that vertic argillisol, vertic calcisol, calcic vertisol, and calcisol are present within the lower Clear Fork, in comparison to gleyed calcisol, calcic vertisol, vertisol, and calcisol in the middle and upper units (Zhu 2015), based on the Mack et al. (1993) classification system. The rare occurrence of gleyed features and the abundance of

calcisols indicate that water logged or reducing environments were uncommon on the Early Permian landscape. Since the analysis of paleosols was not the subject of this thesis, a fuller stratigraphic analysis of these beds (see section 6.4) is required to infer upward changes.

6.2.4 Pease River Group

The Lower to Middle Permian Pease River Group comprises the San Angelo and Blaine Formations (see Nelson and Hook 2005). The San Angelo Formation is a sandy conglomeratic unit, sourced from the Llano Uplift, with large braided and meandering streams in the lower section and muddy coastal-plain deposits in the upper interval. The formation intertongues westward in the subsurface with red mudstone and reflects a rapid progradation of the shoreline to the west, followed by gradual retreat. The Blaine Formation consists of variegated mudstone (reddish-brown and gray-green) interstratified with extensive gypsum and marine dolomite beds, interpreted as a combination of tidal flat and sabkha deposits (Smith 1974) on a broad, low relief, shallow marine shelf. Overlying the Pease River Group are the Middle to Late Permian Whitehorse, Cloud Chief, and Quartermaster formations, which are unconformably overlain by the Late Triassic Dockum Group. Erosion dominated most of the Triassic Period and continued into the Jurassic, when the Gulf of Mexico began to open; during the Cretaceous, postrifting transgressions occurred and marine strata were deposited on the continent (Tabor and Montañez 2004).

An impoverished, fragmentary record of terrestrial vertebrates, namely large herbivores, is known from the San Angelo Formation (Olson 1962), but no record of such fossils exists in the Blaine Formation. Plant fossils are rarely found in the San Angelo Formation, but precocious flora such as the cycad *Dioonitocarpidium* and the conifer *Podozamites* are found in some coastal-plain channels in the Blaine Formation, although elsewhere, they are only known from

the Mesozoic (DiMichele et al. 2001, 2004). The paucity of soil profiles in the Pease River Group reflects unfavourable conditions for soil development, as diagnostic features such as root traces and soil structures only occur along some channels, suggesting that stream corridors were the only source of fresh water for plant-growth and soil formation (DiMichele et al. 2006).

6.2.5 Long-term Paleoenvironmental Trends Summary

The Permo-Pennsylvanian section of north-central Texas records upward changes in paleosol types, plant biomes, and depositional environments. An upward increase in aridification was inferred based on proxies such as paleosols and plant biomes, within the equatorial regions of Pangea (Robinson 1973; Mack and James 1986; Parrish 1993; West et al. 1993; Kessler et al. 2001; Mack 2003; DiMichele et al. 2006; Tabor and Poulsen 2008; Tabor 2013). In the Markley Formation (Bowie Group), coals are present along with everwet plants and poorly-drained paleosols typical of humid climates. In contrast, in the Archer City Formation (Bowie Group), Wichita Group, Clear Fork Formation, and Pease River Group, vertic paleosols are present and seed plants with features indicative of (semi)arid conditions replaced the everwet plants.

Although paleosols and plant fossils are useful when identifying long-term changes in paleoclimate (10^6–10^7 yr; Tabor 2013; Fig. 1-5), higher order or intraformational changes are beyond the resolution of these proxies. Determining upward changes in paleoclimate within a formation using these proxies may be problematic because their presence, absence or type is linked to their position on the landscape (Wright et al. 1991; Kraus 1999; Tabor and Montañez 2004; DiMichele et al. 2006). For example, the level of development (maturity) of paleosols commonly increases away from channels, since those in close proximity to rivers tend to experience cycles of wetting and drying and rapid sedimentation, impeding the development of pedogenic features (Tabor and Montañez 2004). By integrating sedimentological and

petrographic data with classic indicators (plants and paleosols), we are able to identify upward changes in paleoclimatic conditions at a formational level. Using this approach, we evaluated the conditions that existed during the deposition of the Early Permian Clear Fork Formation. Although most of the stratigraphic changes within the formation were subtle, upward changes in channel body type and occurrence, as well as the mineralogy of the carbonate and evaporite occurrences, probably reflect changes in paleoclimate.

Meandering channel-bodies are common throughout the formation, but based on the sedimentary features in the lower unit, the channels transported sediments with stronger flows than in the middle and upper units, implying the periodic availability of considerable volumes of water on the landscape for the lower unit. For example, the sandy lateral accretion sets of the meandering channel body at Red Tank in the lower member are composed of trough and planar cross-beds with ripple cross-lamination but lack evidence of drying up (e.g. rill casts and desiccation cracks), suggesting perennial flow conditions. However, the occurrence of tabular sandstones at three sites (NSCQ, MB, and CCP), the localized debris-flow deposits at MB, and avulsive meandering bodies at MB and KWTP in the middle unit collectively suggest that the landscape received intermittent high rainfall which generated high-magnitude, short-lived floods (Fig. 6-4). Since the tabular sandstones were composed of coarser sediments, flows were capable of entraining these grains most likely in the proximal reaches and transporting them basinward where they were deposited as extensive sheets. This can be attributed to periodic short-term climatic changes, although sediment supply from different source areas cannot be ruled out (see section 2.7.2).

The upward change from primarily calcite and ankerite (cements, isolated crystals and reworked clasts) in the lower unit to dolomite (rhombs, interlocked patches, cements, reworked clasts, and

beds) and gypsum (cements, nodules, and beds) with minor celestine (cements) in the middle and upper units reflects a progressive evolution of shallow phreatic groundwater in an evaporation-dominated environment. This model accords with the analogue from the arid plains of the Channel Country (Cendón et al. 2010; Tweed et al. 2011), where a saline groundwater body with a water table at ~10 m depth, total dissolved solids (TDS) of more than 50,000 mg/L locally, and Na-Cl type brines commonly at gypsum saturation is present below the floodplains (Cendón et al. 2010).

In the lower unit, the presence of calcite and ankerite-bearing clasts derived from weakly developed calcic paleosols (Sarkar 1988; Marriott and Wright 1993; Khadkikar et al. 1998; Gómez-Gras and Alonso-Zarza 2003; Meléndez et al. 2011) suggest that rainfall did not exceed 650 mm/yr and some soils were waterlogged with locally reducing conditions (Blatt et al. 1980; Tucker and Wright 1990; Royer 1999; Mack et al. 2010). In the middle and upper units, dolomite cement was formed by primary precipitation rather than the replacement of calcite through a reaction with Mg-rich waters (Khalaf 1990), as evident by the lack of petrographic evidence of precursor calcite (e.g., dolomite crystals with cloudy cores and clear rims, cement overgrowths, and obliteration of primary fabrics: Scholle and Ulmer-Scholle 2003). The presence of almost stoichiometric, primary dolomite (see appendix B) with no precursor calcite and evaporite minerals (gypsum and celestine) in the upper unit suggests that precipitation was less than 250-300 mm/yr (threshold for gypsum precipitation; Birkeland 1999).

In modern settings, low-temperature dolomite is formed by (a) dissimilatory sulphate-reducing bacteria in anoxic, (hyper)saline environments such as coastal lagoons or lakes in Brazil and Australia (Vasconcelos and McKenzie 1997; Wright and Wacey 2005), and (b) methanogenic metabolic activity and crystal nucleation on the cell walls of microorganisms (not sulphate

reducers) that release Mg, Ca, and Fe during weathering in anaerobic freshwater aquifers (Roberts et al. 2004). Other mechanisms have been recognized in the rock record (summarised in Henares et al. 2016) including: (1) mixing of saline brines and fresh groundwater (El-Sayed et al. 1991; Ye and Mazzullo 1993; Colson and Cojan 1996); (2) Mg enrichment as fluids move through clays (Hutton and Dixon 1981; Spötl and Wright 1992; Armenteros et al. 1995); and (3) calcite precipitation resulting in groundwater enriched in Mg^{2+} and depleted in Ca^{2+} (Pimentel et al. 1996; McQueen et al. 1999; Worden and Burley 2003; Schmid et al. 2006); the findings from this thesis is consistent with the latter mechanism. In continental settings, Mg^{2+} is derived from weathering of Mg-rich bedrock (Nesbitt and Wilson 1992; Spötl and Wright 1992; Schmid et al. 2006) and aeolian dust, some from dolomitic tidal flats (Kessler et al. 2001). Salinization of soils can also occur due to aeolian transport of loose, fine-grained salt-rich sediments from saline desert landscapes such as playa lakes (Gill 1996; Liu et al. 2011).

Based on the upward changes in physical geology and mineralogy within the formation, it is clear that paleoclimatic conditions were increasing in aridity up-section, punctuated by periods of more humid conditions. Although the mineralogy of the carbonate and evaporite beds suggests that groundwater was consistently increasing in salinity up-section, the occurrence of tabular sandstones and avulsive meandering bodies in the middle unit suggest that there were periods with intermittent high rainfall capable of generating antidunes and entraining coarser grains. Although we attribute these changes to the paleoclimate, we cannot ignore the potential impact of long-term tectonics, which uplifts and tilts mountain ranges, increasing the rate of sediment supply and deposition in nearby basins (Gibling et al. 2011). Comparing the underlying, marine-influenced Lueders Formation to the continental beds of the Clear Fork Formation, it is unclear whether the relative change in sea level was related to global fluctuations in climatic conditions

that affected the equatorial regions (the waxing and waning of ice sheets in southern Gondwana could have contributed to eustatic changes; Fielding et al. 2008).

In terms of the depositional environment, the Clear Fork Formation is broadly similar to the middle and upper Wichita Group (Petrolia, Waggoner Ranch, and Lueders Formations), and the Blaine Formation. In the Clear Fork Formation and middle to upper Wichita Group, mud-rich meanderbelts are predominant with average grain sizes ranging from very fine to fine sand, with the fine sediment grade attributed to the denudation of source areas to the east and north (Hentz 1988). The formation also contains similar proportions of sandstone and mudstone suggesting that they were probably derived from the same sediment source. The ephemeral beds identified in the middle to upper Wichita Group also resemble the localized debris-flow deposits in the Clear Fork Formation (Fig. 5-1). Although, the beds were interpreted differently, we agree that these deposits were laid down during episodic high energy floods that recycled carbonate clasts from the adjacent paleosols. In the middle to upper Wichita Group and Clear Fork Formation, ubiquitous variegated laminated claystone is also present in the abandoned channels and floodplain ponds. Interestingly, although the laminated beds in the Clear Fork Formation yield leaves preserved exquisitely as '3D goethite petrifaction' (Looy 2013), the plant remains within the middle to upper Wichita Group are commonly not well-preserved (mostly as hash). The upper Clear Fork unit is similar to the Blaine Formation, as both sections contain beds of dolomite and gypsum with few channel bodies and the landscape contained sparse vegetation and paleosols.

In contrast, the braided channels described by Nelson et al. (2013) and the tabular sandstones were not identified within the middle to upper Wichita Group. Also, we recognize that some of the mudstone beds in the Clear Fork Formation were originally deposited as bedload (mud

aggregates) in the channels, whereas in the middle to upper Wichita Group, the mud-rich beds were interpreted as suspension deposits by Hentz (1988). Another key difference is the absence of smectite within the Clear Fork Formation (Fe-rich chlorite, illite, and kaolinite; appendix D) in comparison to the middle to upper Wichita Group (smectite, illite, and kaolinite; Tabor and Montañez 2004; DiMichele et al. 2006).

The Bowie and lower Wichita Groups (Nocona Formation), and the San Angelo Formation are noticeably different from the Clear Fork Formation. In the underlying Bowie and lower Wichita Groups, there are multistory gravel- and sand-bed braided channel bodies with chert-pebble conglomerate and prominent trough and tabular cross-beds. Although the Clear Fork Formation contains mixed-load meandering channels, the channel bodies are sandier and coarser-grained in the Bowie and lower Wichita Groups, ranging from very coarse sandstone to fine sand (in comparison to fine sand to silt in the Clear Fork Formation). Crevasse splay sandstone and levee deposits of siltstone and mudstone are a prominent component of the landscape during the deposition of the Bowie and lower Wichita Groups, but in the Clear Fork Formation, crevasse splays are very thin, finer-grained, and uncommon, and levee deposits are not characteristic of these channels. Also, the proportion of sandstone and conglomerate in the Bowie and lower Wichita Groups is much higher than in the mud-rich Clear Fork Formation, a result of the close proximity to and the greater availability of detritus from the uplands. An interesting change in conditions is noted between the deposition of the Markley and Archer City Formations (Bowie Group). Although the Archer City Formation and Wichita Group share similar paleosols and plant types to the Clear Fork Formation, the Markley Formation contains coals, everwet plants, and immature paleosols indicative of humid conditions. Similar to the Clear Fork Formation and middle to upper Wichita Group, ephemeral channels and fossiliferous floodplain ponds are

common in the Bowie and lower Wichita Groups. The overlying San Angelo Formation is also significantly different from the Clear Fork Formation, as it contains large braided and sandy meandering streams, especially in the lower part of the section. The coarser quartzose material in the San Angelo Formation was sourced from the Llano Uplift to the south, whereas the sediment source for the Clear Fork Formation was from the Ouachita, Wichita, and Arbuckle Mountains to the east and north. In the absence of paleosols and plant fossils, it is difficult to speculate about the climatic conditions, although the climate was probably wetter, as coarser grains were entrained and transported.

Based on the stratigraphic changes throughout the Permo-Pennsylvanian section and the regional tectonic perspective (Fig. 6-5), it is very likely that the Clear Fork Formation was deposited on the lower coastal plain of the Eastern Shelf, during a quiescent (tectonic) period. The similarity of the underlying Wichita Group and the Clear Fork Formation implies long-term stability in drainage patterns and provenance as indicated by Figures 6-1 to 6-3. Nelson et al. (2013) noted that the facies typical of the lower coastal plain are poorly represented in the Clear Fork Formation due to the lack of evidence for inland transgressions (limestone beds), and we attribute this observation to the long distance from the coastline. Furthermore, Holterhoff (2009a, 2009b) also suggested that the Clear Fork Group (or Formation) represents a highstand systems tract, implying lowered sea levels, since sedimentation rates were consistently low.

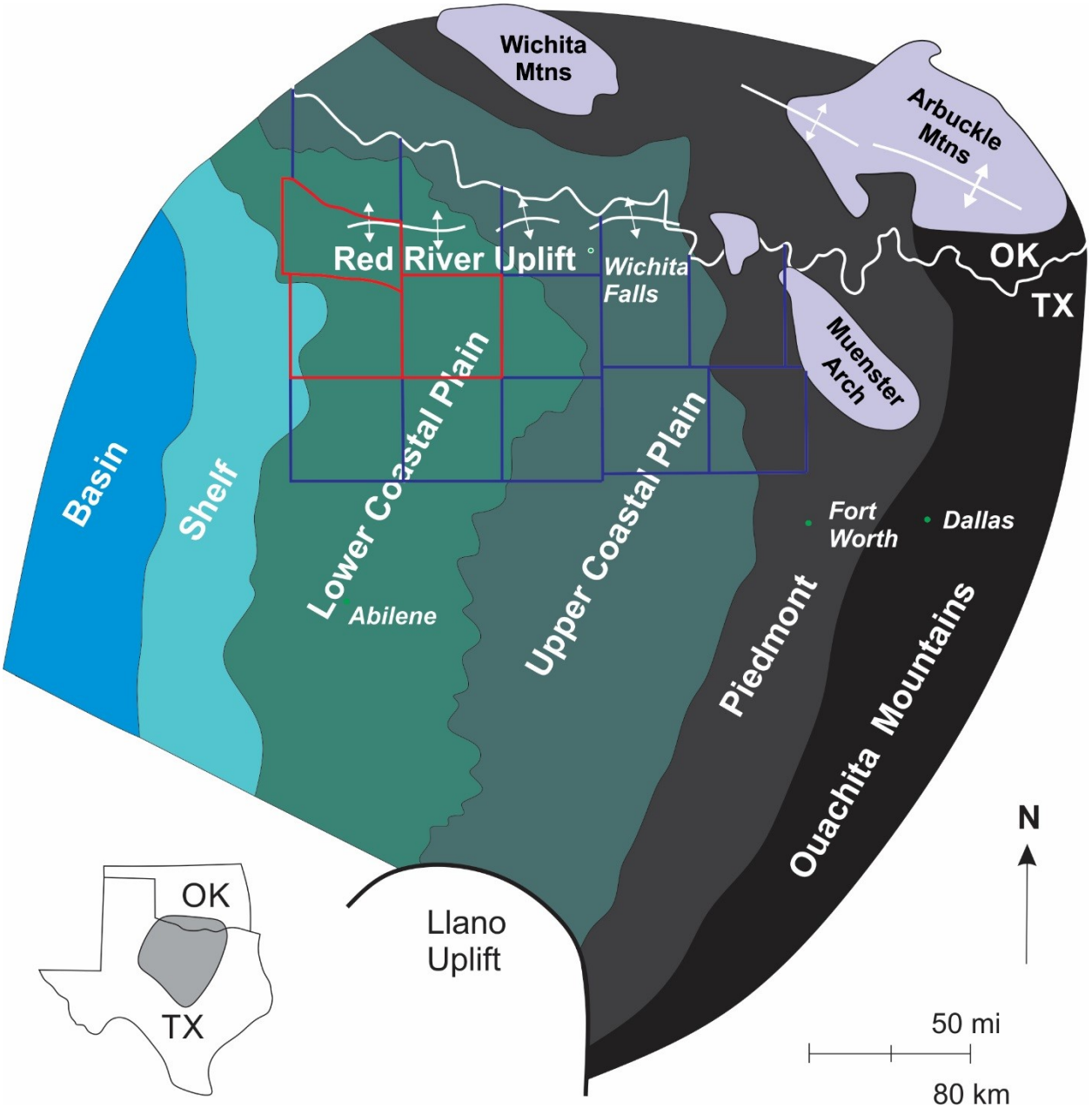

Figure 6-5 Paleogeographic map of north-central Texas illustrating the source areas and physiographic regions during the middle to late Bowie times. The blue lines are the county boundaries; the red lines highlight the three counties in which the Clear Fork Formation was exposed and studied in this thesis. Modified from Hentz (1988).

6.3 AGE DATING IN THE EASTERN SHELF

Age dating in the Eastern Shelf is based primarily on marine fossils, such as fusulinids, ammonoids, and nautiloids (Tabor and Montañez 2004). The Wolfcampian-Leonardian boundary lies close to the Elm Creek Limestone in the Albany Group, which is equivalent to the base of the Petrolia Formation in the Wichita Group (Roth 1931; Dunbar and Skinner 1937; Plummer and Scott 1937; Henbest 1938; Miller and Youngquist 1947). However, the Leonardian-Guadalupian boundary is not well constrained, since it is based on a few ammonoids found in the Blaine Formation (DiMichele et al. 2004). Although an exact age is not known for the Clear Fork Group (Formation in north-central Texas), it is widely considered as Leonardian in age, equivalent to the Kungurian Stage on the international time scale (Wardlaw 2005; Lucas 2006; Nelson et al. 2013). The lack of biostratigraphic or chronostratigraphic control in these continental beds presents an additional challenge, making interbasinal and intra-stage correlations difficult and somewhat unrealistic (e.g. Lucas 2006; Schneider et al. 2006; Montañez et al. 2007). In order to place this body of work within a wider (global) context, we have summarized the key findings of other Early Permian sections within surrounding areas (New Mexico and Oklahoma; Table 6-2; Fig. 6-6) and the conditions within the equatorial regions of Pangea (western North America).

Table 6-2 Late Paleozoic (Wolfcampin and Leonardian) strata deposited under semiarid to arid climatic conditions in New Mexico and Oklahoma, which are equivalent to or slightly older than the Clear Fork Formation (Modified from Soreghan et al. 2008).

Location	Group/Formation	Thickness and Facies	References
Eastern Shelf, Midland Basin, Texas	Leonardian Clear Fork Formation	350 m thick fine-grained fluvio-continental deposits, predominantly interlayered red shale with minor sandstone, conglomerate, dolomite, and evaporites. Up-section increase in dolomite and gypsum beds with an upward decrease in fossil occurrence.	Nelson et al. 2013; this thesis
Bravo Dome field, New Mexico	Wolfcampian Abo Formation-Leonardian Tubb Sandstone	150 m thick strata comprise matrix-supported, arkosic, pebbly conglomerate and poorly sorted arkosic sandstone of fluvial channels intercalated with significant well-sorted massive siltstone of eolian origin (loessite). Aridisols, Inceptisols and Entisol contain abundant dolomite.	Kessler et al. 2001
Hugoton embayment of the Andarko Basin, Kansas-Oklahoma	Leonardian Cedar Hills Member of Hennessey Shale	35-60 m thick reddish-brown silty shale unit with several greenish-gray siltstone layers composed of quartzose sediments and rare fine-grained sandstone.	Fay 1962
	Upper Leonardian Nippewalla Group	150 m; bedded evaporites, mainly halite, gypsum, and anhydrite, red-bed mudstones, siltstones, sandstones, and rare grey mudstones deposited in perennial and saline lakes, salt pans, saline and dry mudflats, sand flats, and sand dunes.	Benison and Goldstein 2001
Orogrande Basin, New Mexico	Wolfcampian Abo Formation	120–420 m of red mudstone, very fine and fine-grained sandstone, siltstone, and conglomerate. Unit consists of deep fine-grained fluvial channels with seasonally exposed point bars, crevasse channels, lacustrine carbonates with periodic desiccation cracks, loessites, and calcic/vertic paleosols with sparse ichnofauna and flora.	Mack et al. 2003

Location	Group/Formation	Thickness and Facies	References
Orogrande Basin, New Mexico	Leonardian Yeso Formation	100-600 m; unit consists of four members: Meseta Blanca (very fine sandstone interbedded with gray shale and tan dolomite), red siltstone-dolomite, fossiliferous limestone with chert nodules and some silicified fossils, and sandstone-limestone. Marine and nonmarine depositional environments, with extensive loess deposits.	Mack and Suguio 1991; Mack and Dinterman 2002
Chama Basin, New Mexico	Wolfcampian Cutler Group	620 m of brown and orange siltstone, multistoried sandstone beds, and minor intraformational and extraformational conglomerate of an ephemeral braided to anastomosed stream environment.	Lucas and Krainer 2005

6.4 LATE PALEOZOIC PALEOCLIMATE IN EQUATORIAL PANGEA

Paleoclimatic proxies from the Clear Fork Formation and the larger Permo-Pennsylvanian section in north-central Texas suggest that conditions were becoming increasingly more arid up-section (Tabor and Montañez 2004; DiMichele et al. 2006). However, this trend is not localised but is also apparent from equivalent sections in Oklahoma and New Mexico (Table 6-2), as well as from a large number of Late Pennsylvanian–Early Permian studies. For example, paleoclimatic indicators such as coal, laterite, and bauxite, which are indicative of humid tropical climates, are common within the Late Pennsylvanian section but are replaced by indicators of dry climate, such as vertisols, calcrete, eolianite, and evaporite in the Lower Permian strata of Pangea (e.g. Mack and James 1986; Patzkowsy et al. 1991; Kessler et al. 2001; Gibbs et al. 2002; Mack 2003; Schneider et al. 2006; Montañez et al. 2007; Tabor and Poulsen 2008; Soreghan et al. 2008; Giles et al. 2013; Tabor 2013). Tabor and Poulsen (2008) concluded that the northward continental drift of most of Pangea, increasing atmospheric pCO_2, and deglaciation could explain most of the low-latitude climate record, whereas changing atmospheric pCO_2 and orbitally-driven glacial–interglacial cycles could account for higher resolution climate variability in Pangea.

Studies have also shown that the rate of transition from relatively humid to arid climate varied significantly based on the geographic position of the basins (Tabor and Poulsen 2008). In western equatorial Pangea, the transition was rapid (< 2 Ma near the Permo-Pennsylvanian boundary: Tabor and Montañez 2004; Montañez et al. 2007), whereas in central Pangea, the transition was protracted over much longer time-scales (~ 20 Ma; Ziegler et al. 2003; Schneider et al. 2006; Roscher and Schneider 2006). In the eastern tropical Tethyan blocks, humid

conditions persisted into the Early Permian (Ikonnikov 1984; Gibbs et al. 2002; Rees et al. 2002; Yang et al. 2005).

Based on the summary by Tabor and Poulsen (2008), this upward drying trend was punctuated by relatively humid intervals (10^4 to 10^6 yr) as evident by "fluvial–eolian deposits of the Colorado Plateau (Blakey and Middleton 1983; Loope 1985; Blakey 1990; 1996; Soreghan et al. 1997; Retallack 2005a; Mountney 2006), Permian cyclothems of the U.S. midcontinent (West et al.1993; Calder 1994; Tandon and Gibling 1994; Miller et al. 1996), and Permian eolian strata of the Pennines Basin (Clemmensen 1991; Frederiksen et al. 1998)". Although the authors noted that these events can be linked to changes in the water table and landscape, in the Clear Fork Formation, pluvial events are also recognized based on the occurrence of coarse-grained tabular sandstones with upper flow regime bedforms and highly avulsive meandering bodies overlying fine-grained meandering channels with lower flow regime bedforms (see Chapter 2).

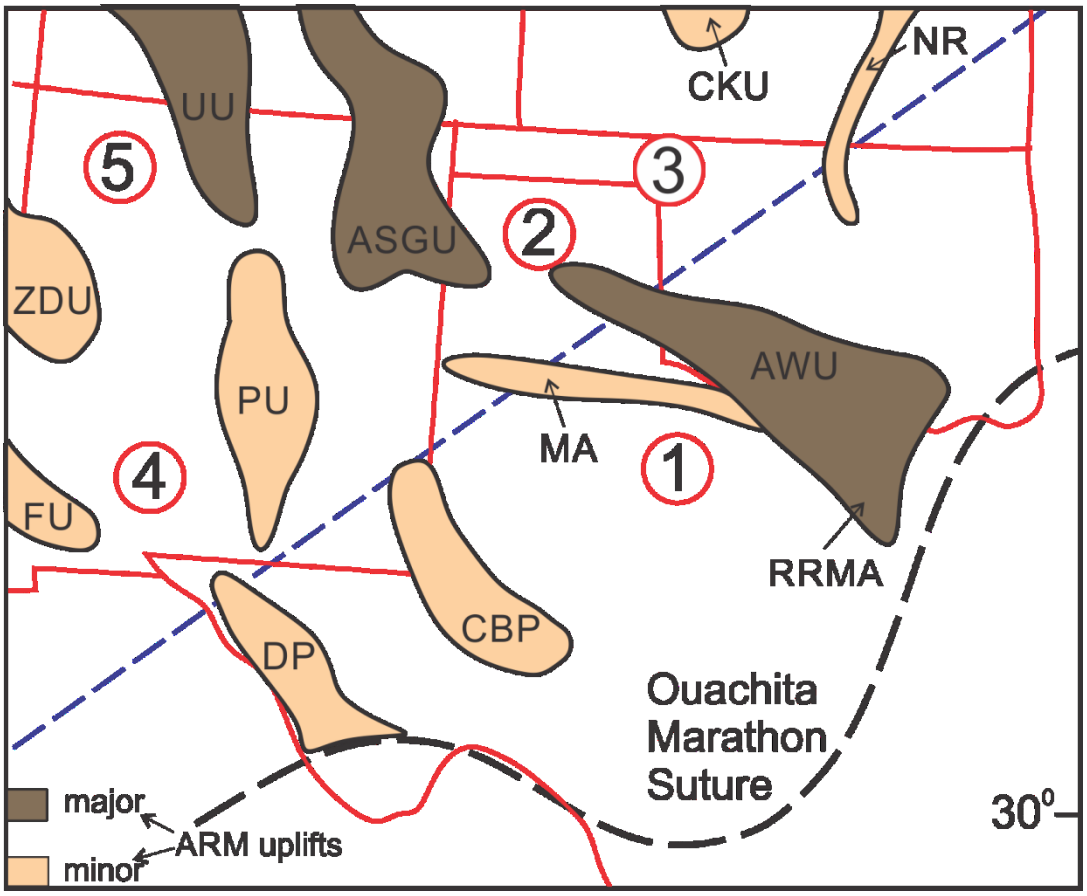

Figure 6-6 Paleogeographic map showing distribution of highlands and localities described in Table 5-2 (circled numbers). Shaded areas are uplifts of the Ancestral Rocky Mountains (ARM); major uplifts refer to those associated with significant basement-derived conglomeratic strata, whereas 'minor' uplifts lack such strata. Dashed blue line approximate the location of the equator during the Permian. Circled numbers: Eastern Shelf, Midland Basin, Texas (1); Bravo Dome field, New Mexico (2); Hugoton embayment of the Andarko Basin, Oklahoma (3); Orogrande basin, New Mexico (4); and Chama Basin, New Mexico (5). Abbreviations of uplifts are as follows: Apishapa-Sierra Grande uplift (ASGU); Amarillo- Wichita uplift (AWU); Central Basin platform (CBP); Central Kansas uplift (CKU); Diablo platform (DP); Florida uplift (FU); Marathon arch (MA); Nemaha ridge (NR); Pedernal uplift (PU), Red River-Muenster arch (RRMA); Uncompahgre uplift (UU); Zuni-Defiance uplift (ZDU). Modified from Soreghan et al. (2008).

6.5 LIMITATIONS AND FURTHER WORK

This thesis focuses on various topics, which provide a solid foundation for further studies in the Permo-Pennsylvanian section of north-central Texas. However, like other studies, some areas require further investigation. The following are my recommendations for future work:

- We studied the characteristics of fossiliferous channel bodies, which were commonly less than 8 m thick, whereas Nelson et al. (2013) identified larger, sandier channel bodies (8-15 m) which were not investigated in this study. By revisiting these and other sites, the upward trends identified in the Clear Fork Formation could be further refined. Also, further analysis can be conducted in the upper unit to identify potential patterns in the occurrence of dolomite and gypsum beds.
- Based on our current understanding from the underlying beds, there is a strong need to refine the sedimentology of these groups, applying modern techniques and ideas. For instance, in the Wichita Group, it is likely that pedogenic mud aggregates were formed on the landscape, provided that the climatic conditions were suitable and the soils contain expandable clays. By sampling these beds, we can further delineate the paleoclimatic conditions in the equatorial regions of Pangea. Since the sediments of the Eastern Shelf were shallowly buried with limited deformation, this area is ideal for the investigation of fine-grained terrestrial depositional systems, which are represented in several formations.
- In this study, we identified the depositional systems in which the plants grew and were eventually preserved. However, no attempt was made to determine the distribution and abundance of fossil taxa in specific facies. Using the method outlined by Bashforth et al. (2010), slabs of rocks with a fixed size can be collected from the outcrops and plant materials including their state of fragmentation and pertinent taphonomic information can be recorded.

Using various statistical approaches, the relative abundance of plant types can be determined, including dominance-diversity patterns.

- Although leaves are exceptionally well-preserved in variegated laminated mudstone deposits, as at Colwell Creek Pond (Chapter 4), the quality of preservation varied markedly between the underlying groups (contained poorly-preserved leaves) and the Clear Fork Formation. This is highly unusual, since wetter conditions would have been ideal for plant growth but were not favourable for preservation. Further sedimentological and geochemical analyses are required to determine the controlling factor for preservation.
- Although a petrographic-based model is presented in this thesis, the use of stable isotopic analyses ($^{18}O/^{16}O$, $^{13}C/^{12}C$, and $^{87}Sr/^{86}Sr$) can provide records of past environmental conditions, including temperature, salinity, pH and humidity, which can help to further refine our understanding of the origin and source of the carbonate and evaporite beds. For example, calcrete stable isotope data can offer information on the vegetation types, palaeoclimatic constraints, and the levels of atmospheric pCO_2 during the Phanerozoic (Alonso-Zarza and Arenas 2004). Strontum isotopes have been used to link cementation and replacement processes to the influx of highly radiogenic waters (Scholle and Ulmer-Scholle 2003).
- To estimate mean annual precipitation (MAP) from the vertisols within the study area, bulk geochemical analyses can be used, followed by the application of CIA-K ($[Al_2O_3/ (Al_2O_3 + CaO + Na_2O)] \times 100$; Sheldon et al., 2002) and CALMAG ($[Al_2O_3/ (Al_2O_3 + CaO + MgO)] \times 100$; Nordt and Driese, 2010a). Although these functions need to be carefully applied, it would be interesting to determine how applicable these techniques are to quantifying paleoclimatic parameters for these ancient red-beds and generally, characterising upward changes in paleosols.

- The provenance of the sediments was not determined as part of this study, but paleoflow data suggest that flows ranged from northwest to south, in a similar direction as the underlying beds. Detrital-zircon geochronology can be used to test these observations by determining the provenance of the grains and comparing the results to other studies within the Permian Basin, such as Soreghan and Soreghan (2013).
- In Chapter 3, we estimated the thermal maturity of the Clear Fork Formation by reviewing the vitrinite reflectance of coals and carbonaceous shales in older rocks, several counties away from the study area or within an adjacent basin. Future researchers should consider using other indicators from within the formation. For instance, the variation in colour of pollen grains and spores can be used as an index for thermal alteration (TAI; Zhao 1984). Illite crystallinity index, which is determined by measuring the half-peak-width of the 10Å illite peak on oriented mineral aggregate preparations of the <2µm size fractions (Kubler 1967, 1968), can also be used as a paleothermal indicator by characterising the grade of diagenesis. Borehole measurements can be used to relate profiles of temperature with depth allowing palaeo-temperature reconstructions.
- Loess deposits have been identified within Lower to Middle Permian rocks in Oklahoma (Giles et al. 2013) and in various basins in southwest USA (e.g. Kessler et al. 2001; Soreghan et al. 2002, 2008). Although the Clear Fork Formation lacks obvious eolian features such as distinct loessite layers and dune sands, further work is required to identify wind-blown deposits, since the formation was deposited in close proximity to provinces with loess deposits and lies downwind of easterly derived to seasonally westerly winds (Fig. 6-7).

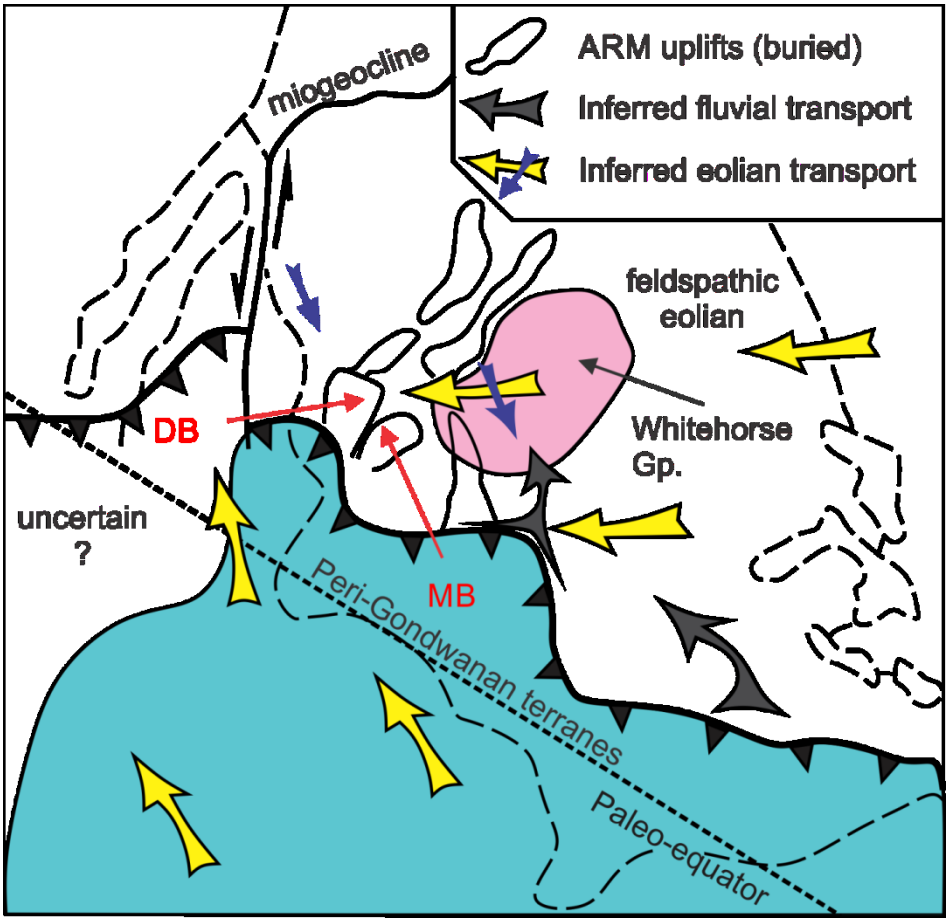

Figure 6-7 Late Paleozoic paleogeography of North America with major orogenic belts, inferred sediment dispersal paths (fluvial and eolian), and prevailing wind direction (modified from Soreghan and Soreghan 2013). DB: Delaware Basin; MB: Midland Basin. Blue arrows indicate zonal circulation which predominated in the Middle Pennsylvanian and yellow arrows indicate monsoonal circulation which predominated during the Permian.

- Presently, it is unclear whether the absence of scroll topography in the meandering channel bodies is the result of surficial weathering, masking by Permian vegetation and pedogenic processes, or (similar to the levee deposits and crevasse splays) they were not characteristic of these rivers. Our research at North Soap-Creek Quadrangle suggests that scroll bars were not originally present. However, additional work could be done at other sites to identify these features in the field and/or explain their absence. In essence, more analysis of the interface and connections between channels and floodplains is needed.

CHAPTER 7 CONCLUSIONS

The Lower Permian Clear Fork Formation of north-central Texas, ~350 m thick, is a fluvial redbed deposit with extensive paleosols and well-preserved plant and vertebrate fossils. The formation was deposited on the western, equatorial margin of Pangea under semi-arid to arid conditions in a tectonically quiescent basin.

This thesis focused on the spatial and stratigraphic variations of alluvial systems through the formation. Fluvial style was assessed using photomosaics of cliffs, facies analysis of measured sections, and paleoflow. Since these deposits are mostly fine-grained, integrating petrographic analyses with sedimentological information was extremely important. The analysis of 77 thin sections was supplemented by grain size analysis for 6 samples containing pedogenic mud aggregates. The mineralogical composition of 83 bulk samples and 23 samples of the <2 μ fraction was determined using XRD, especially for clays. Semi-quantitative geochemical data for 22 samples were obtained using SEM/EDS analysis, and total organic carbon content was determined for 9 samples.

Fine-grained meandering systems are the dominant fluvial style, with individual channels up to 5 m deep contain accretion deposits that dip steeply at ~15° (maximum 22°); the calculated discharge is low, from 64-127 m^3s^{-1}. Quartz-rich, mud-rich, and mud- and quartz-rich systems were identified. Sandy quartz-rich systems comprise dunes and ripples that migrated up the inclined surfaces, resulting in lateral accretion of point bars and good evidence for helicoidal flow. In contrast, mud-rich systems comprise ripple cross-laminated mudstone to very fine sandstone, with oblique accretion the dominant process as sediment was plastered onto accretionary benches and channel banks; channel-base dunes provide local evidence for helicoidal flow. Mud- and quartz-rich systems are the most common meandering style, with

accretion surfaces commonly exhumed on flat-ground and in places defining a complete point bar. Thick intervals of massive to weakly ripple cross-laminated mudstone are interspersed with thin layers of ripple cross-laminated sandstone, representing a combination of lateral and oblique accretion. The cemented sandstones preserved the exhumed topography from erosion. Ripple crests were strongly skewed (swept) relative to channel flow, assumed parallel to the strike of the inclined beds. Where flow was directed up the beds, falling water levels allowed ripple crests to continue migration low in the channel, an interpretation supported by the abundance of rill casts that implies that the channels dried up almost completely. Where flow was directed downwards, we infer re-entry of overbank flood waters into the channel during waning flow.

Inclined muddy beds in the mud- and quartz-rich channels are composed of sand-sized mud aggregates that are sutured together and flattened by compaction, commonly about twice the size of associated quartzose grains. The aggregates are interpreted as pedogenic in origin, formed under hot, seasonal climates from soils containing swelling clays. Washed into the channels, they behaved as bedload and the difference in grain size reflects their lower density, although both grains were entrained at very low velocities ranging from 1.2-1.5 cms^{-1}. The Clear Fork occurrence is among very few known examples where these delicate features have been preserved, due to (a) the encasing clay matrix and hematite rims, (b) partial buffering by detrital and ferruginous grains along with the early formation of rhombs and cements, (c) the rapid burial of aggregates within the migrating point bar set in a rigid “compartment” cut into tough and relatively non-compactible paleosols, and (d) shallow and slow long-term burial.

In the abandoned meandering channels, laminated mudstone yields exquisite plant materials preserved as 3D goethite petrifactions. The laminae are variegated with insignificant organic content, do not contain carbonates or unusual clays, and lack exposure features, bioturbation and

roots. Preservation of lamination is related to the absence of benthic fauna, probably due to the evolutionary delay in freshwater colonization until the Early Permian, and low productivity, high sedimentation rate, elevated salinity, and limited bottom- or pore-water oxygenation may further have inhibited organisms. The plant materials were derived from seed plants growing in the adjacent riparian zone, and the excellent preservation is attributed to early biomineralization and rapid burial in the absence of burrowing organisms. The abandoned channels appear to have been sites of unusual water availability for plants in an otherwise arid landscape, as indicated by floodplain paleosol types. Standing water bodies persisted for centuries to a few millennia based on lamina counts and were probably fed by (a) floodwater from neighbouring rivers, (b) rainwater flow along tie channels or floodplain depressions, or bank slumps, and (c) groundwater discharge below a spring line. Water was retained in these channels because of the fine-grained, impermeable nature of the underlying floodplain deposits and the flood-derived clay, which can seal channel incisions and reduce seepage.

Laterally extensive tabular sandstones cut across channel and muddy floodplain deposits in the middle Clear Fork. These sandstone sheets contain scours filled with plane beds and antidunes, indicating high energy, episodic flows in broad, sandbed channels, which were sourced from upland areas to the north and east. A small occurrence of debris-flow deposits was also identified in the middle interval, and contained carbonate clasts, bones, and plant fragments, deposited by high-intensity floods that were capable of recycling the adjacent paleosols. In the upper interval, stromatolite beds were present at the base of channel bodies within a mudstone interval that contained bedded dolomite and gypsum, which were formed in playa lakes on the landscape.

Upward trends in the formation reflect progressive aridification of equatorial Pangea. Previous studies have inferred semi-arid to arid conditions based on paleosols such as vertisols and

aridisols, seed plants replacing late Pennsylvanian wetland assemblages, and an upward decrease in plant and vertebrate fossil sites, which suggests increasingly intolerable conditions, although the effects of taphonomy and limited sampling cannot be ruled out. Sedimentological data indicate that floods were of higher intensity in the meandering channels in the lower unit than the upper interval, but in the middle unit, the landscape received intermittent, high-magnitude, short-lived floods, bringing coarser quartzose sediments derived from source areas into the basin. Petrographic data for early diagenesis demonstrate an upward change from calcite and ankerite (cements, isolated crystals and reworked clasts) to dolomite (rhombs, interlocked patches, cements, reworked clasts, and beds) with gypsum (nodules and beds) and minor celestine and barite cements. This trend implies increasingly evaporative groundwater conditions, although no upward change in clay mineralogy (illite, Fe-chlorite, and kaolinite) was identified.

The Channel Country region of central Australia shares various similarities with the Clear Fork Formation, making it an appropriate analogue. In both cases, the basins are tectonically stable and experience arid to semi-arid climatic conditions. Obliquely and laterally accreted mud- and sand-rich channels drain uplands and flow for several hundred kilometres across an extensive low-gradient plain, but unlike the Clear Fork channels which flowed into the Permian sea to the west, the rivers in the Channel Country flow into Lake Eyre (internally drained). The geometry of the channel bodies is also similar with low width: thickness ratios. Pedogenic mud aggregates were formed in the mud-rich floodplains containing swelling clays and are reworked as bedload by channels along with quartzose grains. In both cases, the groundwater is saline, due to evaporation.

In comparison to the underlying and overlying beds, the Clear Fork Formation resembles the middle to upper Wichita Group and overlying Blaine Formation but is distinctly different from

the Bowie and lower Wichita Groups and the San Angelo Formation. Similar to the Clear Fork Formation, the middle to upper Wichita Group is composed of (a) mud-rich meanderbelts with an average grain size ranging from very fine to fine sand, (b) ephemeral beds formed from short-lived, high-energy floods, and (c) ubiquitous variegated, laminated claystone in abandoned channels and floodplain ponds. The overlying Blaine Formation is similar to the upper Clear Fork unit, containing beds of dolomite and gypsum with few channel bodies and sparse vegetation and paleosols. Key differences include (a) the absence of tabular sandstones identified in the Clear Fork Formation and (b) the presence of smectite in the middle to upper Wichita Group. Unlike the Clear Fork Formation, the underlying Bowie and lower Wichita Groups contains (a) multistory gravel- and sand-bed braided channel bodies with chert-pebble conglomerate and prominent trough and tabular cross-beds, (b) crevasse splay sandstone and levee deposits, and (c) a higher proportion of sandstone and conglomerate, due to the close proximity to the upland areas. The overlying San Angelo Formation contains large braided and sandy meandering streams sourced from the Llano Uplift to the south.

Based on the stratigraphic changes throughout the Permo-Pennsylvanian section and the regional tectonics, the Clear Fork Formation was probably deposited on the lower coastal plain of the Eastern Shelf similar to the Wichita Group, implying long-term stability in drainage patterns and provenance. The inferred paleoclimatic trend is consistent with other studies from the equatorial regions of Pangea, where conditions were becoming increasingly more arid, due to the northward continental drift of most of Pangea, increasing atmospheric pCO_2, and deglaciation.

REFERENCES

Abdullatif, O.M., 1989, Channel-fill and sheet-flood facies sequences in the ephemeral River Gash, Kassala, Sudan: Sedimentary Geology, v. 63, p. 171–184.

Adams, J.E., Frenzel, H.N., Rhodes, M.L., and Johnson, D.P., 1951, Starved Pennsylvanian Midland Basin: AAPG Bulletin, v. 35, p. 2600–2607.

Alexander, J., and Fielding, C.R., 1997, Gravel antidunes in the tropical Burdekin River, Queensland, Australia: Sedimentology, v. 44, p. 327–337.

Algeo, T.J., and Scheckler, S.E., 1998, Terrestrial-marine teleconnections in the Devonian: Links between the evolution of land plants, weathering processes, and marine anoxic events: Royal Society of London Philosophical Transactions, ser. B, v. 353, p. 113–130.

Al-Hashimi, W.S., and Hemingway, J.E., 1973, Recent dedolomitization and the origin of the rusty crusts of Northumberland: Journal of Sedimentary Research, v. 43, p. 82–91.

Allaby, A., and Allaby, M., 1999, Dictionary of earth sciences: Oxford University Press, London.

Allen, J.R.L., 1968, Current ripples; their relation to patterns of water and sediment motion: Amsterdam, North-Holland Pub. Co., xiii, 433 p.

Allen, J.P., Fielding, C.R., Rygel, M.C., and Gibling, M.R., 2013, Deconvolving signals of tectonic and climatic controls from continental basins: An example from the Late Paleozoic Cumberland Basin, Atlantic Canada: Journal of Sedimentary Research, v. 83, p. 847–872.

Alley, N.F., 1998, Cainozoic stratigraphy, palaeoenvironments and geological evolution of the Lake Eyre Basin: Palaeogeography, Palaeoclimatology, Palaeoecology, v. 144, p. 239–263.

Alonso-Zarza, A.M., and Arenas, C., 2004, Cenozoic calcretes from the Teruel Graben, Spain: microstructure, stable isotope geochemistry and environmental significance: Sedimentary Geology, v. 167, p. 91–108.

Anderson, R.Y., and Dean, W.E., 1988, Lacustrine varve formation through time: Palaeogeography, Palaeoclimatology, Palaeoecology, v. 62, p. 215–235.

Anderson, J.S., Reisz, R.R., Scott, D., Frobisch, N.B., and Sumida, S.S., 2008, A stem batrachian from the Early Permian of Texas and the origin of frogs and salamanders: Nature, v. 453, p. 515–518.

Arakel, A.V., 1986, Evolution of calcrete in palaeodrainages of the Lake Napperby area, Central Australia: Palaeogeography, Palaeoclimatology, Palaeoecology, v. 54, p. 283–303.

Arakel, A.V., and McConchie, D., 1982, Classification and genesis of calcrete and gypsite lithofacies in paleodrainage systems of inland Australia and their relationship to carnotite mineralization: Journal of Sedimentary Research, v. 52, p. 1149–1170.

Armenteros, I., Bustillo, M.A., and Blanco, J.A., 1995, Pedogenic and groundwater processes in a closed Miocene basin (northern Spain): Sedimentary Geology, v. 99, p. 17–36.

Aslan, A., and Autin, W.J., 1998, Holocene flood–plain soil formation in the southern lower Mississippi Valley: Implications for interpreting alluvial paleosols: Geological Society of America Bulletin, v. 110, p. 433–449.

Baird, D., 1958, New records of Paleozoic diplopod Myriapoda: Journal of Paleontology, v. 32, p. 239-241.

Barnes, V.E., Hentz, T.F. and Brown, L.F., 1987, Geologic Atlas of Texas; Wichita Falls – Lawton Sheet: University of Texas, Austin, Bureau of Economic Geology.

Bashforth, A.R., Cleal, C.J., Gibling, M.R., Falcon-Lang, H.J., and Miller, R.F., 2014, Paleoecology of early Pennsylvanian vegetation on a seasonally dry tropical landscape (Tynemouth Creek Formation, New Brunswick, Canada): Review of Palaeobotany and Palynology, v. 200, p. 229–263.

Bashforth, A.R., DiMichele, W.A., and Eble, C.F., in press, Dryland vegetation from the Middle Pennsylvanian of Indiana (Illinois Basin): The dryland biome in glacioeustatic, paleobiogeographic, and paleoecologic context: Journal of Paleontology.

Bateman, R.M., 1991, Palaeoecology, *in* Cleal, C.J., ed., Plant fossils in geological investigation: the palaeozoic: Chichester, UK, Ellis-Horwood, p. 34–116.

Batenburg, L.H., 1982, “Compression species” and “petrifaction species” of Sphenophyllum compared: Review of Palaeobotany and Palynology, v. 36, p. 335–359.

Bathurst, J.C., Thorne, C.R., and Hey, R.D., 1977, Direct measurements of secondary currents in river bends: Nature, v. 269, p. 504–506.

Baucon, A., Ronchi, A., Felletti, F., and de Carvalho, C.N., 2014, Evolution of crustaceans at the edge of the end-Permian crisis: Ichnonetwork analysis of the fluvial succession of Nurra (Permian–Triassic, Sardinia, Italy): Palaeogeography, Palaeoclimatology, Palaeoecology, v. 410, p. 74–103.

Behrensmeyer, A.K., 1988, Vertebrate preservation in fluvial channels: Palaeogeography, Palaeoclimatology, Palaeoecology, v. 63, p. 183–199.

Bein, A., and Land, L.S., 1983, Carbonate sedimentation and diagenesis associated with Mg-Ca-chloride brines; the Permian San Andres Formation in the Texas Panhandle: Journal of Sedimentary Research, v. 53, p. 243–260.

Benison, K.C., and Goldstein, R.H., 2001, Evaporites and siliciclastics of the Permian Nippewalla Group of Kansas, USA: a case for non-marine deposition in saline lakes and saline pans: Sedimentology, v. 48, p. 165–188.

Bercovici, A., Diez, J.B., Broutin, J., Bourquin, S., Linol, B., Villanueva-Amadoz, U., López-Gómez, J., and Durand, M., 2009, A palaeoenvironmental analysis of Permian sediments in Minorca (Balearic Islands, Spain) with new palynological and megafloral data: Review of Palaeobotany and Palynology, v. 158, p. 14–28.

Birkeland, P.W., 1999, Soils and geomorphology: New York, New York : Oxford University Press.

Bischoff, J.L., Juliá, R., Shanks, W.C., and Rosenbauer, R.J., 1994, Karstification without carbonic acid: Bedrock dissolution by gypsum-driven dedolomitization: Geology, v. 22, p. 995–998.

Blakey, R.C., 1990, Stratigraphy and geologic history of Pennsylvanian and Permian rocks, Mogollon Rimregion, centralArizona andvicinity: Geological Society of America Bulletin, v. 102, p. 1189–1217.

Blakey, R.C., 1996, Permian eolian deposits, sequences, and sequence boundaries, Colorado Plateau: *in* Longman, M.W., and Sonnenfeld, M.D., eds., Palaeozoic Systems of the Rocky Mountain Region, Rocky Mountain Section SEPM, p. 405–426.

Blakey, R.C., and Middleton, L.T., 1983, Permian shoreline eolian complex in central Arizon; dune changes in response to cyclic sea level changes: *in* Brookfield, M.E., and Ahlbrandt, T.S., eds., Eolian Sediments and Processes, International Association of Sedimentologists Congress, v. 38, p. 551–581.

Blatt, H., Middleton, G.V., and Murray, R.C., 1980, Origin of sedimentary rocks: Englewood Cliffs, N.J., Prentice-Hall.

Bluck, B., 1971, Sedimentation in the meandering River Endrick: Scottish Journal of Geology, v. 7, p. 93–138.

Bogaart, P.W., Van Balen, R., Kasse, C., and Vandenberghe, J., 2003, Process-based modelling of fluvial system response to rapid climate change—I: model formulation and generic applications: Quaternary Science Reviews, v. 22, p. 2077–2095.

Boles, J.R., 1978, Active ankerite cementation in the subsurface Eocene of southwest Texas: Contributions to Mineralogy and Petrology, v. 68, p. 13–22.

Bowler, J.M., 1973, Clay dunes: their occurrence, formation, and environmental significance: Earth-Science Reviews, v. 9, p. 315–338.

Bradley, W.H., 1931, Origin and microfossils of the oil shale of the Green River Formation of Colorado and Utah: U.S. Geological Survey Professional Paper 168, 58 p.

Bridge, J.S., 2003, Rivers and floodplains forms, processes, and sedimentary record: Oxford, UK; Malden, MA, USA, Blackwell Pub.

Bridge, J.S., and Jarvis, J., 1982, The dynamics of a river bend: a study in flow and sedimentary processes: Sedimentology, v. 29, p. 499–541.

Brister, B.S., Stephens, W.C., and Norman, G.A., 2002, Structure, stratigraphy, and hydrocarbon system of a Pennsylvanian pull-apart basin in north-central Texas: AAPG bulletin, v. 86, p. 1–20.

Brizga, S.O., and Finlayson, B.L., 1990, Channel avulsion and river metamorphosis: the case of the Thomson River, Victoria, Australia: Earth Surface Processes and Landforms, v. 15, p. 391–404.

Broili, F., 1904, Permische Stegocephalen und Reptilien aus Texas: Palaeontographica, v. 51, p. 1–49.

Brooks, G.R., 2003a, Alluvial deposits of a mud-dominated stream: the Red River, Manitoba, Canada: Sedimentology, v. 50, p. 441–458.

Brooks, G.R., 2003b, Holocene lateral channel migration and incision of the Red River, Manitoba, Canada: Geomorphology, v. 54, p. 197–215.

Brown, L.F., 1973, Pennsylvanian rocks of north-central Texas: An introduction, *in* Brown, L.F., ed., Pennsylvanian depositional systems in North-Central Texas; a guide for interpreting terrigenous clastic facies in a cratonic basin: University of Texas, Austin, Bureau of Economic Geology, p. 1–9.

Brown, F., Cleaves, A., and Erxleben, A., 1973. Pennsylvanian Depositional Systems in North-Central Texas: A Guide for Interpreting Terrigenous Clastic Facies in a Cratonic Basin. Texas Bureau of Economic Geology, Guidebook 14, 122 p.

Brown, L.F., Jr., Solís-Iriarte, R.F, and Johns, D.A., 1990, Regional depositional systems tracts, paleogeography, and sequence stratigraphy, Upper Pennsylvanian and Lower Permian strata, north- and west central Texas: University of Texas, Austin, Bureau of Economic Geology, Report of Investigations 197, 116 p., 27 plates.

Buatois, L.A., and Mángano, M.G., 1993. Ecospace utilization, paleoenvironmental trends, and the evolution of early nonmarine biotas: Geology, v. 21, p. 595–598.

Buatois, L.A., Mángano, M.G., Genise, J.F., and Taylor, T.N., 1998, The ichnologic record of the continental invertebrate invasion: evolutionary trends in environmental expansion, ecospace utilization, and behavioral complexity: Palaios, v. 13, p. 217–240.

Budnik, R.T., 1989, Tectonic structures of the Palo Duro Basin, Texas Panhandle: Report of Investigations 187: University of Texas, Austin, Bureau of Economic Geology, 43 p.

Calder, J.H.,1994, The impact of climate change, tectonismand hydrology on the formation of Carboniferous tropical intermontane mires: the Springhill coal field, Cumberland Basin, Nova Scotia: Palaeocgeography Palaeoclimatology Palaeoecology, v. 106, p. 323–351.

Caldwell, D.E., and Caldwell, S.J., 1980, Fine structure of in situ microbial iron deposits: Geomicrobiology Journal, v. 2, p. 39–53.

Calvo, J.P., Rodriguez-Pascua, M., Martin-Velazquez, S., Jimenez, S., and Vicente, G.D., 1998, Microdeformation of lacustrine laminite sequences from Late Miocene formations of SE Spain: an interpretation of loop bedding: Sedimentology, v. 45, p. 279–292.

Cartwright, I., Weaver, T.R., and Tweed, S.O., 2008, Integrating physical hydrogeology, hydrochemistry, and environmental isotopes to constrain regional groundwater flow: southern Riverine Province, Murray Basin, Australia, *in* Carrillo-Rivera, J.J., and Ortega-Guerrero, M.A., eds., Groundwater Flow Understanding: from local to regional scale: London, London: Taylor and Francis, p. 105–133.

Caudill, M.R., Driese, S.G., and Mora, C.I., 1996, Preservation of a paleo-Vertisol and an estimate of late Mississippian paleoprecipitation: Journal of Sedimentary Research, v. 66, p. 58–70.

Cendón, D.I., Larsen, J.R., Jones, B.G., Nanson, G.C., Rickleman, D., Hankin, S.I., Pueyo, J.J., and Maroulis, J., 2010, Freshwater recharge into a shallow saline groundwater system, Cooper Creek floodplain, Queensland, Australia: Journal of Hydrology, v. 392, p. 150–163.

Chaney, D.S., and DiMichele, W.A., 2007, Paleobotany of the classic redbeds (Clear Fork Group – Early Permian) of north-central Texas, Proceedings of the XVth International Congress on Carboniferous and Permian Stratigraphy: University of Utrecht, the Netherlands, p. 357–366.

Chaney, D.S., Sues, H.D., and DiMichele, W.A., 2005, A juvenile skeleton of the nectridean amphibian *Diplocaulus* and associated flora and fauna from the Mitchell Creek Flats locality (upper Waggoner Ranch Formation; Early Permian), Baylor County, north–central Texas: New Mexico Museum of Natural History and Science Bulletin, v. 30, p. 39–47.

Chaney, D.S., Mamay, S.H., DiMichele, W.A., and Kerp, H., 2009, *Auritifolia* gen. nov., probable seed plant foliage with comioid affinities from the Early Permian of Texas, U.S.A: International Journal of Plant Sciences, v. 170, p. 247–266.

Chivas, A.R., Andrews, A.S., Lyons, W.B., Bird, M.I., and Donnelly, T.H., 1991, Paleoenvironments of Salt Lakes Isotopic constraints on the origin of salts in Australian playas. 1. Sulphur: Palaeogeography, Palaeoclimatology, Palaeoecology, v. 84, p. 309–332.

Clausing, A., and Boy, J.A., 2000, Lamination and primary production in fossil lakes: relationship to palaeoclimate in the Carboniferous-Permian transition, in Hart, M.B., ed.,

Climates: Past and Present: Geological Society of London, Special Publication, v. 181, p. 5–16.

Cleaves, A., 1982, Upper Strawn depositional systems of north-central Texas, *in* Martin, C.A., ed., Petroleum geology of the Fort Worth basin and Bend Arch area, Dallas Geological Society, p. 49-96.

Clemmensen, L.B., 1991. Eolian sequence and erg dynamics: the Permian Corre Sandstone, Scotland: Journal of Sedimentary Petrology, v. 61, p. 768–774.

Cohen, A.S., 1984, Effect of zoobenthic standing crop on laminae preservation in tropical lake sediment, Lake Turkana, East Africa: Journal of Paleontology, v. 58, p. 499–510.

Cole, R.D., and Picard, M.D., 1975, Primary and secondary sedimentary structures in oil shale and other fine grained rocks, Green River Formation (Eocene), Utah and Colorado: Utah Geology, v. 2, p. 49–67.

Colson, J., and Cojan, I., 1996, Groundwater dolocretes in a lake-marginal environment: an alternative model for dolocrete formation in continental settings (Danian of the Provence Basin, France): Sedimentology, v. 43, p. 175–188.

Coulombe, C.E., Dixon, J., and Wilding, L., 1996, Mineralogy and chemistry of Vertisols, *in* Ahmad, N., and Mermut, A.R., eds., Developments in Soil Science: Netherlands, Elsevier Publisher, p. 115–200.

Croke, J., Magee, J., and Price, D., 1996, Major episodes of Quaternary activity in the lower Neales River, northwest of Lake Eyre, central Australia: Palaeogeography, Palaeoclimatology, Palaeoecology, v. 124, p. 1–15.

Cui, B., and Komar, P.D., 1984, Size measures and the ellipsoidal form of clastic sediment particles: Journal of Sedimentary Research, v. 54, p. 783–797.

de Gibert, J.M., and Ekdale, A.A., 2002, Ichnology of a restricted epicontinental sea, Arapien Shale, Middle Jurassic, Utah, USA: Palaeogeography, Palaeoclimatology, Palaeoecology, v. 183, p. 275–286.

de Mowbray, 1980, Sedimentary processes of recent intertidal channels: University of Leeds, Unpublished PhD thesis.

Dean, W.E., and Fouch, T.D., 1983, Lacustrine Environment, *in* Scholle, P.A., Bebout, D.G., and Moore, G.H., eds., Carbonate depositional environments: American Association of Petroleum Geologist Memoir, v. 33, p. 97–130.

Demicco, R.V., and Gierlowski-Kordesch, E.G., 1986, Facies sequences of a semi-arid closed basin: the Lower Jurassic East Berlin Formation of the Hartford Basin, New England, USA: Sedimentology, v. 33, p. 107–118.

Demko, T.M., 1995, Taphonomy of fossil plants in the Upper Triassic Chinle Formation: Unpublished Ph.D. dissertation, University of Arizona, Tucson, 274 p.

Dietrich, W.E., 1987, Mechanics of flow and sediment transport in river bends, *in* Richards, K.S., ed., River Channels: Environment and Process, Institute of British Geographers Special Publication No. 18, Basil Blackwell, Inc., p. 179–227.

Dietrich, W.E., and Smith, J.D., 1983, Influence of the point bar on flow through curved channels: Water Resources Research, v. 19, p. 1173–1192.

Dietrich, W.E., Smith, J.D., and Dunne, T., 1979, Flow and Sediment Transport in a Sand Bedded Meander: The Journal of Geology, v. 87, p. 305–315.

DiMichele, W.A., and Aronson, R.B., 1992, The Pennsylvanian-Permian vegetational transition: a terrestrial analogue to the Onshore-Offshore Hypothesis: Evolution, v. 46, p. 807–824.

DiMichele, W.A., and Phillips, T.L., 1994, Paleobotanical and paleoecological constraints on models of peat formation in the Late Carboniferous of Euramerica: Palaeogeography, Palaeoclimatology, Palaeoecology, v. 106, p. 39–90.

DiMichele, W.A., Mamay, S.H., Chaney, D.S., Hook, R.W., and Nelson, W.J., 2001, An Early Permian flora with Late Permian and Mesozoic affinities from north-central Texas: Journal of Paleontology, v. 75, p. 449–460.

DiMichele, W.A., Hook, R.W., Nelson, W.J., and Chaney, D.S., 2004, An unusual Middle Permian flora from the Blaine Formation (Pease River Group: Leonardian-Guadalupian Series) of King County, West Texas: Journal of Paleontology, v. 78, p. 765–782.

DiMichele, W.A., Kerp, H., Krings, M., and Chaney, D.S., 2005, The Permian peltasperm radiation: evidence from the southwestern United States: New Mexico Museum of Natural History and Science Bulletin, v. 30, p. 67–79.

DiMichele, W.A., Tabor, N.J., Chaney, D.S., and Nelson, W.J., 2006, From wetlands to wet spots: Environmental tracking and the fate of Carboniferous elements in Early Permian tropical floras, in Greb, S.F., and DiMichele, W.A., eds., Wetlands through Time: Geological Society of America, Special Paper, v. 399, p. 223–248.

DiMichele, W.A., Cecil, C.B., Chaney, D.S., Elrick, S.D., and Nelson, W. J., 2014, Fossil floras from the Pennsylvanian-Permian Cutler Group of southeastern Utah: Utah Geological Association Publication, v. 43, p. 491–504.

Donovan, R.N., and Foster, R.J., 1972, Subaqueous shrinkage cracks from Caithness Flagstone Series (middle Devonian) of northeast Scotland: Journal of Sedimentary Research, v. 42, p. 309–317.

Driese, S.G., and Ashley, G.M., 2015, Paleoenvironmental reconstruction of a paleosol catena, the Zinj archeological level, Olduvai Gorge, Tanzania: Quaternary Research, v. 85, p. 133–146.

Dunbar, C.O., and Skinner, J.W., 1937, Permian Fusulinidae of Texas: University of Texas Bulletin no. 3701, v. 3, p. 516–732.

Dunn, K.A., McLean, R.J., Upchurch, G.R., and Folk, R.L., 1997, Enhancement of leaf fossilization potential by bacterial biofilms: Geology, v. 25, p. 1119–1122.

Dunoyer de Segonzac, G., 1970, The transformation of clay minerals during diagenesis and low-grade metamorphism: a review: Sedimentology, v. 15, p. 281–346.

Eberl, D.D., Srodon, J., and Northrup, H.R., 1986, Potassium fixation in smectites by wetting and drying, *in* Davis, J.A., and Hayes, K.F., eds., Geochemical Processes at Mineral Surfaces, American Chemical Society Symposium Series, p. 296–326.

Eberl, D., Velde, B., and McCormick, T., 1993, Synthesis of illite-smectite from smectite at earth surface temperatures and high pH: Clay Minerals, v. 28, p. 49–60.

Eberth, D.A., and Miall, A.D., 1991, Stratigraphy, sedimentology and evolution of a vertebrate-bearing, braided to anastomosed fluvial system, Cutler Formation (Permian-Pennsylvanian), north-central New Mexico: Sedimentary Geology, v. 72, p. 225–252.

Edwards, M.B., Eriksson, K.A., and Kier, R.S., 1983, Paleochannel geometry and flow patterns determined from exhumed Permian point bars in north-central Texas: Journal of Sedimentary Research, v. 53, p. 1261–1270.

Ékes, C., 1993, Bedload-transported pedogenic mud aggregates in the Lower Old Red Sandstone in southwest Wales: Journal of the Geological Society, v. 150, p. 469–471.

Eke, E., Parker, G., and Shimizu, Y., 2014, Numerical modeling of erosional and depositional bank processes in migrating river bends with self-formed width: Morphodynamics of bar push and bank pull: Journal of Geophysical Research, v. 119, p. 1455–1483.

El-Sayed, M., Fairchild, I., and Spiro, B., 1991, Kuwaiti dolocrete: petrology, geochemistry and groundwater origin: Sedimentary Geology, v. 73, p. 59–75.

Ethridge, F.G., and Schumm, S.A., 1978, Reconstructing paleochannel morphologic and flow characteristics: methodology, limitations, and assessment, *in* Miall, A.D., ed., Fluvial Sedimentology, Canadian Society of Petroleum Geologists Memoir, v. 5, p. 703–721.

Evamy, B.D., 1967, Dedolomitization and the development of rhombohedral pores in limestones: Journal of Sedimentary Research, v. 37, p. 1204–1215.

Falcon-Lang, H.J., and Bashforth, A.R., 2005, Morphology, anatomy, and upland ecology of large cordaitalean trees from the Middle Pennsylvanian of Newfoundland: Review of Palaeobotany and Palynology, v. 135, p. 223–243.

Fahnestock, R.K., 1969, Morphology of the Slims River, *in* Bushnell, V.C., and Ragle, R.H., eds., Icefield Ranges Research Project scientific results, New York, American Geographical Society; Montreal, Arctic Institute of North America, p. 161–172.

Fay, R.O., 1962, Geology and mineral resources of Blaine County, Oklahoma, Part I—stratigraphy and general geology of Blaine County: Oklahoma Geological Survey Bulletin, v. 89, p. 9–99.

Fracasso, M.A., and Kolker, A., 1985, Late Permian volcanic ash beds in the Quartermaster-Dewey Lake formations, Texas Panhandle: West Texas Geological Society Bulletin, v. 24, p. 5–10.

Freytet, P., Nadège, T.M., Broutin, J., Debriette, P., Durand, M., El Wartiti, M., Gand, G., Kerp, H., Orszag, F., Paquette, Y., Ronchi, A., and Sarfati, J., 1999, Palaeoecology of non marine algae and stromatolites: Permian of France and adjacent countries: Annales de paléontologie, v. 85, p. 99–153.

Fielding, C.R., 2006, Upper flow regime sheets, lenses and scour fills: Extending the range of architectural elements for fluvial sediment bodies: Sedimentary Geology, v. 190, p. 227–240.

Fielding, C.R., Frank, T.D., Birgenheier, L.P., Rygel, M.C., Jones, A.T., and Roberts, J., 2008, Stratigraphic imprint of the Late Palaeozoic Ice Age in eastern Australia: a record of alternating glacial and nonglacial climate regime: Journal of the Geological Society of London, v. 165, p. 129–140.

Fielding, C.R., Allen, J.P., Alexander, J., and Gibling, M.R., 2009, Facies model for fluvial systems in the seasonal tropics and subtropics: Geology, v. 37, p. 623–626.

Florin, R., 1954, The female reproductive organs of conifers and taxads: Biological Reviews, v. 29, p. 367–389.

Folkman, Y., 1969, Diagenetic dedolomitization in the Albian-Cenomanian Yagur dolomite on Mount Carmel (northern Israel): Journal of Sedimentary Research, v. 39, p. 380–385.

Frank, J.R., 1981, Dedolomitization in the Taum Sauk Limestone (Upper Cambrian), Southeast Missouri: Journal of Sedimentary Research, v. 51, p. 7–18.

Frederiksen, K.S., Clemmensen, L.B., and Lawaetz, H.S., 1998, Sequential architecture and cyclicity in Permian desert deposits, Brodick Beds, Aran, Scotland. Journal of the Geological Society, v. 155, p. 677–683.

Fregenal-Martinez, M.A., and Melendez, N., 1994, Sedimentological analysis of the Lower Cretaceous lithographic limestones of the “Las Hoyas” fossil site (Serrania de Cuenca, Iberian Range, Spain): Geobios, v. 27, p. 185–193.

Galloway, W.E., and Brown Jr, L., 1973, Depositional systems and shelf-slope relations on cratonic basin margin, uppermost Pennsylvanian of north-central Texas: AAPG Bulletin, v. 57, p. 1185–1218.

Galloway, W.E., Whiteaker, T.L., and Ganey-Curry, P., 2011, History of Cenozoic North American drainage basin evolution, sediment yield, and accumulation in the Gulf of Mexico basin: Geosphere, v. 7, p. 938−973.

Galtier, J., and Broutin, J., 2008, Floras from red beds of the Permian Basin of Lodève (Southern France): Journal of Iberian Geology, v. 34, p. 57−72

Gastaldo, R.A., 1992, Regenerative growth in fossil horsetails following burial by alluvium: Historical Biology, v. 6, p. 203–219.

Gastaldo, R., and Demko, T., 2010, Long term hydrology controls the plant fossil record. Taphonomy: processes and bias through time, *in* Allison, P.A., and Bottjer, D.J., eds., Topics in Geobiology, p. 249–286.

Gastaldo, R.A., Pludow, B.A., and Neveling, J., 2013, Mud Aggregates from the Katberg Formation, South Africa: Additional Evidence for Early Triassic Degradational Landscapes: Journal of Sedimentary Research, v. 83, p. 531–540.

Gay, G.R., Gay, H.H., Gay, W.H., Martinson, H.A., Meade, R.H., and Moody, J.A., 1998, Evolution of cutoffs across meander necks in Powder River, Montana, USA: Earth Surface Processes and Landforms, v. 23, p. 651–662.

Ge, Q., Hao, Z., Zheng, J., and Shao, X., 2013, Temperature changes ovelr the past 2000 yr in China and comparison with the Northern Hemisphere: Climate of the Past, v. 9, p. 1153–1160.

Gevers, T.W., Frakes, L.A., Edwards, L.N., and Marzolf, J.E., 1971, Trace fossils from the Lower Beacon sediments (Devonian), Darwin Mountains, southern Victoria Land, Antarctica: Journal of Paleontology, v. 45, p. 81–94.

Ghinassi, M., Billi, P., Libsekal, Y., Papini, M., and Rook, L., 2013, Inferring Fluvial Morphodynamics and Overbank Flow Control From 3D Outcrop Sections of A Pleistocene Point Bar, Dandiero Basin, Eritrea: Journal of Sedimentary Research, v. 83, p. 1066–1084.

Ghinassi, M., Nemec, W., Aldinucci, M., Nehyba, S., Özaksoy, V., and Fidolini, F., 2014, Plan-form evolution of ancient meandering rivers reconstructed from longitudinal outcrop sections: Sedimentology, v. 61, p. 952–977.

Ghosh, P., Sarkar, S., and Maulik, P., 2006, Sedimentology of a muddy alluvial deposit: Triassic Denwa Formation, India: Sedimentary Geology, v. 191, p. 3–36.

Gibbs, M.T., Rees, P.M., Kutzbach, J.E., Ziegler, A.M., Behling, P.J., and Rowley, D.B., 2002, Simulations of Permian climate and comparisons with climate-sensitive sediments: Journal of Geology, v. 110, p. 33–55.

Gibling, M.R., 2006, Width and thickness of fluvial channel bodies and valley fills in the geological record: a literature compilation and classification: Journal of Sedimentary Research, v. 76, p. 731–770.

Gibling, M.R., Sinha, R., Roy, N.G., Tandon, S.K., and Jain, M., 2008, Quaternary fluvial and eolian deposits on the Belan River, India: paleoclimatic setting of Paleolithic to Neolithic archeological sites over the past 85,000 years: Quaternary Science Reviews, v. 27, 391–410.

Gibling, M.R., and Davies, N.S., 2012, Palaeozoic landscapes shaped by plant evolution: Nature Geoscience, v. 5, p. 99–105.

Gibling, M.R., Fielding, C.R., and Sinha, R., 2011, Alluvial valleys and alluvial sequences: towards a geomorphic assessment. From River to Rock Record: The Preservation of Fluvial Sediments and Their Subsequent Interpretation: SEPM, Special Publication, v. 97, p. 423–447.

Gibling, M.R., Nanson, G.C., and Maroulis, J.C., 1998, Anastomosing river sedimentation in the Channel Country of central Australia: Sedimentology, v. 45, p. 595–619.

Gibling, M.R., and Rust, B.R., 1993, Alluvial Ridge-and-Swale Topography: A Case Study from the Morien Group of Atlantic Canada, *in* Marzo, M., and Puigdefábregas, C., eds., Alluvial Sedimentation: Oxford, UK, Blackwell Publishing Ltd., p. 133–150.

Gibling, M.R., Tandon, S.K., Sinha, R., and Jain, M., 2005, Discontinuity-bounded alluvial sequences of the southern gangetic plains, India: Aggradation and degradation in response to monsoonal strength: Journal of Sedimentary Research, v. 75, p. 369–385.

Gibling, M.R., Tantisukrit, C., Uttamo, W., Thanasuthipitak, T., and Haraluck, M., 1985, Oil shale sedimentology and geochemistry in Cenozoic Mae Sot basin, Thailand: Bulletin American Association of Petroleum Geologists, v. 69, p. 767–780.

Gierlowski-Kordesch, E.H., 1998, Carbonate deposition in an ephemeral siliciclastic alluvial system: Jurassic Shuttle Meadow Formation, Newark Supergroup, Hartford basin, USA: Palaeogeography, Palaeoclimatology, Palaeoecology, v. 140, p. 161–184.

Gierlowski-Kordesch, E.H., and Gibling, M.R., 2002, Pedogenic mud aggregates in rift sedimentation, *in* Renaut, R., and Ashley, G.M., eds., Sedimentation in Continental Rifts, Society for Sedimentary Geology Special Publication, v. 73, p. 195–206.

Gierlowski-Kordesch, E.H., and Rust, B.R., 1994, The Jurassic East Berlin Formation, Hartford Basin, Newark Supergroup (Connecticut and Massachusetts): A saline lake- playa-alluvial plain system, *in* Renaut, R.W., and Last, W.M., eds., Sedimentology and Geochemistry of Modern and Ancient Saline Lakes: Society for Sedimentary Geology Special Publication, v. 50, p. 249–265.

Gilbert, M.C., 1982, Geology of the Eastern Wichita Mountains, with a brief discussion of unresolved problems, *in* Gilbert, M.C., and Donovan, R.N., eds., Geology of the Eastern Wichita Mountains, Southwestern Oklahoma: Oklahoma Geological Survey Guidebook 21, p. 1–28.

Giles, J.M., Soreghan, M.J., Benison, K.C., Soreghan, G.S., and Hasiotis, S.T., 2013, Lakes, loess, and paleosols in the Permian Wellington Formation of Oklahoma, USA: implications for paleoclimate and paleogeography of the Midcontinent: Journal of Sedimentary Research, v. 83, p. 825–846.

Gill, T., 1996, Eolian sediments generated by anthropogenic disturbance of playas: Human impacts on the geomorphic system and geomorphic impacts on the human system: Geomorphology, v. 17, 207–228.

Gleason, J.D., Patchett, P.J., Dickinson, W.R., and Ruiz, J., 1995, Nd isotopic constraints on sediment sources of the Ouachita-Marathon fold belt: Geological Society of America Bulletin, v. 107, p. 1192–1210.

Goldberg, M., 1967, Supratidal dolomitization and dedolomitization in Jurassic rocks of Hamakhtesh Haqatan, Israel: Journal of Sedimentary Petrology, v. 37, p. 760–773.

Golonka, J., Ross, M.I., and Scotese, C.R., 1994, Pangea: Global Environments and Resources, *in* Embry, A.F., Beauchamp, B., and Glass, D.J., eds., Canadian Society of Petroleum Geologists, Memoir, Canadian Society of Petroleum Geologists, p. 1–47.

Gómez-Gras, D., and Alonso-Zarza, A.M., 2003, Reworked calcretes: their significance in the reconstruction of alluvial sequences (Permian and Triassic, Minorca, Balearic Islands, Spain): Sedimentary Geology, v. 158, p. 299–319.

Gruszka, B., and Zieliński, T., 2008, Evidence for a very low-energy fluvial system: a case study from the dinosaur-bearing Upper Triassic rocks of Southern Poland: Geological Quarterly, v. 52, p. 239–252.

Guccione, M.J., 1993, Grain-size distribution of overbank sediment and its use to locate channel positions, *in* Marzo, M., and Puigdefabregas, C., eds., Alluvial Sedimentation: International Association of Sedimentologists, Special Publications, v. 17, p. 185–194.

Guccione, M.J., Burford, M.F., and Kendall, J.D., 1999, Pemiscot Bayou, a large distributary of the Mississippi River and a possible failed avulsion: Fluvial Sedimentology VI. Special Publication of the International Association of Sedimentologists, v. 28, p. 211–220.

Hackley, P.C., Guevara, E.H., Hentz, T.F., and Hook, R.W., 2009, Thermal maturity and organic composition of Pennsylvanian coals and carbonaceous shales, north-central Texas: Implications for coalbed gas potential: International Journal of Coal Geology, v. 77, p. 294–309.

Hale, W., Saunders, Venetia A., and Margham, J. P., 2005, Collins Dictionary of Biology (New ed.). Glasgow: Collins.

Hallsworth, E., and Beckmann, G., 1969, Gilgai in the Quaternary: Soil Science, v. 107, p. 409–420.

Ham, W.E., 1973, Regional geology of the Arbuckle Mountains, Oklahoma: Oklahoma Geological Survey Special Publication, v. 73, p. 1–55.

Hanor, J.S., 2000, Barite–celestine geochemistry and environments of formation: Reviews in Mineralogy and Geochemistry, v. 40, p. 193–275.

Hartley, A.J.,Weissmann, G.S., Bhattacharayya, P., Nichols, G.J., Scuderi, L.A., Davidson, S.K., Leleu, S., Chakraborty, T., Ghosh, P., and Mather, A.E., 2013, Soil development on modern distributive fluvial systems: preliminary observations with implications for interpretation of paleosols in the rock record, *in*, Driese, S., ed., New Frontiers in Paleopedology and Terrestrial Paleoclimatology: SEPM (Society for Sedimentary Geology) Special Publication, v. 104, p. 149–158.

Hay, R.L., Guldman, S.G., Matthews, J.C., Lander, R.H., Duffin, M.E., Kyser, T.K., 1991, Clay mineral diagenesis in core KM-3 of Searles Lake, California: Clays and Clay Minerals, v. 39, p. 84–96.

Henares, S., Arribas, J., Cultrone, G., and Viseras, C., 2016, Muddy and dolomitic rip-up clasts in Triassic fluvial sandstones: Origin and impact on potential reservoir properties (Argana Basin, Morocco): Sedimentary Geology, v. 339, p. 218–233.

Henbest, L.G., 1938, Notes on the ranges of Fusulinidae in the Cisco Group (restricted) of the Brazos River region, north-central Texas: The University of Texas, no. 3801, p. 237–247.

Hentz, T.F., 1988, Lithostratigraphy and paleoenvironments of Upper Paleozoic continental red beds, north-central Texas--Bowie (new) and Wichita (revised) groups: Report of investigations, University of Texas at Austin, Bureau of Economic Geology, v. 170, 45 p.

Hentz, T.F., and Brown, L.F., 1987, Geologic atlas of Texas, Wichita Falls-Lawton sheet: Bureau of Economic Geology.

Heroux, Y., Chagnon, A., and Bertrand, R., 1979, Compilation and correlation of major thermal maturation indicators: AAPG Bulletin, v. 63, p. 2128–2144.

Hesselbo, S.P., and Trewin, N.H., 1984, Deposition, diagenesis and structures of the Cheese Bay Shrimp Bed, Lower Carboniferous, East Lothian: Scottish Journal of Geology, v. 20, p. 281–296.

Hotton, N., III, Feldmann, R.M., Hook, R.W., and DiMichele, W.A., 2002, Crustacean-bearing continental deposits in the Petrolia Formation (Leonardian Series, Lower Permian) of north-central Texas: Journal of Paleontology, v. 76, p. 486–494.

Houseknecht, D.W., 1983, Tectonic-sedimentary evolution of the Arkoma Basin and guidebook to deltaic facies, Hartshorne sandstone, SEPM Midcontinent Section.

Hubble, G., 1984, The cracking clay soils: definition, distribution, nature, genesis and use, *in* McGarity, J.W., Hoult, E.H., and So, H.B., eds., The properties and utilization of cracking clay soils, Reviews in Rural Science, v. 5, p. 3–13.

Hunt, J.M., 1996, Petroleum Geochemistry and Geology, 2nd edition: New York, W.H. Freeman and Company, 743 p.

Hutton, J., and Dixon, J., 1981, The chemistry and mineralogy of some South Australian calcretes and associated soft carbonates and their dolomitisation: Journal of the Geological Society of Australia, v. 28, p. 71–79.

Ielpi, A., and Ghinassi, M., 2014, Planform architecture, stratigraphic signature and morphodynamics of an exhumed Jurassic meander plain (Scalby Formation, Yorkshire, UK): Sedimentology, v. 61, p. 1923–1960.

Ikonnikov, A.B., 1984. Notes on geology of bauxite deposits in China, *in* Jacob, Jr. Jr., and Leonard., eds., Bauxite, Proceeding of the 1984 Bauxite Symposium, American Institute of Mining and Metallurgical Engineers, p. 539–555.

Ingersoll, R.N., Graham, S.A., and Dickson, W.R., 1995, Remnant ocen basins, *in* Busby, C.J., and Ingersoll, R.V., eds., Tectonics of Sedimentary Basins, Blackwell, Oxford, p. 363–391.

Jackson, W., 1964, Depositional topography and cyclic deposition in west-central Texas: AAPG Bulletin, v. 48, p. 317–328.

Jackson, R.G., 1976, Depositional model of point bars in the lower Wabash River: Journal of Sedimentary Research, v. 46, p. 579–594.

Jackson, R.G., 1981, Sedimentology of muddy fine-grained channel deposits in meandering streams of the American Middle West: Journal of Sedimentary Petrology, v. 51, p. 1169–1192.

James, N.P., Bone, Y., and Kyser, T.K., 1993, Shallow burial dolomitization and dedolomitization of mid-Cenozoic, cool-water, calcitic, deep-shelf limestones, Southern Australia: Journal of Sedimentary Petrology, v. 63, p. 528–538.

Johnson, M., 1994, Thin section grain size analysis revisited: Sedimentology, v. 41, p. 985–999.

Johnson, G.D., 2012, Possible origin of the xenacanth sharks *Orthacanthus texensis* and *Orthacanthus platypternus* in the Lower Permian of Texas, USA: Historical Biology, v. 24, p. 369–379.

Jones, B., Pleydell, S.M., Ng, K.C., and Longstaffe, F.J., 1989, Formation of poikilotopic calcite–dolomite fabrics in the Oligocene–Miocene Bluff formation of Grand Cayman, British West Indies: Bulletin of Canadian Petroleum Geology, v. 37, p. 255–265.

Jones, J.O., and Hentz, T.F., 1988, Permian strata of north-central Texas, *in* Hayward, O.T., ed., South-Central Section of the Geological Society of America Centennial field guide: Boulder, Colorado Geological Society of America, p. 309–316.

Julien, P.Y., 1995, Incipient Motion: Chapter 7, *in* Julien, P.Y., ed., Erosion and Sedimentation, Cambridge, Cambridge University Press, p. 149–152.

Kasvi, E., Vaaja, M., Alho, P., Hyyppä, H., Hyyppä, J., Kaartinen, H., and Kukko, A., 2013, Morphological changes on meander point bars associated with flow structure at different discharges: Earth Surface Processes and Landforms, v. 38, p. 577–590.

Katz, A., 1971, Zoned dolomite crystals: The Journal of Geology, v. 79, p. 38–51.

Kay, B.D., and Angers, D.A., 2000, Soil structure, *in* Sumner, M.E., ed., Handbook of Soil Science: Boca Raton, Florida, CRC Press, p. 229–276.

Kenny, R., 1992, Origin of disconformity dedolomite in the Martin Formation (Late Devonian, Northern Arizona): Sedimentary Geology, v. 78, p. 137–146.

Kelts, K., and Hsü, K.J., 1978, Freshwater carbonate sedimentation, *in* Lerman, A., ed., Lakes: Springer, New York, p. 295–323.

Kerp, J.H., 1988, Aspects of Permian palaeobotany and palynology. X. The West-and Central European species of the genus Autunia Krasser emend. Kerp (Peltaspermaceae) and the form-genus Rhachiphyllum Kerp (callipterid foliage): Review of Palaeobotany and Palynology, v. 54, p. 249–360.

Kessler, J.L.P., Soreghan, G.S., and Wacker, H.J., 2001, Equatorial Aridity in Western Pangea: Lower Permian Loessite and Dolomitic Paleosols in Northeastern New Mexico, U.S.A: Journal of Sedimentary Research, v. 71, p. 817–832.

Khadkikar, A.S., Merh, S.S., Malik, J.N., and Chamyal, L.S., 1998, Calcretes in semi-arid alluvial systems: formative pathways and sinks: Sedimentary Geology, v. 116, p. 251–260.

Khalaf, F.I., 1990, Occurrence of phreatic dolocrete within Tertiary clastic deposits of Kuwait, Arabian Gulf: Sedimentary Geology, v. 68, p. 223–239.

Khalaf, F.I., 2007, Occurrences and genesis of calcrete and dolocrete in the Mio-Pleistocene fluviatile sequence in Kuwait, northeast Arabian Peninsula: Sedimentary Geology, v. 199, p. 129–139.

King, P.B., 1937, Geology of the Marathon region, Texas: U.S. Geological Survey, Professional Paper, v. 187, 148 p.

Kinne, O., 1970, 4. Salinity, 4.3. Animals, 4.3.1. Invertebrates, in Kinne, O., eds., Marine Ecology: A Comprehensive, Integrated Treatise of Life in Oceans and Coastal Waters: London, New York, Wiley-Interscience, p. 821–996.

Knighton, A.D., and Nanson, G.C., 1993, Anastomosis and the continuum of channel pattern: Earth Surface Processes and Landforms, v. 18, p. 613–625.

Knighton, A.D., and Nanson, G.C., 1994a, Flow transmission along an arid zone anastomosing river, Cooper Creek, Australia: Hydrological Processes, v. 8, p. 137–154.

Knighton, A.D., and Nanson, G.C., 1994b, Waterholes and their significance in the anastomosing channel system of Cooper Creek, Australia: Geomorphology, v. 9, p. 311–324.

Knighton, A.D., and Nanson, G.C., 1996, Anabranching rivers: their cause, character and classification: Earth Surface Processes and Landforms, v. 21, p. 217–239.

Knox, J.C., 1993, Large increases in flood magnitude in response to modest changes in climate: Nature, v. 361, p. 430–432.

Kok, C.J., and Van Der Velde, G., 1994, Decomposition and macroinvertebrate colonization of aquatic and terrestrial leaf material in alkaline and acid still water: Freshwater Biology, v. 31, p. 65–75.

Konhauser, K.O., Fyfe, W.S., Ferris, F.G., and Beveridge, T.J. 1993. Metal sorption and mineral precipitation by bacteria in two Amazonian river systems: Rio Solimões and Rio Negro, Brazil: Geology, v. 21, p. 1103–1106.

Koster, E.H., Rust, B.R., and Gendzwill, D.J., 1980, The ellipsoidal form of clasts with practical applications to fabric and size analyses of fluvial gravels: Canadian Journal of Earth Sciences, v. 17, p. 1725–1739.

Kocurek, G. and Kirkland, B.L., 1998, Getting to the source: aeolian influx to the Permian Delaware basin region: Sedimentary Geology, v. 117, p. 143–149.

Kraus, M.J., 1999, Paleosols in clastic sedimentary rocks: their geologic applications: Earth-Science Reviews, v. 47, p. 41–70.

Krings, M., Klavins, S.D., DiMichele, W.A., Kerp, H., and Taylor, T.N., 2005, Epidermal anatomy of *Glenopteris splendens* Sellards nov. emend., an enigmatic seed plant from the Lower Permian of Kansas (USA): Review of Palaeobotany and Palynology, v. 136, p. 159–180.

Kübler, B., 1967, La cristallinité de l'illite et les zones tout á fair supérieures du métamorphisme, *in* Etages Tectoniques, Colloque de Neuchâtel 1966: Univ. Neuchâtel, á la Baconnière, Suisse, p. 105–121.

Kubler, B., 1968, Evaluation quantitative du metamorphism par la cristallinite de l'Illite: Bullet Centre Rech, Pau-SNPA, v. 2, p. 385–397.

Labandeira, C.C., and Allen, E.G., 2007, Minimal insect herbivory for the Lower Permian Coprolite Bone Bed site of north-central Texas, USA, and comparison to other Late Paleozoic floras: Palaeogeography, Palaeoclimatology, Palaeoecology, v. 247, p. 197–219.

Langford, R., and Bracken, B., 1987, Medano Creek, Colorado, a model for upper-flow-regime fluvial deposition: Journal of Sedimentary Petrology, v. 57, p. 863–870.

Larned, S.T., Schmidt, J., Datry, T., Konrad, C.P., Dumas, J.K., and Diettrich, J.C., 2010, Longitudinal river ecohydrology: flow variation down the lengths of alluvial rivers: Ecohydrology, v. 4, p. 532–548.

Laveine, J-P., and Dufour, F., 2013, The bifurcate "outer-inner" semi-pinnate frond of the Permo-Pennsylvanian seed-fern *Neurodontopteris auriculata*, type species of the genus *Neurodontopteris*: Palaeontographica, v. 289B, p. 75–177.

Leopold, L.B., and Wolman, M.G., 1960, River meanders: Geological Society of America Bulletin, v. 71, p. 769–794.

Li, H., and Taylor, D.W., 1998, *Aculeovinea yunguiensis* gen. et sp. nov., a new taxon of gigantopterid axis from the Upper Permian of Guizhou province, China: International Journal of Plant Science, v. 159, p. 1023–1033.

Li, H., and Taylor, D.W., 1999, Vessel-bearing stems of *Vasovinea tianii* gen. et sp. nov. (Gigantopteridales) from the Upper Permian of Guizhou province, China: American Journal of Botany, v. 86, p. 1563–1575.

Liu, D., Abuduwaili, J., Lei, J., and Wu, G., 2011, Deposition rate and chemical composition of the aeolian dust from a bare saline playa, Ebinur Lake, Xinjiang, China: Water, Air and Soil Pollution, v. 218, 175–184.

Löhr, S., Grigorescu, M., and Cox, M., 2013, Iron nodules in ferric soils of the Fraser Coast, Australia: relicts of laterisation or features of contemporary weathering and pedogenesis?: Soil Research, v. 51, p. 77–93.

Loch, R.J., 1991, Bedload transport of mud as pedogenic aggregates in modern and ancient rivers: Sedimentology, v. 38, p. 157–160.

Lojka, R., Drábková, J., Zajíc, J., Sýkorová, I., Franců, J., Bláhová, A., and Grygar, T., 2009, Climate variability in the Stephanian B based on environmental record of the Mšec Lake deposits (Kladno-Rakovník Basin, Czech Republic): Palaeogeography, Palaeoclimatoloty, Palaeoecology, v. 280, p. 78–93.

Long, D., 2011, Architecture and depositional style of fluvial systems before land plants: a comparison of Precambrian, early Paleozoic and modern river deposits, *in* North, C.P., Davidson, S., and Leleu, S., eds., From river to rock record: the preservation of fluvial sediments and their subsequent interpretation: Tulsa, Oklahoma, USA, SEPM Special Publication, v. 97, p. 37–71.

Loope, D.B., 1985. Episodic deposition and preservation of eaolian sands: a late Palaeozoic example from southeastern Utah: Geology, v. 13, p. 73–76.

Looy, C.V., 2013, Natural history of a plant trait: branch-system abscission in Paleozoic conifers and its environmental, autecological, and ecosystem implications in a fire-prone world: Paleobiology, v. 39, p. 235–252.

Looy, C.V., and Duijnstee, I.A., 2013, Characterizing morphologic variability in foliated Paleozoic conifer branches – A first step in testing its potential as proxy for taxonomic composition: New Mexico Museum of Natural History and Science Bulletin, v. 60, p. 215–223.

Looy, C., Kerp, H., Duijnstee, I., and DiMichele, B., 2014, The late Paleozoic ecological-evolutionary laboratory, a land-plant fossil record perspective: The Sedimentary Record, v. 12, p. 4-18.

Lotsari, E., Vaaja, M., Flener, C., Kaartinen, H., Kukko, A., Kasvi, E., Hyyppä, H., Hyyppä, J., and Alho, P., 2014, Annual bank and point bar morphodynamics of a meandering river

determined by high–accuracy multitemporal laser scanning and flow data: Water Resources Research, v. 50, p. 5532–5559.

Lucas, S.G., 2006, Global Permian tetrapod biostratigraphy and biochronology: Geological Society, London, Special Publications, v. 265, p. 65–93.

Lucas, S.G., and Anderson, O.J., 1993, Stratigraphy of the Permian-Triassic boundary in southeastern New Mexico and West Texas: Geology of the Carlsbad Region, New Mexico and West Texas: 44th NMGS Fall Field Conference Guidebook, New Mexico Geological Society, Socorro, NM, p. 219–230.

Lucas, S.G., and Krainer, K., 2005, Cutler Group (Permo-Carboniferous) stratigraphy, Chama basin, New Mexico: *in* Lucas, S.G., Zeigler, K.E., and Spielmann, J.A., eds., The Permian of Central New Mexico: New Mexico Museum of Natural History and Science Bulletin, v. 31, p. 90–100.

Lucas, S.G., Voigt, S., Lerner, A.J., and Nelson, W.J., 2011, Late Early Permian continental ichnofauna from Lake Kemp, north-central Texas, USA: Palaeogeography, Palaeoclimatology, Palaeoecology, v. 308, p. 395–404.

Ludlam, S.D., 1981, Sedimentation rates in Fayetteville Green Lake, New York, USA: Sedimentology, v. 28, p. 85–96.

Lütters, S., and Hanert, H.H., 1989, The ultrastructure of chemolithoautotrophic Gallionella ferruginea and Thiobacillus ferrooxidans as revealed by chemical fixation and freeze-etching: Archives of Microbiology, v. 151, p. 245–251.

Machette, M.N., 1985, Calcic soils of southwestern United States, *in* Weide, D.L., ed., Soils and Quaternary geology of the southwestern United States: Boulder, Colorado, Geological Society of America Special Papers p. 1–21.

Mack, G.H., 2003. Lower Permian Terrestrial Palaeoclimate Indicators in New Mexico and Their Comparison to Palaeoclimate Models: New Mexico Geological Society Guidebook, v. 54, p. 231–240.

Mack, G.H., and Dinterman, P.A., 2002, Depositional environments and paleogeography of the Lower Permian (leonardian) Yeso and correlative formations in New Mexico: Mountain Geologist, v. 39, p. 75–88.

Mack, G.H., Leeder, M., Perez-Arlucea, M., and Bailey, B.D., 2003, Early Permian silt-bed fluvial sedimentation in the Orogrande basin of the Ancestral Rocky Mountains, New Mexico, USA: Sedimentary Geology, v. 160, p. 159–178.

Mack, G.H., and James, W.C., 1986, Cyclic sedimentation in the mixed siliciclastic–carbonate Abo-Hueco transitional zone (Lower Permian), southwestern New Mexico: Journal of Sedimentary Petrology, v. 56, p. 635–647.

Mack, G.H., Suguio, K., 1991. Depositional environments of the Yeso Formation (Lower Permian), southern Caballo Mountains, New Mexico: Rocky Mountain Association of Geologists, v. 13, p. 45–49.

Mack, G.H., Tabor, N.J., and Zollinger, H.J., 2010, Palaeosols and sequence stratigraphy of the Lower Permian Abo Member, south-central New Mexico, USA: Sedimentology, v. 57, p. 1566–1583.

Magee, J.W., Bowler, J.M., Miller, G.H., and Williams, D.L.G., 1995, Stratigraphy, sedimentology, chronology and palaeohydrology of Quaternary lacustrine deposits at Madigan Gulf, Lake Eyre, South Australia: Palaeogeography Palaeoclimatology Palaeoecology, v. 113, p. 3–42.

Magee, J.W., Miller, G.H., Spooner, N.A., and Questiaux, D., 2004, Continuous 150 ky monsoon record from Lake Eyre, Australia: Insolation-forcing implications and unexpected Holocene failure: Geology, v. 32, p. 885–888.

Makaske, B., and Weerts, H.J., 2005, Muddy lateral accretion and low stream power in a sub-recent confined channel belt, Rhine-Meuse delta, central Netherlands: Sedimentology, v. 52, p. 651–668.

Mamay, S.H., 1989, *Evolsonia*, a new genus of Gigantopteridaceae from the Lower Permian Vale Formation, north-central Texas: American Journal of Botany, v. 76, p. 1299–1311.

Mamay, S.H., Chaney, D.S., and DiMichele, W.A., 2009, *Comia*, a seed plant possibly of peltaspermous affinity: A brief review of the genus and description of two new species from the Early Permian (Artinskian) of Texas, *C. greggii* sp. nov. and *C. craddockii* sp. nov: International Journal of Plant Sciences, v. 170, p. 267–282.

Mamy, J., and Gaultier, J.P., 1975, Etude de l'e´volution de l'ordre cristallin dans la montmorillonite en relation avec la diminution d'exchangeabilite´ du potassium: International Clay Conference Proceedings, p. 149–155.

Maroulis, J.C., and Nanson, G.C., 1996, Bedload transport of aggregated muddy alluvium from Cooper creek, central Australia: A flume study: Sedimentology, v. 43, p. 771–790.

Marren, P.M., McCarthy, T.S., Tooth, S., Brandt, D., Stacey, G.G., Leong, A., and Spottiswoode, B., 2006, A comparison of mud- and sand-dominated meanders in a downstream coarsening reach of the mixed bedrock-alluvial Klip River, eastern Free State, South Africa: Sedimentary Geology, v. 190, p. 213–226.

Marren, P.M., and Woods, K.L.M., 2011, Inundation of anabranching river flood plain wetlands: the Ovens River, Victoria, Australia, *in* Abesser, C., Nutzmann, G., Hill, M.C., Bloschl, G., and Lakshmanan, E., eds., Conceptual and Modelling Studies of Integrated Groundwater, Surface Water, and Ecological Systems: IAHS Publication, p. 229–234.

Marriott, S.B., and Wright, V.P., 1993, Palaeosols as indicator of geomorphic stability in two Old Red Sandstone alluvial suites, South Wales: Journal of the Geological Society, v. 150, p. 1109–1120.

Marriott, S.B., and Wright, V.P., 1996, Sediment recycling on Siluro-Devonian floodplains: Journal of the Geological Society, v. 153, p. 661–664.

Marriott, S.B., and Wright, V.P., 2004, Mudrock deposition in an ancient dryland system: Moor Cliffs Formation, Lower Old Red Sandstone, southwest Wales, UK: Geological Journal, v. 39, p. 277–298.

McBride, E., 1989, Stratigraphy and sedimentary history of pre-Permian Paleozoic rocks of the Marathon uplift, *in* Hatcher, R., Thomas, W., and Viele, G., eds., The Appalachian – Ouachita Orogen in the United States, Geological Society of America, The Geology of North America, v. F-2, p. 603–620.

McCaffrey, M.A., Lazar, B., and Holland, H.D., 1987, The evaporation path of seawater and the coprecipitation of Br^- and K^+ with halite: Journal of Sedimentary Research, v. 57, p. 928−937.

McCahon, T., and Miller, K., 1997, Climatic significance of natric horizons in Permian (Asselian) palaeosols of north-central Kansas, USA: Sedimentology, v. 44, p. 113−125.

McElwain, J.C., and Punyasena, S.W., 2007, Mass extinction events and the plant fossil record: Trends in Ecology and Evolution, v. 22, p. 548–557.

McGarry, D., 1996, Structure and grain size distribution of Vertisols, *in* Ahmad, N., and Mermut, A., eds., Vertisols and Technologies for Their Management: Amsterdam, Elsevier, p. 231–302.

McKee, E., Crosby, E.T., and Berryhill Jr, H., 1967, Flood deposits, Bijou Creek, Colorado, June 1965: Journal of Sedimentary Research, v. 37, p. 829–851.

McQueen, K.G., Hill, S.M., and Foster, K.A., 1999, The nature and distribution of regolith carbonate accumulations in southeastern Australia and their potential as a sampling medium in geochemical exploration: Journal of Geochemical Exploration, v. 67, p. 67–82.

Meléndez, A., Alonso-Zarza, A.M., and Sancho, C., 2011, Multi-storey calcrete profiles developed during the initial stages of the configuration of the Ebro Basin's exorrheic fluvial network: Geomorphology, v. 134, p. 232–248.

Menounos, B., Clague, J., Gilbert, R., and Slaymaker, O., 2005, Environmental reconstruction from a varve network in the southern Coast Mountains, British Columbia, Canada: The Holocene, v. 15, p. 1163–1171.

Mertes, L.A., 1997, Documentation and significance of the perirheic zone on inundated floodplains: Water Resources Research, v. 33, p. 1749–1762.

Miall, A.D., 1974, Paleocurrent analysis of alluvial sediments: a discussion of directional variance and vector magnitude: Journal of Sedimentary Research, v. 44, p. 1174–1185.

Miall, A.D., 1985, Architectural-element analysis: a new method of facies analysis applied to fluvial deposits: Earth-Science Reviews, v. 22, p. 261–308.

Miall, A.D., 1996, The geology of fluvial deposits: sedimentary facies, basin analysis, and petroleum geology: Berlin, New York, Springer.

Michael, G.E., Anders, D.E., and Law, B.E., 1993, Geochemical evaluation of Upper Cretaceous Fruitland Formation coals, San Juan Basin, New Mexico and Colorado: Organic Geochemistry, v. 20, p. 475–498.

Miller, J.R., 1991, Development of anastomosing channels in south-central Indiana: Geomorphology, v. 4, p. 221–229.

Miller, M.F., 1984, Distribution of biogenic structures in Paleozoic nonmarine and marine-margin sequences: an actualistic model: Journal of Paleontology, v. 58, p. 550–570.

Miller, M.F., and Labandeira, C., 2002, Slow Crawl Across the Salinity Divide: Delayed Colonization of Freshwater Ecosystems by Invertebrates: GSA Today, v. 12, p. 4–10.

Miller, K.B., McCahon, T.J., and West, R.R., 1996, Lower Permian (Wolfcampian) palaeosol-bearing cycles of the U.S. Midcontinent: evidence of climatic cyclicity: Journal of Sedimentary Research, v. 66, p. 71–84.

Miller, A.K., and Youngquist, W., 1947, Lower Permian cephalopods from the Texas Colorado River Valley: University of Kansas Paleontological Contributions no. 2, Mollusca, v. 1, p. 1–15

Milner, A.R., and Schoch, R.R., 2013, Trimerorhachis (Amphibia: Temnospondyli) from the Lower Permian of Texas and New Mexico: cranial osteology, taxonomy and biostratigraphy: Neues Jahrbuch für Geologie und Paläontologie-Abhandlungen, v. 270, p. 91–128.

Minter, N.J., Krainer, K., Lucas, S.G., Braddy, S.J., and Hunt, A.P., 2007, Palaeoecology of an Early Permian playa lake trace fossil assemblage from Castle Peak, Texas, USA: Palaeogeography Palaeoclimatology Palaeoecology, v. 246, p. 390–423.

Mohrig, D., Heller, P.L., Paola, C., and Lyons, W.J., 2000, Interpreting avulsion process from ancient alluvial sequences: Guadalope-Matarranya system (northern Spain) and Wasatch Formation (western Colorado): Geological Society of America Bulletin, v. 112, p. 1787–1803.

Montañez, I.P., Tabor, N.J., Niemeier, D., DiMichele, W.A., Frank, T.D., Fielding, C.R., Isbell, J.L., Birgenheier, L.P., and Rygel, M.C., 2007, CO_2-forced climate and vegetation instability during late paleozoic deglaciation: Science, v. 315, p. 87–91.

Montgomery, S.L., and Dixon, W.H., New depositional model improves outlook for Clear Fork infill drilling: Oil and Gas Journal, v. 96, p. 94–98.

Moore, D.M., and Reynolds, R.C., 1997, X-ray Diffraction and the Identification and Analysis of Clay Minerals: New York, Oxford University Press, 378 p.

Mora, C.I., Sheldon, B.T., Elliott, W.C., and Driese, S.G., 1998, An oxygen isotope study of illite and calcite in three Appalachian Paleozoic vertic paleosols: Journal of Sedimentary Research, v. 68, p. 456–464.

Morris, R., 1989, Stratigraphy and sedimentary history of post-Arkansas Novaculite Carboniferous rocks of the Ouachita Mountains, *in* Hatcher, R., Thomas, W., and Viele, G., eds., The Geology of North America—The Appalachian–Ouachita Orogen in the United States: The Appalachian–Ouachita orogen in the United States: The Geological Society of America, The Geology of North America, Geological Society of America, The Geology of North America, v. F-2, p. 501–602.

Morozova, G.S., and Smith, N.D., 2000, Holocene avulsion styles and sedimentation patterns of the Saskatchewan River, Cumberland Marshes, Canada: Sedimentary Geology, v. 130, p. 81–105.

Mountney, N.P., 2006, Periodic accumulation and destruction of aeolian erg sequences in the Permian Cedar Mesa Sandstone, White Canyon, southern Utah, USA: Sedimentology, v. 53, p. 789–823.

Müller, R., Nystuen, J.P., and Wright, V.P., 2004, Pedogenic mud aggregates and paleosol development in ancient dryland river systems: Criteria for interpreting alluvial mudrock origin and floodplain dynamics: Journal of Sedimentary Research, v. 74, p. 537–551.

Munsell Color, 1994, Munsell Soil Color Charts (revised edition): New Windsor, New York, Munsell Color, 10 p.

Murry, P.A., and Johnson, G.D., 1987, Clear Fork vertebrates and environments from the Lower Permian of north-central Texas: Texas Journal of Science, v. 39, p. 253–266.

Nádor, A., Lantos, M., Toth-Makk, A., and Thamo-Bozso, E., 2003, Milankovitch-scale multi-proxy records from fluvial sediments of the last 2.6 Ma, Pannonian Basin, Hungary: Quaternary Science Reviews, v. 22, p. 2157–2175.

Nadon, G., 1994, The genesis and recognition of anastomosed fluvial deposits: data from the St. Mary River Formation, southwestern Alberta, Canada: Journal of Sedimentary Research, v. 64, p. 451–463.

Nance, D., and Linnemann, U., 2008, The Rheic Ocean: Origin, evolution, and significance: GSA Today, v. 18, p. 4–12.

Nanson, G.C., 1980, Point bar and floodplain formation of the meandering Beatton River, northeastern British Columbia, Canada: Sedimentology, v. 27, p. 3–29.

Nanson, G.C., Price, D.M., Jones, B.G., Maroulis, J.C., Coleman, M., Bowman, H., Cohen, T.J., Pietsch, T.J., and Larsen, J.R., 2008, Alluvial evidence for major climate and flow regime changes during the middle and late Quaternary in eastern central Australia: Geomorphology, v. 101, p. 109–129.

Nanson, G.C., Price, D.M., and Short, S.A., 1992, Wetting and drying of Australia over the past 300 ka: Geology, v. 20, p. 791–794.

Nanson, G.C., Rust, B.R., and Taylor, G., 1986, Coexistent mud braids and anastomosing channels in an arid-zone river: Cooper Creek, central Australia: Geology, v. 14, p. 175–178.

Nanson, G.C., Young, R., Price, D., and Rust, B., 1988, Stratigraphy, sedimentology and late Quaternary chronology of the Channel Country of western Queensland, *in* Warner, R.F., ed., Fluvial Geomorphology of Australia: Sydney, Academic Press, p. 151–175.

Nanson, G.C., Jones, B.G., Price, D.M., and Pietsch, T.J., 2005, Rivers turned to rock: Late Quaternary alluvial induration influencing the behaviour and morphology of an anabranching river in Australia's monsoon tropics: Geomorphology, v. 70, p. 398–420.

Nash, D.J., and Smith, R.F., 2003, Properties and development of channel calcretes in a mountain catchment, Tabernas Basin, southeast Spain: Geomorphology, v. 50, p. 227–250.

Naugolnykh, S.V., 1999, A new species of *Compsopteris* Zalessky from the Upper Permian of the Kama River Basin (Perm Region): Paleontological Journal, v. 33, p. 686–697.

Nelson, W.J., Hook, R.W., and Tabor, N., 2001, Clear Fork Group (Leonardian, Lower Permian) of North-Central Texas, *in* Johnson., K.S., ed., Pennsylvanian and Permian geology and petroleum in the southern Midcontinent, 1998 symposium., Oklahoma Geological Survey Circular, p. 167–169.

Nelson, W.J., Hook, R.W., and Chaney, D.S., 2013, Lithostratigraphy of the Lower Permian (Leonardian) Clear Fork Formation of north-central Texas, *in* Lucas, S.G., Dimichele, W.A., Barrick, J.E., Schneider, J.W., and Spielmann, J.A., eds., The Carboniferous-Permian Transition, New Mexico Museum of Natural History and Science Bulletin, p. 286–311.

Nesbitt, H.W., and Wilson, R.E., 1992, Recent Chemical Weathering of Basalts: American Journal of Science, v. 292, p. 740–777.

Nettleton, I.M., Martin, S., Hencher, S., and Moore, R., 2005, Debris flow types and mechanisms, *in* Winter, M., Macgregor, F., and Shackman, L., eds., Scottish Road Network Landslides Study, Trunk Roads: Network Management Division Published Report Series, p. 45–67.

Netto, R.G., Balistieri, P.R.M.N., Lavina, E.L.C., and Silveira, D.M., 2009, Ichnological signatures of shallow freshwater lakes in the glacial Itararé Group (Mafra Formation, Upper Carboniferous – Lower Permian of Paraná Basin, S Brazil): Palaeogeography, Palaeoclimatology, Palaeoecology, v. 272, p. 240–255.

Neubauer, F., Liu, Y., Genser, J., Rieser, A.B., Friedl, G., Ge, X., and Thoeni, M., 2010, Quaternary celestine and gypsum extensional veins in a folded hypersaline lake infill: the Qaidam basin, western China: Austrian Journal of Earth Sciences, v. 103, p. 81–91.

Nicholas, R.L., and Waddell, D.E., 1989, The Ouachita system in the subsurface of Texas, Arkansas, and Louisiana, *in* Hatcher, R., Thomas, W., and Viele, G., eds., The Appalachian-Ouachita orogen in the United States, Geological Society of America, v. F-2, p. 661–672.

Niem, A.R., 1977, Mississippian pyroclastic flow and ash-fall deposits in the deep-marine Ouachita flysch basin, Oklahoma and Arkansas: Geological Society of America Bulletin, v. 88, p. 49–61.

Norrish, K., and Pickering, J.G., 1983, Clay minerals, *in* Soils: an Australian Viewpoint: CSIRO, Melbourne, Academic Press, London, p. 281–308.

North, C.P., and Taylor, K.S., 1996, Ephemeral-fluvial deposits: integrated outcrop and simulation studies reveal complexity: AAPG bulletin, v. 80, p. 811–830.

Olsen, H., 1989, Sandstone-body structures and ephemeral stream processes in the Dinosaur Canyon Member, Moenave Formation (Lower Jurassic), Utah, U.S.A: Sedimentary Geology, v. 61, p. 207–221.

Olson, E.C., 1958, Fauna of the Vale and Choza: 14. Summary, review, and integration of the geology and the faunas: Fieldiana Geol, v. 10, p. 397–448.

Olson, E.C., 1989, The Arroyo Formaton (Leonardian: Lower Permian) and Its Vertebrate Fossils: Texas Memorial Museum Bulletin, v. 35, p. 25.

Olson, E.C., and Bolles, K., 1975, Permo-Carboniferous fresh water burrows: Fieldiana Geology, v. 35, p. 271–290.

Olson, E.C., and Mead, J.G., 1982, The Vale Formation (Lower Permian): its vertebrates and paleoecology: Texas Memorial Museum Bulletin, v. 29, p. 46.

Oriel, S.S., McKee, E.D., and Crosby, E.J., 1967, Paleotectonic investigations of the Permian system in United States: Washington, U.S, Geological Survey Professional Paper, 271 p.

Page, K.J., and Nanson, G.C., 1996, Stratigraphic architecture resulting from Late Quaternary evolution of the Riverine Plain, south-eastern Australia: Sedimentology, v. 43, p. 927–945.

Page, K.J., Nanson, G.C., and Frazier, P.S., 2003, Floodplain formation and sediment stratigraphy resulting from oblique accretion on the Murrumbidgee River, Australia: Journal of Sedimentary Research, v. 73, p. 5–14.

Paphitis, D., 2001, Sediment movement under unidirectional flows: an assessment of empirical threshold curves: Coastal Engineering, v. 43, p. 227–245.

Parrish, J.T., 1993, Climate of the supercontinent Pangaea. Journal of Geology, v. 101, p. 215–233.

Patzkowsy, M.E., Smith, L.H., Markwick, P.J., Engberts, C.J., and Gyllenhaal, E.D., 1991, Application of the Fujita–Ziegler palaeoclimate model: Early Permian and Late Cretaceous examples: Palaeogeography Palaeoclimatology Palaeoecology, v. 86, p. 67–85.

Petersen, G.W., Chester, G., and Lee, G.B., 2006. Quantitative determination of calcite and dolomite in soils: Journal of Soil Science, v. 17, p. 328–338.

Phillips, T.L., 1979, Reproduction of heterosporous arborescent lycopods in the Mississippian-Pennsylvanian of Euramerica: Review of Palaeobotany and Palynology, v. 27, p. 239–289.

Phillips, T.L., and DiMichele, W.A., 1992, Comparative ecology and life-history biology of arborescent lycopods in Late Carboniferous swamps of Euramerica: Annals of the Missouri Botanical Garden, v. 79, p. 560–588.

Pimentel, N., Wright, V., and Azevedo, T., 1996, Distinguishing early groundwater alteration effects from pedogenesis in ancient alluvial basins: examples from the Palaeogene of southern Portugal: Sedimentary Geology, v. 105, p. 1–10.

Piper, D.J., and Slatt, R.M., 1977, Late Quaternary clay-mineral distribution on the eastern continental margin of Canada: Geological Society of America Bulletin, v. 88, p. 267–272.

Pittermann, J., Stuart, S.A., Dawson T.E., Moreau, A., 2012, Cenozoic climate change shaped the evolutionary ecophysiology of the Cupressaceae conifers: Proceedings of the National Academy of Sciences, v. 109, p. 9647–9652.

Plummer, F.B., and Scott, G., 1937, Upper Paleozoic ammonites in Texas: University of Texas Bulletin no. 3701, v. 3, p. 1–516.

Pokorný, P., Klimešová, J., and Klimeš, L., 2000, Late Holocene history and vegetation dynamics of a floodplain alder carr: a case study from eastern Bohemia, Czech Republic: Folia Geobotanica, v. 35, p. 43–58.

Prevec, R., Labandeira, C. C., Neveling, J., Gastaldo, R. A., Looy, C. V., and Bamford, M., 2009, Portrait of a Gondwanan ecosystem: a new late Permian fossil locality from KwaZulu-Natal, South Africa: Review of Palaeobotany and Palynology, v. 156, p. 454–493.

Price, A.R., 1982, Western Arabian Gulf echinoderms in high salinity waters and the occurrence of dwarfism: Journal of Natural History, v. 16, p. 519–527.

Potter, P.E., Heling, D., Shimp, N.F., and VanWie, W., 1975, Clay mineralogy of modern alluvial muds of the Mississippi River Basin: Bulletin du Centre de Recherches de Pau, v. 9, p. 353–389.

Probert, M.E., Fergus, I.F., Bridge, B.J., McGarry, D., Thompson, C.H., and Russel, J.S., 1987, The Properties and Management of Vertisols: Wallington, U.K, CAB International/IBSRAM, 20 p.

Puigdefabregas, C., 1973, Miocene point-bar deposits in the Ebro Basin, Northern Spain: Sedimentology, v. 20, p. 133–144.

Purkait, B., 2010, Analysis of current directions in the bends of an ephemeral river and its geological implications: Frontiers of Earth Science, v. 4, p. 417–426.

Rasbury, E.T., Hanson, G.N., Meyers, W.J., Holt, W.E., Goldstein, R.H., and Saller, A.H., 1998, U-Pb dates of paleosols: Constraints on late Paleozoic cycle durations and boundary ages: Geology, v. 26, p. 403–406.

Raymond, A., Lambert, L., Costanza, S., Slone, E.J., and Cutlip, P.C., 2010, Cordaiteans in paleotropical wetlands: an ecological re-evaluation: International Journal of Coal Geology, v. 83, p. 248–265.

Rees, P.M., Ziegler, A.M., Gibbs, M.T., Kutzbach, J.E., Behling, P.J., and Rowley, D.B., 2002, Permian phytogeographic patterns and climate data/model comparisons: Journal of Geology, v. 110, p. 1–3.

Regan, T.R., and Murphy, P.J., 1986a, Faulting in the Matador Uplift area, Texas: Stone and Webster Engineering Corp. Boston, Topical Report ONWI/SUB/86/E512-05000-T48, p. 169.

Remy, W., and Remy, R., 1975, Beiträge zur Kenntnis des Morpho-Genus *Taeniopteris* Brongniart: Argumenta Palaeobotanica, v. 4, p. 31–37.

Retallack, G.J., 2005a. Permian greenhouse crises, *in* Lucas, S.G., and Ziegler, K.E., eds., The Nonmarine Permian: New Mexico Musuem Natural History aand Science Bulletin, v. 30, p. 256–269.

Rice, D.D., 1993, Composition and origins of coalbed gas, *in* Law, B.E., and Rice, D.D., eds., Hydrocarbons from Coal: AAPG Studies in Geology, v. 38, p. 159–184

Robbins, E.I., and Rhodehamel, E.C., 1976, Geothermal gradients help predict petroleum potential of Scotian Shelf: Oil and Gas Journal, v. 74, p. 143–145.

Roberts, J.A., Bennett, P.C., Gonzalez, L.A., Macpherson, G.L., and Milliken, K.L., 2004, Microbial precipitation of dolomite in methanogenic groundwater: Geology, v. 32, p. 277–280.

Robinson, P.L., 1973, Palaeoclimatology and continental drift, *in* Tarling, D.H., and Runcorn, S.K., eds., Implications of Continental Drift to the Earth Sciences: London, I. Academic Press, p. 449–476.

Romer, A.S., 1928, Vertebrate faunal horizons in the Texas Permo-Carboniferous red beds: Univ Texas Bull, v. 2801, p. 67–108.

Roscher, M., and Schneider, J.W., 2006, Permocarboniferous climate: Early Pennsylvanian to Late Permian climate development of central Europe in a regional and global context: Journal of Geological Society London Special Publication, v. 265, p. 95–136.

Roth, R., 1931, New information on the base of the Permian in north-central Texas: Journal of Paleontology, v. 5, p. 295.

Roth, R., Newell, N.D., and Burma, B.H., 1941, Permian pelecypods in the lower Quartermaster Formation, Texas: Journal of Paleontology, v. 15, p. 312–317.

Rothwell, G.W., 1982, New interpretations of the earliest conifers: Review of Palaeobotany and Palynology, v. 37, p. 7–28.

Rowland, J.C., Lepper, K., Dietrich, W.E., Wilson, C.J., and Sheldon, R., 2005, Tie channel sedimentation rates, oxbow formation age and channel migration rate from optically stimulated luminescence (OSL) analysis of floodplain deposits: Earth Surface Processes and Landforms, v. 30, p. 1161–1179.

Royer, D.L., 1999, Depth to pedogenic carbonate horizon as a paleoprecipitation indicator?: Geology, v. 27, p. 1123–1126.

Ruppel, C., Von Herzen, R.P., and Bonneville, A., 1995, Heat flux through an old (~175 Ma) passive margin: Offshore southeastern United States: Journal of Geophysical Research: Solid Earth, v. 100, p. 20037–20057.

Rust, B.R., Gibling, M.R., and Legun, A.S., 1984, Coal Deposition in an Anastomosing-Fluvial System: the Pennsylvanian Cumberland Group South of Joggins, Nova Scotia, Canada, *in* Rahmani , R.A., and Flores, R.M., eds., Sedimentology of coal and coal-bearing sequences, International Association of Sedimentologists Publications, p. 105–120.

Rust, B.R., and Legun, A.S., 1983, Modern anastomosing-fluvial deposits in arid Central Australia, and a Carboniferous analogue in New Brunswick, Canada: Modern and ancient

fluvial systems, Special Publication of the International Association of Sedimentologists, v. 6, p. 385–392.

Rust, B.R., and Nanson, G.C., 1989, Bedload transport of mud as pedogenic aggregates in modern and ancient rivers: Sedimentology, v. 36, p. 291–306.

Rust, B.R., and Nanson, G.C., 1991, Reply: Sedimentology, v. 38, p. 157–160.

Rygel, M.C., and Gibling, M.R., 2006, Natural geomorphic variability recorded in a high-accommodation setting: Fluvial architecture of the Pennsylvanian Joggins Formation of Atlantic Canada: Journal of Sedimentary Research, v. 76, p. 1230–1251.

Rygel, M.C., Gibling, M.R., and Calder, J.H., 2004, Vegetation-induced sedimentary structures from fossil forests in the Pennsylvanian Joggins Formation, Nova Scotia: Sedimentology, v. 51, p. 531–552.

Sambrook Smith, G.H., Best, J.L., Leroy, J.Z., and Orfeo, O., 2015, The alluvial architecture of a suspended sediment dominated meandering river: the Río Bermejo, Argentina: Sedimentology, p. n/a–n/a.

Sander, P.M., 1987, Taphonomy of the Lower Permian Geraldine bonebed in Archer County, Texas: Palaeogeography, Palaeoclimatology, Palaeoecology, v. 61, p. 221–236.

Sarkar, S., 1988, Petrology of caliche-derived peloidal calcirudite/calcarenite in the Late Triassic Maleri Formation of the Pranhita–Godavari Valley, south India: Sedimentary Geology, v. 55, p. 263–282.

Savage, B., Watson, T., Ono, O., and Honda, A., 2010, Natural systems evidence for the alteration of clay under alkaline conditions: An example from Searles Lake, California: Applied Clay Science, v. 47, p. 72–81.

Schachat, S.R., Labandeira, C.C., Gordon, J., Chaney, D., Levi, S., Halthore, M.N., and Alvarez, J., 2014, Plant–insect interactions from the Early Permian (Kungurian) Colwell Creek Pond, North-Central Texas: the early spread of herbivory in riparian environments: International Journal of Plant Sciences, v. 175, p. 855–890.

Scheihing, M.H., 1980, Reduction of wind velocity by the forest canopy and the rarity of non-arborescent plants in the Upper Carboniferous fossil record: Argumenta Palaeobotanica, v. 6, p. 133–138.

Scheihing, M.H., and Pfefferkorn, H.W., 1984, The taphonomy of land plants in the Orinoco Delta: a model for the incorporation of plant parts in clastic sediments of Late Carboniferous age of Euramerica: Review of Palaeobotany and Palynology, v. 41, p. 205–240.

Schmid, S., Worden, R.H., and Fisher, Q.J., 2006, Sedimentary facies and the context of dolocrete in the Lower Triassic Sherwood Sandstone Group: Corrib field west of Ireland: Sedimentary Geology, v. 187, p. 205–227.

Schneider, J.W., Korner, F., Roscher, M., and Kroner, U., 2006, Permian climate development in the northern peri-Tehys area— Lodeve basin, French Masif Central, compared in a European and Global context: Palaeogeography Palaeoclimatology Palaeoecology, v. 243, p. 92–117.

Scholle, P.A., and Ulmer-Scholle, D.S., 2003, A Color Guide to the Petrography of Carbonate Rocks: Grains, Textures, Porosity, Diagenesis: Tulsa, Oklahoma, American Association of Petroleum Geologists, v. 77, 474 p.

Schumann, R.R., 1989, Morphology of Red Creek, Wyoming, an arid-region anastomosing channel system: Earth Surface Processes and Landforms, v. 14, p. 277–288.

Schumm, S.A., Erskine, W.D., and Tilleard, J.W., 1996, Morphology, hydrology, and evolution of the anastomosing ovens and King Rivers, Victoria, Australia: Geological Society of America Bulletin, v. 108, p. 1212–1224.

Schwab, F.L., 1976, Modern and ancient sedimentary basins: Comparative accumulation rates: Geology, v. 4, p. 723–727.

Scotese, C.R., 1999, PALEOMAP Animations ‘Paleogeography’: Department of Geology, University of Texas.

Shanahan, T.M., Overpeck, J.T., Beck, J.W., Wheeler, C.W., Peck, J.A., King, J.W., and Scholz, C.A., 2008, The formation of biogeochemical laminations in Lake Bosumtwi, Ghana, and their usefulness as indicators of past environmental changes: Journal of Paleolimnology, v. 40, p. 339–355.

Sharma, S., Joachimski, M., Sharma, M., Tobschall, H.J., Singh, I.B., Sharma, C., Chauhan, M.S., and Morgenroth, G., 2004, Late glacial and Holocene environmental changes in Ganga plain, Northern India: Quaternary Science Reviews, v. 23, p. 145–159.

Shields, A., 1936, Application of similarity principles and turbulence research to bedload movement (English translation from German): Hydrodynamics Laboratory, California Institute of Technology, Publication No. 167.

Shirsath, S., Bhattacharyya, T., and Pal, D., 2000, Minimum threshold value of smectite for vertic properties: Soil Research, v. 38, p. 189–202.

Shukla, U.K., Singh, L.B., Srivastava, P., and Singh, D.S., 1999, Paleocurrent patterns in braid-bar and point-bar deposits: Examples from the Ganga River, India: Journal of Sedimentary Research, v. 69, p. 992–1002.

Sibley, D.F., and Gregg, J.M., 1987, Classification of dolomite rock textures: Journal of Sedimentary Research, v. 57, p. 967–975.

Simon, S.S.T, Gibling, M.R., DiMichele, W.A., Chaney, D.S., Looy, C.V., and Tabor, N.J., 2016, An abandoned-channel fill with exquisitely preserved plants in redbeds of the Clear Fork Formation, Texas, USA: an Early Permian water-dependent habitat on the arid plains of Pangea: Journal of Sedimentary Research, v. 86, p. 944-964

Slingerland, R., and Smith, N., 2004, River avulsions and their deposits: Annual Review of Earth and Planetary Sciences, v. 32, p. 257–285.

Smith, G.E., 1974, Depositional systems, San Angelo Formation (Permian), North Texas --facies control of red-bed copper mineralization: Bureau of Economic Geology, University of Texas at Austin.

Smith, R.M.H., 1987, Morphology and depositional history of exhumed Permian point bars in the southwestern Karoo, South Africa: Journal of Sedimentary Petrology, v. 57, p. 19–29.

Smith, R.M.H., 1993, Sedimentology and ichnology of floodplain paleosurfaces in the Beaufort Group (Late Permian), Karoo sequence, South Africa: Palaios, v. 8, p. 339–357.

Smith, D.G., and Putnam, P.E., 1980, Anastomosed river deposits: modern and ancient examples in Alberta, Canada: Canadian Journal of Earth Sciences, v. 17, p. 1396–1406.

Smith, N.D., Morozova, G.S., and Gibling, M.R., 2014, Channel enlargement by avulsion-induced sediment starvation in the Saskatchewan River: Geology, v. 42, p. 355–358.

Smith, D.G., and Smith, N.D., 1980, Sedimentation in anastomosed river systems; examples from alluvial valleys near Banff, Alberta: Journal of Sedimentary Research, v. 50, p. 157–164.

Smoot, J.P., 1991, Sedimentary facies and depositional environments of early Mesozoic Newark Supergroup basins, eastern North America: Palaeogeography Palaeoclimatology Palaeoecology, v. 84, p. 369–423.

Smoot, J.P., and Olsen, P.E., 1988, Massive mudstones in basin analysis and paleoclimatic interpretation of the Newark Supergroup, *in* Manspeizer., W., ed., Triassic-Jurassic rifting, continental breakup and the origin of the Atlantic Ocean and passive margins: New York, Elsevier, p. 249–274.

Soreghan, G.S., Elmore, R.D., Katz, B., Cogoini, M., and Banerjee, S., 1997, Pedogenically enhanced magnetic susceptibility variations preserved in Paleozoic loessite: Geology, v. 25, p. 1003–1006.

Soreghan, G.S., Elmore, R.D., and Lewchuk, M.T., 2002, Sedimentologic-magnetic record of western Pangean climate in upper Paleozoic loessite (lower Cutler beds, Utah): Geological Society of America Bulletin, v. 114, p. 1019–1035.

Soreghan, G.S., Keller, G.R., Gilbert, M.C., Chase, C.G., and Sweet, D.E., 2012, Load-induced subsidence of the Ancestral Rocky Mountains recorded by preservation of Permian landscapes: Geosphere, v. 8, p. 654–668.

Soreghan, G.S., and Soreghan, M.J., 2013, Tracing clastic delivery to the Permian Delaware Basin, USA: implications for paleogeography and circulation in westernmost Equatorial Pangea: Journal of Sedimentary Research, v. 83, p. 786–802.

Soreghan, M.J, Soreghan, G.S, And Hamilton, M., 2002, Paleowinds inferred from detrital-zircon geochronology of upper Paleozoic loessite, western equatorial Pangea: Geology, v. 30, p. 695–698.

Soreghan, G.S., Soreghan, M.J., and Hamilton, M.A., 2008, Origin and significance of loess in late Paleozoic western Pangaea: A record of tropical cold?: Palaeogeography, Palaeoclimatology, Palaeoecology, v. 268, p. 234–259.

Southard, J.B., and Boguchwal, L.A., 1990, Bed configurations in steady unidirectional water flows. Part 2. Synthesis of flume data: Journal of Sedimentary Research, v. 60, p. 658–679.

Southard, R.J., Driese, S., and Nordt, L., 2011, Vertisols, *in* Huang, P.M., Li, Y., and Sumner, M.E., eds., Handbook of Soil Science: CRC Press, Boca Raton, Florida, CRC Press, p. 33–97.

Spicer, R.A., 1977, The pre-dispositional formation of some leaf impressions: Palaeontology, v. 20, p. 907–912.

Spötl, C., and Wright, V.P., 1992, Groundwater dolocretes from the Upper Triassic of the Paris Basin, France -- a case-study of an arid, continental diagenetic facies: Sedimentology, v. 39, p. 1119–1136.

Srivastava, P., Parkash, B., and Pal, D.K., 1998, Clay minerals in soils as evidence of Holocene climatic change, central Indo-Gangetic Plains, north-central India: Quaternary Research, v. 50, p. 230–239.

Stear, W.M., 1985, Comparison of the bedform distribution and dynamics of modern and ancient sandy ephemeral flood deposits in the southwestern Karoo region, South Africa: Sedimentary Geology, v. 45, p. 209–230.

Stewart, D., 1983a, Possible Suspended-Load Channel Deposits from the Wealden Group (Lower Cretaceous) of Southern England, *in* Collinson, J.D., and Lewin, J., eds., Modern and ancient fluvial systems: Oxford, UK., Blackwell Publishing Ltd, p. 369–384.

Stewart, D.J., 1981, A meander-belt sandstone of the Lower Cretaceous of Southern England: Sedimentology, v. 28, p. 1–20.

Stewart, D.J., 1983b, Possible Suspended-Load Channel Deposits from the Wealden Group (Lower Cretaceous) of Southern England, *in* Collinson, J.D., and Lewin, J., eds., Modern and Ancient Fluvial Systems: Oxford, UK, Blackwell Publishing Ltd., p. 369–384.

Stiles, C.A., Mora, C.I., and Driese, S.G., 2001, Pedogenic iron-manganese nodules in Vertisols: A new proxy for paleoprecipitation?: Geology, v. 29, p. 943–946.

Sugden, W., 1963, The hydrology of the Persian Gulf and its significance in respect to evaporite deposition: American Journal of Science, v. 261, p. 741–755.

Tabor, N.J., 2007, Permo-Pennsylvanian palaeotemperatures from Fe-oxide and phyllosilicate δ18O values: Earth and Planetary Science Letters, v. 253, p. 159–171.

Tabor, N.J., 2013, Wastelands of tropical Pangea: high heat in the Permian: Geology, v. 41, p. 623–624.

Tabor, N.J., and Montañez, I.P., 2004, Morphology and distribution of fossil soils in the Permo-Pennsylvanian Wichita and Bowie Groups, north-central Texas, USA: implications for western equatorial Pangean palaeoclimate during icehouse-greenhouse transition: Sedimentology, v. 51, p. 851–884.

Tabor, N.J., and Poulsen, C.J., 2008, Palaeoclimate across the Late Pennsylvanian–Early Permian tropical palaeolatitudes: a review of climate indicators, their distribution, and relation to palaeophysiographic climate factors: Palaeogeography, Palaeoclimatology, Palaeoecology, v. 268, p. 293–310.

Talbot, M.R., Holm, K., and Williams, M.A.J., 1994, Sedimentation in low-gradient desert margin systems: A comparison of the Late Triassic of northwest Somerset (England) and the late Quaternary of east-central Australia: Geological Society of America Special Paper 289, p. 97–117.

Tandon, S.K., and Gibling, M.R., 1994, Calcrete and coal in Late Carboniferous cyclothems of Nova Scotia, Canada; climate and sea-level changes linked: Geology, v. 22, p. 755–758.

Tandon, S.K., Gibling, M.R., Sinha, R., Singh, V., Ghazanfari, P., Dasgupta, A., Jain, M., and Jain, V., 2006, Alluvial valleys of the Ganga Plains, India: Timing and causes of incision, *in* Dalrymple, R.W., Leckie, D.A., and Tillman, R.W., eds., Incised Valleys: Tulsa, SEPM Special, p. 15–35.

Tang, Y., Jenden, P.D., Nigrini, A., and Teerman, S.C., 1996, Modeling early methane generation in coal: Energy and Fuels, v. 10, p. 659–671.

Taylor, G., and Woodyer, K.D., 1978, Bank deposition in suspended-load streams, *in* Miall, A.D., ed., Canadian Society of Petroleum Geologists Memoir, p. 257–275.

Termini, D., and Piraino, M., 2011, Experimental analysis of cross-sectional flow motion in a large amplitude meandering bend: Earth Surface Processes and Landforms, v. 36, p. 244–256.

Thomas, R.G., Smith, D.G., Wood, J.M., Visser, J., Calverleyrange, E.A., and Koster, E.H., 1987, Inclined heterolithic stratification-terminology, description, interpretation and significance: Sedimentary Geology, v. 53, p. 123–179.

Thompson, D. M., 1982, Atoka Group (lower– middle Pennsylvanian), northern Fort Worth basin, Texas: Terrigenous depositional systems, diagenesis, and reservoir distribution and quality: Texas Bureau of Economic Geology, Report of Investigations 125, 62 p.

Tissot, B.P., and Welte, D.H., 1984, Petroleum Formation and Occurrence, 2nd Edition: Berlin, Springer-Verlag, 699 p.

Toonen, W.H.J., Kleinhans, M.G., and Cohen, K.M., 2012, Sedimentary architecture of abandoned channel fills: Earth surface Processes and Landforms, v. 37, 459–472.

Tooth, S., 2000, Process, form and change in dryland rivers: a review of recent research: Earth-Science Reviews, v. 51, 67–107.

Tooth, S., and Nanson, G.C., 2000, Equilibrium and nonequilibrium conditions in dryland rivers: Physical Geography, v. 21, p. 183–211.

Trewin, N.H., 1986, Palaeoecology and sedimentology of the Achanarras fish bed of the Middle Old Red Sandstone, Scotland: Transactions of the Royal Society of Edinburgh, Earth Sciences, v. 77, p. 21–46.

Tucker, M.E., 2003, Sedimentary rocks in the field, John Wiley & Sons, 153 p.

Tucker, M.E., and Wright, V.P., 1990, Carbonate sedimentology: London, Blackwell Science, 482 p.

Tunbridge, I.P., 1984, Facies model for a sandy ephemeral stream and clay playa complex the Middle Devonian Trentishoe Formation of North Devon, U.K: Sedimentology, v. 31, p. 697–715.

Tweed, S., Leblanc, M., Cartwright, I., Favreau, G., and Leduc, C., 2011, Arid zone groundwater recharge and salinisation processes; an example from the Lake Eyre Basin, Australia: Journal of Hydrology, v. 408, p. 257–275.

Van Der Meulen, S., 1982, The sedimentary facies and setting of Eocene point bar deposits, Monltobat Formation, Southern Pyrenees, Spain: Geologie en Mijnbouw, v. 6, p. 217–227.

van Gelder, A., Vandenberg, J.H., Cheng, G., and Xue, C.T., 1994, Overbank and channelfill deposits of the modern Yellow-River Delta: Sedimentary Geology, v. 90, p. 293–305.

Van Siclen, D., 1958, Depositional topography – Examples and theory: AAPG Bulletin, v. 42, p. 1897-1913.

Vasconcelos, C., and McKenzie, J.A., 1997, Microbial mediation of modern dolomite precipitation and diagenesis under anoxic conditions (Lagoa Vermelha, Rio de Janeiro, Brazil): Journal of Sedimentary Research, v. 67, p. 378–390.

Vermont Agency of Natural Resources, 2004. Appendix O -- Particle entrainment and transport *in* Vermont Agency of Natural Resources., Vermont Stream Geomorphic Assessment Phase 3 Handbook, p. O1–O5.

Verschuren, D., 1999, Sedimentation controls on the preservation and time resolution of climate-proxy records from shallow fluctuating lakes: Quaternary Science Reviews, v. 18, p. 821–837.

Viele, G.W., and Thomas, W.A., 1989, Tectonic synthesis of the Ouachita orogenic belt, *in* Hatcher Jr., R.D., Thomas, W.A., and Viele, G.W., eds., The Appalachian–Ouachita Orogen in the United States: Boulder, Colorado, Geological Society of America, p. 695–728.

Visser, J., 1986, Sedimentology and taphonomy of a Styracosaurus bonebed in the Late Cretaceous Judith River formation, Dinosaur Provincial Park, Alberta: University of Calgary, Alberta

Wadell, H., 1932, Volume, shape, and roundness of rock particles: Journal of Geology, v. 40, p. 443–451.

Wakelin-King, G.A., and Webb, J.A., 2007, Threshold-dominated fluvial styles in an arid-zone mud-aggregate river: The uplands of Fowlers Creek, Australia: Geomorphology, v. 85, p. 114–127.

Walper, J. L., 1977, Paleozoic tectonics of the southern margin of North America: Gulf Coast Association of Geological Societies Transactions, v. 27, p. 230–239.

Walper, J.L., 1982, Plate tectonic evolution of the Fort Worth Basin, *in* Martin, C.A., ed., Petroleum Geology of the Fort Worth Basin and Bend Arch Area, Dallas Geological Society, p. 237–251.

Wan, M., and Wang, J., 2015, *Nanshanopteris nervosa* gen. et sp. nov., a glenopterid foliage from the Changhsingian Sunan Formation in Yumen, western China: Review of Palaeobotany and Palynology, v. 219, p. 39–51.

Wardlaw, B., 2005, Age assignment of the Pennsylvanian-Early Permian succession of north central Texas: Permophiles, v. 46, p. 21–22.

Warwick, P., and Stanton, R., 1988, Depositional models for two Tertiary coal-bearing sequences in the Powder River Basin, Wyoming, USA: Journal of the Geological Society, v. 145, p. 613–620.

Weissmann, G.S., Hartley, A.J., Scuderi, L.A., Nichols, G.J., Davidson, S.K., Owen, A., Atchley, S.C., Bhattacharyya, P., Chakraborty, T., Ghosh, P., and Nordt, L.C., 2013, Prograding distributive fluvial systems — geomorphic models and ancient examples, *in* Driese, S.G., and Nordt, L.C., eds., New Frontiers in Paleopedology and Terrestrial Paleoclimatology: SEPM (Society for Sedimentary Geology) Special Publication, v. 104, p. 131–147.

Weissmann, G.S., Hartley, A.J., Scuderi, L.A., Nichols, G.J., Owen, A., Wright, S., Felicia, A.L., Holland, F., and Anaya, F.M.L., 2015, Fluvial geomorphic elements in modern sedimentary basins and their potential preservation in the rock record: A review: Geomorphology, v. 250, p. 187-219.

Wellstead, C.F., 1991, Taxonomic revision of the Lysorophia, Permo-Carboniferous lepospondyl amphibians: Bulletin of the American Museum of Natural History, v. 209, p. 1–90.

West, R.R., Archer, A.W., and Miller, K.B., 1993, Role of climate in stratigraphic patterns exhibited by late Palaeozoic rocks exposed in Kansas: Palaeogeography, Palaeoclimatology, Palaeoecology, v. 128, p. 1–16.

White, D., 1929, Flora of the Hermit Shale, Grand Canyon, Arizona: Carnegie Institution of Washington Publication, v. 405, p. 1–221.

Williams, G.E., 1971, Flood deposits of the sand-bed ephemeral streams of central Australia: Sedimentology, v. 17, p. 1–40.

Williams, G.P., 1986, River meanders and channel size: Journal of Hydrology, v. 88, p. 147–164.

Willis, B.J., 1989, Palaeochannel reconstructions from point bar deposits: a three-dimensional perspective: Sedimentology, v. 36, p. 757–766.

Williston, S., 1910, New Permian reptiles: Rhachitomous vertebrae: The Journal of Geology, v. 18, p. 585–600.

Williston, S.W., 1911, American Permian vertebrates: Chicago, University of Chicago Press.

Wilson, M.V., 1977, Paleoecology of Eocene lacustrine varves at Horsefly, British Columbia: Canadian Journal of Earth Sciences, v. 14, p. 953–962.

Wilson, J.H., McLennan, S.M., Glotch, T.D., Rasbury, E.T., Gierlowski-Kordesch, E.H., and Tappero, R.V., 2012, Pedogenic hematitic concretions from the Triassic New Haven Arkose, Connecticut: Implications for understanding Martian diagenetic processes: Chemical Geology, v. 312, p. 195–208.

Wolela, A.M., and Gierlowski-Kordesch, E.H., 2007, Diagenetic history of fluvial and lacustrine sandstones of the Hartford Basin (Triassic-Jurassic), Newark Supergroup, USA: Sedimentary Geology, v. 197, p. 99–126.

Woodyer, K.D., Taylor, G., and Crook, K.A.W., 1979, Depositional processes along a very low-gradient, suspended-load stream: the Barwon River, New South Wales: Sedimentary Geology, v. 22, p. 97–120.

Worden, R.H., and Burley, S.D., 2003, Sandstone Diagenesis: The Evolution of Sand to Stone, *in* Burley, S.D., and Worden, R.H., eds., Sandstone Diagenesis: Recent and Ancient: Oxford, UK Blackwell Publishing Ltd., p. 1–44.

Wren, D. G., Davidson, G. R., Walker, W. G., and Galicki, S. J., 2008, The evolution of an oxbow lake in the Mississippi alluvial floodplain: Journal of Soil and Water Conservation, v. 63, p. 129–135.

Wright, V., Vanstone, S., and Robinson, D., 1991, Ferrolysis in Arundian alluvial palaeosols: evidence of a shift in the early Carboniferous monsoonal system: Journal of the Geological Society, v. 148, p. 9–12.

Wright, I.J., Reich, P.B., Westoby, M., Ackerly, D.D., Baruch, Z., Bongers, F., Cavender-Bares, J., Chapin, T., Cornelissen, J.H.C., Diemer, M., Flexas, J., Garnier. E., Groom, P.K., Gulias, J., Hikosaka, K., Lamont, B.B., Lee, T., Lee, W., Lusk, C., Midgley, J.J., Navas, M.-L., Niinemets, Ü., Oleksyn, J., Osada, N., Poorter, H., Poot, P., Prior, L., Pyankov, V.I., Roumet, C., Thomas, S.C., Tjoelker, M.G., Veneklaas, E.J., and Villar, R., 2004, The worldwide leaf economics spectrum: Nature, v. 428, p. 821–827.

Wright, D.T., and Wacey, D., 2005, Precipitation of dolomite using sulphate-reducing bacteria from the Coorong Region, South Australia: significance and implications: Sedimentology, v. 52, p. 987–1008.

Wright, V.P., and Marriott, S.B., 2007, The dangers of taking mud for granted: Lessons from Lower Old Red Sandstone dryland river systems of South Wales: Sedimentary Geology, v. 195, p. 91–100.

Yang, Y., Li, W., and Long, M., 2005, Tectonic and stratigraphic controls on hydrocarbon systems in the Ordos Basin; a multicycle cratonic basin in central China: American Association of Petroleum Geologists, v. 89, p. 255–269.

Ye, Q.C., and Mazzullo, S.J., 1993, Dolomitization of lower Permian platform facies, Wichita Formation, north platform, Midland basin, Texas: Carbonates and Evaporites, v. 8, p. 55–70.

Zaleha, M.J., 1997a, Fluvial and lacustrine palaeoenvironments of the Miocene Siwalik Group, Khaur area, northern Pakistan: Sedimentology, v. 44, p. 349–368.

Zaleha, M.J., 1997b, Intra-and extrabasinal controls on fluvial deposition in the Miocene Indo-Gangetic foreland basin, northern Pakistan: Sedimentology, v. 44, p. 369–390.

Zambito, J.J., and Benison, K.C., 2013, Extremely high temperatures and paleoclimate trends recorded in Permian ephemeral lake halite: Geology, v. 41, p. 587–590.

Zhang, Z., Gong, D., He, X., Guo, D., and Feng, S., 2009, Reconstruction of the western Pacific warm pool SST since 1644 AD and its relation to precipitation over East China: Science in China Series D-Earth Sciences, v. 52, p. 1436–1446.

Zhao, C., 1984, Thermal alteration of spores and pollen and maturity of organic matter of the Cretaceous System, Songliao basin, northeast China: Geochemistry, v. 3, p. 84–92.

Zhu, L., 2015, Paleosol morphologies and estimations of paleoatmospheric pCO2, North-central Texas. Unpublished MSc thesis, Southern Methodist University, Dallas, Texas.

Ziegler, A.M., Eshel, G., Rees, P.McA., Rothfus, T.A., Rowley, D.B., and Sunderlin, D., 2003, Tracing the tropics across land and sea: Permian to present: Lethaia v. 36, p. 227–254.

Ziegler, A.M., Hulver, M.L., and Rowley, D.B., 1997, Permian world topography and climate, Late glacial and postglacial environmental changes: Pleistocene, Carboniferous-Permian and Proterozoic: Oxford Oxford University Press, p. 111–146.

APPENDIX A: COPYRIGHT PERMISSION LETTERS

August 5, 2016

Journal of Sedimentary Research
3300 Penrose Place
Boulder, CO 80301

I am preparing my Ph.D. thesis for submission to the Faculty of Graduate Studies at Dalhousie University, Halifax, Nova Scotia, Canada. I am seeking your permission to include a manuscript version of the following paper(s) as a chapter in the thesis:

Simon, S., Gibling, M.R., DiMichele, W.A., Chaney, D.S., Looy, C.V., and Tabor, N.J., 2016, An abandoned-channel fill with exquisitely preserved plants in redbeds of the Clear Fork Formation, Texas, USA: an Early Permian water-dependent habitat on the arid plains of Pangea: Journal of Sedimentary Research, v. 86, p. 1-21.

Canadian graduate theses are reproduced by the Library and Archives of Canada (formerly National Library of Canada) through a non-exclusive, world-wide license to reproduce, loan, distribute, or sell theses. I am also seeking your permission for the material described above to be reproduced and distributed by the LAC(NLC). Further details about the LAC(NLC) thesis program are available on the LAC(NLC) website (www.nlc-bnc.ca).

Full publication details and a copy of this permission letter will be included in the thesis.

Yours sincerely,
Sharane Simon

Permission is granted for:

a) the inclusion of the material described above in your thesis.

b) for the material described above to be included in the copy of your thesis that is sent to the Library and Archives of Canada (formerly National Library of Canada) for reproduction and distribution.

Name: Melissa Lester Title: Managing Editor, JSR

Signature: _____ Date: 6 August 2016

5th September 2016

Sedimentology
9600 Garsington Road,
Oxford, OX4 2DQ

I am preparing my Ph.D. thesis for submission to the Faculty of Graduate Studies at Dalhousie University, Halifax, Nova Scotia, Canada. I am seeking your permission to include a manuscript version of the following paper(s) as a chapter in the thesis:

Simon, S., and Gibling, M.R., in press, Fine-grained meandering systems of the Lower Permian Clear Fork Formation of north-central Texas, USA: lateral and oblique accretion on an arid plain: Sedimentology.

Canadian graduate theses are reproduced by the Library and Archives of Canada (formerly National Library of Canada) through a non-exclusive, world-wide license to reproduce, loan, distribute, or sell theses. I am also seeking your permission for the material described above to be reproduced and distributed by the LAC(NLC). Further details about the LAC(NLC) thesis program are available on the LAC(NLC) website (www.nlc-bnc.ca).

Full publication details and a copy of this permission letter will be included in the thesis.

Yours sincerely,
Sharane Simon

Permission is granted for:

a) the inclusion of the material described above in your thesis.

b) for the material described above to be included in the copy of your thesis that is sent to the Library and Archives of Canada (formerly National Library of Canada) for reproduction and distribution.

Name: SHEIK SABAR Title: Farm Hand

Signature: _____ Date: 10/14/16

18th October 2016

Journal of Sedimentary Research

3300 Penrose Place

Boulder, CO 80301

I am preparing my Ph.D. thesis for submission to the Faculty of Graduate Studies at Dalhousie University, Halifax, Nova Scotia, Canada. I am seeking your permission to include a manuscript version of the following paper(s) as a chapter in the thesis:

Simon, S., and Gibling, M.R., in press, Pedogenic Mud Aggregates Preserved In A Fine-Grained Meandering Channel in the Lower Permian Clear Fork Formation, North-Central Texas, USA: Journal of Sedimentary Research.

Canadian graduate theses are reproduced by the Library and Archives of Canada (formerly National Library of Canada) through a non-exclusive, world-wide license to reproduce, loan, distribute, or sell theses. I am also seeking your permission for the material described above to be reproduced and distributed by the LAC(NLC). Further details about the LAC(NLC) thesis program are available on the LAC(NLC) website (www.nlc-bnc.ca).

Full publication details and a copy of this permission letter will be included in the thesis.

Yours sincerely,

Sharane Simon

Permission is granted for:

a) the inclusion of the material described above in your thesis.

b) for the material described above to be included in the copy of your thesis that is sent to the Library and Archives of Canada (formerly National Library of Canada) for reproduction and distribution.

Name: Melissa Lester Title: Managing Editor

Signature: Date: 19 October 2016

APPENDIX B: SUPPLEMENTAL DATA

- Sample preparation for EDS and XRD analysis

A total of 77 unpolished and 17 polished thin sections were made from rock samples (Table 1-2). Despite care in preparation, some weakly consolidated samples partially disintegrated. Sections were studied under plane-polarised light using a Nikon Eclipse E400 Pol petrographic microscope with a Pixe-Link digital camera and PETROG automated stepping stage. Semi-quantitative geochemical data were collected using a TESCAN MIRA 3 LMU Variable Pressure Schottky Field Emission Scanning Electron Microscope (EDS and QBSD detectors) and INCA X-max 80 mm2 EDS system, with a 10 μm spot size and average error margin of 10%. Carbonate crystal size is from Folk (1974). The chemical composition of the carbonates in the form of clasts and cements were also determined based on the CaO, MgO, MnO and FeO contents.

X-ray diffraction (XRD) analysis was conducted on 83 random powder mounts. Finely crushed samples were analysed using a Siemens Kristaloflex diffractometer with Co Kα radiation. Randomly oriented slides were scanned from 2-77^{o} 2θ, with a 0.02^{o} step increment (2 sec counts/step). A total of 24 samples was selected for <2 μm fraction analysis. Approximately 20 g of crushed sample was suspended in a weak solution of sodium hexametaphosphate. After 16 hours, the <2 μm fraction was isolated, flocculated with 4 ml of $MgCl_2$ solution and centrifuged. The clay fraction was re-suspended in a 500 ml cylinder, and a 20 ml aliquot was withdrawn, dried and weighed to determine the appropriate weight (5%) for the internal standard, zincite. After the zincite was dissolved, the sample was centrifuged and smeared on a normal glass slide and a second heat-resistant glass. Using the scan properties described above, XRD analysis was carried out using the normal glass slides. The slides were then placed in a

desiccator containing vapours of ethylene glycol for ~4 hours to investigate peak shifts, after which they were analysed immediately to prevent glycol evaporation, using a 2^{o}-17^{o} 2θ range with a 0.2^{o} step interval. The heat-resistant slides were placed in a preheated furnace at 150°C for at least 30 minutes, and were analysed using a 2^{o}-30^{o} 2θ range with a 0.2^{o} step interval. This process was repeated for 300°C, 500°C, and 650°C to investigate peak shifts. At >500°C, most clay smears started to flake or bubble, precluding XRD analysis. Minerals were identified using tables in Moore and Reynolds (1997) and the JCPDS (Joint Committee on Powder Diffraction Standards) Powder Diffraction File system. No attempt was made to determine the semi-quantitative proportions of clay minerals or the components of mixed-layer clays.

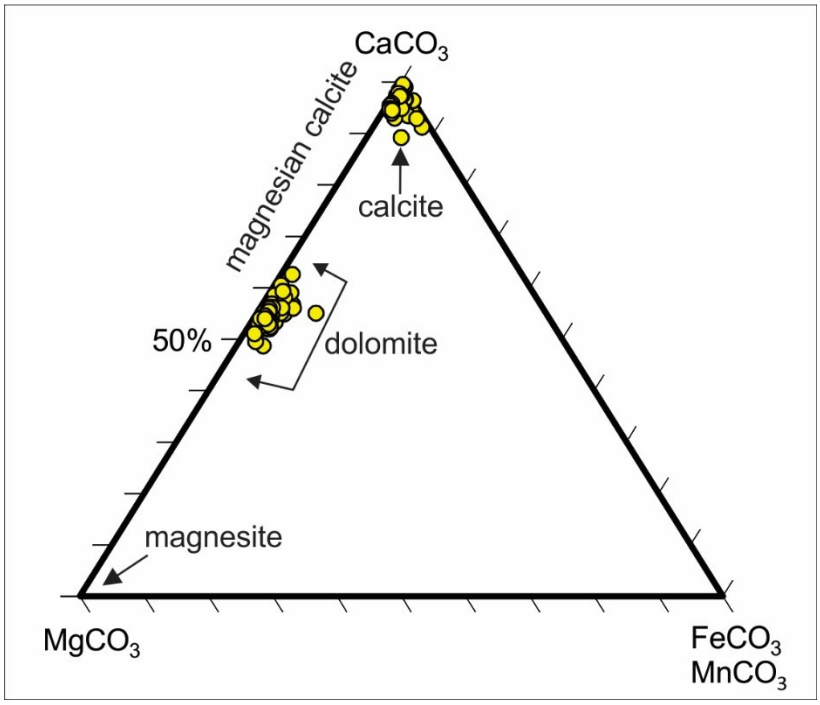

Figure 9-1 Ternary plot of $CaCO_3$-$MgCO_3$-$(Mn+Fe)CO_3$ for (200) points listed in Table 9-1. Structural formulae were calculated based on EDS data.

Table 9-1 Chemical composition of carbonates identified using SEM/EDS analysis. The mean error of each point ranges from ±0.5 wt%. Ankerite was only identified using X-ray diffraction analysis and not SEM/EDS analysis.

Sample	Site	Position	Mineral	Element	$CaCO_3$	$MgCO_3$	$FeCO_3$ & $MnCO_3$
RT 1	1	2	Calcite	LA-1	94.33	1.17	4.49
RT_1	2	3	Calcite	LA-1	96.32	0.00	3.68
RT_1	3	5	Calcite	LA-1	96.05	1.54	2.42
RT_1	3	7	Dolomite	LA-1	52.45	45.32	2.23
RT_1	4	2	Dolomite	LA-1	57.21	41.17	1.62
RT_1	4	8	Calcite	LA-1	97.58	2.42	0.00
RT_1	5	6	Calcite	LA-1	96.59	1.03	2.38
RT_1	6	12	Calcite	LA-1	97.00	1.03	1.97
RT_1	9	1	Calcite	LA-1	97.25	1.58	1.18
RT_1	10	3	Calcite	LA-1	98.91	1.09	0.00
RT_1	11	5	Calcite	LA-1	97.34	1.27	1.40
RT_1	12	1	Calcite	LA-1	97.26	2.09	0.66
RT_1	12	7	Dolomite	LA-1	56.67	38.53	4.79
RT_1	13	2	calcite	LA-1	91.18	1.15	7.67
RT_1	13	3	Calcite	LA-1	93.39	2.24	4.37
RT_1	13	10	Dolomite	LA-1	59.00	38.79	2.21
RT_1	14	4	Calcite	LA-1	96.61	1.13	2.26
RT_1	14	5	Dolomite	LA-1	54.89	40.74	4.38
RT_1	14	7	Dolomite	LA-1	57.94	39.33	2.73
RT_1	14	8	Dolomite	LA-1	58.19	39.46	2.35
RT_1	15	5	Calcite	LA-1	98.92	0.00	1.08
RT_1	16	3	Calcite	LA-1	92.84	1.17	6.00
RT_1	17	3	Calcite	LA-1	92.76	7.24	0.00
RT_1	17	4	Calcite	LA-1	97.09	1.65	1.26
RT_1	17	5	Dolomite	LA-1	57.35	40.20	2.45
RT_1	17	6	Calcite	LA-1	98.84	1.16	0.00
RT_1	17	7	Dolomite	LA-1	58.38	38.87	2.75

Sample	Site	Position	Mineral	Element	$CaCO_3$	$MgCO_3$	$FeCO_3$ & $MnCO_3$
RT_1	17	8	Calcite	LA-1	95.71	3.33	0.96
RT_1	17	9	Dolomite	LA-1	56.01	38.80	5.20
RT_1	17	10	Calcite	LA-1	97.65	2.35	0.00
RT_1	17	12	Dolomite	LA-1	57.88	39.43	2.69
RT_1	17	14	Dolomite	LA-1	58.98	37.68	3.35
RT_3	6	2	Calcite	LA-1	97.21	1.45	1.34
RT_3	7	2	Calcite	LA-1	97.26	1.59	1.15
RT_3	16	1	Calcite	LA-1	97.03	1.56	1.41
BC_4	11	4	Calcite	LA-3	97.73	1.13	1.14
BC_4	7	1	Calcite	LA-3	98.37	1.09	0.54
BC_4	5	1	Calcite	LA-3	97.50	1.03	1.48
BC_4	10	2	Calcite	LA-3	97.63	1.01	1.36
BC_4	5	2	Calcite	LA-3	99.16	0.84	0.00
BC_4	2	8	Calcite	LA-3	99.30	0.00	0.70
BC_4	6	3	Calcite	LA-3	98.91	0.00	1.09
BC_4	7	2	Calcite	LA-3	99.05	0.00	0.95
BC_6	1	1	Calcite	CB	94.03	4.02	1.95
BC_6	1	3	Calcite	CB	97.24	1.41	1.34
BC_6	1	5	Calcite	CB	96.25	1.99	1.76
BC_6	2	4	Calcite	CB	92.91	4.57	2.53
BC_6	2	5	Calcite	CB	97.98	1.08	0.94
BC_6	3	7	Calcite	CB	99.45	0.00	0.55
BC_6	4	4	Calcite	CB	94.80	3.44	1.76
BC_6	5	5	Calcite	CB	96.68	2.29	1.03
BC_6	5	6	Calcite	CB	96.50	1.21	2.29
BC_6	5	11	Calcite	CB	97.37	1.97	0.65
BC_6	6	5	Calcite	CB	96.39	2.52	1.10
BC_6	7	4	Calcite	CB	97.53	2.47	0.00

Sample	Site	Position	Mineral	Element	$CaCO_3$	$MgCO_3$	$FeCO_3$ & $MnCO_3$
BC_6	8	1	Dolomite	CB	60.41	38.46	1.13
BC_6	8	2	Dolomite	CB	60.45	39.55	0.00
BC_6	8	7	Dolomite	CB	58.06	40.22	1.72
BC_6	9	12	Calcite	CB	95.29	2.61	2.10
BC_6	10	2	Calcite	CB	97.23	1.27	1.50
BC_6	10	3	Calcite	CB	89.12	5.46	5.42
BC_6	10	4	Calcite	CB	97.34	1.46	1.20
BC_6	10	8	Dolomite	CB	58.51	40.45	1.03
BC_6	11	3	Dolomite	CB	58.09	39.09	2.82
BC_6	11	4	Calcite	CB	97.59	1.36	1.05
BC_6	11	8	Calcite	CB	97.70	1.59	0.71
BC_6	12	2	Calcite	CB	94.78	2.57	2.65
BC_6	13	10	Calcite	CB	97.16	1.58	1.27
NSCQ_10	1	2	Dolomite	CB	53.52	45.16	1.32
NSCQ_10	1	6	Dolomite	CB	55.68	41.89	2.43
NSCQ_10	2	4	Dolomite	CB	55.82	42.80	1.39
NSCQ_10	2	5	Dolomite	CB	54.01	44.24	1.74
NSCQ_10	2	6	Dolomite	CB	55.63	43.18	1.19
NSCQ_10	3	2	Dolomite	CB	55.40	43.34	1.26
NSCQ_10	3	8	Dolomite	CB	53.97	43.87	2.16
NSCQ_10	4	9	Dolomite	CB	53.70	44.71	1.59
NSCQ_10	5	7	Dolomite	CB	54.64	43.83	1.53
NSCQ_10	5	13	Dolomite	CB	55.55	43.12	1.33
NSCQ_10	6	1	Dolomite	CB	53.70	44.50	1.80
NSCQ_10	6	5	Dolomite	CB	53.42	44.84	1.74
NSCQ_10	6	8	Dolomite	CB	54.56	43.55	1.90
NSCQ_10	6	9	Dolomite	CB	53.52	45.07	1.41
NSCQ_10	8	3	Dolomite	CB	56.26	42.54	1.20

Sample	Site	Position	Mineral	Element	$CaCO_3$	$MgCO_3$	$FeCO_3$ & $MnCO_3$
NSCQ_10	8	8	Dolomite	CB	53.45	44.93	1.62
NSCQ_10	8	11	Dolomite	CB	56.79	41.71	1.50
NSCQ_10	9	1	Dolomite	CB	54.09	44.07	1.84
NSCQ_10	11	3	Dolomite	CB	48.65	47.13	4.22
NSCQ_10	11	6	Dolomite	CB	55.02	42.59	2.39
NSCQ_10	11	9	Dolomite	CB	53.49	44.44	2.07
NSCQ_10	12	6	Dolomite	CB	54.33	43.72	1.95
NSCQ_10	12	7	Dolomite	CB	55.04	43.89	1.07
MB_14	1	10	Dolomite	CB	53.41	44.73	1.87
MB_14	2	1	Dolomite	CB	52.94	44.63	2.44
MB_14	2	3	Dolomite	CB	55.11	43.78	1.11
MB_14	3	1	Dolomite	CB	53.16	43.03	3.82
MB_14	3	9	Dolomite	CB	54.98	35.75	9.27
MB_14	4	3	Dolomite	CB	54.11	44.27	1.62
MB_14	4	5	Dolomite	CB	53.88	44.78	1.34
MB_14	5	5	Dolomite	CB	53.40	44.25	2.34
MB_14	5	8	Dolomite	CB	53.95	43.80	2.25
MB_14	6	1	Dolomite	CB	53.21	44.17	2.62
MB_14	6	8	Dolomite	CB	54.04	44.19	1.76
MB_14	8	9	Dolomite	CB	53.52	44.63	1.85
MB_14	8	11	Dolomite	CB	53.83	44.52	1.65
MB_14	9	5	Dolomite	CB	54.59	43.57	1.84
MB_14	9	7	Dolomite	CB	56.08	41.56	2.37
MB_14	10	7	Dolomite	CB	54.44	43.86	1.70
MB_14	10	8	Dolomite	CB	53.75	43.71	2.54
MB_14	11	2	Dolomite	CB	54.38	43.70	1.92
MB_14	11	3	Dolomite	CB	54.46	43.45	2.09
MB_14	11	7	Dolomite	CB	53.74	44.62	1.63

Sample	Site	Position	Mineral	Element	$CaCO_3$	$MgCO_3$	$FeCO_3$ & $MnCO_3$
MB_14	13	6	Dolomite	CB	54.21	43.69	2.10
MB_14	13	7	Dolomite	CB	55.27	42.85	1.89
KWTP_15	1	1	Dolomite	CB	55.59	42.26	2.16
KWTP_15	1	2	Dolomite	CB	55.28	40.99	3.73
KWTP_15	1	5	Dolomite	CB	59.26	38.75	1.99
KWTP_15	3	3	Dolomite	CB	54.68	43.33	2.00
KWTP_15	3	5	Dolomite	CB	53.47	44.56	1.97
KWTP_15	3	6	Dolomite	CB	54.58	43.31	2.12
KWTP_15	5	5	Dolomite	CB	54.00	43.31	2.69
KWTP_15	5	7	Dolomite	CB	53.23	44.41	2.36
KWTP_15	6	5	Dolomite	CB	53.69	44.37	1.94
KWTP_15	7	3	Dolomite	CB	54.92	42.93	2.15
KWTP_15	8	2	Dolomite	CB	54.85	42.90	2.25
KWTP_15	8	5	Dolomite	CB	53.42	44.37	2.20
KWTP_15	9	1	Dolomite	CB	54.71	42.64	2.65
KWTP_15	9	5	Dolomite	CB	52.11	45.36	2.53
KWTP_15	11	5	Dolomite	CB	53.73	44.30	1.98
MR1_15	1	2	Dolomite	CB	51.97	45.72	2.31
MR1_15	1	4	Dolomite	CB	54.00	43.77	2.23
MR1_15	1	5	Dolomite	CB	49.47	47.92	2.61
MR1_15	1	6	Dolomite	CB	52.43	44.84	2.73
MR1_15	2	1	Dolomite	CB	52.02	44.40	3.58
MR1_15	2	2	Dolomite	CB	54.04	43.81	2.16
MR1_15	2	3	Dolomite	CB	52.79	44.80	2.41
MR1_15	2	5	Dolomite	CB	54.97	41.22	3.80
MR1_15	2	6	Dolomite	CB	51.99	44.75	3.26
MR1_15	3	9	Dolomite	CB	53.81	43.94	2.25
MR1_15	4	3	Dolomite	CB	54.78	43.61	1.61

Sample	Site	Position	Mineral	Element	$CaCO_3$	$MgCO_3$	$FeCO_3$ & $MnCO_3$
MR1_15	4	4	Dolomite	CB	53.38	43.89	2.73
MR1_15	5	1	Calcite	CB	95.74	3.61	0.65
MR1_15	5	2	Dolomite	CB	55.14	43.23	1.63
MR1_15	5	4	Dolomite	CB	53.49	45.14	1.37
MR1_15	5	5	Dolomite	CB	53.00	44.54	2.46
MR1_15	6	5	Dolomite	CB	56.14	42.36	1.51
MR1_15	7	8	Dolomite	CB	53.80	43.67	2.53
MR1_15	8	6	Dolomite	CB	53.65	44.92	1.43
MR1_15	9	6	Dolomite	CB	56.07	40.52	3.41
MR1_15	9	7	Dolomite	CB	54.05	43.70	2.25
MR1_15	10	1	Dolomite	CB	54.17	44.28	1.55
MR1_15	10	2	Calcite	CB	96.63	3.37	0.00
MR1_15	10	3	Calcite	CB	95.32	3.96	0.71
MR1_15	10	4	Dolomite	CB	54.85	43.45	1.70
MR1_15	10	5	Calcite	CB	93.86	4.53	1.61
MR1_15	10	6	Calcite	CB	96.62	3.38	0.00
MR1_15	11	4	Dolomite	CB	53.48	44.27	2.25
MR1_15	11	5	Dolomite	CB	53.34	44.01	2.66
MR1_15	12	4	Calcite	CB	95.37	4.04	0.58
MR1_15	12	6	Dolomite	CB	53.96	43.21	2.83
MR1_15	13	3	Dolomite	CB	62.51	35.68	1.80
MR1_15	13	6	Dolomite	CB	53.32	43.96	2.72
MR1_15	14	1	Dolomite	CB	54.45	44.02	1.53
MR1_15	14	3	Calcite	CB	94.77	4.36	0.87
MR1_15	14	4	Calcite	CB	94.62	4.47	0.91
MR1_15	15	1	Calcite	CB	96.89	3.11	0.00
MR1_15	15	2	Calcite	CB	97.17	2.83	0.00
MR1_15	15	4	Calcite	CB	97.18	2.82	0.00

Sample	Site	Position	Mineral	Element	$CaCO_3$	$MgCO_3$	$FeCO_3$ & $MnCO_3$
MR1_15	16	2	Calcite	CB	94.43	4.16	1.41
MR1_15	16	4	Dolomite	CB	54.51	43.97	1.52
MR1_15	16	6	Dolomite	CB	54.76	42.76	2.48
MR1_15	16	7	Dolomite	CB	56.02	43.98	0.00
MR1_ 17	1	5	Dolomite	LA-3	52.60	45.01	2.39
MR1_ 17	1	6	Dolomite	LA-3	53.46	45.07	1.47
MR1_ 17	1	8	Dolomite	LA-3	54.01	43.57	2.42
MR1_ 17	2	4	Dolomite	LA-3	52.36	44.15	3.50
MR1_ 17	3	6	Dolomite	LA-3	52.58	45.49	1.93
MR1_ 17	3	9	Dolomite	LA-3	56.12	42.31	1.57
MR1_ 17	3	10	Calcite	LA-3	98.26	1.74	0.00
MR1_ 17	4	1	Dolomite	LA-3	53.66	44.54	1.80
MR1_ 17	5	2	Dolomite	LA-3	56.08	42.32	1.60
MR1_ 17	5	5	Dolomite	LA-3	56.10	41.96	1.94
MR1_ 17	6	1	Dolomite	LA-3	53.60	44.60	1.80
MR1_ 17	6	2	Dolomite	LA-3	54.50	43.85	1.65
MR1_ 17	7	7	Dolomite	LA-3	55.46	44.54	0.00
MR1_ 17	7	10	Dolomite	LA-3	53.65	44.82	1.53
MR1_ 17	7	11	Dolomite	LA-3	55.91	42.59	1.50
MR1_ 17	8	3	Dolomite	LA-3	53.93	44.59	1.47
MR1_ 17	8	5	Dolomite	LA-3	53.76	44.60	1.64
MR1_ 17	9	3	Dolomite	LA-3	54.70	43.16	2.15
MR1_ 17	9	8	Dolomite	LA-3	55.35	42.92	1.73
MR1_ 17	11	8	Dolomite	LA-3	54.01	43.83	2.15
MR1_ 17	11	9	Dolomite	LA-3	53.56	44.35	2.09
MR1_ 17	11	10	Dolomite	LA-3	54.52	43.92	1.56
MR3_4	15	3	Dolomite	LA-3	53.23	45.68	1.08
MR3_4	1	3	Dolomite	LA-3	53.87	44.33	1.80

Sample	Site	Position	Mineral	Element	$CaCO_3$	$MgCO_3$	$FeCO_3$ & $MnCO_3$
MR3_4	2	5	Dolomite	LA-3	53.06	45.68	1.26
MR3_4	6	7	Dolomite	LA-3	51.01	47.29	1.70
MR3_4	14	8	Dolomite	LA-3	52.81	44.21	2.97
MR3_4	15	6	Dolomite	LA-3	53.97	44.92	1.10
MR3_4	15	7	Dolomite	LA-3	53.96	44.20	1.83

APPENDIX C: PETROGRAPHIC DESCRIPTIONS

Channel-base Deposits (CD): Based on XRD, carbonate is present in all samples, and is predominantly calcite and ankerite in the lower unit and dolomite in the middle and upper units, regardless of texture. The composition of detrital grains and clay matrix is similar in all samples. Four distinctive carbonate occurrences were identified in individual samples or parts of samples (Fig. 2-2B, C; 10-1A, B). Calcite-rich clasts up to 10 mm long comprise finely crystalline calcite, radiaxial calcite cement, and sparry vugs. They are embedded in a matrix of detrital grains, mud clasts, and clay (illite, Fe-rich chlorite, kaolinite and mixed-layer clay), with isolated dolomite rhombs and sparry and poikilotopic calcite (Fig. 2-2B), and comprise ~70% of some samples. Dolomitic, siliciclastic and ferruginous clasts in a hematite and clay matrix (Fig. 10-1A) are the most abundant form, especially within the upper unit. Patches of coarsely crystalline, interlocked dolomite rhombs are common in the middle unit, with minor detrital grains, clay, and gypsum and barite cements (Fig. 2-2C). Finally, grains with rims of hematite and clay contain interstitial patches of poikilotopic dolomite cement (Fig. 10-1B).

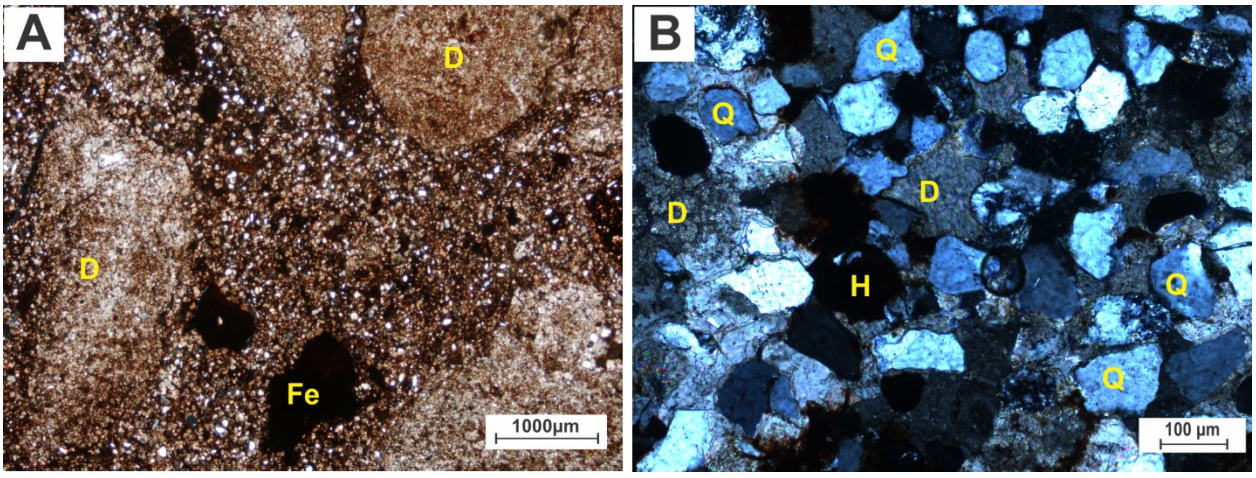

Figure 10-1 Channel-base Deposits (Element CD). (A) Sub-rounded clasts of finely crystalline dolomite and ferruginous clasts in a matrix of detrital grains and hematite-stained clay. Mixing Bowl. (B) Grains composed mainly of angular to sub-rounded monocrystalline quartz, of very fine sand to silt size, with finely crystalline dolomite cement, clay and hematite matrix; other grains include unaltered feldspar, apatite, zircon and Ti-minerals. Mixing Bowl. A-B under cross-polarised light. Quartz (Q), dolomite (D), ferruginous clasts (Fer).

Quartz-rich Inclined Strata (LA-1): At RT, pore-filling calcite and barite cements the detrital grains. The matrix comprises illite, Fe-rich chlorite, kaolinite, mixed-layer clay and hematite, with grain rims (Fig. 2-3G; 10-2A to C). The inner zones of albite and K-feldspar appear partially etched, and some quartz grains show partial overgrowths. Elongate, sand-sized clay aggregates are a minor component, with long axes near-parallel to bedding (Fig. 10-2B). The sandstone scour fill in Storey 1 is cemented by poikilotopic calcite and ankerite (Fig. 2-3A; 10-2C), with apatite grains, vugs filled with blocky calcite, and euhedral dolomite crystals some of which have a hollow interior with clear rims or a calcite core. At MR2, sandstones are cemented by poikilotopic gypsum and celestine; grains are commonly etched, oversized pores are common, and grains typically appear to float in the cements (Fig. 2-3H; 10-2D).

Mud-rich Inclined Strata (LA-2): The inclined beds are composed of detrital grains, a matrix of kaolinite, illite, Fe-rich chlorite and mixed-layer clay, patches of dolomite cement, and minor ferruginous clasts and sand-sized mud aggregates. Hematite-rich laminae and lenses are prominent in red samples (Fig. 2-4D). Couplets of mud and coarser grains are common in grey samples (Fig. 2-4E), with mud-rich laminae averaging 0.9 mm thick, two to three times thicker than the coarser layers. Where grey and red laminae are interbedded, contacts are abrupt but no visible change in framework grain size or abundance is apparent.

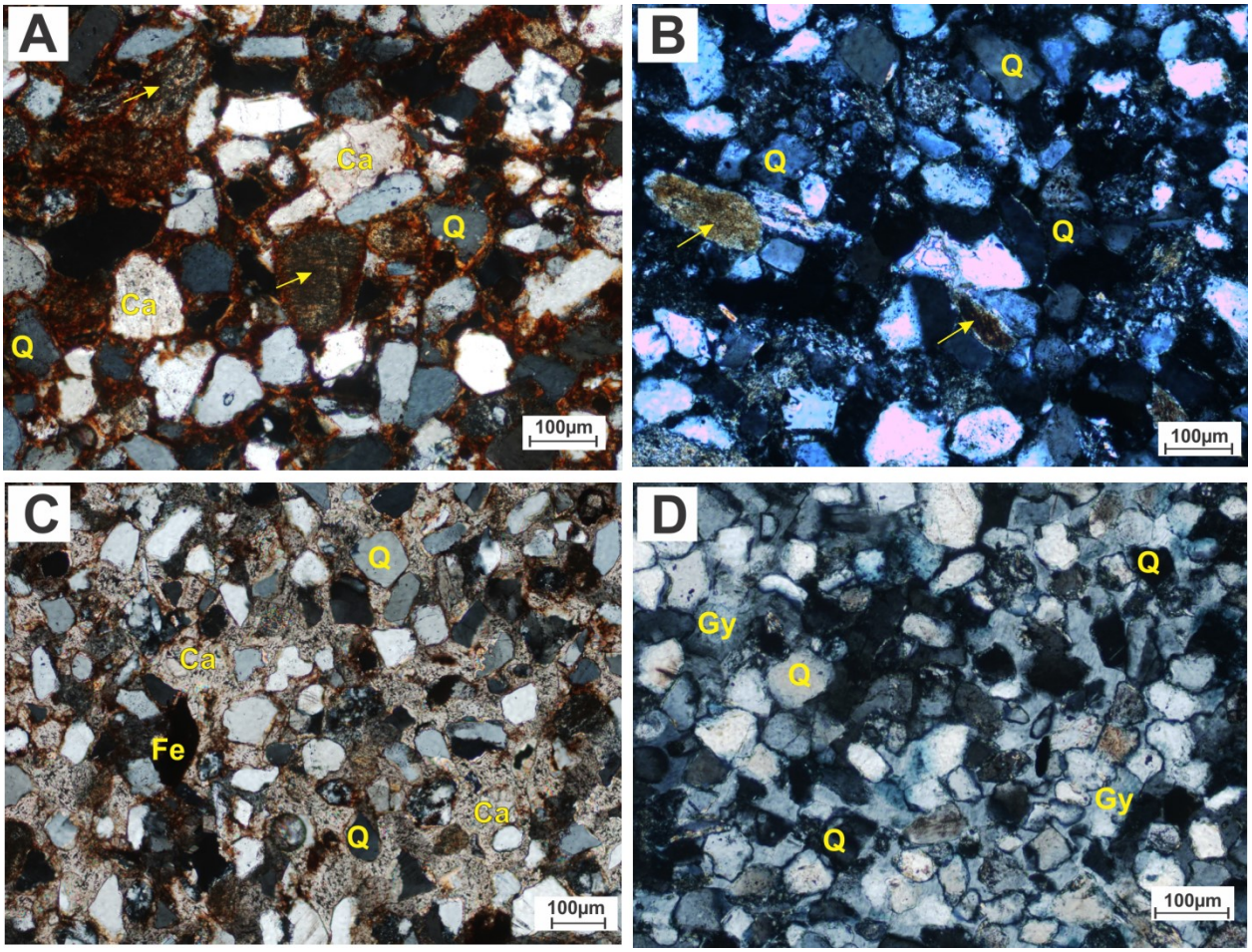

Figure 10-2 Petrographic features of Quartz-rich Inclined Strata (LA-1). A-C from Red Tank, D from Montgomery Ranch 2. (A) Inclined bed composed of subangular to subrounded, very fine- to fine-grained quartz, calcite and other detrital grains (feldspar, monazite, zircon and Ti-minerals) in a matrix of clay and hematite. A few mud aggregates (yellow arrows) are present. (B) Inclined bed with mud aggregates prominent (yellow arrows). (C) Scour fill in Storey 1 with detrital and ferruginous grains cemented by calcite. (D) Grey cemented sandstone with angular to subrounded detrital grains of quartz, feldspar and heavy minerals (ilmenite, Ti-minerals, zircon and garnet), with gypsum cement; the sandstone rests on an erosional surface between sets of quartz-rich inclined strata. A-D under cross-polarised light. Quartz (Q), calcite (Ca), ferruginous clasts (Fer), gypsum (Gy).

Mud- and Quartz-rich Inclined Strata (LA-3): For sandstones in the lower and middle units, detrital grains that include a few quartz grains with partial overgrowths appear to float in a matrix of illite, Fe-rich chlorite, kaolinite, mixed-layer clay and hematite (Fig. 2-6C). Layers with contrasted grain size and variably abrupt or gradational contacts are present, as well as patches of barite, calcite, and dolomite cement (Fig. 2-6C; 10-3A). In the upper unit, finely crystalline dolomite is abundant and the detrital grains are silt-sized (Fig. 10-3B); in rare cases, inequigranular dolomite crystals form patches or line ferruginous or mud clasts (Fig. 10-3C). Six mudstone samples from NSCQ comprise sand-sized mud aggregates with scattered angular to sub-rounded detrital grains (Fig. 2-6D); a detailed account will be published elsewhere. The aggregates are commonly flattened and sutured together, and individual grains were identified by variably reddish brown to grey colour in ordinary light (Fig. 2-6D). Euhedral dolomite crystals and ferruginous grains are also present, as well as thin lenses of detrital grains. Ten mudstone samples from other sites mainly comprise quartz silt that appears to float in a matrix of clay and hematite, with more mud aggregates and coarser quartzose detritus (very fine- to fine-grained sand) at BC. Samples from MR1 and MR3 have few or no distinct mud aggregates and a small percentage of quartzose silt (Fig. 10-3D). Aggregated and non-aggregated muds are composed of illite, Fe-rich chlorite, kaolinite, and mixed-layer clay at each site.

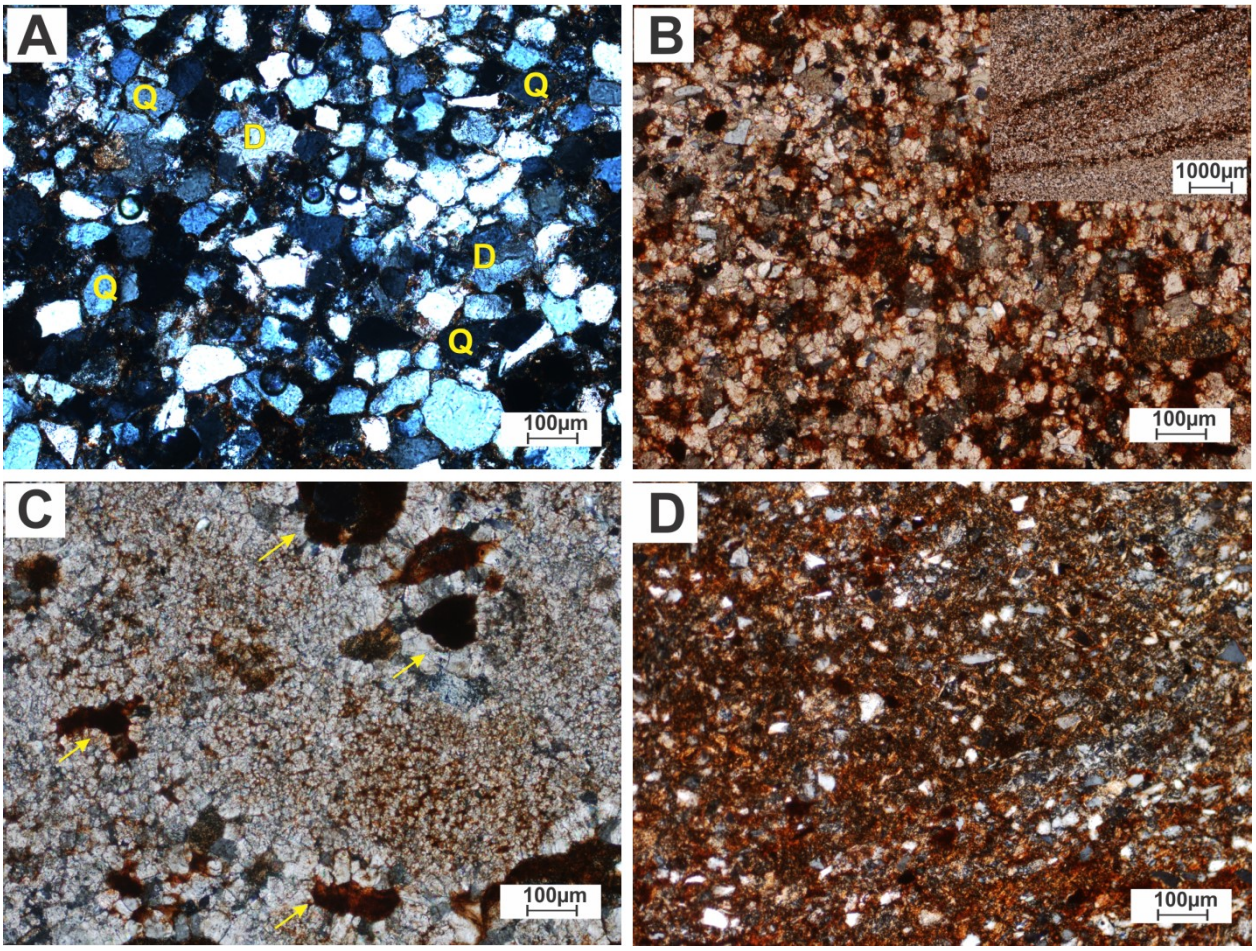

Figure 10-3 Sandstone and siltstone samples from element LA-3. A from North Soap-Creek Quadrangle, and B-D from Montgomery Ranch 1 and 3. (A) Detrital grains cemented by patches of finely crystalline dolomite with a clay and hematite matrix. (B) Dolomite grains with subordinate quartzose silt and a few very fine sand grains, with clay and hematite. Inset shows cross-set with hematite concentration on foresets. (C) Cemented bed with large region of inequigranular dolomite crystals with ferruginous and mud clasts lined with a rim of equant dolomite crystals (yellow arrow). (D) Siltstone composed of detrital silt in matrix of hematite and clay. Quartz (Qz), dolomite (D).

Tabular Sandstone (TS): The sandstone is composed of dolomite-cemented angular to subrounded detrital grains (quartz grains, feldspar, heavy minerals, and lithic fragments) with rims of hematite and clay (illite, Fe-rich chlorite, kaolinite, and mixed-layer clay; Fig. 2-7A, B). Dolomite is also abundant in the conglomerates as finely and coarsely crystalline clasts, interlocked patches of coarsely crystalline rhombs, and inequigranular crystals that fill vugs and line ferruginous or mud clasts (Fig. 10-4A, B). A few flattened mud aggregates are present between the quartz grains.

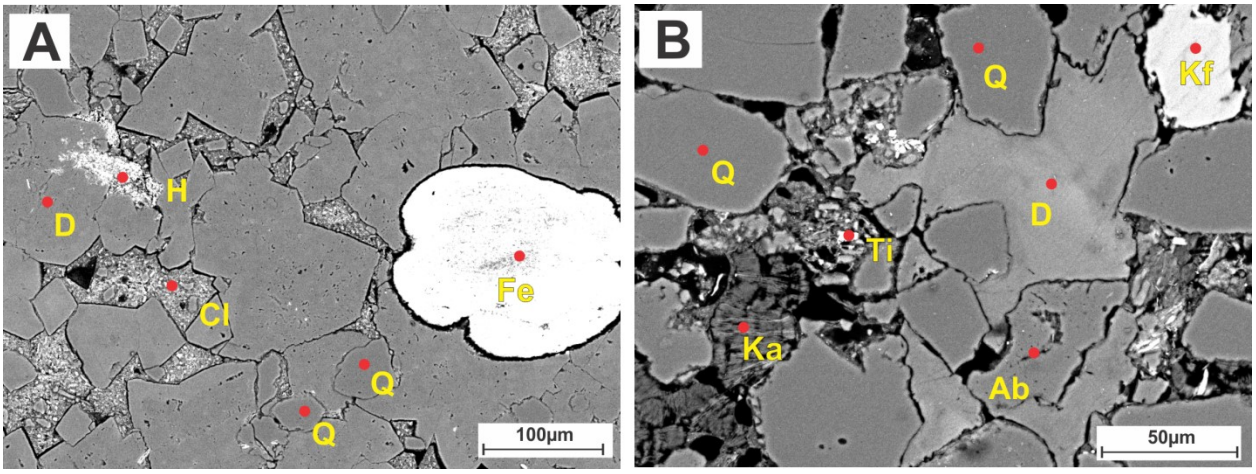

Figure 10-4 Tabular sandstone (element TS). A-B from Mixing Bowl. (A/B) Backscatter images of dolomite-cemented quartz, K-feldspar, albite, Ti-minerals and ferruginous grains with kaolinite and other clay minerals in the pore spaces. Quartz (Q), Kfeldspar (Kf), Dolomite (D), albite (Ab), Ti-minerals (Ti), hematite (Hem), kaolinite (Ka), ferruginous grains (Fer), Clay (Cl).

Laminated Mudstone (LM): The laminae include ungraded, normally and inversely graded layers of silt or clay. A common pattern is grading from silt-sized quartzose and ferruginous grains in a clay matrix to nearly pure clay with hematite (Fig. 10-5A). Silt-rich beds commonly decrease upward through the units, but CCP is clay-rich throughout (Fig. 10-5B). Laminar contacts are commonly abrupt and planar to wavy, with erosion evident in places. As with other mud-rich facies, the laminae contain Fe-rich chlorite, illite, kaolinite, and mixed-layer clay, with hematite prominent in red laminae and goethite in yellow laminae.

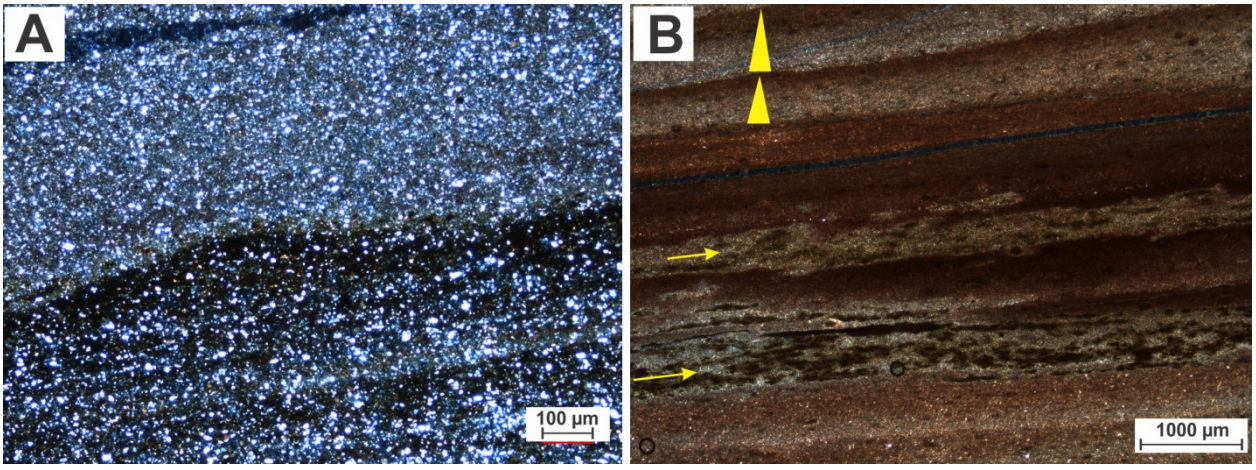

Figure 10-5 Laminated mudstone (element LM). A from Mouth of Brushy Creek, B from Colwell Creek. (A) Silt-rich laminae composed of quartz and other detrital grains within clay matrix with local hematite. Lower part shows grading from silt-rich to clay and hematite, with scour at base of thick upper silt layer. (B) Clay-rich laminae with varying amount of iron oxides and hydroxides. The greenish-black layers (yellow arrow) contain some organic material, possibly plant fragments. Note laminae that grade from fine silt to clay (yellow triangles), and abrupt and slightly erosional bases to some laminae. A and B under cross-polarised light.

Disrupted Mudstone (DM): Grains include sand-sized mud aggregates coated with clay and hematite (Fig. 2-8H) and silt-sized detrital grains that appear to float in a clay and hematite matrix (Fig. 10-6A, B). Illite, muscovite, kaolinite and Fe-rich chlorite are present. Apatite grains were derived from bone material (Fig. 10-6A). Cracks are filled with detrital grains, mud aggregates, larger mud clasts, clay and hematite, and microfaults show sharp and straight or wavy surfaces.

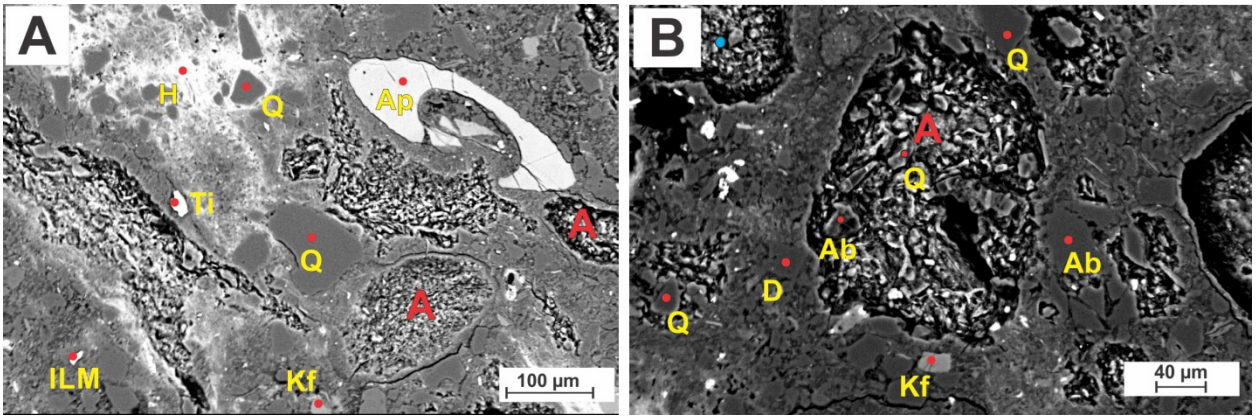

Figure 10-6 Disrupted mudstone (element DM) at Know Where to Park. (A/B) Backscatter images of the disrupted beds. Mud aggregates were partially plucked in the thin section preparation and the internal features are visible. Detrital grains range in size from sand to silt-sized particles and are present around and within the mud aggregates. Mud aggregates (A), apatite (Ap), quartz (Q), Ti-minerals (Ti), hematite (H), ilmenite (ILM), albite (Ab), K-feldspar (Kf), dolomite (D).

Massive Mudstone (MM): Samples from channel fills have similar textures at all sites, and commonly comprise very fine-grained sand to silt in an abundant clay and hematite matrix (Fig. 10-7A to B). In contrast, mudstone sheets vary considerably between sites. They comprise illite, Fe-rich chlorite, kaolinite and mixed-layer clay, silt and hematite accompanied by rare coarse sand-sized mud clasts, isolated or grouped euhedral dolomite rhombs, and vugs filled with dolomite crystals (Fig. 10-7C to D). Dolomite is especially prominent in the upper unit.

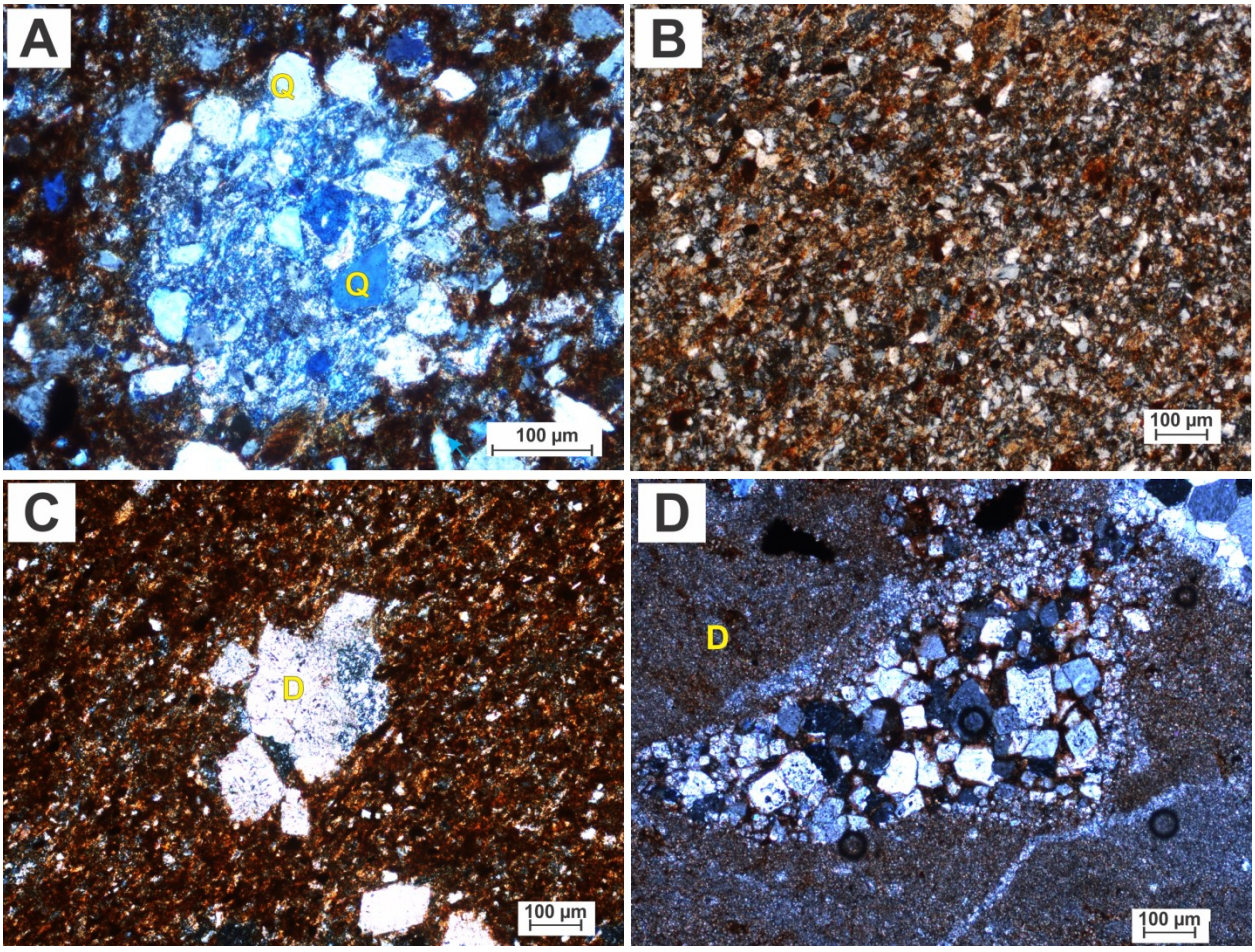

Figure 10-7 Massive mudstone (element MM). A, B, and D from Know Where to Park and C from Montgomery Ranch 3. (A) Very fine-grained sandstone to coarse siltstone (mostly sub-angular to sub-rounded quartz) within a clay and hematite matrix. A redoximorphic spot 0.3 mm wide is present.. (B) Fine- to medium-grained siltstone. Sample is associated with inclined strata. (C) Mudstone with fine- to medium-grained silt in a clay and hematite matrix, with vugs filled with medium crystalline, euhedral to subhedral dolomite crystals. (D) Finely crystalline dolomite with vugs filled with loosely packed, medium crystalline, euhedral to subhedral dolomite crystals. A-D are under cross-polarized light. Quartz (Q), dolomite (D).

APPENDIX D: CLAY MINERALOGY

Table 11-1 Samples used to conduct XRD clay analysis with a description of their relative position on the landscape and key differences based on the peak intensities.

Site	Samples	Descriptions	Key differences in spectra
Brushy Creek	BC 1	Accretion deposit (LA-3), mud- and quartz-rich channel	The intensity of the illite peak at 10Å in BC 3 is greater than BC 1. The intensity of the chorite and kaolinite peak at 7Å in BC 1 is greater than BC 3.
	BC 3	Abandoned fill, mud- and quartz-rich channel	
Know Where To Park	KWTP 2	Basal deposits, mud-rich channel	The peaks in samples KWTP 2, 6. 11, and Pa have low intensities, which can be a function of the clay crystallinity or the percentage of clay in the sample, in comparison to the zincite standard.
	KWTP 6	Accretion deposit (LA-2), mud-rich channel	
	KWTP Pa	Floodplain deposit (paleosol)	
	KWTP 11	Accretion deposit (LA-2), mud-rich channel	The peak intensities of the mixed layer clays (11-13Å) are much higher in the KWTP 11, 12, and 14 samples than the KWTP 17 sample. The chlorite peak at 14 Å is slightly less intense than the other samples.
	KWTP 12		
	KWTP 14	Abandoned fill, mud-rich channel	
	KWTP 17	Accretion deposit (LA-2), mud-rich channel	
Mixing Bowl	MB 10	Basal deposits, mud-rich channel	For sample MB 10, the peak intensity of the chorite and kaolinite peak at 7Å is lower than MB 15 and MB 18 samples.
	MB 15	Abandoned fill, mud-rich channel	
	MB 18	Accretion deposit (LA-2), mud-rich channel	
Montgomery Ranch 1	MR1_10	Floodplain deposit (paleosol)	For samples MR1_13 and MR1_18, the intensity of the chlorite peak at at 14 Å is less intense than the other samples. The peak intensity of the mixed layer clays is higher in the MR1_10 sample than the other samples.
	MR1_13	Accretion deposit (LA-3), mud- and quartz-rich channel	
	MR1_18		
	MR1_21		

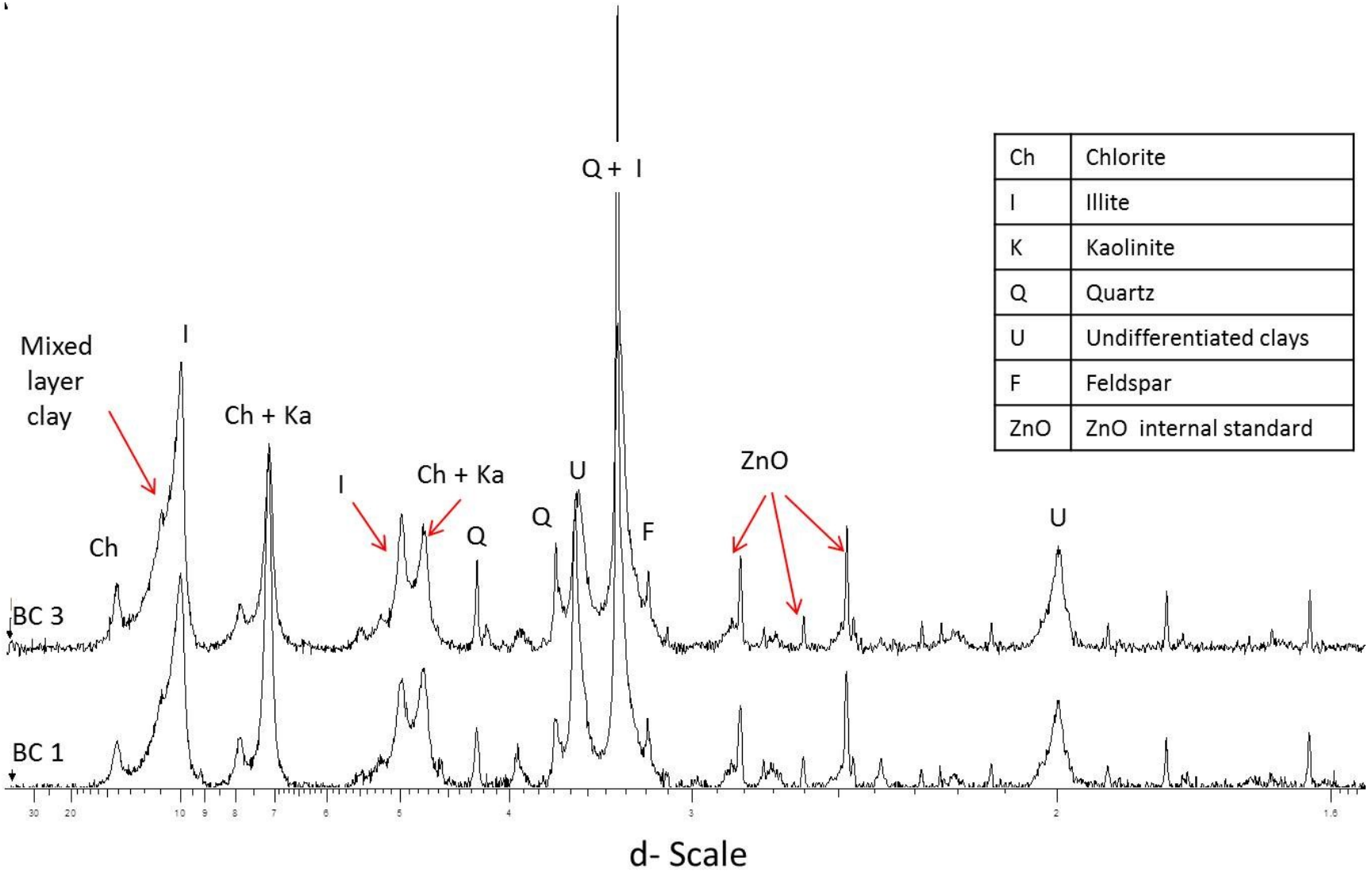

Figure 11-1 Spectra of <2µm clay fraction from the Mouth of Brushy Creek site. Illite, Fe-chlorite, and kaolinite are the main clay types present in the lateral accretion deposits (BC1) and the abandoned channel fill (BC3). See Table 11-1 for a description of the key differences.

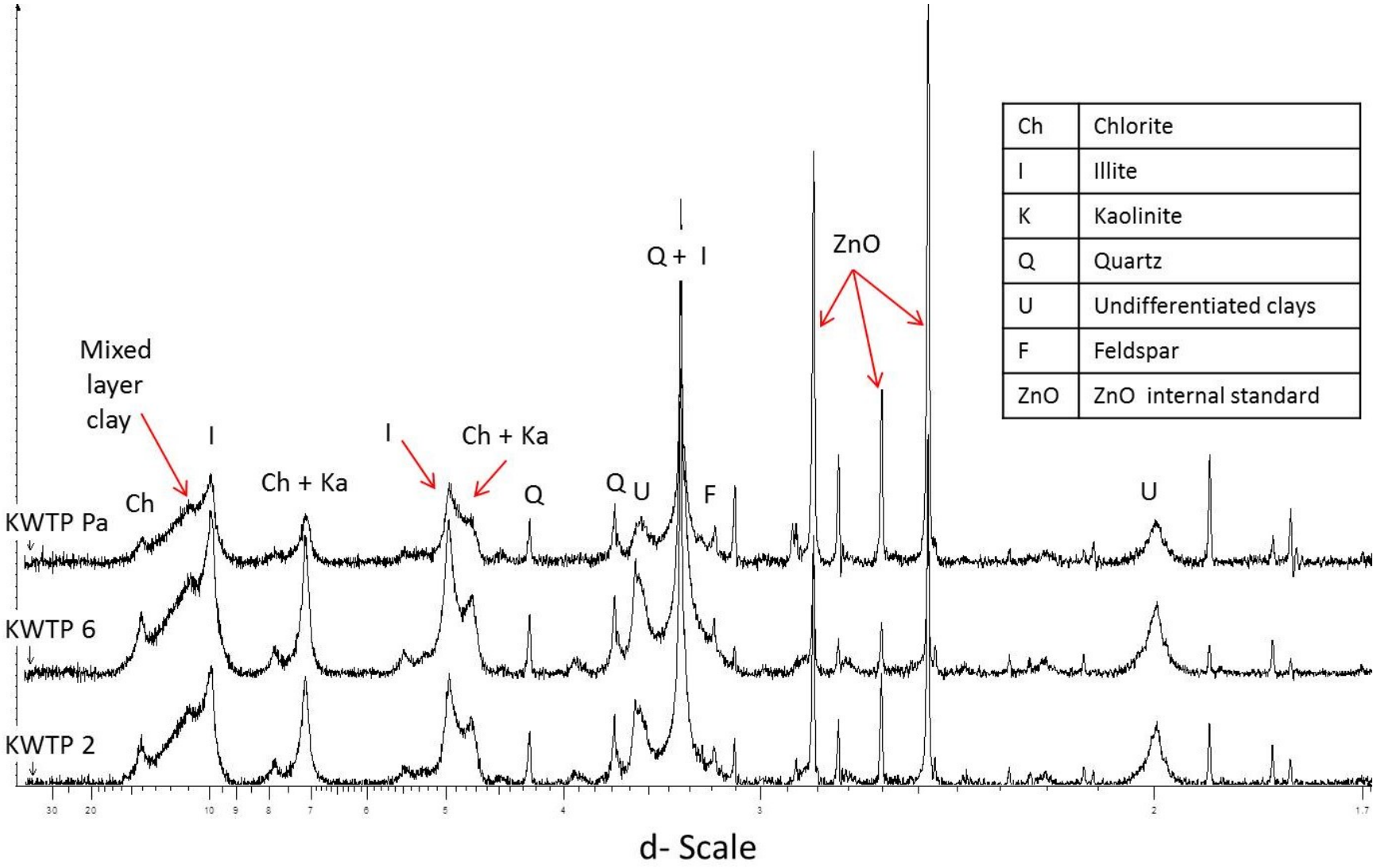

Figure 11-2 Spectra of <2µm clay fraction from the Know Where To Park site. Illite, Fe-chlorite, and kaolinite are the main clay types present in the paleosols (KWTP Pa), channel lag (KWTP 2), and the accretion deposits (KWTP 6). See Table 11-1 for a description of the key differences.

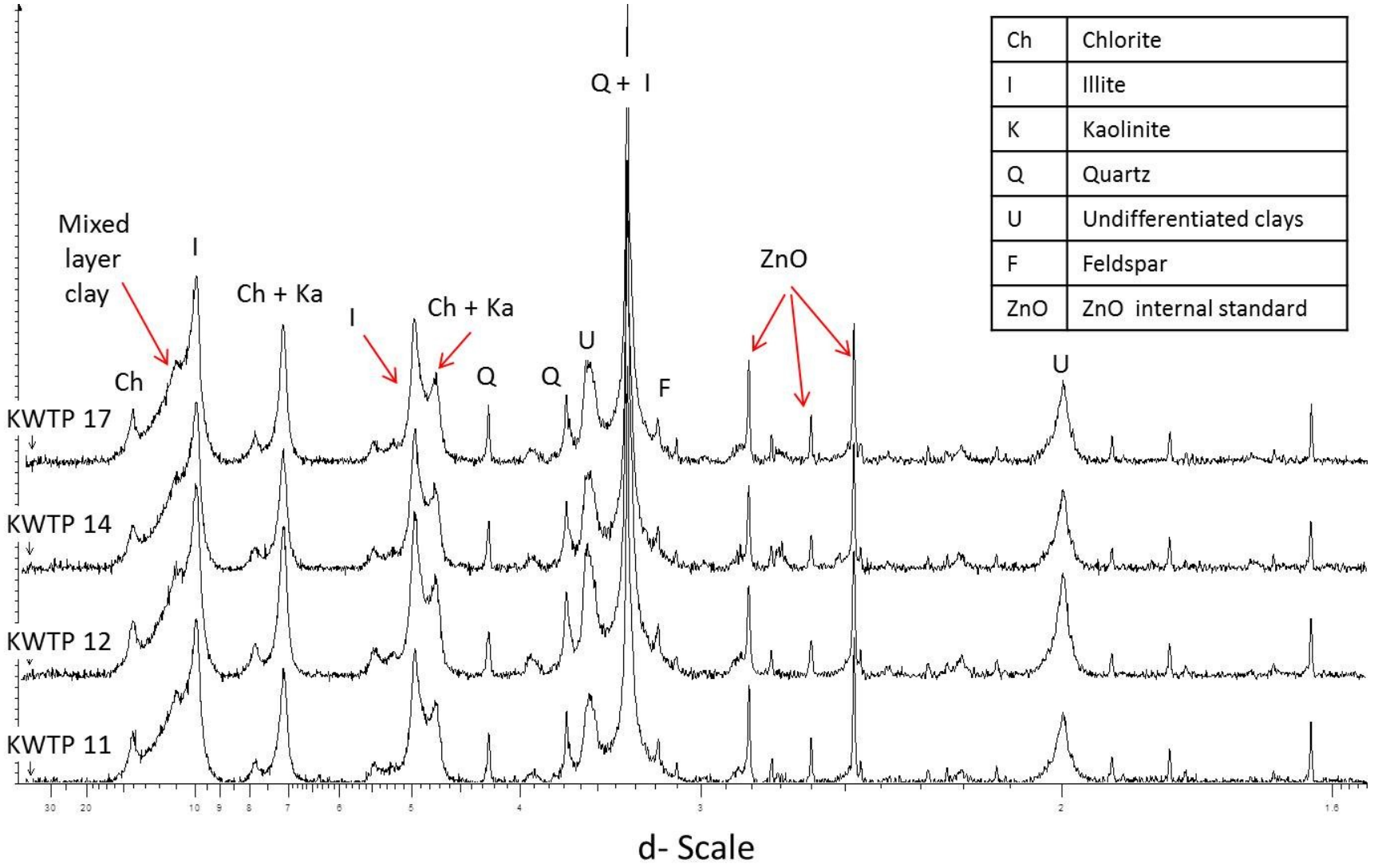

Figure 11-3 Spectra of <2µm clay fraction from the Know Where To Park site. Illite, Fe-chlorite, and kaolinite are the main clay types present in the abandoned channel fill (KWTP 14), and accretion deposits (KWTP 11, 12, and 17). See Table 11-1 for a description of the key differences.

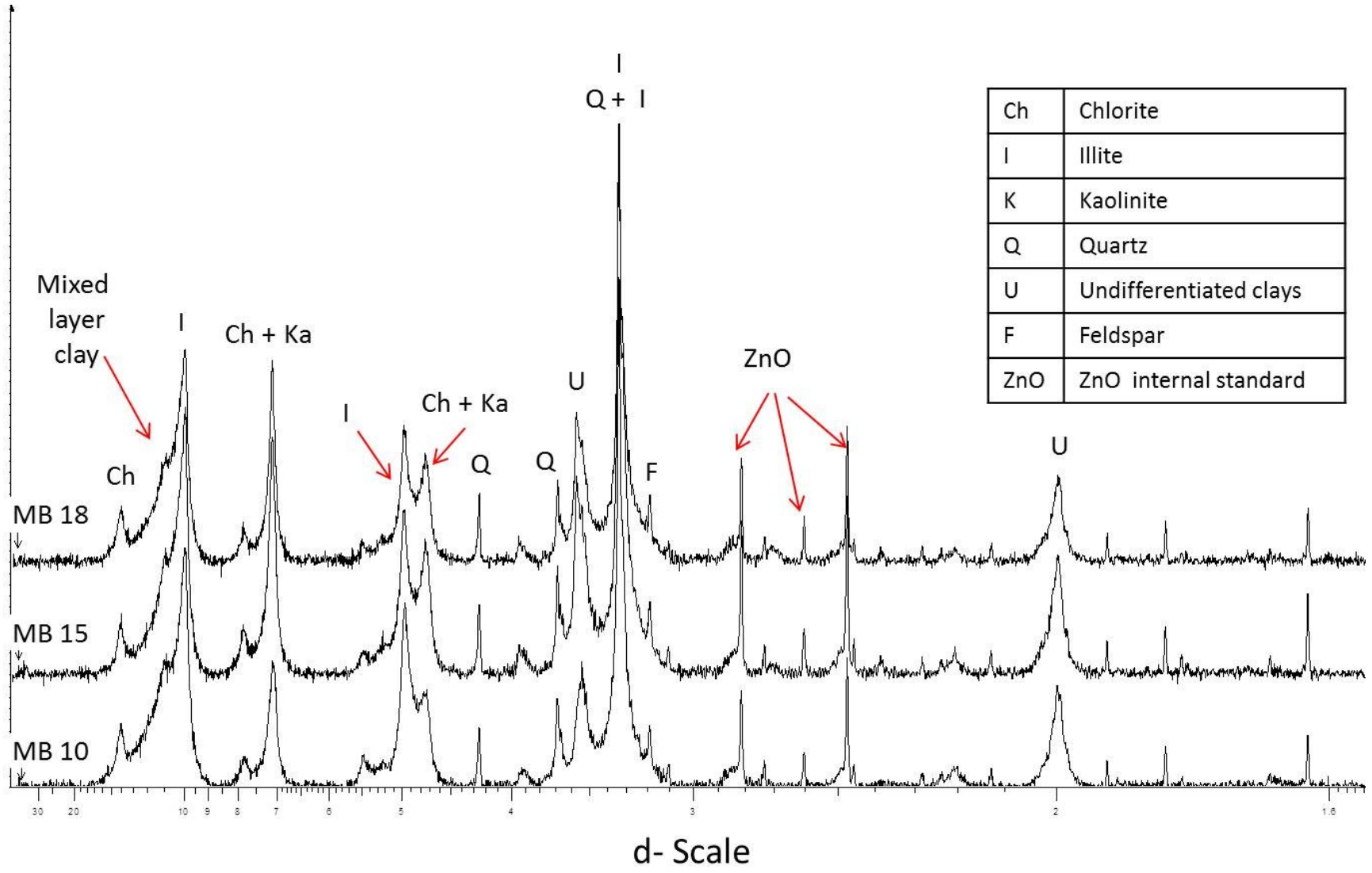

Figure 11-4 Spectra of <2µm clay fraction from the Mixing Bowl site. Illite, Fe-chlorite, and kaolinite are the main clay types present in the channel lag (MB 10), abandoned channel fill (MB 15), and accretion deposits (MB 18). See Table 11-1 for a description of the key differences.

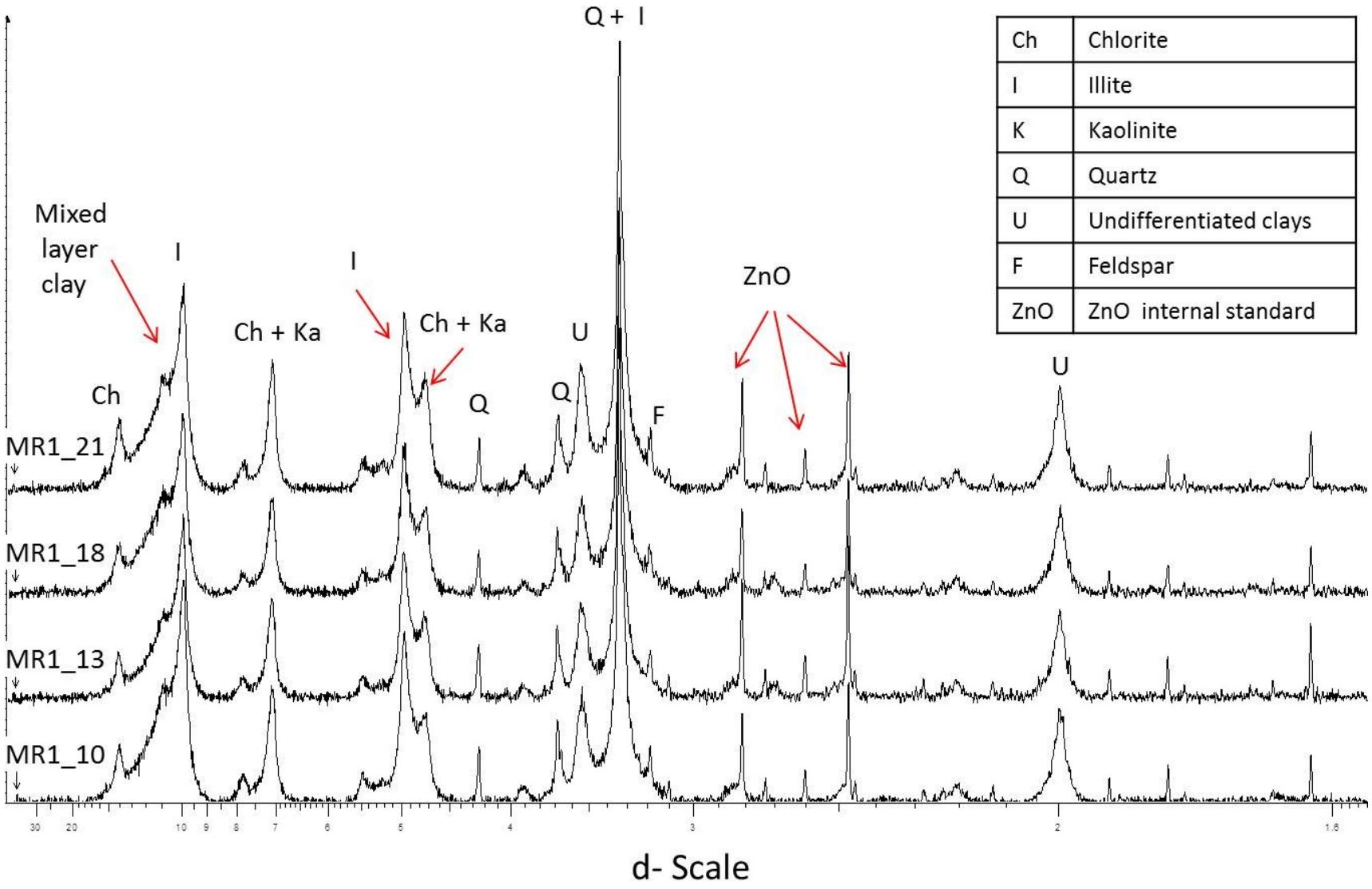

Figure 11-5 Spectra of <2µm clay fraction from the Montgomery Ranch 1 site. Illite, Fe-chlorite, and kaolinite are the main clay types present in paleosols (MR1_10) and accretion deposits (MR1_13, 18, 21). See Table 11-1 for a description of the key differences.